



ALK in the pathogenesis of cancer

A thesis submitted for the degree of
Doctor of Philosophy

Nina Prokoph

University of Cambridge

Newnham College

August 2020



This project has received funding from the European Union's Horizon 2020

Marie Skłodowska-Curie Innovative Training Networks (ITN-ETN) under grant agreement No.: 675712

Declaration

I hereby declare that this thesis is the result of my own work and includes nothing which is the outcome of work done in collaboration except as declared in the preface and specified in the text.

It is not substantially the same as any that I have submitted, or, is being concurrently submitted for a degree or diploma or other qualification at the University of Cambridge or any other University or similar institution except as declared in the preface and specified in the text. I further state that no substantial part of my dissertation has already been submitted, or, is being concurrently submitted for any such degree, diploma or other qualification at the University of Cambridge or any other University of similar institution except as declared in the preface and specified in the text.

It does not exceed the prescribed word limit (60,000 words) for the Biology Degree Committee.

Nina Prokoph

Abstract

ALK in the pathogenesis of cancer¹

Nina Prokoph

Anaplastic Lymphoma Kinase (ALK) has been implicated in the pathogenesis of many types of cancer including Anaplastic Large Cell Lymphoma (ALCL) and neuroblastoma (NB). ALK is an ideal drug target as its endogenous expression is limited to neuronal cells during neonatal development, although resistance to ALK-targeted therapy has been observed. In this thesis I explore potential mechanisms of resistance to the ALK inhibitors that have been approved for ALK+ non-small cell lung cancer (NSCLC) including crizotinib, alectinib, ceritinib, brigatinib and lorlatinib.

To define a global landscape of resistance mechanisms, patient-centric studies require many pre- and post-treatment tumour specimens taken from a sufficient number of patients, which is not possible for a rare cancer such as ALK+ ALCL or ALK driven NB. Hence, genome-wide CRISPR overexpression screens were conducted in ALCL and NB cell lines.

We show that resistance to ALK inhibition by crizotinib in ALCL can be driven by aberrant upregulation of interleukin-10 receptor alpha (IL10RA). Elevated IL10RA expression rewires the STAT3 signalling pathway bypassing otherwise critical phosphorylation of STAT3 by NPM1-ALK. IL-10RA expression does not correlate with response to standard chemotherapy in paediatric patients suggesting that a combination of crizotinib with chemotherapy could prevent ALK-inhibitor resistance-specific relapse.

In the case of ALK-driven NB resistance to ALK inhibition is associated with expression of the serine/threonine-protein kinase PIM1. While both ALK-driven and ALK-negative NB cells were insensitive to several small-molecule pan-PIM kinase inhibitors, knockdown of PIM1 by RNA interference sensitized cells to ALK inhibition and the combination of ALK inhibitors with the PIM1 inhibitor AZD1208 demonstrated mild synergy. Therefore, our data suggest the potential for combined pharmacological inhibition of ALK and PIM1 in patients with ALK-driven NB.

Finally, given the above investigations largely focused on cell line-based models whereby *in vitro* culture conditions may cause rapid phenotypic and genotypic divergence of patient-derived cells from the originating tumour, we developed two paediatric ALK+ ALCL patient-derived xenograft (PDX) models from liquid biopsy samples of chemotherapy-refractory and crizotinib resistant patients. *In vivo* investigation showed that second generation ALK inhibitor brigatinib led to a reduction in the mean tumour volume relative to either vehicle or crizotinib treatment. This suggests brigatinib as a treatment option for crizotinib resistant ALCL patients.

In summary, this study has identified potential mechanisms of ALK inhibitor resistance particularly in NPM1-ALK positive ALCL and ALK-driven NB.

Acknowledgements

I have been extremely lucky to meet wonderful people, who have guided and supported me on my scientific journey. I will name them in the order that they crossed my way.

Ralf Jauch opened the door for my research adventure when he invited me to join Prasana Kolatkar's lab in Singapore. Eight years later he remains my untouchable role model of a supervisor. He has an indescribable talent to create the most encouraging and collaborative work environment one can dream of:

Kamesh Narasimhan taught me that there is nothing wrong about feeling stupid.

Calista Keow Leng Ng's heartily guidance taught me all the wet-lab knowledge that I still cherish from.

Elena Haas worked alongside me when I moved back to Germany to continue with my Master's. Together we learned to acknowledge negative results as important results.

Jianming Liu accepted me for my final Master thesis project and this way set the ground stone for two fruitful years at AstraZeneca. He was the most caring of my supervisors.

Neil Henderson introduced me into the world of biomarkers and clinical samples and helped me tremendously to develop better documentation techniques.

John Steele played a major part in my overall happiness and development when he supported me to move from Gothenburg to Shanghai. I am immensely grateful for his encouragement, suggestions, and perspective. I always experience an energetic happiness even days after meeting him. Although not superman, John is my hero.

Xiaolin Zhang was a wonderful host and allowed me to play in his research paradise. He is bursting with energy – if I would have only met him once in my life, his image would still have stayed in my memory. But what made the most impression on me was his modesty.

Qiuli Guo's natural cheerfulness, and her mode of interaction with scientific colleagues completed my experience in the Middle Kingdom.

Suzanne Turner attracted me to move to the United Kingdom and provided me with complete independence and freedom. I am thankful for everything I could learn that way.

Nicola Probst has been the most important person during my PhD. She was my sunshine during an extremely work-intensive time in the lab.

Isaia Barbieri infected me with fresh enthusiasm and energy. It is such a pleasure to show him new results as his creative mind finds new avenues in a matter of seconds and his feedback is the most encouraging that I have ever encountered.

There are three people that inspired me without their knowledge: Katarina Höll, Donatella Luciani and Sofia Chen.

The labs based at the Addenbrooke's hospital have been filled with people, past and present, that made sure I kept the same level of sanity. Specifically, **Jamie Matthews** and **Rogier ten Hoopen** shared kindness and laughter with me; **Hugo Larose** was irreplaceable as he called out when I was getting demotivated, working too hard or being not rational or focused; **Jun Mun Liew** was a calm anchor; **Sorcha Forde** was my companion while carrying out the CRISPR screens and this way halved my suffering; **Liam Lee** established numerous methods that I hugely profited from.

The biggest joy of my PhD has been to work alongside my undergraduate students **Tu Truong, Nicola Probst, Guido Lewik, Tugce Gül** and **Klaas Bahnsen**. They have been great teachers.

In this context, I would like to thank the German Academic Exchange Service (Deutscher Akademischer Austauschdienst, DAAD), the Bayer Science and Education Foundation, Erasmus+, the German Academic Scholarship Foundation (Studienstiftung des deutschen Volkes) and Research Internships in Science and Engineering (RISE) worldwide for supporting my students financially. Both DAAD and RISE worldwide are funded by the German Federal Ministry of Education and Research.

In addition, I would like to thank the European Union for their generous financial support under the Horizon 2020 Marie Skłodowska-Curie Innovative Training Network with grant agreement no. 675712. Being part of a group of 15 PhD students across Europe taught me a great deal about the value of collaboration in science. Most importantly, I would like to thank **Stephen Ducray, Huan-Chang Liang, Ivonne Montes-Mojarro, Cosimo Lobello, Geeta Sharma** and **Serena Stadler** for their support and **Roberto Chiarle** and **Luca Mologni** for been fantastic role models.

The first part of my PhD I spend at Cambridge Life Sciences in Ely: Special thanks goes to **Keith Rawson** and **Danielle Mack** for their time and patience.

It feels like I have spent a decade in a dark tissue culture room, which I could not have endured without music from the Red Hot Chili Peppers, Kurt Vile, Bon Iver, Hozier, Cigarettes After Sex, Mumford & Sons, Of Monsters and Men, The Lumineers, The Decemberists, and Hollow Coves.

Finally, I would like to thank the patients and families that have provided samples.

Declaration of Assistance Received

The following people contributed to the success of my PhD projects. I thank each of you for your time and friendliness.

Experiments or data analysis carried out by students that worked under my supervision:

- 1) Klaas Bahnsen (University of Dresden, Germany):
 - Analysis of all microarray data
- 2) Tugce Gül (University of Bonn, Germany):
 - Construction and validation of NSCLC cell line H3122 stably expressing lenti dCAS-VP64_Blast and lenti MS2-P65-HSF1_Hygro
 - Design and introduction of guide sequences into lenti sgRNA(MS2)_Puro backbone vector for the following genes: *KIT*, *MET*, *EGFR*, *ABCB1*, *KRAS*, *HER-2*, *IGF-1R*
- 3) Guido Lewik (University of Bochum, Germany):
 - RT-qPCR based validation of CRISPR hits using TKI-resistant ALCL cell lines
- 4) Nicola Probst (University of Applied Sciences Biberach, Germany):
 - Establishment of alectinib-resistant and crizotinib-resistant SUDHL-1 cell line
 - RT-qPCR based validation of CRISPR hits using TKI-resistant ALCL cell lines
 - Design and introduction of guide sequences into lenti sgRNA(MS2)_Zeo backbone vector for the following genes: *STAT3*, *NPM1*, *MYC*, *MKNK1*, *IL10RA*, *IL10*, *P2RY6*, *SH2D2A*, *FOXN2*, *HELZ2*, *HOXD8*, *RORC*, *GPR161*, *PRKACA*, *ADORA2A*, *PGBD1*, *HDAC8*, *ABCB1*, *EGFR*, *KRAS*, *ALK*, *HER-2*, *IGF-1R*, *KIT*, *MET*
 - Functional validation of candidates identified from the screens in SU-DHL-1 and Mac-2A.
- 5) Tu Truong (University of Applied Sciences Biberach, Germany):
 - Construction and validation of Mac-2A and SU-DHL-1 cell lines stably expressing lenti dCAS-VP64_Blast and lenti MS2-P65-HSF1_Hygro
 - Optimization of Golden Gate Cloning using Bsmbl for the introduction of guide sequences into lenti sgRNA(MS2)_Zeo backbone vector

Experiments or data analysis carried out by collaborators:

- 1) Liam Lee (University of Cambridge, UK)
 - Design and introduction of guide sequences into lenti sgRNA(MS2)_Zeo backbone vector coding for the following genes: *ARHGEF9*, *BCL10*, *BDNF*, *COPZ2*, *CRK*, *CLYBL*, *EGR4*, *EML2*, *EREG*, *ETV1*, *FAIM2*, *FOS*, *FOXP1*, *KRAS*, *MET*, *MFSD2A*, *MYC*, *NIN*, *NKX2-4*, *NPY*, *NR4A2*, *PIK3CD*, *PIM1*, *PLEKHG6*, *PRKACA*, *PRRX2*, *PSD2*, *PTGES*, *RORC*, *RRAS*, *SAGE1*, *SAMD4A*, *SEMA4A*, *SLC7A3*, *SPDEF*, *SSBP3*, *SURF2*, *UBIAD1*, *UTF1*, *YAP1*.
 - Transformation and amplification of the human CRISPR activation library
 - Quantification of isolated amplicons by qPCR reactions using KAPA Library Quantification Kit
 - Cell-titre blue based validation of CRISPR dCas9 overexpression screen hits in SH-SY5Y

- 2) Martin Zimmerman (Hannover Medical School, Germany), Jamie D. Matthews (University of Cambridge, UK):
 - Survival analysis
- 3) Serena Stadler (University of Giessen, Germany):
 - Analysis of 94 BFM samples with immunoperoxidase labelling technique
- 4) Jack Monahan (EMBL-EBI, Cambridge, UK):
 - RNA-seq analysis
- 5) Huan-Chang Liang (Medical University of Vienna, Austria):
 - Immunohistochemistry staining for IL-10RA & IL-10RB
- 6) Vikas Malik (Columbia University Irving Medical Center, USA):
 - ChIP-seq analysis
- 7) Luca Pandolfini (University of Cambridge, UK):
 - Analysis of Human Protein Atlas RNA-seq datasets
- 8) Shi-Lu Luan (University of Cambridge, UK):
 - Design and introduction of guide sequences into the lentiCRISPR v2 backbone vector coding for *IL10RA*
- 9) Stephen P. Ducray, Hugo Larose (University of Cambridge):
 - RT-qPCR based investigation of ALK knockdown with an inducible shRNA/crizotinib inhibition on IL10, IL10RA and IL10RB mRNA expression
- 10) Geeta Sharma (University of Milano-Bicocca, Italy):
 - RT-qPCR of lorlatinib-resistant K299 xenograft tumours
- 11) Ricky Trigg (University of Cambridge, UK):
 - Illustrations: Figure 1, Figure 4, Figure 14, Figure 19A, Figure 21, Figure 29J, Figure 31B
 - Cell-titre blue based PIM1 inhibitor validation in several NB cell lines.
- 12) Ivonne Montes-Mojarro (Tübingen University Hospital, Germany), Lakshmi Venkatraman (Royal Belfast Hospital for Sick Children, UK), Sandra Höglner (Medical University of Vienna, Austria), Simone Tangermann (Medical University of Vienna, Austria), Lukas Kenner (Medical University of Vienna, Austria), Liz Hook (University of Cambridge, UK), Olivier Giger (University of Cambridge, UK):
 - Pathological assessment, quantification and image generation of tissue microarrays
- 13) Elif Karaca & Qi Wang (Boston Children's Hospital and Harvard Medical School, USA)
 - Genome-wide Cas9 mini knockout screen and analysis
- 14) Jamie Matthews, Ricky Trigg, Harriet Kendrick-Thomas, Fallon Miller, Laura O'Reilly and Holly Bloy (University of Cambridge, UK):
 - Mouse handling

Collaborators that generously provided patient samples, reagents, equipment and/or data:

- 1) Andishe Attarbaschi (St Anna Children's Hospital, Vienna, Austria)
- 2) AstraZeneca
- 3) Isaia Barbieri (University of Cambridge, UK)

- 4) Assaf C. Bester (Beth Israel Deaconess Medical Center, USA)
- 5) Laurence Brugières (Gustave Roussy Cancer Center, France)
- 6) G.A. Amos Burke (Addenbrooke's Hospital, UK)
- 7) David R. Camidge (University of Colorado Cancer Center, USA)
- 8) Roberto Chiarle (University of Torino, Italy)
- 9) Ming-Qing Du (University of Cambridge, UK)
- 10) Falko Fend (Tübingen University Hospital, Germany)
- 11) F. Hoffmann-La Roche: Johannes Noe, Eveline Nüesch, Malgorzata Nowicka
- 12) Carlo Gambacorti-Passerini (University of Milano-Bicocca, Monza, Italy)
- 13) Birgit Georger (Gustave Roussy Cancer Center, France)
- 14) Inflection Biosciences
- 15) Andrea Janíková (University Hospital Brno, Czech Republic)
- 16) Robert Johnston (Royal Belfast Hospital for Sick Children, UK)
- 17) Wolfram Klapper (UKSH Campus Kiel, Germany)
- 18) Anne Lambilliotte (Hôpital Jeanne de Flandre, France)
- 19) Judith Landman-Parker (Hospital Armand Trousseau, France)
- 20) Olaf Merkel (Medical University of Vienna, Austria)
- 21) Luca Mogni (University of Milano-Bicocca, Monza, Italy)
- 22) Matthew J. Murray (Addenbrooke's Hospital, UK)
- 23) Hélène Pacquement (Institut Curie, France)
- 24) Shahid Pervez (Aga Khan University Hospital, Pakistan)
- 25) Pfizer
- 26) Šárka Pospíšilová (CEITEC, Czech Republic)
- 27) Gudrun Schleiermacher (Institut Curie, France)
- 28) Owen Smith (Our Lady's Children's Hospital, Ireland)
- 29) Gilles Vassal (Gustave Roussy Cancer Center, France)
- 30) Wilhelm Woessmann (University Hospital Hamburg-Eppendorf, Germany)
- 31) Kent Yip (Ipswich Hospital NHS Trust, UK)

Technical service providers used:

- 1) DNA Sequencing Facility (Department of Biochemistry, University of Cambridge, UK):
 - Sanger Sequencing reactions of PCR amplicons or plasmids
- 2) NIHR BRC Cell Phenotyping Hub (Department of Medicine, University of Cambridge, UK):
 - FACS cell sorting on an FACSAria™ Fusion 2 (BD Biosciences)
- 3) Massachusetts General Hospital Next Generation Sequencing Facility (Department of Molecular Biology, Harvard University, USA):
 - HiSeq RapidRun reactions
- 4) Human Research Tissue Bank team (Addenbrooke's Hospital, Cambridge, UK):
 - Embedding of formalin-fixed tissue & sectioning of FFPE-blocks
 - Staining of FFPE tissue sections for ALK and CD30

Table of Content

DECLARATION	I
ABSTRACT	II
ACKNOWLEDGEMENTS.....	III
DECLARATION OF ASSISTANCE RECEIVED.....	V
LIST OF FIGURES	XIII
LIST OF TABLES	XV
ABBREVIATIONS.....	XVII
CHAPTER 1 INTRODUCTION	1
1.1 ANAPLASTIC LYMPHOMA KINASE (ALK) IN THE PATHOGENESIS OF CANCER	2
1.2 ALK+ ALCL.....	5
1.2.1 Clinical Features of Paediatric ALCL.....	5
1.2.2 Frontline Treatment for Paediatric ALCL	7
1.2.3 Treatment of Refractory/Relapsed Disease	14
1.3 ALK-DRIVEN NB.....	19
1.3.1 Clinical Features of NB	19
1.3.2 ALK in NB	19
1.3.3 Targeting ALK in ALK-driven NB	20
1.4 ALK+ NSCLC	22
1.4.1 Clinical Features of ALK+ NSCLC	22
1.4.2 Targeting ALK in ALK+ NSCLC.....	22
1.5 RESISTANCE MECHANISMS TO ALK INHIBITORS	23
1.5.1 ALK-dependent resistance mechanisms	23
1.5.2 ALK-independent resistance mechanisms	25
1.6 APPROACHES TO IDENTIFYING ACQUIRED RESISTANCE MECHANISMS TO TKIs.....	25
1.6.1 CRISPR-based genome-wide screens.....	27
1.7 AIMS OF THE PHD	30
CHAPTER 2 MATERIALS & METHODS.....	31
2.1 KEY REAGENTS AND RESOURCES	32
2.2 PATIENT SAMPLES	40
2.2.1 NHL-BFM90 trial cohort.....	40
2.2.2 NHL-BFM95 trial cohort	41
2.2.3 ALCL99 trial cohort	42
2.2.4 UK cohort.....	43
2.2.5 MAPPYACTS trial cohort.....	44
2.2.6 Brno cohort	45

2.2.7	Pakistan cohort	46
2.2.8	Vienna cohort.....	46
2.3	ANIMAL STUDIES	47
2.3.1	Generation of lorlatinib-resistant K299 xenografts	47
2.3.2	Generation of ALCL PDX.....	48
2.4	IMMUNOPEROXIDASE LABELLING TECHNIQUE FOR ANTI-ALK AUTOANTIBODY DETECTION.....	49
2.4.1	Preparation of COS-1 NPM1-ALK transfectants	49
2.4.2	Immunostaining of COS-1 NPM1-ALK transfectants.....	49
2.5	PROTEIN MICROARRAY ASSAY FOR ALK AUTOANTIBODY DETECTION	50
2.5.1	Antigen spotting process	50
2.5.2	Processing of microarray slides.....	50
2.6	CELL LINES AND CELL CULTURE	51
2.7	IC ₅₀ DETERMINATION	51
2.8	CELLULAR PROLIFERATION.....	51
2.9	APOPTOSIS ANALYSIS	51
2.10	GENERATION OF TKI-RESISTANT ALCL CELL LINES.....	51
2.11	SEQUENCING OF THE NPM1-ALK KINASE DOMAIN REGION	52
2.12	RT-QPCR	52
2.13	WESTERN BLOT	54
2.14	SGRNA CLONING.....	55
2.15	GENOME-SCALE CAS9 TRANSCRIPTIONAL ACTIVATION SCREEN.....	57
2.15.1	Genome-scale Cas9 transcriptional activation screen design	57
2.15.2	Generation of dCas9 and MS2 expressing cell lines	59
2.15.3	Transformation, amplification and preparation of lentiviral sgRNA libraries	59
2.15.4	Transduction of ALCL cell lines using lentiviral CRISPR libraries	60
2.15.5	Preparation of HiSeq libraries for the screen readout.....	60
2.16	GENOME-SCALE CAS9 MINI KNOCKOUT SCREEN.....	62
2.16.1	Genome-scale Cas9 knockout screen design.....	62
2.16.2	CRISPR Mini Knockout Screen.....	63
2.17	SHORT-HAIRPIN RNA (SHRNA) KNOCKDOWN.....	66
2.18	DRUG SYNERGY EXPERIMENTS.....	66
2.19	IMMUNOHISTOCHEMISTRY (IHC).....	66
2.20	CHROMATIN IMMUNOPRECIPITATION (CHIP) qPCR	67
2.21	ENFORCED IL10RA OVEREXPRESSION.....	68
2.22	MRNA SEQUENCING	68
2.23	BIOINFORMATICS ANALYSIS	68
2.23.1	ChIP-seq Data Analysis	68
2.23.2	Survival Analysis	68
2.23.3	CRISPR Overexpression Screen Deconvolution and Analysis.....	69
2.23.4	CRISPR Mini Knockout Screen Deconvolution and Analysis	69

2.23.5	mRNA-Seq Data Analysis	69
2.23.6	Gene Set Enrichment Analysis (GSEA) and Gene Ontology (GO) Analysis	69
2.23.7	Gene Expression Analysis	69
2.23.8	Co-Expression Analysis	70
2.23.9	Analysis of Public Gene Expression Datasets	70
2.23.10	Waterfall Plot	70
CHAPTER 3 BYPASS RESISTANCE LANDSCAPE TO CRIZOTINIB INHIBITION IN ALCL.....		71
3.1	INTRODUCTION	72
3.1.1	Aims	73
3.2	VALIDATION OF THE dCAS9-VP64 INDUCED OVEREXPRESSION PHENOTYPE	73
3.3	CRISPR OVEREXPRESSION SCREENS IDENTIFY GENES MODULATING CRIZOTINIB SENSITIVITY IN ALCL CELL LINES	74
3.4	VALIDATION OF CANDIDATE GENES IDENTIFIED IN THE SCREEN	76
3.4.1	Overexpression-based validation of Candidate Genes Modulating ALK TKI Sensitivity in ALCL Cell Lines	76
3.4.2	Knockout-based validation of Candidate Genes Modulating ALK TKI Sensitivity in ALCL Cell Lines	79
3.4.3	Validation of Candidate Genes Modulating ALK TKI Sensitivity in Resistant ALCL Cell Lines.....	81
3.4.4	Validation of Candidate Genes Modulating ALK TKI Sensitivity in a Resistant Orthotopic ALCL Cell Line Xenograft Model	81
3.4.5	Validation of Candidate Genes Modulating ALK TKI Sensitivity in ALCL Patients	82
3.5	DISCUSSION.....	86
CHAPTER 4 IL10RA MODULATES ALK TKI SENSITIVITY IN ALK+ ALCL.....		87
4.1	INTRODUCTION	88
4.1.1	Aims	89
4.2	IL10RA IS EXPRESSED IN ALCL IN AN NPM1-ALK-INDEPENDENT MANNER.....	89
4.3	IL10RA OVEREXPRESSION MODULATES SENSITIVITY TO ALK INHIBITION	92
4.4	KNOCKOUT OF IL10RA/IL10RB/IL10 FURTHER SENSITIZES ALCL CELLS TO ALK INHIBITION.....	97
4.5	STAT3 IS ACTIVATED INDEPENDENTLY OF NPM1-ALK THROUGH THE IL10/IL10R SIGNALING PATHWAY ON CRIZOTINIB INHIBITION	97
4.6	HIGH EXPRESSION OF IL10RA AT DIAGNOSIS IS NOT PREDICTIVE OF CLINICAL OUTCOME FOR PATIENTS TREATED WITH STANDARD CHEMOTHERAPY	101
4.7	DISCUSSION.....	103
CHAPTER 5 BRIGATINIB IS EFFECTIVE IN A PDX OF CRIZOTINIB-RESISTANT ALK+ ALCL		104
5.1	INTRODUCTION	105
5.1.1	Aims	106
5.2	PATIENT TREATMENT HISTORY AND SAMPLE COLLECTION.....	107
5.3	BRIGATINIB IS EFFECTIVE IN A PDX OF CRIZOTINIB-RESISTANT ALK+ ALCL	107

5.4	DISCUSSION.....	109
CHAPTER 6 OVEREXPRESSION OF PIM1 IN ALK+ MALIGNANCIES DECREASES		
SENSITIVITY TO BRIGATINIB AND CERITINIB..... 113		
6.1	INTRODUCTION.....	114
6.1.1	Aims.....	115
6.2	VALIDATION OF CANDIDATE RESISTANCE GENES IN ALK-DRIVEN NB CELLS EXPOSED TO ALK INHIBITORS IDENTIFIED IN A GENOME-WIDE CRISPR-CAS9 OVEREXPRESSION SCREEN	115
6.3	PIM1 INHIBITION ENHANCES THE SENSITIVITY OF HIGH-RISK ABERRANT ALK-EXPRESSING NB TO ALK INHIBITION REGARDLESS OF MYCN STATUS	117
6.3.1	High expression of PIM1 in NB is associated with advanced, high risk disease independent of MYCN amplification	117
6.3.2	Inhibition of PIM1 alone lacks potency in ALK-expressing NB but enhances the efficacy of ALK inhibitors.....	117
6.3.3	Knockdown of PIM1 sensitizes NB cells to ALK inhibitors	119
6.4	OVEREXPRESSION OF PIM1 IN ALK+ ALCL CELL LINES DECREASES SENSITIVITY TO ALK INHIBITORS.....	119
6.5	DISCUSSION.....	120
CHAPTER 7 DETECTION AND CLINICAL SIGNIFICANCE OF ANTI-ALK AUTOANTIBODIES. 122		
7.1	INTRODUCTION.....	123
7.1.1	Humoral Immune Response against ALK in ALK+ ALCL.....	123
7.1.2	Humoral Immune Response against ALK in ALK+ NSCLC	124
7.1.3	Aims.....	124
7.2	A PIPELINE TO QUANTIFY ALK AUTOANTIBODY TITRES IN ALK+ MALIGNANCIES	125
7.2.1	2D-Epoxy is the best slide activation chemistry for antigen binding.....	126
7.2.2	A reduced teflon mask increases the signal intensity.....	127
7.2.3	Evaluation of ALK and control proteins	127
7.2.4	Final slide layout	129
7.3	PROTEIN MICROARRAY ASSAY CROSS-VALIDATION.....	130
7.4	DISCUSSION.....	134
CHAPTER 8 DISCUSSION 135		
8.1	INTRODUCTION.....	136
8.2	THE USE OF ALK INHIBITORS FOR THE TREATMENT OF PAEDIATRIC ALK+ ALCL.....	136
8.2.1	Crizotinib in combination with multi-agent chemotherapy could be used as a consolidation therapy before allogenic SCT for paediatric ALK+ ALCL patients after relapse ..	136
8.2.2	Brigatinib could offer a bridge to transplant for paediatric ALK+ ALCL patients after CNS relapse.....	137
8.3	THE USE OF ALK INHIBITORS FOR THE TREATMENT OF ALK-DRIVEN NB.....	137
8.4	A COLLABORATIVE APPROACH TO COLLATE AND INTEGRATE DATA WILL BE CRUCIAL TO MAKING PROGRESS IN THE TREATMENT OF PAEDIATRIC CANCERS	138

CHAPTER 9	APPENDIX	139
9.1	APPENDIX 1: LIST OF PEER-REVIEWED PAPERS AND REVIEWS	140
9.1.1	Primary research articles	140
9.1.2	Review article.....	140
REFERENCE LIST		141

List of Figures

Figure 1	Domain structure and aberrant forms of Anaplastic Lymphoma Kinase (ALK)	2
Figure 2	Different categories of ALK+ malignancies	3
Figure 3	Management of childhood ALCL.....	17
Figure 4	ALK in NB.....	20
Figure 5	ALK-dependent or ALK-independent resistance mechanisms in ALK+ NSCLC	23
Figure 6	Types of in vitro experimental designs to identify putative TKI resistance mechanisms	27
Figure 7	Technologies to perturb gene function in mammalian cells for pooled genetic screens	28
Figure 8	The genome-scale Cas9 transcriptional activation screen employed to identify bypass resistance mechanisms to ALK TKIs.....	58
Figure 9	The genome-scale Cas9 knockout screen employed to identify bypass resistance mechanisms to ALK TKIs	62
Figure 10	ABCB1 overexpression induces resistance to crizotinib	74
Figure 11	The dCas9-VP64-based CRISPR activation system induces overexpression of various genes in different ALCL cell lines	74
Figure 12	CRISPR Overexpression Screens Identify Genes Modulating Crizotinib Sensitivity in ALCL Cell Lines.....	75
Figure 13	CRISPR Overexpression Screens Identified STAT3 and NPM1 to Modulate Crizotinib Sensitivity in ALCL Cell Lines.....	76
Figure 14	Overexpression of candidate genes identified from the SAM screen induce resistance to crizotinib	78
Figure 15	Overexpression-based validation of candidate genes.....	78
Figure 16	CRISPR knockout screen dataset by Ng et al. identifies MYC and RORC as vulnerabilities in ALK+ and ALK- ALCL.....	79
Figure 17	Knockout-based analysis	80
Figure 18	Hit validation in resistant ALCL cell lines	81
Figure 19	Hit validation in a resistant orthotopic ALCL cell line xenograft model.....	82
Figure 20	Validation of Candidate Genes Modulating ALK TKI Sensitivity in ALCL Patients	84
Figure 21	Schematic of the IL10 signalling pathway	88
Figure 22	IL10RA is Expressed in ALCL Patient Tumour Tissue	90
Figure 23	IL10 signaling is represented in ALCL cell lines	91
Figure 24	Transcription of IL10RA is independent of NPM1-ALK expression and activity.....	92
Figure 25	IL10RA Overexpression Modulates Sensitivity to ALK Inhibition	94
Figure 26	IL10 Overexpression does not Modulate Sensitivity to ALK Inhibition	96
Figure 27	Plasmid-based IL10RA Overexpression Modulates Sensitivity to Crizotinib Inhibition ...	96
Figure 28	CRISPR-based knockout of IL10RA/IL10RB/IL10 is not lethal, but sensitizes ALCL cell lines to ALK inhibition	98

Figure 29	STAT3 is Activated Independently of NPM1-ALK through the IL10/IL10R Signaling Pathway on Crizotinib Inhibition	101
Figure 30	Initial High Expression of IL10RA is not Predictive of Clinical Outcome for Patients Treated with Chemotherapy.....	102
Figure 31	Established cell lines maintain crizotinib responsiveness of the original tumour	108
Figure 32	Tumour volume over time in MGS-A-x PDX mice	110
Figure 33	Brigatinib is effective in the treatment of a PDX of crizotinib-resistant ALK+ ALCL	111
Figure 34	Validation of CRISPR dCas9 overexpression screen hits in SH-SY5Y and CHLA-20 cells	116
Figure 35	High expression of PIM1 in NB is associated with advanced, high risk disease independent of MYCN amplification	117
Figure 36	Response of ALK+ and ALK- NB cell lines to PIM inhibition	118
Figure 37	ALK inhibitors and AZD1208 exhibit mild synergism in KELLY cell lines.....	118
Figure 38	Knockdown of PIM1 sensitizes NB cells to ALK inhibitors	119
Figure 39	Overexpression of PIM1 in ALK+ ALCL cell lines decreases sensitivity to ALK inhibitors	120
Figure 40	Production, quality control (QC) and processing of microarray slides.....	125
Figure 41	Effect of slide activation chemistry	126
Figure 42	Effect of the Teflon mask	127
Figure 43	Antigens utilized in the microarray assay	128
Figure 44	A typical slide layout	129
Figure 45	Correlation between anti-ALK autoantibody titre and anti-ALK autoantibody concentration levels in paediatric ALK-positive ALCL patients enrolled in the ALCL-99 trial	131
Figure 46	Outcomes of paediatric ALK+ ALCL patients according to the magnitude of the antibody response to ALK	132
Figure 47	Outcomes of paediatric ALK+ ALCL patients according to the magnitude of the antibody response against ALK in combination with their minimal disseminated disease (MDD) status	133

List of Tables

Table 1	ALK+ NSCLC inhibitor landscape	4
Table 2	Definition of clinical terms in NHL	6
Table 3	Treatment outcomes for paediatric patients with ALCL after frontline multi-agent chemotherapy with or without methotrexate (MTX) or vinblastine (VBL)	7
Table 4	Treatment strategies for childhood ALCL	8
Table 5	Past, ongoing and planned clinical trials for paediatric ALCL	10
Table 6	Factors used for stratification of paediatric ALK+ ALCL patients into different risk groups	11
Table 7	Clinical trials evaluating ALK inhibitors in NB	21
Table 8	Sensitizing (S) and resistance (R) mutations to ALK inhibitors	24
Table 9	Previously published CRISPRn screens on drug resistance using GeCKO A v2 and B libraries	29
Table 10	Previously published CRISPRa screens on drug resistance	30
Table 11	Key Reagents and Resources	32
Table 12	Clinical trials from which samples have been acquired	40
Table 13	Clinical Information of Paediatric ALCL Patients Recruited onto the NHL-BFM90 Trial	41
Table 14	Clinical Information of Paediatric ALCL Patients Recruited onto the NHL-BFM95 Trial	42
Table 15	Clinical Information of Paediatric ALCL Patients Recruited onto the ALCL99 Trial that provided FFPE tissue specimens	43
Table 16	Clinical Information of the Paediatric ALCL Patient from the UK Cohort	44
Table 17	Clinical Information of Paediatric ALCL Patients Recruited onto the MAPPYACTS Trial	44
Table 18	Clinical Information of T-cell Lymphoma Patients from the Brno Cohort	45
Table 19	Clinical Information of T-cell Lymphoma Patients from the Pakistan Cohort	46
Table 20	Clinical Information of T-cell Lymphoma Patients from the Vienna Cohort	47
Table 21	Starting and final TKI concentrations used to generate TKI resistant ALCL cell lines	52
Table 22	PCR Using Q5 High-Fidelity DNA Polymerase	52
Table 23	PCR cycle conditions used to amplify the NPM1-ALK kinase domain region	52
Table 24	RT-qPCR primers	53
Table 25	List of antibodies used to detect proteins by Western blot	54
Table 26	Oligonucleotides used to generate dsDNA fragments containing the 20 bp target sequence	55
Table 27	Phosphorylation and annealing of single-stranded sgRNA oligonucleotides	57
Table 28	Golden Gate assembly	57
Table 29	PCR cycle conditions used for Golden Gate assembly	57
Table 30	Antibiotic concentrations that were used for the selection of the transduced cell lines	59
Table 31	PCR amplification of virally integrated guides	60
Table 32	Oligonucleotides used for HiSeq library preparation	61

Table 33	PCR cycle conditions used to amplify the sgRNAs' guide sequence region and to append the Illumina (HiSeq) compatible adapters and barcodes	61
Table 34	sgRNAs cloned for the CRISPR Mini Knockout Screen	63
Table 35	Oligonucleotides used for HiSeq library preparation	65
Table 36	Oligonucleotides used to generate dsDNA fragments containing the target shRNA sequence that were cloned into pLKO.1-puro.....	66
Table 37	Antibodies used to detect proteins by IHC.....	67
Table 38	ChIP-qPCR Sequencing Primers	68
Table 39	Candidate genes and their relevance in ALCL and other cancers	77
Table 40	Baseline characteristics of Paediatric ALCL Patients Recruited to the ALCL99 Trial	130

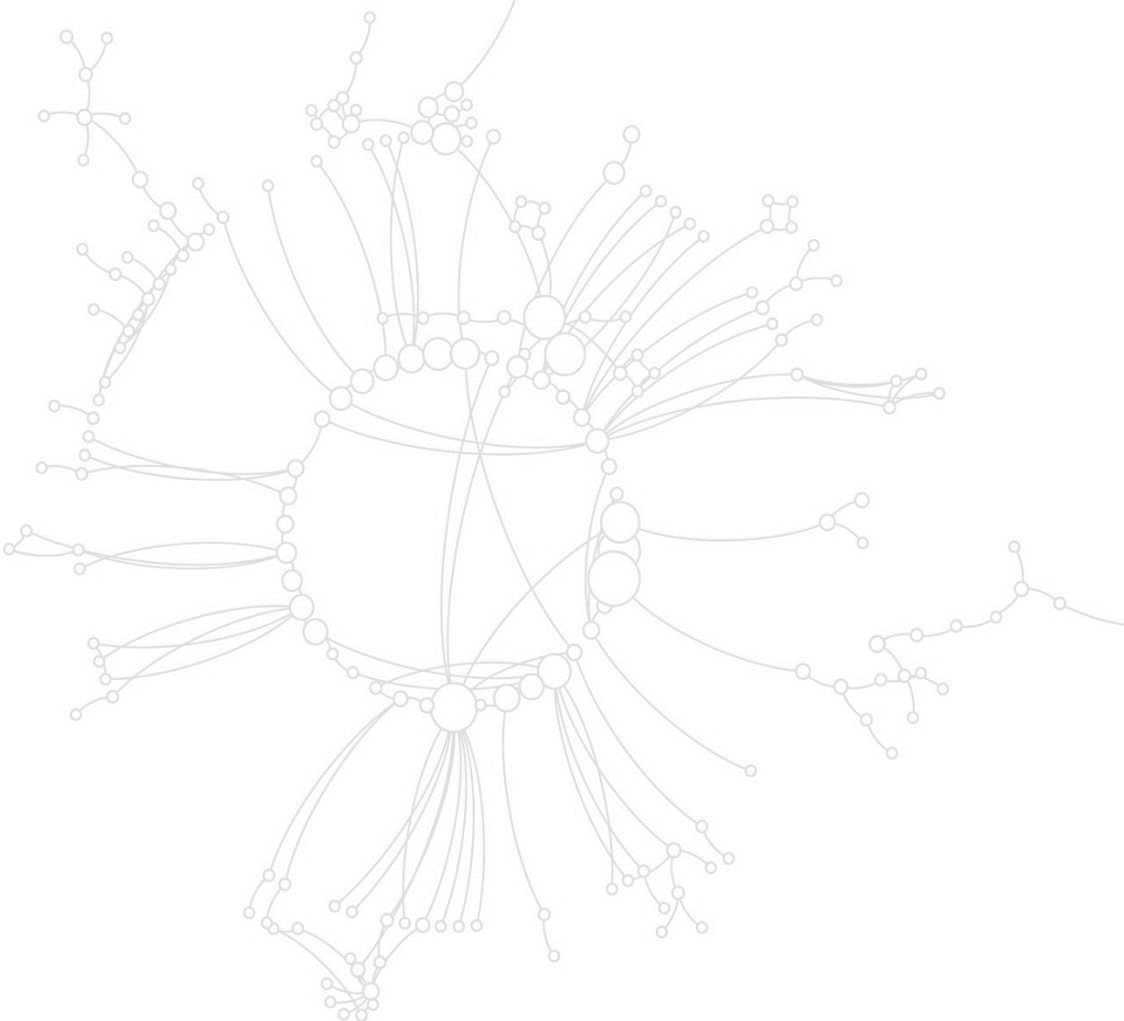
Abbreviations

AITL	Angioimmunoblastic T-cell lymphoma
ALCL	Anaplastic large cell lymphoma
ALK	Anaplastic lymphoma kinase
ANOVA	Analysis of variance
ATC	Anaplastic thyroid cancer
b.i.d.	bis in die (lat), twice a day
BSA	Bovine serum albumin
BV	Brentuximab vedotin
CAS9	CRISPR-associated protein 9
CNS	Central Nervous System
COG	Children's Oncology Group
CR	Complete response
CRISPR	Clustered regularly interspaced short palindromic repeats
CRISPRa	CRISPR activation
CRISPRi	CRISPR interference
CRISPRn	CRISPR nuclease
DLBCL	Diffuse large B cell lymphoma
dCAS9	Dead Cas9
ECACC	European collection of authenticated cell cultures
ED50	Median effective dose
EDTA	Ethylenediaminetetraacetic acid
EFS	Event-free survival
EICNHL	European Inter-group for Childhood Non-Hodgkin Lymphoma
EML4	Echinoderm microtubule-associated protein-like 4
ESCC	Oesophageal squamous cell carcinoma
FBS	Fetal bovine serum
gDNA	Genomic DNA
GeCKO	Genome-Scale CRISPR Knock-Out
GOF	Gain-of-function
GSEA	Gene set enrichment analysis
HL	Hodgkin Lymphoma
HR	Hazard ratio
HSF1	Heat shock transcription factor 1
ICE	Ifosfamide, carboplatin and etoposide
IHC	Immunohistochemistry
IMT	Inflammatory myofibroblastic tumour
InDels	Insertions or deletions

IRC	Independent review committee
ITCC	Innovative Therapies for Children with Cancer
JAK-STAT	Janus kinase-signal transducer and activator of transcription
JUN	Jun proto-oncogene
KO	Knockout
KRAB	Krüppel-associated box
LB	Lysogeny broth
LOF	Loss-of-function
MAGeCK	Model-based analysis of genome-wide CRISPR/Cas9 knockout
MAPPYACTS	Molecular Profiling for Pediatric and Young Adult Cancer Treatment Stratification
MDD	Minimal disseminated disease
MLE	Maximum likelihood estimation
MOI	Multiplicity of Infection
MRD	Minimal residual disease
MTX	Methotrexate
NB	Neuroblastoma
NCBI	National Center for Biotechnology Information
NHEJ	Non-homologous end joining
NHL	Non-Hodgkin Lymphoma
NHL-BFM	Non-Hodgkin Lymphoma-Berlin-Frankfurt-Münster
NMD	Non-sense-mediated decay
NPM	Nucleophosmin
NSCLC	Non-small cell lung cancer
NT	Non-targeting
ORF	Open reading frame
ORR	Overall response rate
OS	Overall survival
PAM	Photospacer adjacent motif
PBS	Phosphate-buffered saline
PCA	Principle component analysis
PD	Progressive Disease
PD-L1	Programmed death-ligand 1
PDX	Patient-derived xenograft
PFS	Progression-Free Survival
PI	Propidium iodide
PR	Partial Response
PTC	Premature termination codon
PTCL-NOS	Peripheral T-cell lymphoma not otherwise specified
QC	Quality control
RCC	Renal cell carcinoma

RIPA	Radioimmunoprecipitation assay
RMC	Renal medulla carcinoma
RNAi	RNA interference
RTK	Receptor tyrosine kinase
SAM	Synergistic activation mediator
SCT	Stem Cell Transplantation
SD	Standard deviation
SFOP	French Society for Paediatric oncology
sgRNA	Single guide RNA
shRNA	short-hairpin RNA
SOC	Serous ovarian carcinoma
TAE	Tris-acetate-EDTA
TKI	Tyrosine kinase inhibitor
tracrRNA	trans-activating CRISPR RNA
TSS	Transcription start site
VBL	Vinblastine
WES	Whole exome sequencing
WGS	Whole genome sequencing
WT	Wild type

CHAPTER 1 Introduction



1.1 Anaplastic lymphoma kinase (ALK) in the pathogenesis of cancer

The *ALK* gene encodes a receptor tyrosine kinase (RTK), which consists of an intracellular tyrosine kinase domain, a trans-membrane domain and an extracellular ligand-binding domain² (**Figure 1A-B**). As a gene first discovered from the investigation of the t(2;5) chromosomal translocation, generating nucleophosmin (NPM)-ALK, in anaplastic large cell lymphoma (ALCL)³ (**Figure 1B**), ALK has been thoroughly investigated for its oncogenic capacity².

ALK regulates cellular proliferation, apoptosis and differentiation by activation of multiple pathways⁴, including rat sarcoma (RAS)/mitogen-activated protein kinase (MAPK), phosphoinositide 3-kinase (PI3K)/AKT/molecular target of rapamycin (mTOR), Janus kinase (JAK)-signal transducer and activator of transcription (STAT), phospholipase C γ (PLC γ), sonic hedgehog (SHH) and jun proto-oncogene (JUN)¹⁻⁵ (**Figure 1C**).

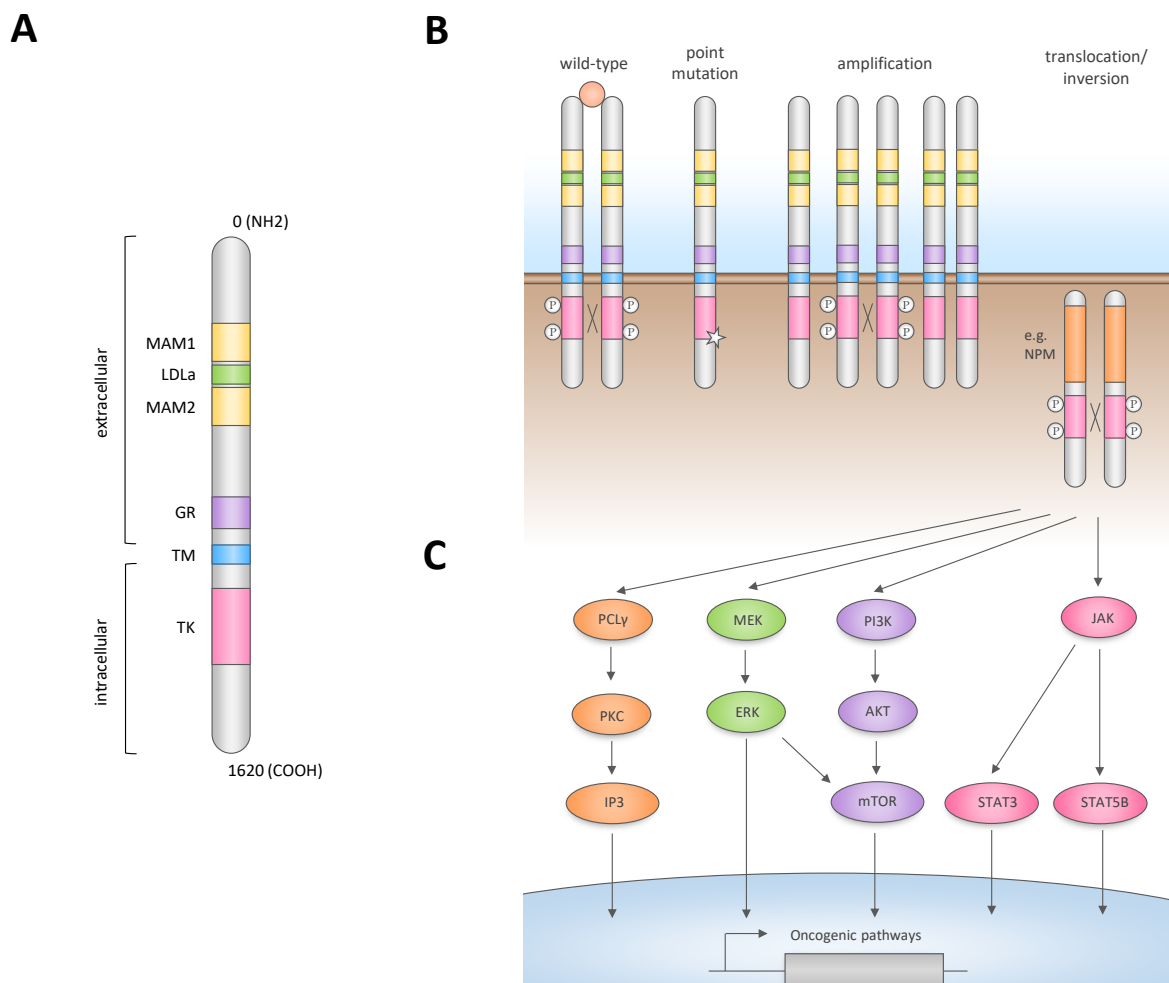


Figure 1 Domain structure and aberrant forms of Anaplastic Lymphoma Kinase (ALK)

(A) The N-terminal extracellular domain comprises two MAM domains flanked by a low-density lipoprotein class A (LDLa) domain, and a glycine-rich (GR) domain. The C-terminal intracellular region comprises the tyrosine kinase (TK) domain. **(B)** In the wild-type receptor, ligand-induced dimerisation of the extracellular region permits auto- and transphosphorylation of the kinase domain and subsequent recruitment of signal transducers. Aberrant forms of ALK expressed in cancer are ligand-independent due to point mutations in the kinase domain, gene amplification, or gene fusion. **(C)** NPM1-ALK signals through the PLC γ /PKC, MEK/ERK, PI3K/AKT and JAK/STAT pathways. Modified from Trigg et al.⁶.

Thus, ALK has been implicated in the pathogenesis of many types of cancers that can be categorized by the specific types of alteration (**Figure 2**): translocations, overexpression and point mutations of ALK² (**Figure 1B**).

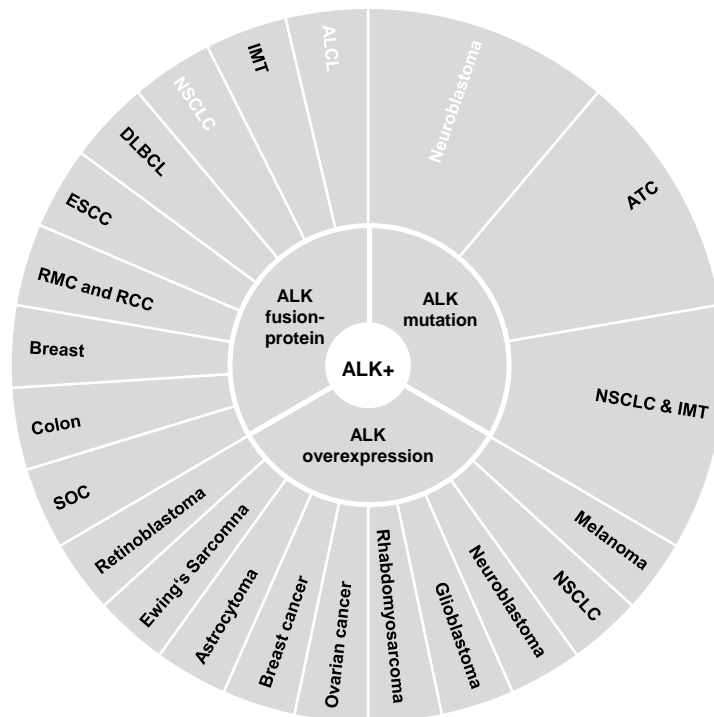


Figure 2 Different categories of ALK+ malignancies

ALK-related malignancies that are studied in this thesis are highlighted in white. DLBCL: diffuse large B cell lymphoma; ATC: anaplastic thyroid cancer; ESCC: oesophageal squamous cell carcinoma; IMT: inflammatory myofibroblastic tumour; RCC: renal cell carcinoma; RMC: renal medulla carcinoma; SOC: serous ovarian carcinoma.

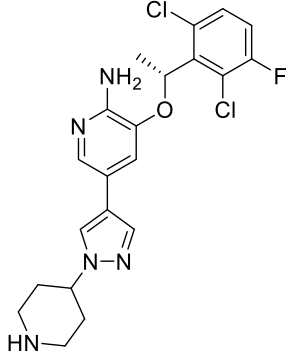
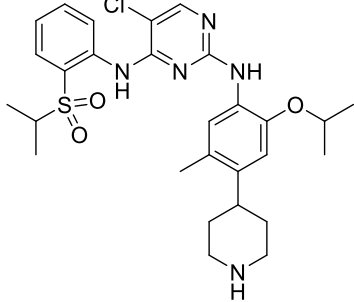
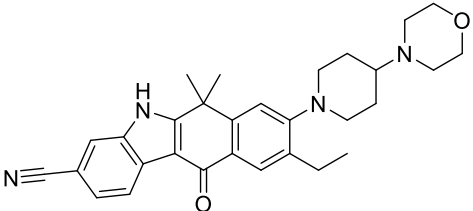
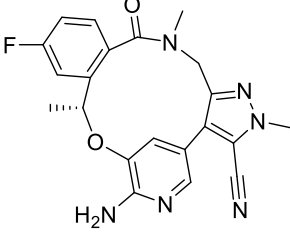
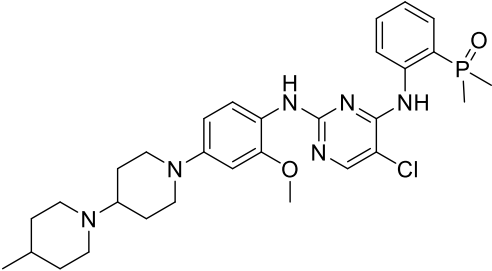
Overexpression of ALK and amplification of the *ALK* gene have been reported in various types of cancer cell lines and patient samples, including inflammatory myofibroblastic tumour (IMT)⁷, neuroblastoma (NB)⁸, melanoma⁹, non-small cell lung cancer (NSCLC)¹⁰, rhabdomyosarcoma, glioblastoma², breast cancer¹¹, oesophageal cancer¹², retinoblastoma, Ewing's sarcoma and astrocytoma².

Point mutations and focal deletion of *ALK*, without translocation, have been identified in relatively limited types of cancer to date including anaplastic thyroid cancer¹³, NSCLC¹⁴, and in both familial¹⁵ and sporadic NB¹⁶ (**Figure 4**).

In contrast, ALK is frequently translocated in human cancers with twenty-two fusion partner genes¹⁷ including Nucleophosmin 1 (*NPM1*)³, ring finger protein 213 (*RNF213*), 5-aminoimidazole-4-carboxamide ribonucleotide formyltransferase/IMP cyclohydrolase (*ATIC*), TRK-fused gene (*TFG*), moesin (*MSN*), tropomyosin 3/4 (*TPM3/4*), myosin heavy chain 9 (*MYH9*) and clathrin heavy chain (*CLTC*)² in ALCL, and echninoderm microtubule-associated protein-like 4 (*EML4*)¹⁸, Kif5b kinesin family member 5B (*KIF5B*), TRK-fused gene (*TFG*), Kinesin light chain 1 (*KLC1*), protein tyrosine phosphatase non-receptor type 3 (*PTPN3*) and striatin (*STRN*) in NSCLC². To add to the complexity, within the different ALK fusions there are examples of several breakpoint variants, as illustrated by the EML4–ALK translocations observed in NSCLC, by which multiple EML4 exon breakpoints fuse in-frame with exon 20 of ALK¹⁹. Comparisons of the different ALK fusion proteins suggest that they display differences in

signalling and in transforming tumourigenic potential¹⁷. The fusion partner of ALK generally determines the initiation of transcription, subcellular localization, dimerization, activation² and therefore the molecular and physiological function of ALK. Several pharmaceutical companies have developed potent ALK inhibitors (**Table 1**).

Table 1 ALK+ NSCLC inhibitor landscape

Name	Chemical structure	Company	Global Status
Crizotinib		Pfizer	FDA approval for advanced NSCLC whose tumours are ALK+ (26/08/2011) or ROS1+ (11/03/2016)
Ceritinib		Novartis	FDA approval (29/04/2014) for advanced ALK-rearranged NSCLC patients who experience disease progression on or who are intolerant to crizotinib. FDA broadens ceritinib approval to firstline treatment for ALK+ metastatic NSCLC (30/05/2017).
Alectinib		Hoffmann-La Roche	FDA approval (11/12/2015) EU approval (21/02/2017) for advanced NSCLC whose tumours are ALK+.
Lorlatinib		Pfizer	FDA approval (02/11/2018) for patients with ALK+ metastatic NSCLC whose disease has progressed on crizotinib and at least one other ALK inhibitor for metastatic disease or whose disease has progressed on alectinib or ceritinib as the first ALK inhibitor therapy for metastatic disease
Brigatinib		Takeda	FDA approval (28/04/2017) for ALK+ metastatic NSCLC patients who have progressed on or are intolerant to crizotinib and lorlatinib.

The following paragraphs largely from sections of a review published in *Cancers* (Prokoph & Larose et al.)²⁰, which can be found in Appendix 1.

1.2 ALK+ ALCL

1.2.1 Clinical Features of Paediatric ALCL

In 1982, Stein and colleagues¹⁹ described tumours formed of neoplastic cells of unknown origin found in Hodgkin's Lymphoma (HL), expressing the CD30 antigen (Ki-1, Ber-H2)²¹⁻²². Approximately 77% of these tumours also expressed a T cell antigen, 20% showed B cell antigens and the rest were of a null-cell phenotype expressing neither B nor T cell-distinguishing cell surface proteins. In 1988, the entity was for the first time described as ALCL, which is the name used to this day²³. In 1989, a French group identified a translocation (t(2;5)(p23;q35)) in a subset of ALCL²⁴⁻²⁵, breakpoints of which were successfully cloned by Steve Morris and Tom Look in 1994, revealing the fusion of the nucleolar phosphoprotein gene *NPM1* with that of a newly described gene, *ALK*³. However, it was not until 2008 that ALCL was split into two provisional entities; ALK+ ALCL and ALK- ALCL, which were confirmed in the 2017 version of the WHO classification of tumours of haemopoietic and lymphoid tissues.

ALCL is primarily a paediatric tumour, accounting for 15% of all paediatric Non-Hodgkin Lymphoma (NHL) with an annual incidence ranging from 1.2 per million in children under 15 years to approximately 2 per million in young adults between 25-34 years²⁶, with approximately 80 new paediatric cases diagnosed in Europe each year²⁷. ALCL shows a bimodal age distribution; whilst the majority of paediatric cases are ALK+, about 50-60% of adult ALCL cases are ALK-. It is estimated that 90% of paediatric ALCL show aberrant expression of ALK fusion proteins and of those, approximately 75% express NPM-ALK²⁸. ALK+ ALCL cases show improved survival rates over ALK- ones, although this could be due to the skewed age distribution with ALK- disease largely diagnosed in an adult population²⁹. However, considering only paediatric cases, overall survival (OS) rates (see **Table 2** for clinical terms) are still higher for ALK+ paediatric patients than for ALK- ones, with an event-free survival (EFS) of 65-75% for ALK+ ALCL depending on the treatment regimen compared to 15-46% for ALK- ALCL³⁰⁻³³.

Table 2 Definition of clinical terms in NHL

The first received response criteria for NHL were published in 1999³⁴, updated in 2007³⁵ by an International Working Group and 2013³⁶ termed as the Lugano Classification. The definition of response criteria in this table is based on the Lugano Classification³⁶ and the refinement of the Lugano classification in the era of immunotherapy³⁷. (*) 5-point scale according to Lugano Classification³⁶: 1, no uptake above background; 2, uptake \leq mediastinum; 3, uptake $>$ mediastinum but \leq liver; 4, uptake $>$ liver; 5, uptake markedly $>$ liver and/or new lesions.

Clinical term	Definition
Overall survival (OS)	The length of time from either the date of diagnosis or the start of cancer treatment that a patient is still alive ³⁸ .
Event-free survival (EFS)	The length of time after primary cancer treatment ends that the patient remains free of complications/events that the treatment was intended to prevent/delay ³⁸ .
Progression-free survival (PFS)	The length of time during and after cancer treatment that a patient lives with the disease but it does not get worse ³⁸ .
Complete Response (CR), Complete Remission (CR)	A complete metabolic response measured by positron emission tomography-computed tomography (PET-CT) or a complete radiological response measured by CT ³⁶ . Lymph nodes: on PET-CT, score 1, 2, or 3 with/without a residual mass on 5-point scale*; on CT, target nodes/nodal masses must regress to ≤ 1.5 cm in longest diameter ³⁷ . No bone marrow involvement or extralymphatic sites involved ³⁶ .
Partial Response (PR), Partial Remission (PR)	A partial metabolic response measured by positron PET-CT or a complete radiological response measured by CT ³⁶ . On PET-CT score 4 or 5 with reduced uptake compared with baseline and residual mass(es) of any size. On CT $\geq 50\%$ decrease in SPD (sum of the product of the perpendicular diameters for multiple lesions) of up to 6 target measurable nodes and extranodal sites ³⁶⁻³⁷ .
Progressive Disease (PD)	A progressive metabolic disease measured by positron PET-CT or a progressive disease measured by CT ³⁶ . On PET-CT, score 4 or 5 with an increase in intensity of uptake from baseline and/or new fluorodeoxyglucose-avid foci consistent with lymphoma at preliminary or end-of-treatment assessment ³⁷ . On CT, an individual node/lesion must be abnormal with: longest diameter > 1.5 cm and increase by $\geq 50\%$ from product of the perpendicular diameters lowest point and an increase in longest diameter or short diameter from the lowest point (0.5 cm for lesions ≤ 2 cm / 1.0 cm for lesions > 2 cm) ³⁷ . New/clear progression of preexisting nonmeasured lesions or regrowth of resolved lesions ³⁷ . A new node > 1.5 cm or a new extranodal site > 1.0 cm (both in any axis) or < 1.0 cm in any axis or assessable disease of any size that must be unequivocal attributable to lymphoma ³⁷ . New/recurrent bone marrow involvement ³⁷ .
Stable Disease (SD)	No metabolic disease measured by positron PET-CT or a stable disease measured by CT ³⁶ . Target nodes, extranodal lesions: on PET-CT, score 4 or 5 with no significant change in fluorodeoxyglucose uptake from baseline at interim or end of treatment; on CT: $< 50\%$ decrease from baseline in SPD (sum of the product of the perpendicular diameters for multiple lesions) of up to 6 measurable nodes and extranodal sites ³⁶ .
Allogenic SCT	Stem cell transplantation that uses stem cells from a donor whose human leukocyte antigens (HLA) are acceptable matches to the patient's.
Autologous SCT	Stem cell transplantation that uses a person's own stem cells.
Intrathecal injection	A route of administration for drugs via an injection into the spinal canal, or into the subarachnoid space so that it reaches the cerebrospinal fluid (CSF). This way the drug is not stopped by the blood brain barrier ³⁸ .
Minimal disseminated disease (MDD)	Detection of NPM-ALK transcript via e.g. RT-qPCR in bone marrow or peripheral blood samples from an ALK+ ALCL patient at diagnosis ³⁹ .
Recommended phase II dose (RP2D)	Identified in phase I clinical trials, the RP2D is defined as the highest dose with acceptable toxicity ⁴⁰ .
Reduced Intensity Conditioning (RIC)	RIC conditioning as tested by Fukano et al. ⁴¹ in ALK+ ALCL is composed of (i) total body irradiation of ≤ 500 cGy as a single fraction or ≤ 800 cGy fractionated, (ii) < 9 mg/kg of busulfan, (iii) ≤ 140 mg/m ² melphalan, (vi) < 10 mg/kg thiotepa.
BEAM conditioning	Carmustine [bis-chloroethylnitrosourea=BCNU]-etoposide-cytarabine [Ara-C]-melphalan

1.2.2 Frontline Treatment for Paediatric ALCL

Fortunately, paediatric ALCL patients are relatively chemo-sensitive with high response rates to diverse chemotherapy regimens as proven by various studies; EFS and OS vary between 65-75% and 70-90% respectively independent of treatment duration, drugs used or their dosages (**Table 3**)^{31–33,42–44}.

Given that ALCL was not recognised as a distinct form of NHL until 1989, most patients prior to this time would have been treated as B or T-cell NHL. The NHL-Berlin-Frankfurt-Münster (NHL-BFM) working group enrolled paediatric patients with B or T-cell NHL in three different trials (NHL-BFM83, NHL-BFM86, NHL-BFM90)^{33,45–46}. Though the trials were not primarily aimed at ALCL, a retrospective paper found that the protocols used led to an 83% 9-year EFS, and an 9-year OS of 81% for CD30-positive ALCL patients⁴⁶.

Table 3 Treatment outcomes for paediatric patients with ALCL after frontline multi-agent chemotherapy with or without methotrexate (MTX) or vinblastine (VBL)
Intermediate dose MTX high-dose cytarabine (IDM-HiDAC), not applicable (N/A). Reproduced from Prokoph & Larose et al.²⁰.

	Study Designation	Paediatric patients	Treatment duration (months)	EFS (-year)	OS (-year)	Grade 3/4 toxicity
Multi-agent chemotherapy +/- MTX	NHL-BFM83, 86 ⁴⁶	62	2-5	81% (9)	83% (9)	N/A
	HM89 ³¹	82	8	66% (3)	83% (3)	N/A
	UKCCSG-B-NHL-9001, 9002/9602, 9003 ⁴⁴	72	N/A	59% (5)	65% (5)	One toxic death
	POG9315 (APO arm) ⁴²	85	11	71% (5)	88% (4)	neutropenia/thrombocytopenia (35%)
	POG9315 (IDM-HiDAC arm) ⁴²	90	11	71% (4)	88% (4)	neutropenia/thrombocytopenia (70%)
	CCG-5941 ⁴³	86	11	68% (5)	80% (5)	neutropenia (82%), thrombocytopenia (66%), anemia (38%)
	LNH-92 ⁴⁷	55	11	69% (5)	74% (5)	neutropenia, hepatic events
	NHL-BFM90 (K1 arm) ³³	9	2-3	100% (5)	N/A	N/A
	NHL-BFM90 (K2 arm) ³³	65	2-3	73% (5)	N/A	N/A
	NHL-BFM90 (K3 arm) ³³	14	4-5	76% (5)	N/A	N/A
	EICNHL-ALCL99 (MTX1-arm) ²⁸	175	4-5	74% (2)	90% (2)	hematologic toxicity (79%), infection (50%), stomatitis (21%)
	EICNHL-ALCL99 (MTX3-arm) ²⁸	177	4-5	75% (2)	95% (2)	hematologic toxicity (64%), infection (32%), stomatitis (6%)
	HM91 ³¹	82	7	66% (3)	83% (3)	N/A
Multi-agent chemotherapy + VBL	EICNHL-ALCL99-VBL ³¹	110	17-18	70% (2)	94% (2)	neutropenia (29%)
	ANHL0131 (APO arm) ⁴⁸	64	12	74% (3)	84% (3)	neutropenia (39%), infections (22%)
	ANHL0131 (APV arm) ⁴⁸	61	12	79% (3)	86% (3)	neutropenia (84%), infections (43%)

NHL-BFM90 was the first trial to sort 89 paediatric ALCL patients into independent arms of the study (**Table 3**), although presence of the ALK translocation was not used as inclusion criteria for this trial³³. The treatment protocol (**Table 4**) was based on the previous NHL-BFM studies, using retrospective results of ALCL patients enrolled in these studies. ALCL patients were enrolled into one of three arms according to disease severity: arm K1 for stages I and II if completely resected (9 patients), K2 for stage II non-resected and stage III (65 patients), and K3 for stage IV (14 patients). Because CD30-positive ALCL resembled B-cell NHL closely, the first protocol trialled was that used for B-cell NHL, which used methotrexate. Thus, the arms K1 to K3 tested increasing doses of methotrexate. NHL-BFM90 led to a 5-year EFS of 100%, 73% and 79% respectively for arms K1, K2 and K3. The treatment regimen lasted between 2 to 5 months compared to 7 or 8 months respectively for HM89 and HM91 (**Table 4**), which are both protocols that were tested by the French Society for Paediatric oncology (SFOP) at that time. As a result, and because the drug doses were comparatively lower – all with comparable EFS rates – the NHL-BFM working group recommended its NHL-BFM90 protocol as a gold standard^{31,33,49-50}.

Table 4 Treatment strategies for childhood ALCL

Treatment strategies for childhood ALCL. ARA-C, cytarabine; BV, Brentuximab vedotin; Cyc, cyclophosphamide; CZ, crizotinib; Daun, daunorubicin; Doxo, doxorubicin; Eto, etoposide; IDM-HiDAC, intermediate dose MTX high-dose Cytarabine; Ifo, ifosfamide; I/T, intrathecal; IV, Intravenous; MTX, methotrexate; TT, topotecan; VBL, vinblastine; VCR, vincristine; VND, Vindesine. Not detailed: prednisone, prednisolone, dexamethasone and food supplements. (*) Randomized into MTX1 or MTX3 arm. Reproduced from Prokoph & Larose et al.²⁰.

Trial Acronym	Other	Cyc	Ifo	Doxo	Eto	MTX (I/T)	MTX (IV)	ARA-C (IV)	ARA-C (I/T)	VCR	VND	VBL
HM89 ³¹												
HM91 ³¹												
NHL-BFM90 (K1/2 arm) ³³												
NHL-BFM90 (K3 arm) ³³												
POG9315 (APO arm) ⁴²												
POG9315 (IDM-HiDAC arm) ⁴²												
CCG-5941 ⁴³												
LNH-92 ⁴⁷	+Daun											
NHL-BFM95 (R1/2) ⁵¹												
NHL-BFM95 (R3/4) ⁵¹												
EICNHL-ALCL99 (MTX1-arm) ²⁸												
EICNHL-ALCL99 (MTX3-arm) ²⁸												
EICNHL-ALCL99-VBL ⁵²						*						
ANHL0131 (APO arm) ⁴⁸												
ANHL0131 (APV arm)												
COG-ADVL1212 (Course A/C/D)	+CZ +TT											
COG-ADVL1212 (Course B)	+CZ											
COG-ANHL12P1 (Course A)	+CZ/BV											
COG-ANHL12P1 (Course B)	+CZ/BV											

Given the high risk of short-term side effects associated with methotrexate such as oral and gastrointestinal mucositis, sometimes leading to sepsis and toxic death⁵¹, lower concentrations of methotrexate administered in shorter pulses were applied in a subsequent NHL-BFM trial in 1995 (NHL-BFM 95, **Table 4**). NHL-BFM95 stratified patients into lower risk (stages I and II, arms R1 and R2) and high-risk patients (stages III and IV, arms R3 and R4). Patients in arms R1/R2 and R3/R4 were treated with 1 g/m² and 5 g/m² methotrexate infusions respectively. In both cases, half the patients were randomized to be given the infusion over 4 hours, while the other half were given the infusion over 24 hours. The trial found that the 4-hour infusion and the 1 g/m² dose were not inferior but were less toxic than the 24-hour infusion and 5 g/m² injection.

The European Inter-group for Childhood Non-Hodgkin Lymphoma (EICNHL) launched the first randomized trial for ALCL patients under 22 years of age (**Table 5**), regardless of ALK status in 1999 – the ALCL99 trial (NCT00006455)^{28,53-54}. ALCL99 enrolled 352 children over 7 years in 11 European countries and Japan. The trial tested four different protocols aiming to achieve three main goals: to lower the amount of methotrexate required, to rid the protocol of intrathecal injections and to test whether vinblastine could be a valuable addition to the protocol. Patients were randomly enrolled into arms methotrexate (MTX)1 and MTX3, which tested the NHL-BFM90 backbone with a 24-hour low-dose (1 g/m²) methotrexate infusion or a high-dose (3 g/m²) 3-hour methotrexate infusion (both without intrathecal injections) respectively. The trial achieved a 2-year EFS of 74.1% and a 2-year OS of 92.5%, and found that the MTX3 arm using a higher dose, but a shorter infusion time for methotrexate was overall less toxic than the MTX1 arm^{28,30-33,55}. Thus, the investigators recommended using short-pulse, high-dose methotrexate without intrathecal injections for reduced toxicity and improved quality of life. In addition, given the comparatively lower dose of anthracycline and alkylating agent employed, it was hoped that the long-term side-effects such as obesity and metabolic syndrome would be reduced^{28,55-56}. Besides the observed short-term toxicity, relapse compared to previous trials (HM89, HM91, NHL-BFM83, NHL-BFM86, and NHL-BFM90) averaging at 20-40% with some children experiencing multiple events²⁸. Whilst these children tend to remain chemo-sensitive, they still suffer the long-term side effects of toxic chemotherapy⁵⁵.

Table 5 Past, ongoing and planned clinical trials for paediatric ALCL

Allo, allogeneic; AC, alectinib; auto, autologous; BV, Brentuximab vedotin; CR, ceritinib; CZ, crizotinib; Cyc, cyclophosphamide; ARA-C, cytarabine; Dexa, Dexamethasone; Doxo, doxorubicin; Eto, etoposide; Ifo, ifosfamide; MTX, methotrexate; SCT, stem cell transplantation; TT, topotecan; VBL, vinblastine; VCR, vincristine. (*) as stated on ClinicalTrials.gov webpage. Reproduced from Prokoph & Larose et al.²⁰.

	ClinicalTrials.gov Identifier	Trial Acronym	Treatment	Phase	Time frame*	Location	No (ALCL)*
Frontline	NCT00006455	EICNHL-ALCL99 ^{52,55}	ALCL99 (Cyc, MTX, Ifo, Eto, ARA-C, Doxo) +/- VBL	III	1999-2005	Europe, Japan	487
	NCT00059839	COG-ANHL0131 ⁵⁷	APO (Doxo, MTX, VCR) +/- VBL	III	2003-2014	USA	125
	NCT01979536	COG-ANHL12P1 ⁵⁸	CZ/BV + (Dexa, Ifo, MTX, ARA-C, Eto)/(Dexa, MTX, Cyc, Doxo)	II	2013-2020	USA	140
	NCT02729961	NCI-2016-00396 ⁵⁹	BV+CR	I/II	2017-2023	USA	30
	N/A	EICNHL-ALCL-VBL	ALCL99/VBL	N/A	Planned	Europe	106
Relapse	NCT00317408	EICNHL-ALCL-RELAPSE ⁶⁰	allo SCT/BEAM-conditioning + auto SCT/VBL	N/A	2004-2014	Europe	96
	NCT00354107	COG-ANHL06P1 ⁶¹	SGN-30, Ifo, Carboplatin, Eto	I/II	2007-2010	USA	5
	NCT01492088	C25002 ⁶²	BV	I/II	2012-2018	Worldwide	36
	NCT00939770	COG-ADVL0912 ^{63,64}	CZ	I	2009-2020	USA	26
	NCT01606878	COG-ADVL1212 ⁶⁵	CZ + (Cyc, TT)/	I	2013-2018	USA	65
	NCT02034981	AcSé ⁶⁶	CZ	II	2013-2022	France	24
	N/A	UMIN000016991 ^{67,68}	(VCR, Dexa, Doxo)	II	2015-2020	Japan	10
	N/A	UMIN000028075 ⁶⁹	AC	I/II	2017-2022	Japan	23
	N/A	ITCC053/CRISP ⁷⁰	CZ	IB	2016-2021*	Europe	82
	NCT03703050	ALCL-Nivo	Nivolumab	II	2018-2026	Europe	38
	NCT01742286	N/A	CR	I	2013-2019	Europe	8
	N/A	JPLSG-ALCL-RIC18	SCT	N/A	2017-2026	Japan	18

1.2.2.1 Vinblastine: Adjusting Frontline Therapy to Reduce Relapse and Toxicity

Two small retrospective studies conducted by the SFOP showed that vinblastine could reduce the risk of treatment failure, even for patients who had relapsed on chemotherapy⁷¹⁻⁷². Hence, as part of the ALCL99 protocol, vinblastine was trialled in high-risk patients (those with mediastinal, lung, liver or spleen involvement, or biopsy-proven skin lesions) who were eligible for the sub-trial, ALCL99-VBL (Table 3, Table 4). High-risk patients were first randomized into either the MTX1-VBL or MTX3-VBL arms, and then half were randomly selected to receive weekly Vinblastine at 6 mg/m², in addition to the MTX1 or MTX3 protocol they were already in, followed by weekly vinblastine only injections for 1 year on its own as a maintenance treatment⁵². Results showed a significant improvement over the first year of treatment with regards to EFS, but no significant difference overall with relapse being delayed rather than prevented⁵². Vinblastine was further trialled as a frontline therapy in the Children's Oncology Group

(COG) trial ANHL0131 (NCT00059839), in addition to the chemotherapy backbone, which used low-dose methotrexate infusions – vinblastine replaced vincristine. Similar to the European trial, it did not find any significant difference between the 3-year OS or EFS as compared to standard chemotherapy, but did show that weekly vinblastine administration was more toxic than the ‘no vinblastine’ arm⁴⁸. For both ANHL0131 and ALCL99-VBL, the vinblastine dose started at 6 mg/m², but had to be reduced to 4 mg/m² due to toxicity in 41 of 61 patients.

The experience with single agent vinblastine in relapse therapy (discussed below) suggested that low-dose, long-term single agent vinblastine could be as effective as is standard short-term multi-agent chemotherapy in low risk patients (see **Table 6** for criteria used to stratify patients into risk groups). Therefore, a new EICNHL trial, ALCL-VBL, will investigate Vinblastine as a single-agent frontline treatment (administered weekly for 18 months, then every other week for 6 months, at 6 mg/m²), in patients negative for minimal disseminated disease (MDD), a prognostic factor previously associated with a lower risk of treatment failure⁷³⁻⁷⁴. The goal will be to assess whether vinblastine could replace the ALCL99 protocol, at least for low risk patients – though it may not improve the OS and EFS rates, the hope is that it will be less toxic overall. Patients who can be cured by vinblastine are spared both acute (stomatitis, neutropenia, infections, 1 – 2% treatment related mortality) and late (risk of secondary malignancies, infertility, cardiac toxicity, obesity, metabolic syndrome) toxicity of the multi-agent chemotherapy which includes etoposide, alkylators and anthracyclines. A further advantage for single agent vinblastine therapy is that patients can be treated as outpatients. Unfortunately, the long duration of the treatment protocol with weekly hospital visits for 2 years may prove to be a logistical barrier. In addition, this could provide a low toxicity chemotherapy backbone forming a new basis to study the addition of targeted therapies.

Table 6 Factors used for stratification of paediatric ALK+ ALCL patients into different risk groups
AIEOP, Associazione Italiana di Ematologia e Oncologia Pediatrica; BFM, Berlin-Frankfurt-Münster; MDD, minimal disseminated disease; MRD, minimal residual disease; UKCCSG, UK Children’s Cancer and Study group; SFOP, Société Française d’Oncologie Pédiatrique.

Factor	Relevance for risk stratification
Mediastinal involvement	Although in disagreement with results from the NHL-BFM-30 trial ³³ , four independent studies by the SFOP ³¹ , the UKCCSG ⁴⁴ , the BFM ⁷⁵ as well as a combined study by the three ⁷⁶ found mediastinal involvement to be predictive of a high risk of treatment failure. Based on those results, the ALCL99 trial used mediastinal involvement for risk stratification ^{28,52} .
Visceral involvement (liver, spleen, lung)	Although in disagreement with results from the NHL-BFM-30 trial ³³ , four independent studies by the SFOP ³¹ , the UKCCSG ⁴⁴ , the BFM ⁷⁵ as well as a combined study by the three ⁷⁶ found visceral involvement to be predictive of a high risk of treatment failure. Based on those results, the ALCL99 trial used visceral involvement for risk stratification ^{28,52} .
Skin involvement	Skin involvement is described as a negative prognostic marker in two BFM group studies ^{46,75} . Skin lesions were associated with increased relapse risk in a combined follow-up study of BFM, SFOP and UKCCSG ⁷⁶ . Based on those results, the ALCL99 trial used skin involvement for risk stratification ^{28,52} .
Histopathology	Lymphohistiocytic subtype correlated with lower EFS in two clinical trials (HM89 and HM91) ³¹ . Small cell or lymphohistiocytic subtype was associated with increased relapse risk in the ALCL99 trial ^{77,78} and an independent BFM group study ⁷⁹ . Additional histology based prognostic factors were described, but not yet validated in an independent study ⁸⁰⁻⁸⁶ .

Factor	Relevance for risk stratification
Small cell or lymphohistiocytic subtype (SC/LC) + MDD	Patients can be stratified into three biological/pathological risk groups (bpRG): high risk (bpHR): MDD+ with SC/LC subtype, low risk (bpLR): MDD- without SC/LC subtype, intermediate risk (bpIR): all remaining patients. 10-year PFS was 40%, 75% and 86% for bpHR, bpIR and bpLR, respectively ⁷⁸ .
Quantitative detection of NPM1-ALK in the bone marrow or peripheral blood at diagnosis (MDD)	MDD (detected by RT-qPCR) in bone marrow samples was associated with lower 5-year PFS ($41 \pm 11\%$ for MDD+ patients compared to 100% for MDD- patients) ⁷³ , reduced 5-year EFS ($38 \pm 9\%$ MDD+ patients compared to $82 \pm 7\%$ for MDD- patients) ⁷⁹ and lower 5-year OS ($60 \pm 9\%$ MDD+ patients compared to $86 \pm 7\%$ for MDD- patients) ⁷⁹ . MDD (detected by RT-qPCR) in bone marrow and peripheral blood samples was associated with lower 5-year PFS ($54 \pm 6\%$ for MDD+ patients compared to $87 \pm 5\%$ for MDD- patients) ³⁹ , reduced 5-year EFS ($51 \pm 5\%$ MDD+ patients compared to $83 \pm 5\%$ for MDD- patients) ⁷⁴ and lower 5-year OS ($79 \pm 4\%$ MDD+ patients compared to $91 \pm 3\%$ for MDD- patients) ⁷⁴ . Those results were confirmed in a 10-year follow-up study of the ALCL99 trial ⁷⁸ .
Quantitative detection of NPM1-ALK in the bone marrow or peripheral blood at diagnosis during treatment course (MRD)	MRD (detected by RT-qPCR) in bone marrow and peripheral blood samples before the second course of chemotherapy was associated with reduced 5-year EFS (69% MDD+ patients compared to 19% for MDD- patients) ⁷⁴ and lower 5-year OS ($65 \pm 9\%$ MDD+ patients compared to $92 \pm 5\%$ for MDD- patients) ⁷⁴ and increased cumulative incidence of relapse ($81 \pm 8\%$ MDD+ patients compared to $31 \pm 9\%$ for MDD- patients) ⁷⁴ . This had first been explored in a small cohort of relapsed patients that presented with NPM1-ALK transcript level increase in bone marrow samples ⁸⁷ .
Anti-ALK autoantibody titre	Anti-ALK autoantibodies can be detected in >90% of paediatric ALK+ ALCL patients at diagnosis ^{39,88-93} . Patients can be stratified into risk groups according to the anti-ALK autoantibody titre at diagnosis with cut-off at $\leq 1/750$. Two studies combining patients recruited onto NHL-BFM90 ³³ /NHL-BFM95 ⁹⁴ and NHL-BFM95 ⁹⁴ /AIEOP LNH-97 ⁹⁵ /ALCL99 ²⁸ described that titres inversely correlated with relapse risk ^{91,92} . Those results were confirmed by an independent study in Japanese children ⁹³ .
Course of anti-ALK autoantibody titre	Patients can be stratified into risk groups according to the decrease in the anti-ALK autoantibody titre from diagnosis to the end of therapy: patients who showed a titre-decrease of maximal two dilution steps (≤ 2) or patients who showed a titre-decrease of more than two dilution steps (>2). 10-year EFS was $91 \pm 5\%$ or $70 \pm 6\%$ for patients in the ≤ 2 or >2 group ⁹² .
Anti-ALK autoantibody titre + MDD	Patients can be stratified into three biological risk groups (bRG): high risk (bHR): MDD+ and anti-ALK autoantibody titre $\leq 1/750$, low risk (bLR): MDD- and anti-ALK autoantibody titre $>1/750$, intermediate risk (bIR): all remaining patients. 5-year PFS was 28%, 68% and 93% for bHR, bIR and bLR, respectively. 5-year OS was 71%, 83% and 98% for bHR, bIR and bLR ³⁹ . Those results were confirmed by an independent study in Japanese children ⁹³ .
Time to relapse, failure or progression	Relapsed patients can reach a second remission by chemotherapy and allogenic SCT ^{71,96-98} . Time to relapse/failure/progression serves as prognostic factor ^{71,97,98} whereby shorter time to first relapse is an indicator for another relapse with 50% of patients that progress during first-line therapy experiencing another relapse ⁹⁸ .
Infiltration of the CNS	Only a low number of patients presents with CNS infiltration ^{95,97,99,100} ; in the biggest cohort analyzed so far, 26/618 (4%) patients were CNS positive ¹⁰⁰ . In this study, 3-year OS after CNS relapse was 49% ¹⁰⁰ .
CD3	CD3+ patients that were treated with autologous SCT had lower 5-year EFS ($18 \pm 12\%$ for CD3+ patients compared to $72 \pm 9\%$ for CD3- patients) ⁹⁷ . However, no further relapse occurred in patients with CD3+ first relapse that were treated with allogenic SCT ⁹⁷ . Based on those results, the ALCL-Relapse trial used C3 positivity for risk stratification ^{77,98} . In this study, 5/6 CD3+ patients that progressed during first-line therapy experienced another relapse compared to 3/11 CD3- patients. However, for other patient groups this effect was not pronounced ⁹⁸ .
Bone marrow involvement	Depending on the analysis method used bone marrow involvement ranges from uncommon ^{28,31-33,44,101,102} to common ^{73,79} . Due to high concordance between NPM1-ALK transcripts by RT-qPCR of bone marrow and peripheral blood samples ⁷⁹ , Damm-Welk et al. hypothesized that this is due to circulating tumours cell rather than true bone marrow infiltration ¹⁰³ . Bone marrow involvement (detected by RT-qPCR) was associated with a higher relapse risk ($50 \pm 10\%$ for patients with bone marrow involvement compared to $15 \pm 7\%$ for patients without) ⁷⁹ , lower 5-year PFS ($41 \pm 11\%$ for patients with bone marrow involvement compared to 100% for patients without) ⁷³ and reduced OS ⁹⁷ .

1.2.2.2 Development of Targeted Agents for Frontline Therapy

1.2.2.2.1 Targeting ALK

With EFS and OS rates having barely changed since the NHL-BFM first tested its B-cell NHL protocol on ALCL patients in the 1980s, there is a clear need for new, less toxic therapies for patients in all risk groups. For ALCL, ALK provides an ideal drug target for those cases that are ALK+ particularly as endogenous ALK expression is limited to neuronal cells during neonatal development¹⁰⁴ which should limit toxic side-effects. However, initial interest in the development of ALK inhibitors was largely non-existent amongst pharmaceutical companies due not only to the favourable survival rates of these patients, but also its orphan disease status. Over a decade later in 2007, ALK was identified to be fused to EML4 in 6.7% of NSCLC patients as a result of a chromosomal inversion¹⁸ and subsequently the first phase I clinical trial of Pfizer's ALK/MET/ROS1 inhibitor crizotinib was initiated in 2008¹⁰⁵. Other ALK inhibitors have followed and since crizotinib's FDA approval in 2011 for advanced ALK+ NSCLC, ceritinib (Novartis) and alectinib (Hoffmann-La Roche) were likewise approved in 2014 and 2015 respectively¹⁰⁶⁻¹⁰⁸. Two more ALK inhibitors – lorlatinib (Pfizer) and brigatinib (Takeda) – have recently been granted breakthrough therapy designation and FDA accelerated approval respectively¹⁰⁹. These drugs have been slowly filtering through to the treatment of ALCL and other ALK-related malignancies in children.

Although, ALK inhibitors have been tested mainly in pediatric relapsed and refractory ALK+ ALCL patients (discussed below), the safety of crizotinib and combination chemotherapy have already been shown in a phase I trial in children with ALK-related malignancies (NCT01606878), and final data will soon be available from the phase II frontline trial of crizotinib administered in combination with ALCL99 in the USA (NCT01979536).

Interestingly, a phase I/II open-label dose-finding study of ceritinib combined with Brentuximab vedotin (BV, SGN-35; discussed below) for frontline treatment of ALK+ ALCL patients 12 years and older opened recruitment in 2018 (NCT02729961). This trial will provide important information regarding new targeted agent combination strategies not involving standard chemotherapy.

1.2.2.2.2 Targeting CD30

The consistent expression of CD30 (a protein expressed almost exclusively on activated B and T cells) on ALCL provides another therapeutic target¹¹⁰⁻¹¹¹. The first mouse-human chimeric anti-CD30 antibody SGN-30 was developed by Seattle Genetics and tested in a phase I/II pilot study in combination with ifosfamide, carboplatin and etoposide (ICE) in five children with recurrent ALCL (COG-ANHL06P1, NCT00354107). However, serious adverse events (pleural effusion, ascites, neutrophil count decrease, capillary leak syndrome, skin and subcutaneous tissue disorders) led to the termination of the study⁶¹. Sometime after, the activity of SGN-30 was further improved by conjugation with the antimicrotubule agent monomethyl auristatin E (MMAE). The resulting antibody-drug conjugate BV binds to CD30 on the cell surface initiating its internalization, followed by trafficking to the lysosomal compartment with eventual release of MMAE via proteolytic cleavage¹¹². Binding of MMAE to tubulin disrupts the microtubule network, induces cell cycle arrest, and results in apoptotic death of the CD30-expressing cell¹¹³. An initial phase I clinical trial of BV (NCT00430846) was conducted in adults with CD30-positive

lymphomas that had failed systemic chemotherapy. The two adult patients with ALCL enrolled into the study both achieved complete remission (CR)¹¹⁴. Following this, a phase II study of BV in adults with relapsed or refractory systemic ALK+ and ALK- ALCL was initiated (NCT00866047)¹¹⁵ and in 2011 BV was approved by the FDA for the treatment of relapsed ALCL following failure of at least one multi-agent chemotherapy protocol for adults. An update to this pivotal study provided 4-year follow-up of patients included in the phase 2 study, the median Progression-Free Survival (PFS) was 20 months (25.5 months for ALK+ ALCL patients) and the 4-year OS was 64%¹¹⁶.

Both crizotinib and BV have since been studied in adults with HL (NCT02243436, NCT01578967, NCT02098512, NCT01874054, NCT00848926, NCT02298283, NCT02227433, NCT02939014, NCT01716806) and NHL (NCT01805037, NCT02462538, NCT01657331, NCT01909934, NCT01352520, NCT01950364, NCT02139592, NCT02419287, NCT02939014, NCT00866047, NCT02280785) in a frontline setting with promising results. Additionally, BV and combination chemotherapy has been trialed in young patients with newly diagnosed HL (NCT02166463).

This has encouraged a randomized phase II COG study for paediatric ALCL (COG-ANHL12P1, NCT01979536) that compares the use of BV to the ALK inhibitor crizotinib administered with a common chemotherapy backbone (ALCL99). This study is the first frontline trial of these targeted agents specifically for children with ALCL. The trial enrolled its first patient in 2013 and results will be available by the end of 2020; to date, 110 patients have been enrolled and updated study results were presented at the EICNHL meeting in November 2017. The BV arm has been closed, as recruitment is now complete; the crizotinib arm re-opened following an FDA-imposed clinical hold in March 2017 due to the occurrence of thrombosis. Catheter-related clots and pulmonary emboli occurred in 10 patients, after which the study committee initially closed the crizotinib arm, but temporarily reopened enrolment after the DSMC reviewed the cases. This is surprising as the robust and sustained activity observed in the Phase I/II COG-ADVL0912 trial (discussed below) provided the rationale for combining crizotinib at 165 mg/m² with conventional chemotherapy. The only grade 3 or 4 drug-related adverse event was a decrease in neutrophil count occurring in 83% patients treated with 165 mg/m² crizotinib¹¹⁷. In future, single agent vinblastine may provide a lower toxicity chemotherapy backbone as mentioned above.

1.2.3 Treatment of Refractory/Relapsed Disease

1.2.3.1 Stem Cell Transplantation (SCT)

Some retrospective studies suggest that OS is over 50% for ALK+ ALCL relapse cases when treated with SCT or continued multi-agent chemotherapy^{71,118-97}, the former being the standard of care for children or adolescents with some other forms of relapsed or refractory NHL (except ALCL)¹¹⁹⁻¹²⁰. Therefore, one treatment option for relapsed or refractory ALCL is SCT and five retrospective studies have been conducted to assess its efficacy.

The NHL-BFM working group were the first to report that SCT is a viable option for relapsed ALCL looking back at ALCL patients treated in the 1990s^{97,121}. Two retrospective Japanese studies also found that relapsed or refractory ALCL patients who received SCT did better than those who did not^{118,122}. For all cases, the risk profile was acceptably low, but this approach was reserved for high-risk ALCL patients who had already relapsed at least once. One of the Japanese studies in particular, showed that 30% of

relapsed patients treated with chemotherapy alone relapsed a second time, which is similar to the 37.5% of patients treated with autologous SCT who relapsed a second time¹¹⁸. However, the patient group was small with only 10 and 8 patients treated in each arm, respectively. Allogenic SCT was more successful, with all 6 patients entering remission¹¹⁸. Collectively, these limited data suggest that allogenic SCT is superior to autologous SCT¹²². A retrospective French trial also showed mixed results, with 45% of patients treated with autologous SCT entering remission, as opposed to 52% treated with chemotherapy alone⁷¹. EICNHL-ALCL-RELAPSE (NCT00317408), which between 2004 and 2011, enrolled ~105 relapsed paediatric ALCL patients sorted into three arms depending on CD3 expression and time to relapse, tested allogenic SCT and autologous SCT with and without BEAM-conditioning in comparison to single agent weekly vinblastine. For early relapsed ALCL (within the first year after initial diagnosis) autologous SCT was not effective with relapses observed in 70% of patients treated with autologous SCT in comparison to 20% of patients treated with allogeneic SCT⁹⁸. Fortunately, patients that relapsed during autologous SCT could be rescued by allogeneic SCT or maintenance therapy achieving an OS rate of 80%⁹⁸. Therefore, the trial established allogeneic SCT as standard consolidation therapy for ALCL patients with progression during frontline multi-agent chemotherapy or relapse after completion of multi-agent chemotherapy⁹⁸. A Japanese study found 5-year EFS rates of 100% and 49%, respectively, in relapsed/refractory ALK+ ALCL patients treated with Reduced Intensity Conditioning (RIC) compared to myeloablative conditioning (MAC) regimens⁴¹. One clinical trial, JPSLG-ALCL-RIC-18, is still ongoing and will specifically test the efficacy of RIC to prepare for allogenic SCT.

1.2.3.2 Vinblastine

One arm of the EICNHL-ALCL-RELAPSE trial recruited patients with late relapse (more than 12 months from initial diagnosis) and CD3-negative ALCL to be treated with single agent weekly vinblastine for 24 months. The trial established that vinblastine achieved both high survival rates and a long-term remission rate of 81%^{98,123}. However, vinblastine was not effective in patients that experienced a relapse within the first year after initial diagnosis⁹⁸. Therefore, the authors suggest that vinblastine should only be tested in low-risk patients defined by CD3-negative relapse with more than one year after initial diagnosis⁹⁸.

1.2.3.3 Development of Future Treatments for Relapsed/Refractory ALCL

1.2.3.3.1 Targeting ALK

As mentioned above, COG was the first group to open a phase I dose-escalation study of an ALK inhibitor (ADV0912, NCT00939770)⁶³. In this trial, crizotinib was administered orally, twice daily in 28-day cycles, as a single agent for an indefinite duration to paediatric patients with ALK+ relapsed or refractory ALCL that had received at least one course of chemotherapy⁶⁴. Those with relapsed ALCL achieved an objective response rate of 90%¹¹⁷ when treated with the recommended phase II dose (RP2D) of 280 mg/m²⁶³. The 10 patients treated at the RP2D in phase I of the study were included in the phase II study. The additional 10 patients that were treated at the RP2D were specifically enrolled in the phase II expansion cohort. Of the 20 patients included in the phase II expansion cohort, 13 responded within 4 weeks of initiating treatment and the remaining 7 within 5 to 8 weeks with CR in

18/20 patients. Two patients came off therapy after experiencing adverse events (AEs), 3 after experiencing disease progression, 12 proceeded to SCT and two continued on crizotinib¹¹⁷.

Three years later a phase I study was also initiated by COG (COG-ADVL1212, NCT01606878) combining crizotinib with conventional chemotherapy for relapsed or refractory paediatric ALCL patients which provided the requisite safety and tolerability data for eventually integrating crizotinib into frontline treatment regimens for children with ALCL (NCT01979536).

In Japan, the trials UMIN000016991 and UMIN000028075 are investigating the efficacy and safety of alectinib or crizotinib respectively as monotherapies for children with recurrent or refractory ALK+ ALCL⁶⁷⁻⁶⁹. UMIN000016991 was the first trial to test an ALK inhibitor, other than crizotinib, for paediatric ALCL patients. Based on this study the Ministry of Health, Labour and Welfare in Japan has approved alectinib for the treatment of recurrent or refractory ALK+ ALCL in 2020¹²⁴. In addition, a first case report described the successful treatment of a girl, who suffered from a CNS relapse, with alectinib¹²⁵. Results for UMIN000028075 are expected in 2022.

In Europe, an Innovative Therapies for Children with Cancer (ITCC) trial is in progress to treat relapsed patients with ALK-, ROS1- or MET-positive malignancies (not limited to ALCL) with crizotinib either as a single agent or in combination with vinblastine in a phase IB safety study. The trial (ITCC053, CRISP) will determine the RP2D of vinblastine in combination with crizotinib by dose escalation of vinblastine with a fixed dose of 150 mg/m² crizotinib. Patients will receive a maximum of 24 cycles corresponding to two years of therapy. Salvage of non-responding patients is anticipated by transfer of patients to the ALCL-Nivo trial discussed below (**Figure 3**). In France, the trans-tumoural, multicentric phase II trial AcSé (NCT02034981) investigates the efficacy and safety of single agent crizotinib in paediatric ALK+ ALCL patients that relapsed from chemotherapy. Although final results are eagerly awaited, preliminary results showed that 5/15 patients progressed and that all cases of progression on crizotinib occurred during the first 3 months following treatment initiation¹²⁶. In addition, the EICNHL is planning to trial an ALK inhibitor in combination with the ALCL99 backbone in paediatric patients with ALK+ relapsed or refractory ALCL (personal communication with Dr. Suzanne Turner).

Even though the final results from the ALK inhibitor trials are still to come, single-agent crizotinib has not yet proven curative since abrupt relapses following crizotinib discontinuation have been described in isolated cases¹²⁷. Hence, crizotinib is currently used to induce second remission as shown in adult relapsed/refractory ALK+ ALCL patients before allogeneic or autologous SCT¹²⁸ (**Figure 3**).

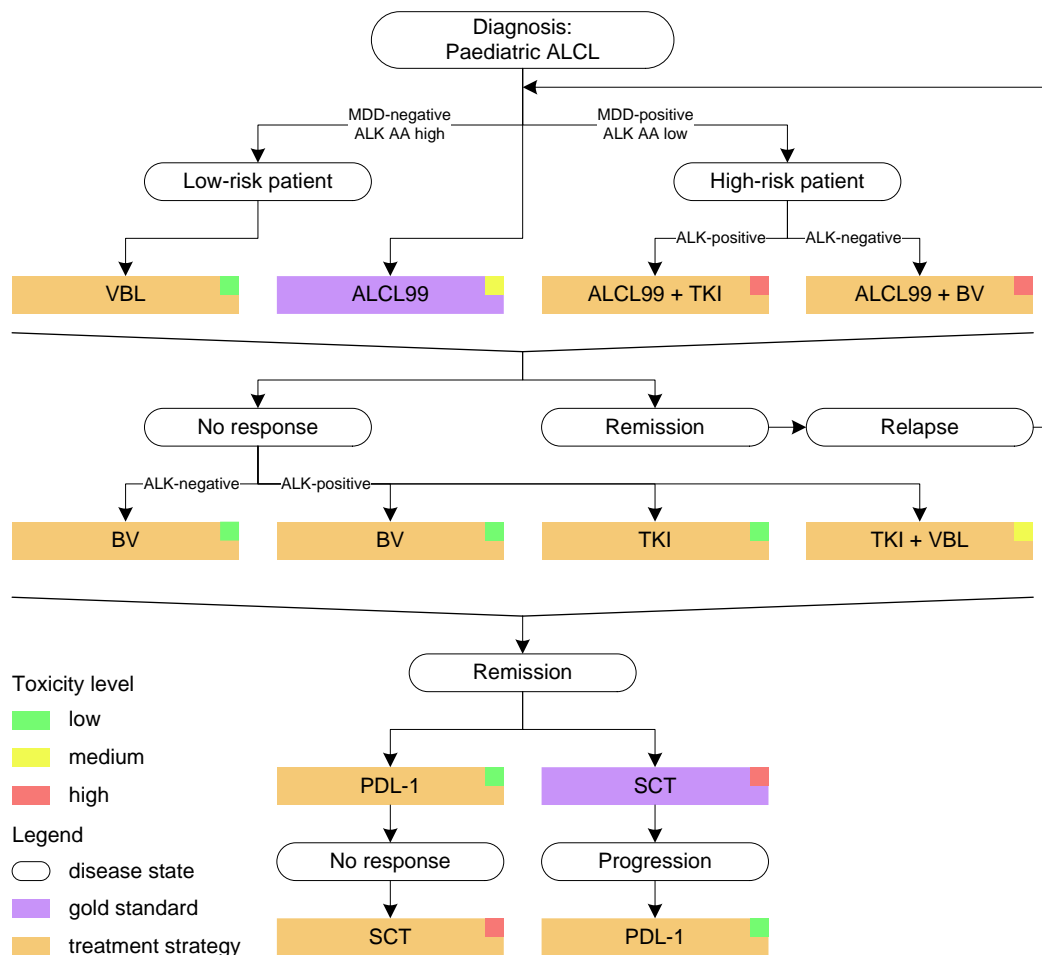


Figure 3 Management of childhood ALCL

AA, auto-antibody; BV, Brentuximab vedotin; MDD, minimal disseminated disease, SCT, stem cell transplantation; TKI, tyrosine kinase inhibitor; VBL, vinblastine. Reproduced from Prokoph & Larose et al.²⁰.

1.2.3.3.2 Targeting CD30

As mentioned earlier, following encouraging results from adult ALCL trials (NCT00430846, NCT00866047), a company-sponsored international phase I/II study of BV in paediatric patients with relapsed or refractory systemic ALCL (NCT01492088) was opened in 2012. Participants received BV 1.4 mg/kg in Phase I and 1.8 mg/kg in Phase II, on day 1 of every 21-day cycle for up to 16 cycles. Of the 17 ALCL patients recruited into the phase II expansion cohort of the trial, the Overall Response Rate (ORR) was 53% and time to progression was 6.3 months. However, 13 patients did not complete the study; 1 patient died, and 12 patients dropped out for unspecified reasons. The most common reported drug-related AE was a decrease in neutrophil and lymphocyte counts with 1 patient experiencing pyrexia and 4 of 17 patients developing neutralizing anti-therapeutic antibodies¹²⁹. Additionally, a major clinical consideration is cumulative peripheral neuropathy that was observed in 36% of patients recruited onto the dose finding study of BV for adults with CD30-positive hematologic malignancies (NCT00430846)¹³⁰. Given the neurologic side effect of BV, prolonged treatment may be difficult to manage in paediatric patients. Thus, this drug is currently mostly used as a bridge to transplant in relapsed ALK+ ALCL patients (Figure 3).

1.2.3.3.3 Immunotherapy

Accumulating evidence indicates that the immune system plays a major role in the pathogenesis of ALK+ ALCL⁸⁸⁻⁹¹. Indeed, it has been shown that ALK+ ALCL cell lines strongly express the cell surface protein, Programmed Cell-Death Ligand 1 (PD-L1; CD274, B7-H1), as determined at both the mRNA and protein levels¹³¹. Furthermore, results of PD-L1 immunostaining of ALK+ ALCL primary patient tumours showed strong PD-L1 expression¹³². Analysis revealed that PD-L1 expression is induced by the chimeric NPM1-ALK tyrosine kinase, via STAT3, confirming a unique function for NPM1-ALK as a promoter of immune evasion by inducing PD-L1¹³². PD-1 and its ligands, PDL-1 and PDL-2, have been shown to be involved in immune suppression with increased expression of PD-1 leading to decreased activation of reactive T-cells inhibiting the PI3K/AKT pathway on ligation by ligand¹³³⁻¹³⁵.

These observations provided a strong rationale to use consolidative anti-PD1/PD-L1 immunotherapy for relapsed or refractory ALK+ ALCL. Indeed, three case reports describe a dramatic and durable response using the anti-PD1 monoclonal antibodies pembrolizumab (Merck) or nivolumab (Bristol-Myers Squibb) for ALCL patients¹³⁶⁻¹³⁸. The first, an adult with ALK- ALCL was treated with pembrolizumab following chemotherapy, BV and SCT¹³⁶. The second, a 19-year old ALK+ ALCL patient was treated with nivolumab, following chemotherapy, BV, crizotinib and SCT¹³⁷. Finally, a case report observed a similar dramatic response to Nivolumab in a relapsed 17-year old patient with ALK+ ALCL after two lines of treatment including chemotherapy and crizotinib¹³⁸. While the 19-year old developed grade 2 pneumonitis, there are no reports of adverse events for the other two patients, pointing towards an acceptable toxicity profile. Interestingly, only the 17-year old patient was tested for PD-1 expression on tumour cells by immunostaining showing strong expression throughout the tumour. It should be noted that several publications have shown both that PD-1 inhibitors can provoke a response even in tumours which do not have strong PD-1 expression, but also that they sometimes fail in tumours which do show strong PD-1 expression¹³⁹. The lack of an obvious biomarker for PD-1 inhibitor efficacy may make clinical decisions difficult when assessing therapeutic approaches for relapsed disease.

With a clear need for a randomized trial of anti-PD-1 monoclonal antibodies in refractory or relapsed ALCL, ALCL-Nivo has been designed as a phase II trial of nivolumab in paediatric and adult relapsed or refractory ALK+ ALCL patients. The trial is testing the objective response to nivolumab at 24 weeks, for patients which have already relapsed on chemotherapy and either an ALK inhibitor or BV. Should there be sufficient response in this first cohort, the trial also plans to test nivolumab as a consolidation therapy after CR of at least two months as a replacement to SCT. Patients in both cohorts will be treated with 24 months of Nivolumab at 3 mg/kg every two weeks, and every four weeks after the first eight weeks for patients in the second cohort (personal communication with Laurence Brugières).

Another potential immunotherapy under investigation, potentially of therapeutic use for ALCL at all stages, is the application of cancer vaccines. Strong expression of the ALK chimera in the majority of ALCL cases combined with near-absent expression of ALK in healthy tissues makes it an ideal candidate for vaccine development. Autoantibodies against ALK as well as cytotoxic and helper T cell responses to ALK have been detected in patients with ALK+ ALCL both at diagnosis and during remission with a significant inverse correlation between ALK-antibody titres and the incidence of relapse¹⁴⁰⁻³⁹. Vaccination using a truncated cDNA of ALK has been reported to induce potent and long-

lasting protection from local and systemic lymphoma growth in mice¹⁴¹⁻¹⁴². This has yet to be trialled in ALCL patients, but as mentioned, pre-clinical models show promising results.

1.3 ALK-driven NB

1.3.1 Clinical Features of NB

NB is an embryonal tumour of the sympathetic peripheral nervous system¹⁴³ accounting for 7–10% of paediatric cancers and representing 15% of all paediatric cancer deaths^{144–146,6}. Deriving from the sympathoadrenal lineage of the neural crest, it presents along the sympathoadrenal axis¹⁴⁷. NB is a complex disease and ranges from regression to treatment-resistant progression, metastasis and death^{147,6}. As such, there has been a substantial collaborative effort to develop accurate risk-classification systems that will assist in determining the appropriate treatment regimen¹⁴³. The COG categorizes NB patients into three prognostic groups according to the risk of death: low, intermediate, and high risk^{148,149}. Patients are assigned to each risk group based mainly on the patient's age at diagnosis, biological features of the tumour (e.g. tumour karyotype, *MYCN* amplification status, International NB Pathology Classification (INPC histopathology classification), and the stage of tumour defined by the International NB Staging System (INSS)¹⁵⁰. Whereas low- and intermediate-risk disease is highly curable, with 5-year survival >90%, high-risk disease is associated with frequent relapse and a 5-year survival of 40–50%^{151,6}. Considering that the majority of newly diagnosed NB patients are high-risk cases (45%) compared to 37% low risk and 18% intermediate risk cases^{152,153}, current research efforts focus on identifying novel therapeutic approaches that will improve the survival rates and long-term effects associated with therapy for high-risk NB patients¹⁵³.

1.3.2 ALK in NB

To identify novel therapeutic approaches that not only achieve superior long-term survival rates but also reduce treatment-induced toxicities, many of the NB research efforts have focused on enhancing our understanding of the molecular basis of high-risk NB¹⁴³.

In 2013, Pugh et al. published a large (n=240) sequencing study applying a combination of whole exome sequencing (WES) (n=221), Whole genome sequencing (WGS) (n=18), or both (n=1) with all samples collected from high-risk NB patients as part of the Therapeutically Applicable Research to Generate Effective Treatments (TARGET) Initiative¹⁵⁴. The three most frequently altered genes from the TARGET study cohort were genes with previously confirmed pathogenic roles in NB^{16,155–158}: *MYCN* (amplified; >20%), *ALK* (missense point mutations; 9%), and *ATRX* (multi-exon focal deletions; 7.1%). Among those genes, *ALK* currently represents the only directly druggable target as *MYCN* (transcription factor) and *ATRX* (chromatin remodeler) both belong to classes of proteins, which are difficult to inhibit directly^{159,160}.

Most ALK-driven NBs express full-length ALK^{161,162,6}. In ALK-driven NB, single-base missense mutations cluster in the ALK kinase domain and promote ligand-independent signaling by disruption of the auto-inhibited conformation of the kinase^{163,6} (**Figure 4**). Mutations at three positions (R1275, F1174, and F1245) account for ~85% of ALK mutations in ALK-driven NB and are hotspots for lower frequency mutations^{164,6} (**Figure 4B**).

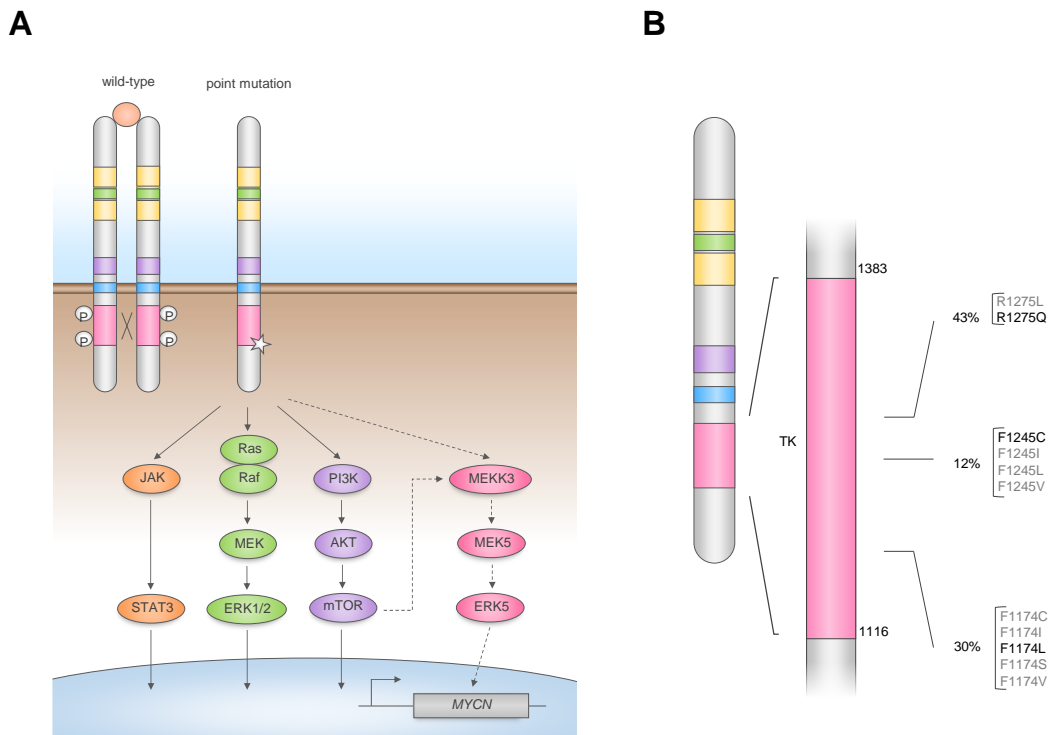


Figure 4 ALK in NB

(A) Full-length ALK signals through the Ras/MAPK, PI3K/AKT and JAK/STAT pathways. In NB, MYCN expression is activated in a pathway mediated by ALK, PI3K/AKT, MEKK3, MEK5 and ERK5 (dashed lines). **(B)** Gain-of-function mutations cluster in the kinase domain of ALK. Modified from Trigg et al.⁶

NB with *ALK* mutations are distributed amongst all of the clinical stages^{155,157,165–168}. However, a study of 1596 NB samples found that *ALK* mutations were associated with poorer survival in high- and intermediate-risk patients^{164,6}. *ALK* mutations correlate with *MYCN* amplification and the cooperative activity of these two oncogenes as been shown to drive NB in mouse and zebrafish models^{169,6}.

Interestingly, *ALK* has been shown to induce transcription of *MYC* in NB cell lines, which could explain the poor prognosis of NB patients harbouring both *MYCN* amplification and *ALK* mutations^{170,6}. Sequencing of matched primary and relapsed NB patient tumour samples showed an increased frequency of *ALK* mutations at relapse^{171–173,6}. Some mutations were found to undergo clonal expansion at relapse, whereas others were confirmed to arise de novo^{174,6}. These observations highlight *ALK* as a driver oncogene in primary and relapsed NB⁶.

Gene amplification is a less common mechanism of *ALK* activation in NB (2–3% cases) leading to increased protein expression and constitutive kinase activity^{175,176,6} (**Figure 1B**). While *ALK* is almost always co-amplified with *MYCN* and therefore tumours harbouring *ALK* amplification tend to afford a poor prognosis^{158,164,177}, mutation and amplification of *ALK* is rare in NB^{174,6}.

1.3.3 Targeting ALK in ALK-driven NB

The results of *ALK* inhibitor trials in ALK+ NSCLC provided the rationale for further evaluation in ALK-driven NB. In 2009, the COG initiated a phase I–II trial of crizotinib in paediatric patients with relapsed or refractory ALK+ solid tumours or ALCL (NCT00939770) (**Table 7**)^{63–64}. Results from NB patients in this trial were discouraging^{63,6}; only 1/11 had a CR and 2/11 had stable disease⁶³. However, this is understandable, since 3/7 tumours from ALK+driven NB patients with progressive disease (PD)

harboured the resistance conferring ALK F1174L mutation^{63,6}. In 2011, a phase I trial of crizotinib was launched for patients aged ≥ 15 years with any ALK+ malignancy other than NSCLC (NCT01121588). In addition, in 2013, COG initiated a phase I trial of crizotinib with combination chemotherapy for patients with high-risk NB and ALCL (NCT01606878)⁶. Encouraging results from this trial provided the rationale for a COG phase III trial evaluating the addition of crizotinib to standard therapy in high-risk NB patients with ALK mutations (NCT03126916)⁶.

Table 7 Clinical trials evaluating ALK inhibitors in NB

ALK inhibitors: Crizotinib, Ceritinib, Entrectinib, Lorlatinib; Cyclin-dependent kinase (CDK)4/6 inhibitor: Ribociclib. (*) as stated on ClinicalTrials.gov webpage. Updated from Trigg et al.⁶.

ClinicalTrials.gov Identifier	Trial Acronym	Treatment	Phase	Time frame*	Location	Ref
NCT00939770	COG-ADVL0912	Crizotinib	I/II	2009-2018	USA	64,178
NCT01121588	PROFILE 1013	Crizotinib	I	2011-2019	Worldwide	179
NCT01606878	COG-ADVL1212	Crizotinib + chemotherapy	I	2013-2018	USA	180
NCT01742286	N/A	Ceritinib	I	2013-2019	Worldwide	181
NCT02034981	AcSé	Crizotinib	II	2013-2022	France	66
NCT02650401	N/A	Entrectinib	I/Ib	2016-2023	USA	182
NCT02780128	NEPENTHE	Ceritinib + Ribociclib	I	2016-2026	USA	183
NCT03213652	N/A	Ensartinib	II	2017-2024	USA	184
NCT03107988	NANT2015-02	Lorlatinib +/- chemotherapy	I	2017-2020	USA	185
NCT03126916	COG-ANBL1531	Crizotinib + chemotherapy	III	2018-2026	USA	186

Other trials are evaluating second and third generation ALK inhibitors alone or in combination with chemotherapy and targeted agents in patients with ALK+driven NB (**Table 7**)⁶:

Ceritinib^{187,188} is undergoing phase I assessment as a monotherapy in relapsed or refractory ALK+ paediatric cancers including NB (NCT01742286). In addition, the Next Generation Personalized Neuroblastoma Therapy (NEPENTHE) trial (NCT02780128) is recruiting patients with relapsed or refractory NB into treatment arms based on actionable genetic alterations. Patients with ALK mutations are treated with ceritinib in combination with ribociclib. The National Cancer Institute (NCI)-COG Paediatric Molecular Analysis for Therapy Choice (MATCH) is a phase II study that involves the stratification of patients into targeted treatments based on genetic profiling (NCT03155620)¹⁸⁹. The ALK inhibitor ensartinib is under assessment for patients with relapsed or refractory NB among other solid tumours, NHL, and histiocytic disorders with genetic alteration of ALK or ROS1 (NCT03213652). A phase I trial is assessing the TRK, ROS1 and ALK inhibitor entrectinib in paediatric patients with relapsed or refractory solid and central nervous system (CNS) tumours with and without TRK, ROS1 and ALK fusions (NCT02650401). Moreover, the New Approaches to Neuroblastoma Therapy consortium opened a phase I trial of lorlatinib in combination with chemotherapy in patients with high-risk NB (NCT03107988)⁶.

1.4 ALK+ NSCLC

1.4.1 Clinical Features of ALK+ NSCLC

Based on GLOBOCAN estimates¹⁹⁰, lung cancer is the leading cause of cancer death in both men and women worldwide¹⁹¹. NSCLC accounts for about 85% of lung cancer cases and remains difficult to treat, particularly in the metastatic setting¹⁹². Approximately 57% of NSCLC patients are diagnosed with metastatic, or advanced disease with a 5-year survival rate of only 5%¹⁹³. Epidemiology studies suggest that approximately 3-5% of NSCLC tumours are ALK+¹⁹⁴, which translates to approximately 75,000 newly diagnosed cases worldwide per year¹⁹¹. This means that NSCLC contributes by far the largest ALK fusion-positive patient population¹⁹⁵ – the EML4–ALK fusion being the most common – with an urgent need for early disease detection. ALK+ NSCLC is associated with a younger age at diagnosis and a non-smoking history¹⁹⁶.

1.4.2 Targeting ALK in ALK+ NSCLC

Surgery remains the treatment of choice if patients are diagnosed at an early disease stage, because NSCLC patients do not respond well to chemotherapy. However, with the discovery of driver mutations, targeted therapies gave new hope to NSCLC patients with advanced and metastatic disease. After ALK was identified to be fused to EML4¹⁸ in NSCLC patients, the first phase I clinical trial was initiated in 2008¹⁹⁷. This phase I clinical trial with Pfizer's crizotinib^{19,198} encouraged the initiation of a phase III, open-label trial to compare the efficacy of crizotinib to that of traditional chemotherapeutics (pemetrexed or docetaxel) in a larger NSCLC patient cohort. The ORR to crizotinib treatment was 65% (vs. 20% with chemotherapy), increasing the median PFS period to 7.7 months for the crizotinib treatment group (vs. 3 months for the chemotherapy treatment group)^{199,200}.

Crizotinib's FDA approval in 2011 was followed by Novartis's ceritinib in 2014 and Hoffmann-La Roche's alectinib in 2015 (**Table 1**). Ceritinib was the first FDA approved drug for patients who have experienced progression on or are intolerant to crizotinib²⁰¹. Ceritinib provided ORR of around 60% across the ASCEND trials in crizotinib-pretreated patients with or without brain metastases (BM)^{202–204}. Alectinib was the first ALK-inhibitor that demonstrated superior efficacy against crizotinib in a randomized, open-label phase III trial (J-ALEX; JapicCTI-132316) in ALK+ NSCLC patients who had received a prior chemotherapy regimen. Moreover, alectinib was superior as an initial treatment compared to crizotinib in chemotherapy naïve ALK+ NSCLC patients in the global phase III ALEX trial (NCT02075840). Additionally, alectinib reduced the risk of progression by 92% compared with crizotinib in patients with brain metastases at baseline (HR =0.08; 95% CI, 0.01–0.61)²⁰⁵.

Two more ALK inhibitors – brigatinib (Takeda, 2017) and lorlatinib (Pfizer, 2018) – have been granted breakthrough therapy designation and FDA accelerated approval. Lorlatinib – a third-generation ALK and ROS1 inhibitor – was specifically designed to increase tumour and central CNS penetration, as up to 50% of patients with ALK+ NSCLC develop CNS metastases during the course of their disease²⁰⁶. Brigatinib is of major interest, as it exhibited a superior inhibitory profile compared to crizotinib, ceritinib, and alectinib²⁰⁷ and demonstrated high activity in crizotinib/ceritinib/alectinib-refractory ALK+ NSCLC patients²⁰⁸.

1.5 Resistance mechanisms to ALK inhibitors

Despite the success of ALK inhibitors, resistance inevitably develops²⁰⁹. For example, the median PFS after treatment with crizotinib in advanced ALK+ NSCLC patients is generally less than one year^{197,210–212}. Resistance to targeted therapies can be either primary/intrinsic, adaptive or acquired²¹³. Primary resistance to a targeted therapy implies an intrinsic lack of response to the treatment. Adaptive resistance denotes disease progression after an initial response when the tumour cells undergo early adaptive changes²¹⁴. Acquired resistance arises from a selection of therapy-resistant clones within a heterogeneous tumour combined with the acquisition of new alterations²¹³.

Resistance mechanisms can be classified as ALK-dependent/'on-target' or ALK-independent/'off-target' (Figure 5). On-target resistance arises, when the initial target – for example ALK – is altered, off-target resistance arises when collateral signalling events are activated²¹⁴.

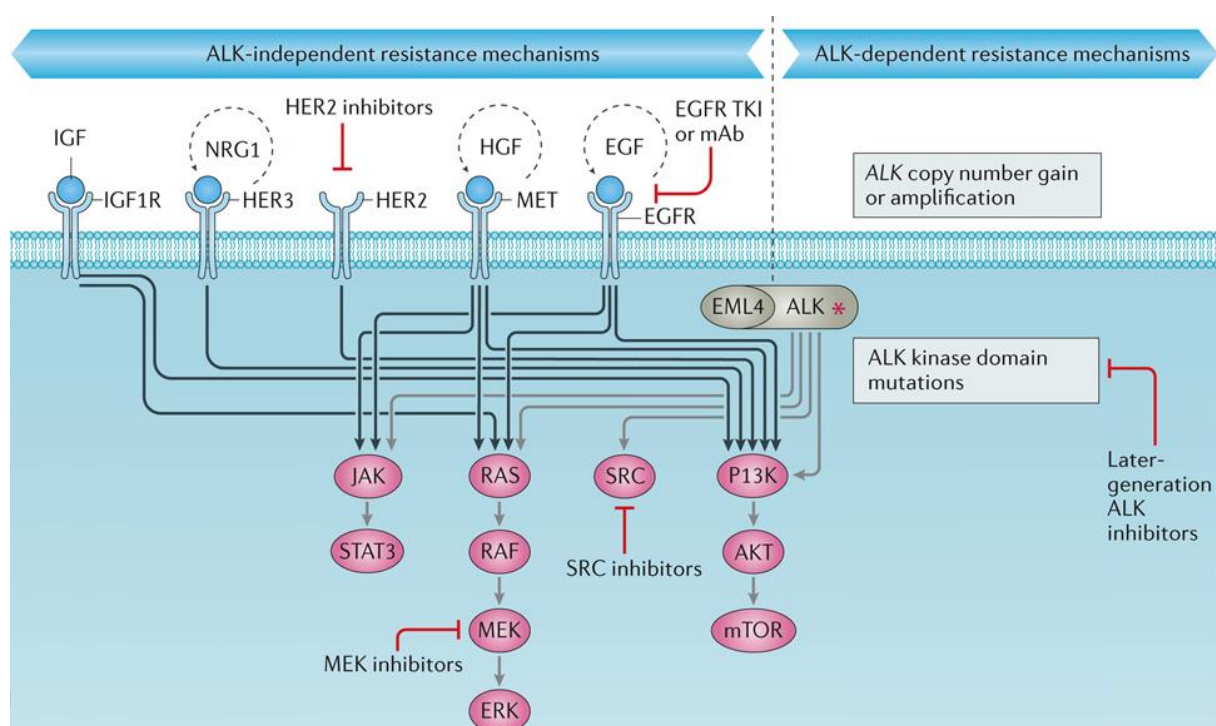


Figure 5 ALK-dependent or ALK-independent resistance mechanisms in ALK+ NSCLC

IGF1R, insulin-like growth factor 1 receptor; HER3, human epidermal growth factor receptor 3; HER2, human epidermal growth factor receptor 2; MET, hepatocyte growth factor receptor; EGFR, epidermal growth factor receptor activate downstream signals through the JAK/STAT, MEK/ERK, and PI3K/AKT and pathways. Modified from Rotow et al.²¹⁴.

1.5.1 ALK-dependent resistance mechanisms

ALK-dependent mechanisms can be induced by secondary mutations in ALK itself impeding the binding of the ALK inhibitor (Table 8). The prototypical mutations leading to ALK TKI resistance are gatekeeper mutations. The first one - L1196M - was reported in a crizotinib resistant EML4-ALK+ NSCLC patient²¹⁵. This mutation was found to occur in 7% of ALK+ NSCLC in a first case series²¹⁶. A further gatekeeper mutation - L1196Q - was initially identified in crizotinib-resistant ALCL cells *in vitro*²¹⁷. The same paper described a I1171N mutant, which was later identified in an adult ALK+ ALCL patient progressing on crizotinib¹²⁸ as well as an alectinib resistant ALK+ NSCLC patient²¹⁸. Sasaki et al. described an F1174L

mutation in the RANBP2-ALK kinase domain of an ALK+ IMT patient²¹⁹. This mutation had earlier been detected in a NB patient²²⁰ and has been shown to reduce ALK sensitivity to crizotinib by increasing ATP binding affinity²²¹. Another mutant variant at the same position, F1174V, was also found in an ALK+ NSCLC patient resistant to crizotinib²¹⁸. The secondary mutation L1152R was reported in a cell line established from a crizotinib resistant ALK+ NSCLC patient²²². A number of other secondary mutations such as S1206Y, G1202R, 1151Tins or G1269A were also found in crizotinib-refractory ALK+ NSCLC patients^{210,223}. Both, S1206Y and G1202R, are located at the solvent front of the kinase domain and interfere with inhibitor binding due to steric hindrance and conformational changes of the kinase. The G1202R mutant is only seen in ~2% of ALK+ NSCLC patients at resistance to early-generation ALK TKIs, but it is the most common resistance mutation (21–43% of cases) in patients treated with later-generation ALK TKIs^{216,224}. G1269A is situated at the end of the ATP-binding pocket of ALK and leads to a decrease in the binding of crizotinib to ALK due to steric hindrance²²³. 1151Tins, F1174C, L1152R and C1156Y near the α C helix do not directly interact with ALK TKI binding and cause resistance via conformational changes that alter kinase activity²¹⁴.

Another ALK-dependent resistance mechanism is amplification of *ALK*. Katayama et al. reported wild type *EML4-ALK* gene amplification in 1/15 patients that progressed on crizotinib²¹⁰. Likewise, Doebele et al. documented wild type *EML4-ALK* gene amplification in 2/12 crizotinib resistant patients²²³. Genomic amplification of the *ALK* locus has also been described to mediate ALK TKI resistance in ALCL cell lines^{225,226}. However, this resistance can be overcome by using increased doses of crizotinib and has not been reported as a resistance mechanism to more potent second-line ALK inhibitors²²⁷.

Table 8 Sensitizing (S) and resistance (R) mutations to ALK inhibitors

Mutation	Biological function	Crizotinib	Alectinib	Certinib	Lorlatinib	Brigatinib
G1123S	Steric hindrance	R	S	R	N/A	N/A
F1127L	Decreased stability of ALK-crizotinib complex	R	S	R	N/A	N/A
1151Tins	Increased ATP affinity for ALK	R	S	R	N/A	N/A
L1152P/R	Loop N-terminal of alpha C	R	S	R	S	S
C1156Y	Loop N-terminal of alpha C, increased kinase activity	R	S	R	S	S
I1171T/N/S	Steric hindrance	R	R	S	N/A	N/A
F1174V/C/L	Conformational changes in the catalytic domain	R	S	R	S	S
V1180L	Gatekeeper residue	R	R	S	N/A	N/A
L1196M/Q	Gatekeeper residue	R	S	S	S	S
L1198F	Near ATP-binding site, steric hindrance	S	R	R	R	S
G1202R	Solvent front, steric hindrance	R	R	R	S	S
D1203N	Solvent front	R	S	S	R	S
S1206C/Y/F	Solvent front	R	S	S	S	R
E1210K	N/A	R	S	S	S	S
F1245C	Near the kinase motif	R	N/A	S	N/A	N/A
G1269A/S	ATP-binding pocket	R	S	S	S	S
R1275Q	ATP-binding pocket	N/A	N/A	R	N/A	N/A

1.5.2 ALK-independent resistance mechanisms

However, ALK-dependent mechanisms described in the previous section account for only approximately 30% of acquired resistance mechanisms noted in relapsed ALK+ NSCLC patients with the rest of the patients relapsing with various ALK-independent mechanisms (**Figure 5**)^{228–230}. ALK-independent resistance is achieved by either activation of alternative RTKs or by triggering downstream signalling components²³¹. These alterations bypass the requirement for ALK activity in the tumour cells². Bypass mechanisms identified thus far, associated with ALK TKI resistance in NSCLC patients, include activation of EGFR²²⁷, HER2²³², KRAS²²³, IGF-1R²³³, SRC²¹⁰ and amplification of *KIT*²²⁷. Aberrantly activated ALK regulates several downstream pathways, including RAS/MAPK²³⁴, PI3K/AKT²³⁵, JAK/STAT²²⁵, PLC/PKC²³⁶ and CRKL/RAP1²³⁷ pathways.

1.6 Approaches to identifying acquired resistance mechanisms to TKIs

Acquired resistance mechanisms to TKIs can be identified by three types of samples or models: 1) Patient tumour samples taken throughout a patient's treatment most importantly at diagnosis and after therapy relapse, 2) mouse cancer models or 3) cancer cell lines established from patient tumour tissue²³⁸.

As a gold standard, putative resistance inducers are identified most often by WES coupled with RNA-Seq, while previously identified biomarkers can be identified by targeted-seq of tumour tissue²³⁸. However, defining a global landscape of resistance mechanisms requires matched presentation-relapse tumour specimens from a sufficiently large number of patients^{238,230,239}. For instance, the cataloguing of epidermal growth factor receptor TKI resistance in NSCLC patients with an incidence rate of 18,252–54,756 newly diagnosed cases per year in the USA is still incomplete with around 30% of relapsed patients currently presenting with 'unknown' resistance mechanisms^{228–230}. This problem is intensified for paediatric malignancies, such as ALK+ ALCL with an incidence rate of approximately 80 newly diagnosed and 16 relapse cases per year in children and adolescents in Europe²⁷ or ALK-driven high-risk NB with an incidence rate of approximately 30 newly diagnosed cases per year²⁴⁰.

This has spurred the development of *in vivo* and *in vitro* experimental approaches that facilitate the proactive identification of resistance mechanisms²³⁸, validation of putative resistance mechanisms or investigation of therapeutic strategies that can re-sensitize the relapsed patients' tumour cells to treatment^{241–243}.

The laboratory mouse (*Mus musculus*) is one of the best *in vivo* models to study disease biology including cancer. In general, three types of mouse models exist: 1) Cell line xenografts, 2) patient-derived xenografts (PDX) derived from tumour explants and 3) genetically engineered mouse models (GEMMs), which can either be transgenic or endogenous²⁴⁴.

With the identification of the importance that tumour heterogeneity and the microenvironment play on acquired resistance to TKIs^{241,245–248}, GEMMs have many advantages compared to cell line xenografts or cell lines²³⁸. GEMMs are also superior to PDXs in terms of microenvironment, as the human stromal components in PDXs are replaced by murine elements and PDXs lack the interaction between immune cells and tumour cells²⁴⁴. However, all GEMMs described to date also exhibit certain shortcomings in mimicking human malignancy arising from the fact that the biology of humans and mice is different²⁴⁹. For example differences in xenobiotic receptor (XR) and cytochrome P450 (CYP) expression levels,

tissue distribution, enzymatic activities, substrate preferences and ligand affinities lead to different rates of drug absorption, distribution, metabolism and excretion in mice and men^{244,250}. In addition, human cells in comparison to mouse cells have decreased cancer susceptibility²⁵¹. Furthermore, there is a species-specific difference in tissue-specific cancer incidence. While mice tend to develop cancer in mesenchymal tissues, most age-related cancers in humans develop in epithelial tissues²⁴⁹. One possible explanation is the replacement of human telomere components with murine ones since telomere dysfunction has an important role in oncogenesis and telomeres maintain chromosomal integrity²⁴⁴.

The most artificial model, which is nevertheless predominantly used, are established cancer cell lines. Even though cancer cell lines are derived from a patient's tumour, those cells that survive the initial culturing process represent only a small proportion of the tumour indicated by the lack of intra-heterogeneity in cell lines^{252–254}. In addition, extended culture can induce genetic and epigenetic modifications with the eventual risk of altering cellular phenotypes²⁵⁵. However, cell line models require far less financial and time commitment compared to *in vivo* models. In addition, the patient population diversity may be better represented *in vitro* as there are typically far more cell lines than PDXs for each disease. For example, while only one paediatric ALK+ ALCL PDX has been described in the literature²⁵⁶, 12 ALK+ ALCL cell lines had been listed by the German Collection of Microorganisms and Cell Cultures (DSMZ) by 2004²⁵⁷; while only two experimentally validated ALK-driven NB PDX models – COG-N-426x (ALK^{F1245C}; MYCN-WT) and COG-N-453x (ALK^{F1174L}; MYCN-amplified) – have been described in the literature, >110 NB cell lines with variable ALK mutation status, had been detailed by 1998²⁵⁸.

In vitro investigations can be further separated into three different types (**Figure 6**) of experimental designs²³⁸. The first type of design involves culturing established cancer cell lines for an extended period of time during which TKI concentrations are gradually increased until resistant clones form (**Figure 6A**). These resistant clones are then compared to the parental TKI sensitive cells to identify potential resistance drivers via molecular and biochemical profiling procedures²³⁸.

The second approach actively generates secondary mutations in the target kinase via random mutagenesis by error-prone PCR²⁵⁹ or by cloning the target kinase cDNA in a mutator strain of competent bacteria²⁶⁰ (**Figure 6B**). Ideally, this process will generate the full spectrum of potential secondary mutations in the target kinase gene. This mixed population of mutant kinase cDNAs should then be transfected or transduced into TKI-sensitive cancer cell lines and cDNAs that induce kinase-dependent resistance will be enriched when the cells are cultured with the respective TKI²³⁸.

The last method focuses on kinase-independent (bypass) mechanisms by individually manipulating the expression level of each gene within the genome via systemic gain- or loss-of-function screen libraries (**Figure 6C, Figure 7**). The main advantages of this approach are the comprehensive scope of the investigation and the unbiased nature of the experiment²³⁸. It relies on pooled cDNA²⁶¹, RNAi²⁶² or Clustered Regularly Interspaced Short Palindromic Repeats (CRISPR)/CRISPR-associated protein 9 (Cas9) libraries²⁶³ (**Figure 7**).

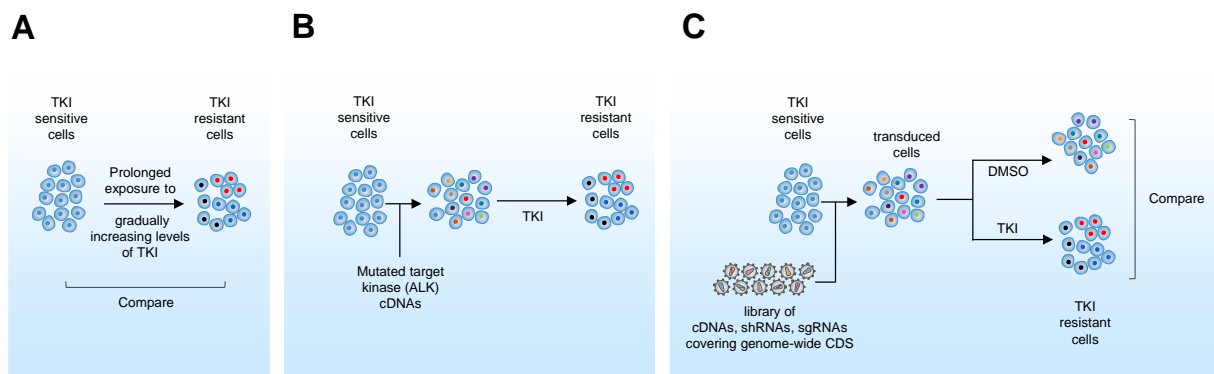


Figure 6 Types of *in vitro* experimental designs to identify putative TKI resistance mechanisms (A) Cancer cells are cultured with gradually increasing concentrations of TKI until TKI resistant cells dominate the population. (B) The target kinase (e.g., ALK) is amplified via error-prone PCR to generate a spectrum of mutated cDNAs that are transfected or transduced into neoplastic cells, which are then exposed to TKIs to select for TKI-resistant clones. (C) Unbiased genome-wide screens can be conducted to artificially induce or repress expression of genes individually to identify those that can induce resistance. See also **Figure 7**.

1.6.1 CRISPR-based genome-wide screens

CRISPR/Cas9 is a gene-editing platform derived from a microbial adaptive immune system²⁶⁴. Several types of CRISPR/Cas systems have been investigated, but the type II system quickly gained popularity as it required only one protein – Cas9, derived from *Streptococcus pyogenes* – to achieve CRISPR RNA-guided DNA recognition and cleavage²⁶⁵⁻²⁶⁶. The first milestone was the discovery that RNA-guided DNA cleavage was only possible when the target DNA sequence was complementary to the CRISPR RNA and possessed a short protospacer adjacent motif (PAM) sequence (5'-NGG for Cas9)²⁶⁵. The second milestone was the discovery that a trans-activating CRISPR RNA (tracrRNA) was essential for CRISPR RNA maturation in the Cas9 system²⁶⁷. The final milestone was the development of a synthetic single guide RNA (sgRNA) that combined the tracrRNA and CRISPR RNA by the addition of a linker loop sequence between the two RNAs²⁶⁵. Soon after CRISPR/Cas9-based loss-of-function (LOF) and gain-of-function (GOF) technologies were developed²⁶⁸⁻²⁷¹ (**Figure 7**).

CRISPR/Cas9-based LOF technologies include CRISPR/Cas9 knockout (CRISPR nuclease = CRISPRn) and CRISPR/dCas9-Krüppel²⁷²-associated box (KRAB) knockdown (CRISPR interference = CRISPRi) technologies (**Figure 7A**). For CRISPR/Cas9-based knockout the Cas9–sgRNA complex is targeted to a specific sequence in the coding region of a gene and cleaves both strands of the DNA^{273,274}. The DNA double-strand break is repaired by non-homologous end joining (NHEJ), an error-prone pathway introducing insertion or deletion mutations that can lead to frameshifts²⁷⁵ and a premature termination codon (PTC) in the expressed transcript, resulting in nonsense-mediated decay (NMD) of the mRNA and aberrant peptide products that are degraded²⁷⁶.

The CRISPR/dCas9-KRAB knockdown system (**Figure 7A**) is based on a catalytically dead Cas9 (dCas9), which is generated when Cas9's two nuclease domains – HNH²⁷⁷ and RuvC-like²⁷⁸ – are mutated²⁶⁴. dCas9 is further fused to a repressor domain such as KRAB. As a result, transcriptional repression is achieved by directly blocking RNA polymerase activity (dCas9) and through effector domain-mediated transcriptional silencing via dCas9-KRAB^{279,280}. The KRAB domain of Kox1, VP16 and p65AD mediates recruitment of Kap1 and HP1 proteins finally leading to transcription silencing through heterochromatin spreading²⁸¹.

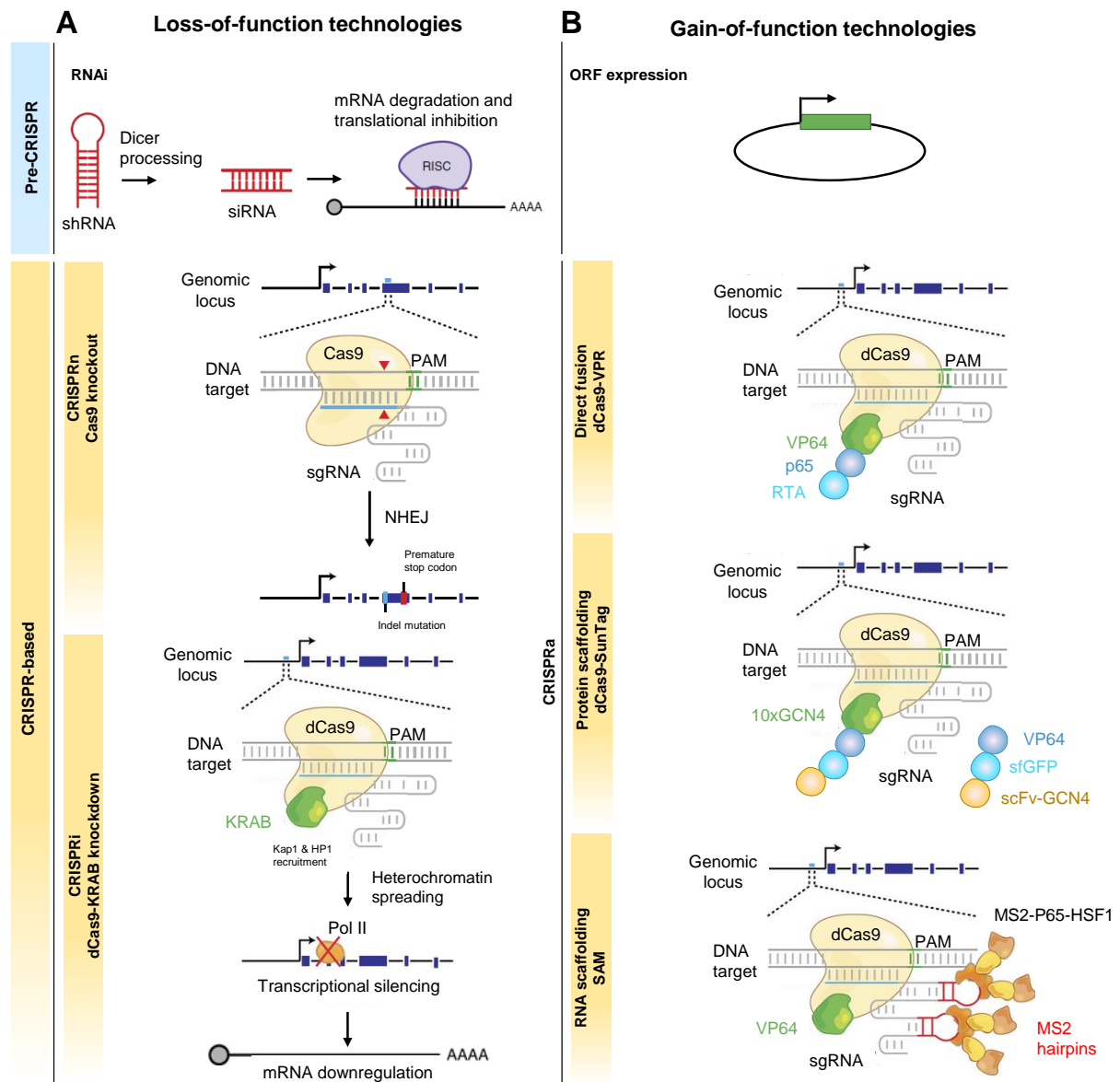


Figure 7 Technologies to perturb gene function in mammalian cells for pooled genetic screens
(A) LOF technologies include RNA interference (RNAi); CRISPR nuclease (CRISPRn), in which Cas9-mediated DNA cleavage directed to the coding region of a gene by a single guide RNA (sgRNA) results in error-prone repair by cellular non-homologous end joining (NHEJ) pathways, thereby disrupting gene function; and CRISPR interference (CRISPRi), in which catalytically dead Cas9 (dCas9) fused to a transcriptional repressor domain (e.g. KRAB) is recruited to the TSS of an endogenous gene, as specified by an sgRNA, to repress transcription.
(B) GOF technologies include overexpression of Open Reading Frames (ORFs) as transgenes; and CRISPR activation (CRISPRa), in which transcriptional activators are recruited via sgRNAs and dCas9 to TSSs of endogenous genes to induce their overexpression. To achieve high levels of overexpression with a single sgRNA, CRISPRa methods recruit more than one transcriptional activator to a given TSS. Multiple activator domains are either directly fused to dCas9 (e.g. VP64, p65 and RTA in the VPR system²⁸²), recruited to a protein scaffold fused to dCas9 (e.g. VP64 fused to superfolder GFP (sfGFP) and an antibody single-chain variable fragment (scFv) targeting a GCN4 epitope, which are recruited to a tandem array of 10 copies of the GCN4 epitope in the SunCas system^{269,283}), or recruited to an RNA scaffold fused to the sgRNA (e.g. p65 and HSF1 transcriptional activation domains fused to MS2 coat protein (MCP), dimers of which are recruited to MS2 RNA hairpins in the Synergistic Activation Mediator (SAM) system²⁷¹). Modified from Kampmann et al.²⁸⁴

CRISPR/Cas9-based GOF technologies include CRISPR activation (CRISPRa) systems such as the CRISPR/dCas9-VP64 overexpression (Synergistic Activation Mediator = SAM) system²⁷¹. Transcriptional activation is achieved by fusion of activator domains such as a tetrameric VP16 (VP64)²⁶⁸ to dCas9, which recruits transcriptional complexes to the TSS of target transcripts as well as an altered sgRNA to recruit accessory transcriptional co-activators (MS2-p65-HSF1) to synergistically interact with the transcriptional complex. Specifically, a hairpin aptamer that selectively binds to the MS2 phage protein was appended to the tetraloop and stem loop no. 2 regions²⁸⁵. Then a separate vector was constructed to express MS2 protein fused to the p65 transcription factor and heat shock transcription factor 1 (HSF1). This allows for additional recruitment of transcriptional activators to the TSS, leading to >500-fold enhanced overexpression in target mRNA levels compared to dCas9-VP64 alone²⁷¹.

The ability to multiplex sgRNAs, and Cas9's capacity to modulate expression of various endogenous genes, inspired the development of CRISPR screen libraries²⁸⁶. The Genome-Scale CRISPR Knock-Out (GeCKO) library was the first genome-wide CRISPR/Cas9-based KO screen library to be published²⁸⁷. As it was demonstrated to be superior compared to RNAi LOF screens (**Figure 7A**), specifically in a TKI resistance research setting, as it identified novel resistance mechanisms against the BRAF inhibitor vemurafenib previously not identified with an RNAi screen²⁶³, many groups have since used it to identify putative drug resistance mechanisms (**Table 9**).

Table 9 Previously published CRISPRn screens on drug resistance using GeCKO A v2 and B libraries²⁸⁸

Selection	Organism	Reference
Vemurafenib	A375	Genome-scale CRISPR-Cas9 knockout screening in human cells ²⁶³
Etoposide	HL60, KBM70	Genetic screens in human cells using the CRISPR-Cas9 system ²⁸⁹
Clostridium septicum α -toxin	mouse embryonic stem cells	Genome-wide recessive genetic screening in mammalian cells with a lentiviral CRISPR-guide RNA library ²⁹⁰
Diphtheria toxin	HeLa	High-throughput screening of a CRISPR/Cas9 library for functional genomics in human cells ²⁹¹
Vemurafenib	A375, HEK293T, BV2	Optimized sgRNA design to maximize activity and minimize off-target effects of CRISPR-Cas9 ²⁹²
Ricin	K562	Genome-Scale CRISPR-Mediated Control of Gene Repression and Activation ²⁶⁹
Sorafenib	Huh7	Genome-wide CRISPR screen reveals SGOL1 as a druggable target of sorafenib-treated hepatocellular carcinoma ²⁹³
Cisplatin	SKOV3, A2780	Loss of ZNF587B and SULF1 contributed to cisplatin resistance in ovarian cancer cell lines based on Genome-scale CRISPR/Cas9 screening ²⁹⁴
Rigosertib	K562	Combined CRISPRi/a-Based Chemical Genetic Screens Reveal that Rigosertib Is a Microtubule-Destabilizing Agent ²⁹⁵

The Weissman group combined CRISPR/Cas9-based KO with CRISPR/dCas9-based activation screens showing accurate complementarity²⁶⁹. A subsequent study by Feng Zhang's group identified mediators of resistance to PLX-4720²⁷¹ by validating CRISPR/dCas9-based activation screens (**Table 10**). This eventually led to the replacement of Open Reading Frame (ORF) overexpression screen technologies (**Figure 7A**), as CRISPR/dCas9-based activation screens hold two key advantages: First, ORF libraries do not replicate the transcript isoform variance. In contrast, guiding dCas9-VP64 upstream of the TSS of genes can induce overexpression of several transcript variants with a single sgRNA²⁷¹. Second, ORF libraries suffer from selection bias as large cDNAs are packaged into lentiviral particles at a much lower efficiency, leading to an overrepresentation of genes with smaller ORFs^{271,296}. In contrast, dCas9-VP64 induces the overexpression of different genes by the 20 bp guide sequence present in the sgRNA.

Table 10 Previously published CRISPRa screens on drug resistance

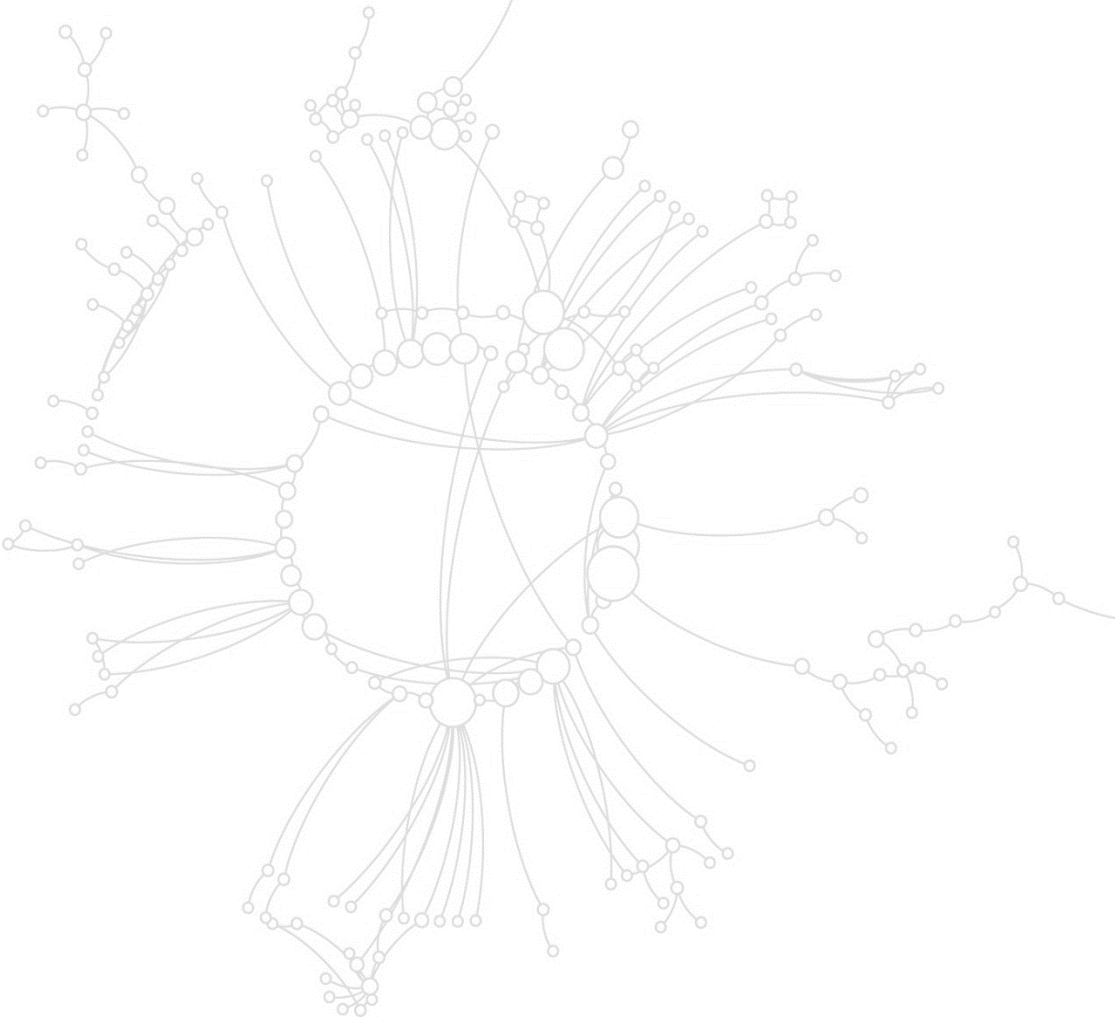
Selection	Organism	Reference
Cytarabine	MOLM14	An Integrated Genome-wide CRISPRa Approach to Functionalize lncRNAs in Drug Resistance ²⁹⁷
Rigosertib	K562	Combined CRISPRi/a-Based Chemical Genetic Screens Reveal that Rigosertib Is a Microtubule-Destabilizing Agent ²⁹⁵
Vemurafenib	A375	Dual direction CRISPR transcriptional regulation screening uncovers gene networks driving drug resistance ²⁹⁸
Vemurafenib	A375	Genome-scale activation screen identifies a lncRNA locus regulating a gene neighbourhood ²⁹⁹
BRAF inhibitor PLX-4720	A375	Genome-scale transcriptional activation by an engineered CRISPR-Cas9 complex ²⁷¹

1.7 Aims of the PhD

This PhD aims to:

- Determine a bypass resistance landscape to ALK inhibition in ALK+ ALCL
- Explore the mechanism by which IL10RA mediates resistance to ALK inhibition in ALK+ ALCL
- Generate and characterize PDX models of ALK+ ALCL
- Explore if PIM1 overexpression mediates resistance to ALK inhibition in ALK-driven NB/ALK+ ALCL
- Establish and validate an assay for the detection of anti-ALK autoantibodies in ALK+ malignancies

CHAPTER 2 Materials & Methods



2.1 Key Reagents and Resources

The reagents or resources (Table 11) and methods described in this chapter of the thesis partly form sections of two separate publications (Trigg, Lee & Prokoph et al.³⁰⁰, Prokoph et al.³⁰¹), which can be found in Appendix 1.

Table 11 Key Reagents and Resources

Reagent or Resource	Source	Identifier
Antibodies		
Anti-GFP antibody	Abcam	Cat#: ab290
Polyclonal anti-Cas9 antibody	Abcam	Cat#: ab204448, 1:2000 dilution
Goat anti-rabbit immunoglobulin/HRP	Agilent technologies	Cat#: P0448, 1:10000 dilution
Rabbit anti-mouse immunoglobulins/HRP	Agilent technologies	Cat#: P0161, 1:10000 dilution
Rabbit anti-human immunoglobulins/HRP	Agilent technologies	Cat#: P0214, 1:100 dilution
Rabbit ALK (D5F3®) XP® antibody	Cell Signalling	Cat#: 3633, 1:1000 dilution
Rabbit Phospho-ALK (Tyr1604) antibody	Cell Signalling	Cat#: 3341, 1:1000 dilution
Rabbit Phospho-STAT3 (Tyr705) antibody	Cell Signalling	Cat#: 9145S, 1:1000 dilution
Rabbit STAT3 antibody	Cell Signalling	Cat#: 4904S, 1:1000 dilution
Rabbit STAT1 antibody	Cell Signalling	Cat#: 9172 S, 1:1000 dilution
Rabbit Phospho-STAT1 (Tyr701) antibody	Cell Signalling	Cat#: 14994 S, 1:1000 dilution
Rabbit Phospho-STAT5 (Tyr694) antibody	Cell Signalling	Cat#: 9359 S, 1:1000 dilution
Mouse STAT5A (4H1) antibody	Cell Signalling	Cat#: 4807 S, 1:1000 dilution
Bond™ Ready-to-Use Primary Antibody Anaplastic Lymphoma Kinase (5A4)	Leica Biosystems Newcastle Ltd	Cat#: PA0306
BOND™ Ready-to-Use Primary Antibody CD30 (JCM182)	Leica Biosystems Newcastle Ltd	Cat#: PA0790
Mouse anti-α-Tubulin	Sigma Aldrich	Cat#: T9026, 1:10000 dilution
Mouse anti-GAPDH	Cell Signalling	Cat#: 97166S, 1:10000 dilution
ALK monoclonal antibody	Thermo Fisher Scientific	Cat#: 35-4300, 1:1000 dilution
Rabbit IL10RA antibody	Abcam	Cat#: ab94811, 1:100 dilution
Rabbit IL10RB antibody	Abcam	Cat#: ab106282, 1:100 dilution
Rabbit IL10 antibody	Abcam	Cat#: ab34843 1:200 dilution
Monoclonal anti-human IgG (Fc specific) antibody	Sigma-Aldrich	Cat#: I6260
Human IgG	Sigma-Aldrich	Cat#: I4506
goat anti-human IgG (H&L) – Affinity Pure, DyLight550 Conjugate	ImmunoReagents	Cat#: GtxMu-003-E2550NHSX
anti-GST antibody	Abcam	Cat#: ab117484
Anti-STAT3 (124H6) antibody	Cell Signalling	Cat#: 9139
Bacteria and Virus Strains		
lenti dCAS-VP64_Blast	²⁷¹ , a gift from Feng Zhang	RRID: Addgene_61425

Reagent or Resource	Source	Identifier
lenti MS2-P65-HSF1_Hygro	²⁷¹ , a gift from Feng Zhang	RRID: Addgene_61426
lenti sgRNA(MS2)_zeo backbone	²⁷¹ , a gift from Feng Zhang	RRID: Addgene_61427
lenti sgRNA(MS2)_puro backbone	²⁷¹ , a gift from Feng Zhang	RRID: Addgene_73795
Human CRISPR Activation Library	²⁷¹ , a gift from Feng Zhang	RRID: Addgene_100000057
lentiCRISPR v2	²⁸⁸ , a gift from Feng Zhang	RRID: Addgene_52961
pMD2.G	A gift from Didier Trono	RRID: Addgene_12259
psPAX2	A gift from Didier Trono	RRID: Addgene_12260
pRSV-Rev	A gift from Didier Trono	RRID: Addgene_12253
pCMVR8.74	A gift from Didier Trono	RRID: Addgene_22036
pLKO.1-puro	³⁰² , a gift from Prof. Bob Weinberg	RRID: Addgene_8453
non-targeting shRNA	³⁰³ , a gift from David Sabatini	RRID: Addgene_1864
pLKO.1 STAT3 shRNA #1	³⁰⁴ , a gift from Roberto Chiarle	TRCN0000020842
pLKO.1 STAT3 shRNA #2	³⁰⁴ , a gift from Roberto Chiarle	TRCN0000020840
pLKO.1_PIM1 shRNA #1	³⁰⁰	TRCN0000010118
pLKO.1_PIM1 shRNA #2	³⁰⁰	TRCN0000199011
FgH1tUTG	³⁰⁵ , a gift from Marco Herold	RRID: Addgene_70183
pHR-SFFV-KRAB-dCas9-P2A-mCherry	²⁶⁹ , a gift from Jonathan Weissman	RRID: Addgene_60954
pSB700 Cerulean-Zhang2.0	³⁰⁶ , a gift from George Church	RRID: Addgene_79378
pSB700 Cerulean-Zhang2.0 puro	²⁹⁷	N/A
pSB700 Cerulean-Zhang2.0 BFP	²⁹⁷	N/A
pSB700 Cerulean-Zhang2.0 RFP	²⁹⁷	N/A
pLVUT-tTR-KRAB	³⁰⁷ , a gift from Patrick Aebischer & Didier Trono	RRID: Addgene_11651
pLVTHM	³⁰⁸ , a gift from Didier Trono	RRID: Addgene_12247
pLVTHM vector containing the H1 promoter ALK-shRNA (A5) cassette	³⁰⁹	N/A
pLX302	³¹⁰ , a gift from David Root	RRID: Addgene_25896
pLX302 IL10RA-V5 puro	³¹¹ , a gift from Kevin Janes	RRID: Addgene_47552
pcDNA™ 3.1 vector	Invitrogen	Cat#: V79020
pcDNA NPM-ALK	a kind gift from Steve Morris	N/A
NEB Stable Competent <i>E. coli</i> (High Efficiency)	New England Biolabs (NEB)	Cat#: C30401
ElectroMAX Stbl4 Competent Cells	Thermo Fisher	Cat#: 11635018
Chemicals, Peptides, and Recombinant Proteins		
T4 PNK	NEB	Cat#: M0201S
10X T4 Ligation Buffer	NEB	Cat#: M0541
BsmB1	NEB	Cat#: R05805
T4 DNA Ligase	NEB	Cat#: M0202S
Pfu DNA Polymerase	Thermo Fisher Scientific	Cat#: EP0571
FastDigest® DpnI	NEB	Cat#: FD1703

Reagent or Resource	Source	Identifier
Agel-HF	NEB	Cat#: R0552S
EcoRI-HF	NEB	Cat#: R0101S
DTT	ThermoFisher	Cat#: 707265ML
SOC Outgrowth Medium	NEB	Cat#: B9020
TransIT-293	MirusBio	Cat#: MIR 2700
Xfect™ Transfection Reagent	Takara Bio	Cat#: 631318
Lipofectamine® 3000 Transfection Reagent	Thermo Fisher Scientific	Cat#: L3000001
Zeocin	InvivoGen	Cat#: Ant-zn-1
Puromycin	Gibco	Cat#: A1113803
Blasticidin	Thermo Fisher Scientific	Cat#: R21001
Hygromycin B	Thermo Fisher Scientific	Cat#: 10687010
Dubbecco's phosphate buffered saline (DPBS)	Sigma-Aldrich	Cat#: D8537
Fetal bovine serum (FBS)	Labtech	Cat#: FCS-SA/500
Dulbecco's Modified Eagle Medium (DMEM), Hi Gluc, pyruvate	Thermo Fisher Scientific	Cat#: 41966029
Roswell Park Memorial Institute (RPMI) 1640	Thermo Fisher Scientific	Cat#: 21875091
Iscove's Modified Dulbecco's Medium (IMDM)	Thermo Fisher Scientific	Cat#: 21980032
Opti-MEM® I Reduced Serum Medium	Thermo Fisher Scientific	Cat#: 51985026
Penicillin/Streptomycin Solution	Thermo Fisher Scientific	Cat#: 15140122
1 x Trypsin- Ethylenediaminetetraacetic acid (EDTA)	Life Technologies	Cat#: 25300054
Insulin-transferrin-selenium	Thermo Fisher Scientific	Cat#: 41400045
Trypan blue	Thermo Fisher Scientific	Cat#: 15250061
Q5® High-Fidelity DNA Polymerase	New England Biolabs	Cat#: M0491S
Herculase II Fusion DNA Polymerase	Agilent	Cat#: 600677
APC-Annexin V	BioLegend	Cat#: 640920
Annexin V Binding Buffer	Thermo Fisher Scientific	Cat#: V13246
Propidium Iodide (PI)	Sigma-Aldrich	Cat#: P4170-10MG
Power SYBR Green PCR Master Mix	ThermoFisher Scientific	Cat#: A25741
Pierce™ RIPA buffer	Thermo Scientific	Cat#: 89900
Immobilon Western Chemiluminescent HRP Substrate	Merck Millipore	Cat#: WBKLS0050
Dimethyl sulfoxide (DMSO)	Sigma-Aldrich	Cat#: D8418
Crizotinib	MedChemExpress	Cat#: HY-50878
Alectinib	MedChemExpress	Cat#: CH5424802
Lorlatinib	MedChemExpress	Cat#: HY-12215
Ceritinib	MedChemExpress	Cat#HY-15656
Brigatinib	MedChemExpress	Cat#: HY-12857
Vinblastine	Sigma-Aldrich	V1377
AZD1208	AstraZeneca	N/A
IBL-101	Inflection Biosciences	N/A
Stattic	MedChemExpress	Cat#: HY-13818
Interleukin-10 human	Sigma-Aldrich	Cat#: H7541-10UG
PhiX Sequencing Control v3	Illumina	Cat#: FC-110-3001
Halt™ Protease Inhibitor Cocktail	Thermo Scientific	Cat#: 87786
Halt™ Phosphatase Inhibitor Cocktail	Thermo Scientific	Cat#: 78420
Restore™ PLUS Western Blot Stripping Buffer	Thermo Scientific	Cat#: 46430
IDetect Super Stain System – HRP	Empire Genomics	Cat#: IDST1007
Target Retrieval Solution, Citrate pH6.1 (10X)	Agilent Dako	Cat#: S2369
Hematoxylin Solution, Gill No. 3	Sigma-Aldrich	Cat#: GHS332
3,3'-Diaminobenzidine (DAB) substrate	Sigma-Aldrich	Cat#: D4293
Aquatex	Merck	Cat#: 108562
Faramount mounting medium	Dako	Cat#: S302580
StabilGuard® Choice	SurModics	Cat#: SG02
DY-633 carboxylic acid carrier dye	Dyomics	Cat#: 633-00

Reagent or Resource	Source	Identifier
ALK protein	Thermo Fisher Scientific	Cat#: PR7396B
Glutathione S-Transferase (GST)	GeneScript	Cat#: Z02039
RNase A	Roche	Cat#: 10109169001
DNase I	Thermo Scientific	Cat#: 18068015
Proteinase K	Thermo Scientific	Cat#: EO0491
Dynabeads™ Protein G	Thermo Scientific	Cat#: 10004D
Lymphoprep	STEMCELL TECHNOLOGIES	Cat#: 07801
cComplete™ Mini EDTA-free Protease Inhibitor Cocktail	Roche	Cat#: 11836170001
Matrigel matrix	Corning	Cat#: 354277
Critical Commercial Assays		
QIAprep Spin Plasmid Kit	Qiagen	Cat#: 27104
EndoFree Plasmid Maxi Kit	Qiagen	Cat#: 12362
RNeasy Plus Mini Kit	Qiagen	Cat#: 74134
High-Capacity RNA-to-cDNA™ Kit	Applied Biosystems	Cat#: 4387406
Q5 High-Fidelity PCR Kit	NEB	Cat#: E0555S
CellTiter-Glo	Promega	Cat#: G7572
CellTiter-Blue® Cell Viability Assay	Promega	Cat#: G8081
Pierce™ BCA Protein Assay Kit	Thermo Scientific	Cat#: 23225
QIAamp DNA Blood Maxi Kit	Qiagen	Cat#: 51194
QIAamp DNA Mini Kit	Qiagen	Cat#: 51304
Q5 High-Fidelity PCR Kit	NEB	Cat#: E0555S
Zymo DNA Clean and Concentrator-5	Zymo research	Cat#: D4003
KAPA Library Quantification Kit	Kapa Biosystems	Cat#: Q32850
TruSeq Stranded mRNA kit	Illumina	Cat#: 20020595
AEC Substrate Kit	BDPharmingen	Cat#: 551015
Avidin/Biotin Blocking Kit	Vector Laboratories	Cat#: SP2001
QIAquick PCR Purification Kit	Qiagen	Cat#: 28106
AMIDot™ Activation Diluent	Cambridge Life Sciences	Cat#: N7214D
AUTOZYME™ RF Wash Buffer	Cambridge Life Sciences	Cat#: N7206D
AUTOZYME™ RF Sample Diluent	Cambridge Life Sciences	Cat#: N7015D
Deposited Data		
CRISPR overexpression screens sgRNA Counts in ALCL cells treated with DMSO or crizotinib	(Prokoph et al.) ³⁰¹	Table S9
CRISPR knockout screens sgRNA Counts in ALCL cells treated with DMSO or crizotinib	(Prokoph et al.) ³⁰¹	Table S10
CRISPR overexpression screens sgRNA Counts in NB cells treated with DMSO, brigatinib or ceritinib	(Trigg, Lee & Prokoph et al.) ³⁰⁰	Supplementary Data 1, Supplementary Data 2
CRISPR knockout screens sgRNA Counts in ALCL cells	³¹²	Supplementary Data 5 Supplementary Data 6
RNA-seq from 2 ALK inhibitor resistant and 2 chemotherapy relapsed ALK+ ALCL patients	(Prokoph et al.) ³⁰¹	N/A
STAT3 ChIP-seq for CD4+ T-cells	³¹³	GEO: GSE21669
STAT3 ChIP-seq for ALCL cell lines	³⁰⁴	GEO: GSE117164
Expression profiling by array from 23 ALK+ ALCL patients, 12 reactive lymph nodes	³¹⁴	GEO: GSE78513
Expression profiling by array from 67 AITL, 73 PTCL-NOS, 17 ALK+ and 18 ALK- ALCL patients; as well as T cells from 9 healthy individuals.	³¹⁵	GEO: GSE58445
Expression profiling by array from 6 AITL, 28 PTCL-NOS, 2 ALK+ and 4 ALK- ALCL patients; as well as T cells from 10 healthy individuals.	³¹⁶	GEO: GSE6338

Reagent or Resource	Source	Identifier
Expression profiling by array from 5 ALK+ and 4 ALK- ALCL patients, 23 T cells and 3 ALK+ ALCL cell lines.	317	GEO: GSE14879
Expression profiling by array from 36 AITL, 45 PTCL-NOS, 20 ALK+, 9 ALK- ALCL patients; as well as 10 T cells and 3 T-cell control cell lines.	318	GEO: GSE19069
Expression profiling by array from 8 PTCL-NOS, 10 ALK+ and 13 ALK- ALCL patients	319	GEO: GSE65823
Expression profiling by array from 61 lymphoma cell lines	320	GEO: GSE94669
Expression profiling by array from 4 ALK+, 2 ALK- and 4 T-cell control cell lines	321	GEO: GSE107951
Expression profiling by array from doxycycline induced or non-induced TS and SU-DHL-1 cells. Expression profiling by array from ALK inhibitor treated TS cells.	322	GEO: GSE6184
Experimental Models: Cell Lines		
Human: DEL (Male, 12 years)	Deutsche Sammlung von Mikroorganismen und Zellkulturen (DSMZ)	Cat#: ACC 338, RRID: CVCL_1170
Human: KARPAS-299 (Male, 25 years)	European Collection of Authenticated Cell Cultures (ECACC)	Cat#: 06072604, RRID: CVCL_1324
Human: SU-DHL-1 (Male, 10 years)	DSMZ	Cat#: ACC 356, RRID: CVCL_0538
Human: SUP-M2 (Female, 5 years)	DSMZ	Cat#: ACC 509, RRID: CVCL_2209
Human: COST (Male, 4 years)	a gift from Roberto Chiarle	RRID: CVCL_9491
Human: TS (Female, 5 years)	³²³ , a gift from Roberto Chiarle	RRID: CVCL_B228
Human: JB6 (Male, 12 years)	a gift from Roberto Chiarle	RRID: CVCL_H633
Human: ManGoSteen = MGS (Female, 7 years)	(Prokoph & Matthews et al., unpublished)	RRID: N/A
Human: MaToKe = MTK (Male, 5 years)	(Prokoph & Matthews et al., unpublished)	RRID: N/A
Human: Mac-2A (Male, 47 years)	³²⁴ , a gift from Olaf Merkel	RRID: CVCL_H637
Human: FE-PD (Female, 46 years)	DSMZ	RRID: CVCL_H614
Human: CHLA-20 (Female, 2 years)	COG	RRID: CVCL_6602
Human: CHLA-90 (Male, 6 years)	COG	RRID: CVCL_6610
Human: CHLA-95 (Female)	COG	RRID: CVCL_6611
Human: CHLA-171 (Male, 8 years)	COG	RRID: CVCL_6597
Human: COG-N-426 (Felix-CL, Male)	COG	RRID: CVCL_LF58
Human: GI-ME-N (Female, 3 years)	DSMZ	Cat#: ACC654; RRID: CVCL_1232
Human: KELLY (Female, 1 year)	ECACC	Cat#: 92110411; RRID: CVCL_2092
Human: LAN-5 (Male, 4 months)	COG	RRID: CVCL_0389
Human: LAN-6 (Male, 6 years)	COG	RRID: CVCL_1363
Human: NB-1643 (Male, 3 years)	COG	RRID: CVCL_5627
Human: NBL-S (Male, 3 years)	DSMZ	Cat#: ACC656; RRID: CVCL_2136
Human: NGP (Male, 2 years)	DSMZ	Cat#: ACC676; RRID: CVCL_2141
Human: SH-SY5Y (Female, 4 years)	ECACC	Cat#: 94030304; RRID: CVCL_0019
Human: LM1 (Female, 13 years)	³²⁵	N/A
Human: HEK293T (Female)	Invitrogen	Cat#: R70007, RRID: CVCL_6911
Monkey: COS-1 (Male)	DSMZ	Cat#: ACC63, RRID: CVCL_0223
Human: DEL CR (Male, 12 years)	(Prokoph et al.) ³⁰¹	N/A
Human: DEL AR (Male, 12 years)	(Prokoph et al.) ³⁰¹	N/A

Reagent or Resource	Source	Identifier
Human: KARPAS-299 CR (Male, 25 years)	²¹⁷ , a gift from Luca Mogni	RRID: CVCL_V404
Human: KARPAS-299 AR (Male, 25 years)	³²⁶ , a gift from Luca Mogni	N/A
Human: KARPAS-299 BR (Male, 25 years)	³²⁷ , a gift from Luca Mogni	N/A
Human: KARPAS-299 LR (Male, 25 years)	³²⁸ , a gift from Luca Mogni	N/A
Human: SU-DHL-1 CR (Male, 10 years)	(Prokoph et al.) ³⁰¹	N/A
Human: SU-DHL-1 AR (Male, 10 years)	(Prokoph et al.) ³⁰¹	N/A
Human: SUP-M2 CR (Female, 5 years)	²¹⁷ , a gift from Luca Mogni	RRID: CVCL_V405
Human: SUP-M2 AR (Female, 5 years)	(Prokoph et al.) ³⁰¹	N/A
Human: SUP-M2 BR (Female, 5 years)	³²⁷	N/A
Human: SUP-M2 LR (Female, 5 years)	³²⁸ , a gift from Luca Mogni	N/A
Human: stable doxycycline inducible NPM1-ALK shRNA TS (Female, 5 years)	³²³ , a gift from Roberto Chiarle	N/A
Human: stable doxycycline inducible NPM1-ALK shRNA SU-DHL-1 (Male, 10 years)	³²³ , a gift from Roberto Chiarle	N/A
Experimental Models: Organisms/Strains		
C.B.17/IcrHanHsd-Prkdc (<i>Mus musculus</i>)	Envigo	Cat#: 88304F
NOD.Cg-Prkdcscid Il2rgtm1Wjl/SzJ (<i>Mus musculus</i>)	Charles River	Cat#005557; RRID: IMSR_ARC:NSG
MGS-A-x	(Prokoph & Matthews et al., unpublished)	RRID: N/A
Software and Algorithms		
FlowJo 10	Treestar	https://www.flowjo.com/
R Statistical Software 3.6	N/A	https://www.r-project.org/
Inkscape 0.92.4	N/A	https://inkscape.org/
MAGeCK	³²⁹	https://sourceforge.net/p/mageck/wiki/Home/
MAGeCK-VISPR	³²⁹	http://bitbucket.org/liulab/mageck-vispr
Salmon	³³⁰	https://github.com/CO-MBINE-lab/salmon
tximport	³³¹	https://bioconductor.org/packages/release/bioc/html/tximport.html
edgeR	³³²	https://bioconductor.org/packages/release/bioc/html/edgeR.html
DESeq2	³³³	http://bioconductor.org/packages/release/bioc/html/DESeq2.html
biomaRt	³³⁴	http://bioconductor.org/packages/release/bioc/html/biomaRt.html
fgsea	³³⁵	http://bioconductor.org/packages/release/bioc/html/fgsea.html
topGO	³³⁶	https://bioconductor.org/packages/release/bioc/html/topGO.html

Reagent or Resource	Source	Identifier
SAM Cas9 activator tool	Zhang lab	http://sam.genome-engineering.org/database/
CRAN: survminer	337	https://cran.r-project.org/web/packages/survminer/index.html
CRAN: survival package in R	338	https://cran.r-project.org/web/packages/survival/index.html
GraphPad Prism 8.2	GraphPad	www.graphpad.com
SRA toolkit	National Center for Biotechnology Information (NCBI)	https://github.com/ncbi/sra-tools
SAMtools	339	http://samtools.sourceforge.net/
Bowtie2	340	http://bowtie-bio.sourceforge.net/bowtie2/index.shtml
BEDTools	341	https://sourceforge.net/projects/bedtools/
IGV	342,343	http://software.broadinstitute.org/software/igv/
GEOquery	344	https://bioconductor.org/packages/release/bioc/html/GEOquery.html
oligo	345	https://www.bioconductor.org/packages/release/bioc/html/oligo.html
arrayQualityMetrics	346	https://bioconductor.org/packages/release/bioc/html/arrayQualityMetrics.html
AnnotationDbi	347	https://bioconductor.org/packages/release/bioc/html/AnnotationDbi.html
limma	348	https://bioconductor.org/packages/release/bioc/html/limma.html
beadarray	349	https://www.bioconductor.org/packages/release/bioc/html/beadarray.html
illuminaHumanv4.db	350	http://bioconductor.org/packages/release/data/annotation/html/illuminaHumanv4.db.html
Human Reference Genome (GRCh38.p12)	Genome Reference Consortium	https://www.ncbi.nlm.nih.gov/assembly/GCF_000001405.38
GENCODE transcriptome annotation version v29	351	https://www.encodegenes.org/human/release_29.html
Human Reference Genome (hg19)	Genome Reference Consortium	https://www.ncbi.nlm.nih.gov/grc/human
Mouse Reference Genome (mm10)	Genome Reference Consortium	https://www.ncbi.nlm.nih.gov/grc/mouse
KEGG: Kyoto Encyclopedia of Genes and Genomes	352	https://www.genome.jp/kegg

Reagent or Resource	Source	Identifier
PrimerBLAST	NCBI	https://www.ncbi.nlm.nih.gov/tools/primer-blast/
PrimerBank	353	https://pga.mgh.harvard.edu/primerbank/
Other		
FACSAria™ Fusion 2 flow cytometer	BD Bioscience	N/A
2100 BioAnalyzer System	Agilent	N/A
Illumina NextSeq500	Illumina	N/A
QuantStudio™ 6 Flex Real-Time PCR System	ThermoFisher	N/A
Accuri C6 flow cytometer	BD Bioscience	N/A
ABI Veriti Thermal Cycler	Applied Biosystems	N/A
30-gauge hypodermic Agani™ needle	VWR	Cat#: 613-5373
Plastic feeding tubes (22ga (black) x 38mm)	Instech Laboratories	Cat#: FTP-22-38
70 µM nylon Falcon™ cell strainer	Thermo Fisher Scientific	Cat#: 352350
5 mL Plastipak™ syringe	Thermo Fisher Scientific	Cat#: 302187
Minisart filters (0.45 µm pore size)	Merck Millipore	Cat#: 16555K
Minisart filters (0.2 µm pore size)	Sartorius Stedim Biotech	Cat#: 17823K
Vivaspin centrifugal filter column with a molecular weight cut-off of 3 kDa	Sartorius Stedim Biotech	Cat#: VS0191
SpectraMax i3	Molecular Devices	N/A
Mini-Protean TGX Precast Gels	Bio-Rad	Cat#: 4561033
Trans-Blot Turbo Transfer Pack	Bio-Rad	Cat#: 1704156
Trans-Blot Turbo Transfer System	Bio-Rad	N/A
Gene Pulser II Electroporation System	Bio-Rad	N/A
Flat-bottom 96-well plates	Corning	Cat#: 167008
96 well V-bottom plates	Greiner bio-one	Cat#: 651201
Black 96-well Cellstar plate	Greiner bio-one	Cat#: 655090
2D-Epoxy functionalized glass slide	PolyAN Molecular Surface Engineering	Cat#: 10400221
3D-Epoxy functionalized glass slide	PolyAN Molecular Surface Engineering	Cat#: 10400205
3D-NHS functionalized glass slide	PolyAN Molecular Surface Engineering	Cat#: 10400405
2D-Aldehyde functionalized glass slide	PolyAN Molecular Surface Engineering	Cat#: 10400325
3D-Aldehyde functionalized glass slide	PolyAN Molecular Surface Engineering	Cat#: 10400305
Dako Pen	Dako	Cat#: S2002
Superfrost™ microscope slides	Thermo Fisher Scientific	Cat#: 10143560W90
Cytocentrifuge	Shandon	N/A
Automated slide processor ZenitUP	A. Menarini Diagnostics	N/A
Port Array 5000TM	Aurora Photonics	N/A
Nano-Plotter™ NP2.1	GeSiM	N/A
AIRWIN ultrasonic humidifier	BOGA Gerätetechnik	N/A
programmable temperature controller	PolyScience	N/A
Bioruptor® Pico	Diagenode	N/A
Nanodrop 1000	ThermoFisher	N/A
LAS-4000 Image Analyzer	Fujifilm/Raytek	N/A
Water-sensitive paper	Quantifoil Instruments	Cat#: 3100-0011
15-mL polypropylene centrifuge tubes	Sarstedt	Cat#: CEN255
Sonication beads	Diagenode	Cat#: C03070001
High sensitivity D1000 ScreenTape	Agilent	N/A

2.2 Patient samples

Patient samples utilized in this thesis include samples collected from patients enrolled to clinical trials (Table 12).

Table 12 Clinical trials from which samples have been acquired
(* as stated on the ClinicalTrials.gov webpage).

NIH study trial registration no.	Description	Study timeframe*	Disease	Patients	Experiment purpose
NCT00006455	ALCL99: Combination chemotherapy in treating children with ALCL	Dec 1999 – N/A	ALCL	42	TMA
N/A	NHL-BFM95	N/A	ALCL	24	TMA
N/A	NHL-BFM90	N/A	ALCL	26	TMA
NCT02613962	MAPPYACTS: Proof -of - concept study to stratify targeted therapies adapted to molecular profiling	Dec 2005 – Dec 2020	ALCL	4	RNA-seq

2.2.1 NHL-BFM90 trial cohort

The BFM group study NHL-BFM90³³ enrolled paediatric patients with B or T-cell NHL, including paediatric ALCL patients, to test increasing doses of methotrexate. From this study, archival paraffin-embedded tissue blocks were used to create tissue microarrays (TMAs) containing cores selected from representative tumour areas as determined by a consultant histopathologist from hematoxylin and eosin–stained sections.

FFPE tissue specimens from individuals with ALK+ ALCL treated in the NHL-BFM90³³ trial were obtained from both male (n = 19) and female (n = 7) paediatric subjects (Table 13) with informed consent and in accordance with the Declaration of Helsinki. The study was approved by the institutional ethics committee of the primary investigator of the NHL-BFM study group. Patients with completely resected Stage 1 disease were treated with different chemotherapy regimens and as such were excluded from this study. Eligibility was confirmed by demonstration of NPM1-ALK positivity of the tumour either by NPM1-ALK polymerase chain reaction, two-color fluorescence in situ hybridization for the t(2;5) or nuclear and cytoplasmic staining for ALK. Staging procedures included bone marrow aspiration cytology and a spinal tap. Bone marrow involvement was defined by cytologically detectable ALCL cells, irrespective of their number. The patient’s treatment consisted of a cytoreductive prephase followed by six chemotherapy courses, as previously described³³.

Table 13 Clinical Information of Paediatric ALCL Patients Recruited onto the NHL-BFM90 Trial

Case no.	Sex	Age group (in years)	Diagnosis	Study	Relapse	Death
1	F	≥ 10	ALCL, ALK+	NHL-BFM90	no	no
2	M	< 10	ALCL, ALK+	NHL-BFM90	no	no
3	M	< 10	ALCL, ALK+	NHL-BFM90	no	no
4	M	< 10	ALCL, ALK+	NHL-BFM90	no	no
5	M	≥ 10	ALCL, ALK+	NHL-BFM90	no	no
6	M	≥ 10	ALCL, ALK+	NHL-BFM90	no	no
7	F	≥ 10	ALCL, ALK+	NHL-BFM90	no	no
8	F	≥ 10	ALCL, ALK+	NHL-BFM90	no	no
9	M	< 10	ALCL, ALK+	NHL-BFM90	no	no
10	M	≥ 10	ALCL, ALK+	NHL-BFM90	no	no
11	M	≥ 10	ALCL, ALK+	NHL-BFM90	no	no
12	F	≥ 10	ALCL, ALK+	NHL-BFM90	no	no
13	M	< 10	ALCL, ALK+	NHL-BFM90	no	no
14	M	< 10	ALCL, ALK+	NHL-BFM90	no	no
15	M	< 10	ALCL, ALK+	NHL-BFM90	no	no
16	F	≥ 10	ALCL, ALK+	NHL-BFM90	no	no
17	M	< 10	ALCL, ALK+	NHL-BFM90	no	no
18	F	< 10	ALCL, ALK+	NHL-BFM90	yes	yes
19	M	≥ 10	ALCL, ALK+	NHL-BFM90	no	no
20	M	< 10	ALCL, ALK+	NHL-BFM90	no	no
21	M	≥ 10	ALCL, ALK+	NHL-BFM90	yes	no
22	F	< 10	ALCL, ALK+	NHL-BFM90	yes	no
23	M	< 10	ALCL, ALK+	NHL-BFM90	no	no
24	M	≥ 10	ALCL, ALK+	NHL-BFM90	yes	no
25	M	≥ 10	ALCL, ALK+	NHL-BFM90	no	no
26	M	< 10	ALCL, ALK+	NHL-BFM90	yes	no

2.2.2 NHL-BFM95 trial cohort

Given the high risk of short-term side effects associated with methotrexate⁵¹, lower concentrations of methotrexate administered in shorter pulses were applied in a subsequent BFM group study, NHL-BFM95⁹⁴. From this study, archival paraffin-embedded tissue blocks were used to create TMAs containing cores selected from representative tumour areas as determined by a consultant histopathologist, from hematoxylin and eosin–stained sections.

FFPE tissue specimens from individuals with ALK+ ALCL treated in the NHL-BFM95⁹⁴ trial were obtained from both male (n = 20) and female (n = 4) paediatric subjects (**Table 14**) with informed consent and in accordance with the Declaration of Helsinki. The study was approved by the institutional ethics committee of the primary investigator of the NHL-BFM study group. Patients with completely resected Stage 1 disease were treated with different chemotherapy-regimens and as such were excluded from this study. Eligibility was confirmed by demonstration of NPM1-ALK positivity of the tumour either by NPM1-ALK polymerase chain reaction, two-color fluorescence in situ hybridization for the t(2;5) or nuclear and cytoplasmic staining for ALK. Staging procedures included bone marrow aspiration cytology and a spinal tap. Bone marrow involvement was defined by cytologically detectable ALCL cells, irrespective of their number. The patient's treatment consisted of a cytoreductive prephase followed by six chemotherapy courses, as previously described³³.

Table 14 Clinical Information of Paediatric ALCL Patients Recruited onto the NHL-BFM95 Trial

Case no.	Sex	Age group (in years)	Diagnosis	Study	Relapse	Death
1	M	>= 10	ALCL, ALK+	NHL-BFM95	no	no
2	M	< 10	ALCL, ALK+	NHL-BFM95	no	no
3	M	>= 10	ALCL, ALK+	NHL-BFM95	no	no
4	M	< 10	ALCL, ALK+	NHL-BFM95	yes	no
5	M	>= 10	ALCL, ALK+	NHL-BFM95	no	no
6	M	< 10	ALCL, ALK+	NHL-BFM95	no	no
7	F	>= 10	ALCL, ALK+	NHL-BFM95	no	no
8	M	< 10	ALCL, ALK+	NHL-BFM95	yes	no
9	M	< 10	ALCL, ALK+	NHL-BFM95	yes	no
10	M	>= 10	ALCL, ALK+	NHL-BFM95	no	no
11	M	< 10	ALCL, ALK+	NHL-BFM95	yes	yes
12	M	>= 10	ALCL, ALK+	NHL-BFM95	no	no
13	M	>= 10	ALCL, ALK+	NHL-BFM95	yes	no
14	M	>= 10	ALCL, ALK+	NHL-BFM95	no	no
15	M	< 10	ALCL, ALK+	NHL-BFM95	no	no
16	M	>= 10	ALCL, ALK+	NHL-BFM95	no	no
17	F	< 10	ALCL, ALK+	NHL-BFM95	yes	yes
18	M	< 10	ALCL, ALK+	NHL-BFM95	no	yes
19	M	< 10	ALCL, ALK+	NHL-BFM95	no	no
20	M	>= 10	ALCL, ALK+	NHL-BFM95	yes	no
21	M	< 10	ALCL, ALK+	NHL-BFMV95	yes	no
22	F	>= 10	ALCL, ALK+	NHL-BFMV95	no	no
23	F	< 10	ALCL, ALK+	NHL-BFMV95	yes	no
24	M	>= 10	ALCL, ALK+	NHL-BFMV95	no	no

2.2.3 ALCL99 trial cohort

The European intergroup trial ALCL99²⁸ (NCT00006455) is a randomized phase III trial that is studying several different regimens of combination chemotherapy to compare how well they work in treating children with ALCL. The study was approved by the institutional ethics committee of the primary investigator of the NHL-BFM study group. Patients with completely resected Stage 1 disease were treated with different chemotherapy-regimens and as such were excluded from this study. Eligibility was confirmed by demonstration of NPM1-ALK positivity of the tumour either by NPM1-ALK polymerase chain reaction, two-color fluorescence in situ hybridization for the t(2;5) or nuclear and cytoplasmic staining for ALK. Staging procedures included bone marrow aspiration cytology and a spinal tap. Bone marrow involvement was defined by cytologically detectable ALCL cells, irrespective of their number. The patient's treatment consisted of a cytoreductive prephase followed by six chemotherapy courses, as previously described³³.

From this study, archival paraffin-embedded tissue blocks were used to create TMAs containing cores selected from representative tumour areas as determined by a consultant histopathologist, from hematoxylin and eosin-stained sections. FFPE tissue specimens from individuals with ALK+ ALCL treated in the ALCL99 trial were obtained from both male (n = 28) and female (n = 14) paediatric subjects (**Table 15**) with informed consent and in accordance with the Declaration of Helsinki.

In addition, serum or plasma samples from individuals with ALK+ ALCL treated in the ALCL99 trial were obtained from both male (n = 53) and female (n = 40) paediatric subjects (**Table 40**) with informed consent and in accordance with the Declaration of Helsinki.

Table 15 Clinical Information of Paediatric ALCL Patients Recruited onto the ALCL99 Trial that provided FFPE tissue specimens

Case no.	Sex	Age group (in years)	Diagnosis	Study	Relapse	Death
1	M	>= 10	ALCL, ALK+	ALCL99	yes	no
2	M	>= 10	ALCL, ALK+	ALCL99	yes	no
3	F	>= 10	ALCL, ALK+	ALCL99	no	no
4	M	>= 10	ALCL, ALK+	ALCL99	no	no
5	M	< 10	ALCL, ALK+	ALCL99	yes	no
6	M	>= 10	ALCL, ALK+	ALCL99	yes	no
7	F	>= 10	ALCL, ALK+	ALCL99	no	no
8	M	>= 10	ALCL, ALK+	ALCL99	no	no
9	M	>= 10	ALCL, ALK+	ALCL99	no	no
10	M	< 10	ALCL, ALK+	ALCL99	yes	no
11	M	>= 10	ALCL, ALK+	ALCL99	no	no
12	M	>= 10	ALCL, ALK+	ALCL99	yes	no
13	M	>= 10	ALCL, ALK+	ALCL99	no	no
14	M	>= 10	ALCL, ALK+	ALCL99	no	no
15	M	>= 10	ALCL, ALK+	ALCL99	yes	no
16	F	>= 10	ALCL, ALK+	ALCL99	yes	no
17	F	>= 10	ALCL, ALK+	ALCL99	no	no
18	M	>= 10	ALCL, ALK+	ALCL99	no	no
19	M	< 10	ALCL, ALK+	ALCL99	yes	no
20	M	>= 10	ALCL, ALK+	ALCL99	no	no
21	M	>= 10	ALCL, ALK+	ALCL99	yes	yes
22	M	>= 10	ALCL, ALK+	ALCL99	no	no
23	F	< 10	ALCL, ALK+	ALCL99	no	no
24	F	>= 10	ALCL, ALK+	ALCL99	no	no
25	F	>= 10	ALCL, ALK+	ALCL99	no	no
26	M	>= 10	ALCL, ALK+	ALCL99	no	no
27	F	>= 10	ALCL, ALK+	ALCL99	no	no
28	M	< 10	ALCL, ALK+	ALCL99	no	no
29	F	>= 10	ALCL, ALK+	ALCL99	no	no
30	M	>= 10	ALCL, ALK+	ALCL99	no	no
31	M	< 10	ALCL, ALK+	ALCL99	no	no
32	M	>= 10	ALCL, ALK+	ALCL99	yes	no
33	F	>= 10	ALCL, ALK+	ALCL99	yes	yes
34	F	>= 10	ALCL, ALK+	ALCL99	no	yes
35	F	>= 10	ALCL, ALK+	ALCL99	yes	no
36	M	>= 10	ALCL, ALK+	ALCL99	no	no
37	F	< 10	ALCL, ALK+	ALCL99	no	no
38	M	>= 10	ALCL, ALK+	ALCL99	no	yes
39	F	>= 10	ALCL, ALK+	ALCL99	yes	yes
40	M	>= 10	ALCL, ALK+	ALCL99	yes	no
41	M	< 10	ALCL, ALK+	ALCL99	no	no
42	M	< 10	ALCL, ALK+	ALCL99	yes	no

2.2.4 UK cohort

FFPE tissues, bone marrow, peripheral blood and related clinical information from a female (n = 1) paediatric patient with ALK+ ALCL (**Table 16**) were obtained after written informed parental consent and according to the Declaration of Helsinki. The study was approved by the Huntington research ethics committee (no. 07/Q0104/16).

Table 16 Clinical Information of the Paediatric ALCL Patient from the UK Cohort

ALCL99 = cyclophosphamide, methotrexate, ifosfamide, etoposide, cytarabine, doxorubicin; CYVE³⁵⁴ = cytarabine, etoposide; N/A = not applicable; VBL = vinblastine.

Characteristics	Patient 1	Patient 2
Sex	F	M
Age at diagnosis	6 years	5 years
Stage at diagnosis	4	4
CNS involvement at diagnosis	No	No
CNS involvement at chemotherapy relapse/refractoriness	Yes	No
CNS involvement at crizotinib relapse/refractoriness	Yes	Yes
1 st -line treatment	ALCL99	ALCL99
2 nd -line treatment	VBL	CYVE
3 rd -line treatment	VBL + iv cytarabine/etoposide with intrathecal hydrocortisone/methotrexate/cytarabine	Crizotinib + intrathecal chemotherapy
4 th -line treatment	VBL + Crizotinib + intrathecal hydrocortisone / methotrexate / cytarabine	CYVE
5 th -line treatment	SCT	Vinblastine + steroids
6 th -line treatment	Crizotinib	N/A
7 th -line treatment	Brentuximab vedotin + VBL	N/A
Samples used for engraftment into NSG mice	Bone marrow taken after 7 th treatment line	Pleural effusion taken before 3 rd treatment line

2.2.5 MAPPYACTS trial cohort

Molecular Profiling for Pediatric and Young Adult Cancer Treatment Stratification (MAPPYACTS, NCT02613962) is a prospective, international, multicentric clinical proof-of-concept study to stratify targeted therapies adapted to molecular profiling of relapsed or refractory paediatric tumours. Molecular screening is carried out on newly biopsied or resected tumour samples obtained at the time of relapse/progression, using high-throughput technologies, primarily WES and RNA Sequencing.

Clinical and molecular data of samples from individuals with ALK+ ALCL treated with crizotinib (n = 2) or combination chemotherapy (n = 2) were obtained from both male (n = 3) and female (n = 1) pediatric subjects included in the MAPPYACTS trial (**Table 17**) with informed consent. The MAPPYACTS trial protocol, amendments and informed consent were approved by the ethics committee and complied with local regulations and the Declaration of Helsinki (no. 2015-A00464-45).

Table 17 Clinical Information of Paediatric ALCL Patients Recruited onto the MAPPYACTS Trial

ALCL99 = cyclophosphamide, methotrexate, ifosfamide, etoposide, cytarabine, doxorubicin; ALCL99* = patient was treated according to ALCL99 recommendations for patients with CNS involvement as specified in Williams et al., 2013⁹⁹; BV = Brentuximab vedotin; CR = Crizotinib; LR = Lorlatinib; Nivo = Nivolumab; VBL = vinblastine. Biopsy sample for RNA-seq was taken at relapse during or after the highlighted treatment line.

Characteristics	Patient 1	Patient 2	Patient 3	Patient 4
Sex	M	M	F	M
Age at diagnosis	16	16	10	11
ALK fusion partner	NPM1-ALK+	NPM1-ALK+	TFG-ALK+	NPM1-ALK+
1 st -line treatment	ALCL99	ALCL99*	ALCL99	ALCL99
2 nd -line treatment	VBL	CR	CR	CR
3 rd -line treatment	CR	Nivo	N/A	N/A
4 th line treatment	BV	N/A	N/A	N/A
5 th line treatment	LR	N/A	N/A	N/A
6 th line treatment	Nivo	N/A	N/A	N/A
CR resistant (R)	R	R	N/A	N/A
ALK mutation status	L1196M	not detected	not detected	not detected

2.2.6 Brno cohort

FFPE tissue specimens from individuals with angioimmunoblastic T-cell lymphoma (AITL, n = 3), peripheral T-cell lymphoma not otherwise specified (PTCL-NOS, n = 4), ALK+ (n = 16) or ALK- (n = 6) ALCL were obtained from both male (n = 19) and female (n = 10) adult subjects (**Table 18**) with informed consent and in accordance with the Declaration of Helsinki. The study was approved by the ethics committee of the University Hospital of Brno, Czech Republic (no. 4-306/13/1). From this cohort, archival paraffin-embedded tissue blocks were used to create TMAs containing cores selected from representative tumour areas as determined by a consultant histopathologist, from hematoxylin and eosin–stained sections.

Table 18 Clinical Information of T-cell Lymphoma Patients from the Brno Cohort
Angioimmunoblastic T-cell lymphoma (AITL), peripheral T-cell lymphomas not otherwise specified (PTCL-NOS).

Case no.	Sex	Age at diagnosis	Diagnosis	Biopsy (Tissue origin)	Relapse	Death
1	M	21	ALCL, ALK+	lymph node	no	no
2	M	46	ALCL, ALK+	infiltrate, subhepatal	no	no
3	M	58	ALCL, ALK+	lymph node, axilla	no	no
4	M	28	ALCL, ALK+	tumour, axilla	no	no
5	M	28	ALCL, ALK+	lymp node	yes	yes
6	F	30	ALCL, ALK+	lymph node, neck	no	no
7	F	66	ALCL, ALK-	skin	yes	no
8	F	81	ALCL, ALK-	lymph node, neck	no	yes
9	M	71	ALCL, ALK-	infiltrate, inguina	no	yes
10	M	61	ALCL, ALK-	nasopharynx	no	yes
11	M	60	ALCL, ALK-	lymph nodes, inguina	no	no
12	M	57	ALCL, ALK-	lymph node, supraclavicula	no	no
13	F	54	ALCL, ALK-	lymph node	yes	no
14	M	51	ALCL, ALK-	lymph node, inguina	no	no
15	M	89	ALCL, ALK-	mandibula	yes	yes
16	M	51	ALCL, ALK-	lymph node, retroperitoneum	no	yes
17	M	56	ALCL, ALK-	lymph node, inguina	no	no
18	F	44	ALCL, ALK-	mesenterium and retroperitoneum with pancreas	no	yes
19	F	60	ALCL, ALK-	lymph node, supraclavicula	no	no
20	M	57	ALCL, ALK-	lymph node	no	no
21	M	66	ALCL, ALK-	lymph node, neck	no	yes
22	M	61	ALCL, ALK-	lymph node, neck	no	yes
23	F	57	AITL	lymph node, neck	yes	yes
24	M	62	AITL	lymph node, axilla	yes	yes
25	F	60	AITL	N/A	yes	yes
26	F	76	PTCL-NOS	lymph node,mesenteric	no	yes
27	M	77	PTCL-NOS	lymph node, neck	no	no
28	M	80	PTCL-NOS	lymph node, groin	yes	yes
29	F	70	PTCL-NOS	lymph node, neck	yes	yes

2.2.7 Pakistan cohort

FFPE tissue specimens from individuals with ALK+ (n = 15) or ALK- (n = 9) ALCL were obtained from both male (n = 19) and female (n = 10) subjects with informed consent and in accordance with the Declaration of Helsinki. The study was approved by the ethics committee of the Huntington research ethics committee (no. 07/Q0104/16). From this cohort, archival paraffin-embedded tissue blocks were used to create TMAs containing cores selected from representative tumour areas as determined by a consultant histopathologist, from hematoxylin and eosin–stained sections.

Table 19 Clinical Information of T-cell Lymphoma Patients from the Pakistan Cohort

Case no.	Sex	Age at diagnosis	Diagnosis	Biopsy (Tissue origin)
1	M	57	ALCL, ALK+	inguinal lymph node
2	M	19	ALCL, ALK+	cervical lymph node
3	F	17	ALCL, ALK+	cervical lymph node
4	M	53	ALCL, ALK+	cervical lymph node
5	M	19	ALCL, ALK+	cervical lymph node
6	M	12	ALCL, ALK+	buccal mucosa
7	M	35	ALCL, ALK+	abdominal mass
8	M	38	ALCL, ALK+	mass right axilla
9	M	12	ALCL, ALK+	paravertebral soft tissue
10	M	2	ALCL, ALK+	cervical lymph node
11	M	59	ALCL, ALK+	groin mass
12	F	20	ALCL, ALK+	right side neck swelling
13	F	61	ALCL, ALK+	mesenteric lymph node
14	M	35	ALCL, ALK+	cervical lymph node
15	M	25	ALCL, ALK+	mesenteric nodule & nodulae anterior part of stomach
16	F	27	ALCL, ALK-	supraclavicular lymph node
17	M	38	ALCL, ALK-	mesenteric lymph node
18	M	67	ALCL, ALK-	left arm swelling
19	M	35	ALCL, ALK-	cervical lymph node
20	M	75	ALCL, ALK-	right supraclavicular
21	M	21	ALCL, ALK-	skin lesion - thigh
22	F	20	ALCL, ALK-	axillary lymph node
23	M	60	ALCL, ALK-	cervical lymph node
24	M	14	ALCL, ALK-	inguinal lymph node

2.2.8 Vienna cohort

FFPE tissue specimens from individuals with AITL (n = 4) or PTCL-NOS (n = 17) were obtained from both male (n = 9) and female (n = 12) adult subjects (**Table 20**) with informed consent and in accordance with the Declaration of Helsinki. The study was approved by the ethics committee of the Medical University of Vienna, Austria (no. 1437/2016). From this cohort, archival paraffin-embedded tissue blocks were used to create TMAs containing cores selected from representative tumour areas as determined by a consultant histopathologist from hematoxylin and eosin–stained sections.

Table 20 Clinical Information of T-cell Lymphoma Patients from the Vienna Cohort
 Angioimmunoblastic T-cell lymphoma (AITL), peripheral T-cell lymphomas not otherwise specified (PTCL-NOS).

Case no.	Sex	Age at diagnosis	Diagnosis	Biopsy (Tissue origin)
1	M	54	AITL	inguinal lymph node
2	F	85	AITL	lymph node
3	M	58	AITL	cervical lymph node
4	F	82	AITL	inguinal lymph node
5	F	64	PTCL-NOS	axillary lymph node
6	F	70	PTCL-NOS	lymph node
7	M	67	PTCL-NOS	cervical lymph node
8	F	62	PTCL-NOS	peritoneum
9	M	58	PTCL-NOS	inguinal lymph node
10	M	54	PTCL-NOS	supraclavicular lymph node
11	F	73	PTCL-NOS	skin
12	F	87	PTCL-NOS	skin
13	F	89	PTCL-NOS	skin
14	M	76	PTCL-NOS	preauricular lymph node
15	M	63	PTCL-NOS	axillary lymph node
16	M	43	PTCL-NOS	inguinal lymph node
17	F	78	PTCL-NOS	inguinal lymph node
18	F	77	PTCL-NOS	axillary lymph node
19	F	65	PTCL-NOS	inguinal lymph node
20	M	55	PTCL-NOS	inguinal lymph node
21	F	77	PTCL-NOS	inguinal lymph node

2.3 Animal Studies

2.3.1 Generation of lorlatinib-resistant K299 xenografts

For the generation of lorlatinib-resistant K299 xenografts, experiments were carried out as previously described³²⁸. Adult female Severe combined immunodeficiency (SCID) (6 weeks old) mice (C.B.17/IcrHanHsd-Prkdc) were kept under standard conditions following the guidelines of the University of Milano-Bicocca ethical committee for animal welfare. The protocol (no. 006/2014) was approved by the Italian Ministry of Health and by the Institutional Committee for Animal Welfare. Lorlatinib was suspended in 0.5% carboxymethylcellulose/0.1% Tween 80. Ten million K299 cells were injected subcutaneously into the left flank of the mice. Once tumours reached an average size of 200 mm³, mice were randomized to receive vehicle alone ($n = 3$) or lorlatinib ($n = 10$, starting dose 0.1 mg/kg), orally, twice daily (b.i.d.). Tumour size was evaluated three times per week with calipers, using the formula: tumour volume (mm³) = $(d^2 \times D)/2$, where D is the longest and d is the shortest diameter. After 21 days, the dose was increased to 0.25 mg/kg b.i.d. and on day 37, to 0.5 mg/kg b.i.d. Each mouse was monitored for tumour growth and the dosage was increased every time the tumour relapsed or on stabilization after partial regression. Treatment was suspended at three different doses: 0.5 mg/kg ($n = 4$), 1 mg/kg ($n = 3$) or 2 mg/kg ($n = 3$).

2.3.2 Generation of ALCL PDX

NOD scid gamma (NSG) mice were obtained from Charles River and housed in individually ventilated cages (IVCs) under sterile pathogen-free conditions at the University of Cambridge, Central Biomedical Services (CBS) animal facilities, Addenbrooke's Hospital, Cambridge in groups of 2–5. At the end of procedures, mice were culled by the Schedule 1 method of cervical dislocation in accordance with UK Home Office guidelines. Animal work was carried out under UK Home Office project licence number P4DBEFF63, and personal licence numbers I27A881AC and IF74BBA96 according to the Animals (Scientific Procedures) Act 1986 and were approved by the University of Cambridge Animal Welfare and Ethical Review Body (AWERB). We have complied with all relevant ethical regulations for animal testing and research in the UK.

For ALCL PDX establishment, MCs were isolated from a bone marrow (Patient 1) or pleural effusion (Patient 2) sample by gradient centrifugation at 800 x g for 20 minutes at room temperature with brakes off using Lymphoprep according to the standard protocol. Afterwards, MCs were washed once in PBS containing 2% FBS. MCs were suspended in Matrigel diluted 1:2 with PBS and a total volume of 300 µL was injected subcutaneously into the left flank of NSG mice at 6-8 weeks of age using a 30-gauge hypodermic Agani™ needle. Mice were euthanized once tumours reached 15 mm in any direction, tumours were disaggregated and tumour cells vially frozen in 90% FBS, 10% DMSO.

For cell line establishment from ALCL PDX tumours, tumours were disaggregated in a petri dish using a 70 µm nylon Falcon™ cell strainer and the plunger of a 5 mL Plastipak™ syringe, applying light to medium mechanical force. Afterwards, limiting dilutions were prepared in IMDM supplemented with 20% FBS and 100 U/mL penicillin/streptomycin to establish cell lines.

For in vivo ALCL PDX studies, viably frozen PDX cells were thawed, washed in PBS containing 2% FBS and suspended in Matrigel diluted 1:2 with PBS before 0.5×10^6 cells per mouse in a total volume of 300 µL were injected subcutaneously into the left flank of NSG mice at 6-8 weeks of age using a 30-gauge hypodermic Agani™ needle. Mice were monitored for health and tumour size by animal technicians daily. Animals were shaved around the tumour area to assist with precision of measurement and callipers used to measure both the length and width of the tumour. Tumours were measured with manual calipers and tumour volumes estimated using the modified ellipsoid formula: $V = ab^2/2$, where a and b (a > b) are length and width measurements. Once tumours reached 400 mm³, mice were randomly split into three treatment groups and treated daily with the following agents by oral gavage using 22 gauge plastic feeding tubes at 10 µL per gram body weight: vehicle (PBS, 10% DMSO; n = 8), crizotinib (100 mg/kg; n = 8) or brigatinib (25 mg/kg; n = 8). Mice were euthanized once tumours reached 15 mm in any direction.

For immunohistochemistry (IHC), tumours were fixed in 10% neutral-buffered formalin for 24 hours, then paraffin-embedded and 3 µm sections cut from central regions. To generate blocks of the established cell lines, 2×10^7 cells were embedded in 0.5 mL of 1% agar diluted in PBS and processed as above. Tissue sections were stained with hematoxylin and eosin or with antibodies against ALK and CD30.

2.4 Immunoperoxidase labelling technique for Anti-ALK Autoantibody Detection

2.4.1 Preparation of COS-1 NPM1-ALK transfectants

COS-1 cells were seeded to approx. 1×10^6 cells/mL in 20 mL Dulbecco's Modified Eagle Medium (DMEM) containing 10% FBS in a T75 cell culture flask at 37 °C in a 5% CO₂ cell culture incubator. When the cells reached 50-60% confluence, they were transfected with pcDNA3 NPM1-ALK or pcDNA™ 3.1 vector as negative control using Lipofectamine® 3000 Transfection Reagent following the manufacturers protocol.

After 24 hours, the cell culture medium from the transfected COS-1 cells was discarded and the cells washed three times with Dubbecco's phosphate buffered saline. After washing, the cells were harvested with 10 mL of 1 x trypsin-EDTA for 2 min at 37 °C in a 5% CO₂ cell culture incubator. The trypsin was inactivated by adding an equal volume of DMEM containing 10% FBS, the cell suspension subject to centrifugation for 5 minutes at 290 x g and the cell pellet re-suspended in DMEM containing 10% FBS to reach a final concentration of $6-8 \times 10^5$ cells/mL. The cell suspension was kept on ice thereafter.

Test slides were prepared by varying the volume from 50 – 200 µL cell suspension to each well of the cytocentrifuge. After centrifugation, the Superfrost™ microscope slides were air-dried for 5 minutes and subsequently stained in Hematoxylin Solution, Gill No. 3. A volume of cells resulting in an appropriate cell density on the slides were chosen to prepare a large batch of cytocentrifuge slides. The slides were air-dried for 1 hour before fixation in 100% acetone for 10 minutes. After the fixation step the slides were air-dried for another hour until wrapping them back-to-back in pairs in aluminium foil for long-term storage at -20 °C. Several slides were immunostained at this stage to find the efficiency of transfection as described below.

2.4.2 Immunostaining of COS-1 NPM1-ALK transfectants

COS-1 NPM1-ALK transfectants were equilibrated at room temperature for 15 minutes before opening the cover foil and the cell spots circled using a Dako wax pen. 100 µL of each serum dilution (1:50, 1:100, 1:250, 1:750, 1:2250, 1:6750, 1:20250, 1:60750 in PBS) were added to a single spot of COS-1 NPM1-ALK transfectants. PBS was used as negative control, and ALK monoclonal antibody (1:1000 dilution) as a positive control. The highest dilution (1:50) was used to check for any background signal on COS-1 pcDNA™ 3.1 vector only transfectants.

Slides were incubated for 1 hour at room temperature in a humidified chamber until washing in PBS for 5 minutes. Afterwards, the cell spots were incubated with 100 µL of polyclonal rabbit anti-human IgG/HRP (1:100 dilution in PBS) for 30 minutes. The slides were then washed in PBS for 5 minutes before 3,3'-Diaminobenzidine (DAB) substrate was applied and incubated for eight minutes. After another wash in PBS, slides were counterstained in hematoxylin solution, Gill No. 3, rinsed with tap water, dried and the cover slide mounted with faramount mounting medium.

The highest dilution of the serum/plasma sample at which staining of the NPM1-ALK transfectants was still observed was taken as the titre of the antibody.

2.5 Protein Microarray Assay for ALK Autoantibody Detection

In collaboration with Cambridge Life Sciences (Keith Rawson and Danielle Mack, Ely, UK), a protein microarray assay was developed to determine the presence of ALK autoantibodies in patient serum, plasma, or frozen whole blood.

2.5.1 Antigen spotting process

The ALK protein solution was prepared by buffer exchange with a Vivaspin centrifugal filter column with a molecular weight cut-off of 3 kDa in TrisT (50 mM Tris, 0.01% Tween 20, pH 7.4). The concentrated protein solution was diluted to a final concentration of 150 µg/mL with TrisT containing DY-633 carboxylic acid carrier dye (2 µg/mL final) that was filtered with a Minisart NML 0.2 µm hydrophilic filter and transferred into a 96 well V-bottom plate. The dye was used to subsequently monitor the spotting process with Port Array 5000TM. 7.5 pL of triplicate droplets of recombinant ALK (150, 75, 37.5, 18.75 µg/mL) were spotted onto functionalized glass slides with the Nano-PlotterTM NP2.1 controlled by NPC16 NP2/E software. Functionalized glass slides were kind gifts from PolyAN Molecular Surface Engineering, Germany. 2D-Epoxy, 3D-Epoxy, 3D-NHS, 2D-Aldehyde and 3D-Aldehyde functionalized glass slides were tested for their suitability to bind the antigens during the optimization process. 2D-Epoxy glass slides were used in the final assay. Glutathione S-Transferase (150 µg/mL in PBS buffer), and monoclonal anti-human IgG (Fc specific) antibody were spotted as negative and positive controls. Human IgG was spotted to generate a standard curve (200, 100, 50, 25, 12.5 µg/mL). Humidity during the spotting process was kept at 65% with an AIRWIN ultrasonic humidifier controlled by a microprocessor controller CT-1. The protein solutions were cooled to 15 °C by using a programmable temperature controller connected to the microplate holder in the Nano-Plotter. The glass slides were dried for 2 hours before coating of the protein spots with triplicate spots of 7.5 pL microarray stabilizer StabilGuard[®] Choice. During the spotting process, antigen spotting was monitored with water-sensitive paper glued onto plain glass slides. After spotting, slides were scanned using a Port Array 5000TM and visually quality checked for separation of spots. Two slides from each print run were tested in a microarray assay as described in the section below with anti-GST antibody (1:200 dilution), healthy human plasma controls and positive human patient plasma controls, while remaining slides were stored at 4 °C until usage.

2.5.2 Processing of microarray slides

Microarray slides were pre-warmed for 1 hour at room temperature before they were processed using the automated slide processor ZenitUP controlled by the ZenitUP 2.12.51 software package. The slides were blocked with 50 µL of AMIDot[™] Activation Diluent and incubated for 30 minutes at room temperature before the plates were washed six times with 50 µL of AUTOZYME[™] RF Wash Buffer. Sample (50 µL) diluted in AUTOZYME[™] RF Sample Diluent was then transferred to the well and incubated for 30 minutes at room temperature before the plates were washed with 50 µL of AUTOZYME[™] RF Wash Buffer. After six washes, a goat anti-human IgG (H&L) – Affinity Pure, DyLight550 Conjugate (1:200 dilution) was used as a reporter. Readings were taken using the Port Array 5000TM.

2.6 Cell lines and cell culture

The ALCL cell lines DEL³⁵⁵, Karpas 299 (K299)²⁴, SU-DHL-1³⁵⁶, SUP-M2³⁵⁷, Mac-2A and TS (SUP-M2 derived) were cultured in Roswell Park Memorial Institute (RPMI) 1640 medium supplemented with 10% FBS and 1% penicillin and streptomycin (PS).

The NB cell lines CHLA-15, CHLA-20, CHLA-42, CHLA-90, CHLA-95, CHLA-171, COG-N-426 (Felix), NB-1643, NB-EBC1, NBL-S and the ALCL cell lines MGS and MTK were cultured in IMDM supplemented with 20% FBS, 1% insulin-transferrin-selenium and 1% PS. CHP-134, GI-ME-N, IMR-32, KELLY, LA-N-1, LA-N-5, LA-N-6, NGP, SK-N-BE(1), SK-N-BE(2), SK-N-FI, SMS-KAN, SMS-KCNR and SMS-LHN cells were cultured in RPMI 1640 supplemented with 10% FBS, 1% ITS and 1% PS.

SH-SY5Y and 293FT cells were cultured in DMEM supplemented with 10% FBS and 1% PS.

All cells were grown at 37°C in a humidified incubator with 5% CO₂. All cells were mycoplasma-free and subjected to periodic in-house testing.

2.7 IC₅₀ determination

For IC₅₀ determination, ALCL cell lines were seeded in flat-bottom 96-well plates at approximately 0.5 x 10⁵ cells/mL, treated with decreasing concentrations of ALK TKIs and cultured for 48 hours. Crizotinib, alectinib, lorlatinib and brigatinib were obtained from MedChemExpress and dissolved in 100% dimethyl sulfoxide (DMSO) at a concentration of 1 mM and stored at -20 °C until usage. The end-point viability for each condition was measured with the CellTiter-Blue® Cell Viability Assay in a black 96-well Cellstar plate following the manufacturer's protocol and analyzed on a SpectraMax i3.

2.8 Cellular proliferation

To determine cellular proliferation rates, 0.25 x 10⁵ cells/mL were plated in 6-well plates. Each day, 100 µL of cell suspension was transferred to a well of a 96-well plate, and the cell titre was measured by the CellTiter-Blue Cell Viability Assay. The signal was measured using a SpectraMax i3 plate reader.

2.9 Apoptosis analysis

Approximately 500,000 cells were collected, washed with cold PBS, then washed once with and resuspended in 100 µL of the binding buffer provided with the Annexin V Apoptosis Detection Kit APC following the manufacturer's protocol. Fluorochrome-conjugated Annexin V (5 µL/reaction) was added to the 100 µL cell suspension. Cells were incubated for 30 minutes at room temperature. Afterwards, APC-Annexin V was removed from the cells by centrifugation, washed once in 1 x Annexin V Binding Buffer, then cells were resuspended in 100 µL of 1 x Annexin V Binding Buffer containing 1 mg/mL propidium iodide (PI). The cells were stored in an ice box in the dark until analysis with an Accuri C6 flow cytometer. At least 20,000 events were collected per sample and these data were analyzed with FlowJo software.

2.10 Generation of TKI-resistant ALCL cell lines

ALK inhibitor resistant cell lines were established as described previously²¹⁷. Briefly, ALCL cells were seeded at approximately 0.5 x 10⁶ cells/mL. Crizotinib or alectinib were added at a starting concentration (**Table 21**), and cells were maintained in fresh drug containing medium changed every 48-72 hours.

Cells were passaged once they reached confluence. After every two passages at a given concentration of drug, the concentration of ALK TKI was increased in half-log intervals until a final concentration (**Table 21**) was achieved. The resulting pool of resistant cells was maintained in TKI containing media thereafter.

Table 21 Starting and final TKI concentrations used to generate TKI resistant ALCL cell lines

Cell line	Crizotinib		Alectinib	
	Starting concentration	Final concentration	Starting concentration	Final concentration
DEL	25 nM	200 nM	5 nM	100 nM
K299	50 nM	300 nM	5 nM	80 nM
SU-DHL-1	10 nM	100 nM	5 nM	50 nM
SUP-M2	50 nM	600 nM	5 nM	100 nM

2.11 Sequencing of the NPM1-ALK kinase domain region

For mutation analyses, genomic DNA was isolated from each of the resistant ALCL cell lines with the QIAamp DNA Mini Kit. The NPM1-ALK kinase domain region was amplified by PCR with the Q5 High-Fidelity PCR Kit from genomic DNA (gDNA) extracts as described in **Table 22** using cycle numbers specified in **Table 23**. Primers were used as described previously³⁵⁸: NPM1-ALK_seq_F 5'-TGCATATTAGTGGACAGCAC-3' and NPM1-ALK_seq_R 5'-GACTCGAACAGAGATCTCTG-3'. Amplicons were purified with the Zymo DNA Clean and Concentrator-5 kit and then Sanger sequenced by the DNA Sequencing Facility service (University of Cambridge).

Table 22 PCR Using Q5 High-Fidelity DNA Polymerase

Component	Start conc.	Amount [μ L]	Final conc.
5X Q5 Reaction Buffer	10x	5	1x
dNTPs	10 mM	0.5	200 μ M
Forward Primer	10 μ M	1.25	0.5 μ M
Reverse Primer	10 μ M	1.25	0.5 μ M
Template DNA	variable	variable	< 1,000 ng
Q5 High-Fidelity DNA Polymerase	2,000 units/ml	0.25	0.02 U/ μ l
Nuclease-free water		variable	
Total		25	

Table 23 PCR cycle conditions used to amplify the NPM1-ALK kinase domain region

Cycle number	Denature	Anneal	Extend
1	98 °C, 30 sec	N/A	N/A
2-25	98 °C, 10 sec	65 °C, 30 sec	72 °C, 30 sec
26	N/A	N/A	72 °C, 2 min

2.12 RT-qPCR

Total RNA was extracted with the RNeasy Plus Mini Kit and quantified using a Nanodrop 1000. RNA (1 μ g per cell line) was then reverse transcribed using the High-Capacity RNA-to-cDNA™ Kit. Reverse transcription (RT) reactions were diluted 1/10 and 10 ng (equivalent to the input RNA amount) was used as the template DNA for qPCR using the Power SYBR Green PCR Master Mix with standard reaction conditions on the QuantStudio™ 6 Flex Real-Time PCR System. Double delta Ct ($\Delta\Delta$ Ct) analysis was

conducted with normalization to GAPDH (ΔCt) and then relative expression level comparison to the negative control expressing scrambled sgRNA ($\Delta\Delta Ct$). All qPCR reactions were performed in technical triplicates. RT-qPCR primers used are listed in **Table 24**.

Table 24 RT-qPCR primers
All primers were retrieved from PrimerBank^{353,359} and synthesized by Sigma-Aldrich.

Gene	Forward primer	Reverse primer
ADORA2A	CGCTCCGGTACAATGGCTT	TTGTTCCAACCTAGCATGGGA
ARHGEF9	AATGAGCACTGAGCGTCACTA	AGCAGGGTCCTATCTCGCTG
BCL10	TCTGGACACCCTTGTTGAATCT	TGAAAAGGTTCACTGCTAC
BDNF	CTACGAGACCAAGTGCAATCC	AATCGCCAGCCAATTCTCTTT
COPZ2	ATTGTGGATGGCGGTGTGATT	TCCTGGCAGACTGAAGAACC
CRK	GCGGAGTAGCTGGTACTGG	GCGGAGTTCTCTGAGACG
CLYBL	GAAGGTCGGGCCTCAAGTAG	TTGCCGGCGTAGAGAATATC
EGR4	TCCTCGTCAAGTCCACTGAAG	CAGGAGTCGGCTAAGTCCC
EML2	GTGGCGGGAACCACTAAGG	CCACACCGAGAGCATGTGA
EREG	GTGATTCCATCATGTATCCCAGG	GCCATTCATGTCAGAGCTACACT
ETV1	TGGCAGTTTTTGGTAGCTCTTC	CGGAGTGAACGGCTAAGTTTATC
FAIM2	AGTTCGTCGAGTCTTTGTCAGA	TGGGTCCAGAACAGCAAGC
FOS	GGGGCAAGGTGGAACAGTTAT	CGGCTTGGAGTGTATCAGTCA
FOXP1	ATGATGCAAGAATCTGGGACTG	AGCTGGTTGTTTGTTCATTCTC
KRAS	GAGTACAGTGCAATGAGGGAC	CCTGAGCCTGTTTTGTGTCTAC
MET	AGCAATGGGGAGTGTAAGAGG	CCCAGTCTTGTACTCAGCAAC
MFSD2A	GGGAGCAGAGAGAACCCTATG	AGGTGTAGGTGCAAAACAAGAC
MYC	GTCAAGAGCGCAACACACAAC	TTGGACGGACAGGATGTATGC
NIN	CGTGATGGTCACCTGAACCG	CGTCCACTCTCATCGAAAGACT
NKX2-4	ACCCACGCTACTCGTCAATCT	CCTGCCGTTTCATCTTGTAAC
NPY	CGCTGCGACACTACATCAAC	CTCTGGGCTGG ATCGTTTTCC
NR4A2	ACCACTCTTCGGGAGAATACA	GGCATTGGTACAAGCAAGGT
PIK3CD	TCAACTCACAGATCAGCCTCC	CGCGAAAGTCGTTCACTTCT
PIM1	GAGAAGGACCGGATTTCCGAC	CAGTCCAGGAGCCTAATGACG
PLEKHG6	CCGCCCTACAGAAGCTGAAG	GGATAATGGTCGAGAAGCTCAGGA
PRKACA	ACCCTGAATGAAAAGCGCATC	CGTAGGTGTGAGAACATCTCCC
PRRX2	GCACCACGTTCAACAGCAG	TCCTTGGCCTTGAGACGGA
PSD2	GGATGGCCTGTCAGACTCAGA	CAGCCTGCTAAACTCGTTGTT
PTGES	TCCTAACCCTTTTGTGCGCTG	CGCTTCCCAGAGGATCTGC
RORC	GTGGGGACAAGTCGTCTGG	AGTGCTGGCATCGGTTTCG
RRAS	GACCCCACTATTGAGGACTCC	CGGTCGTTAATGGCGAACAC
SAGE1	TACCAGGATCTGCATTCTACC	CTGTGGGACCAGTT GACAAGA
SAMD4A	TCGAGGCTTTGGGCAATCC	GAGCTGACGAATCCACTGGT
SEMA4A	AGCCAGCGAGTTTGACTTCTT	CGTGGCGGATGACGTTGAA
SLC7A3	GCCATCCATTGTGATCTGCTT	GTGGTTCCCAATCAGGTTGTC
SPDEF	CAGTGCCCGGTCATTGACA	CAGCCGGTATTGGTGCTCT
SSBP3	GGAACACCCATTATGCCAGT	GACCCATCGGGAAGTTGGAC
SURF2	GGGAGCTGCAAGTGATGACAG	CGGTACACGGTCGTCTCTCT
UBIAD1	AGTGTGCCTCCTACGTGTTG	CAGGACACCGTGGGATCTG
UTF1	CGCCGCTACAAGTTCTTAAA	GGATCTGCTCGTCGAAGGG
YAP1	TAGCCCTGCGTAGCCAGTTA	TCATGCTTAGTCCACTGTCTGT
GAPDH	GGAGCGAGATCCCTCCAAAAT	GGCTGTTGTCATACTTCTCATGG
NPM1	GGAGGTGGTAGCAAGGTTCC	TTCACTGGCGCTTTTTCTTCA
MKNK1	AGATGGGCAGTAGCGAAC	AGCAATTCAGAGGTCAGCTTG
SH2D2A	GACTTCCCTGAGGACCGAAG	GCTTGCCCTGTTTGATGATTG
HELZ2	ATCTACATCCGGGAGTATTTCCA	TCGTGCGTCAGGCAACAGTA
IL10RA	CCTCCGTCTGTGTGGTTTGAA	CACTGCGGTAAGGTCATAGGA
PGBD1	TGCCTGGGATAACCACCCT	ATGAGCTGATCCGTGGGGAA
GPR161	TGGATCTTTGGTGTAGTGTGGT	ATGACCCCGAGGGTTAGCAT
P2RY6	GTGTCTACCGCGAGAACTTCA	CCAGAGCAAGGTTTAGGGTGTA
NPM-ALK	CTGTACAGCCAACGGTTTCC	GGCCAGACCCGAATGAGG

2.13 Western Blot

Protein lysates were prepared by lysing 1 million cells in 40 μ L radioimmunoprecipitation assay (RIPA, 25mM Tris HCL pH 7.6, 150mM NaCl, 1% NP-40, 1% sodium deoxycholate, 0.1% SDS) buffer supplemented with Halt Protease and Phosphatase Inhibitor Cocktail for 30 minutes on ice. Cellular debris were removed by centrifugation at 16,000 x g for 20 minutes at 4 °C and the supernatant stored at -20 °C until usage. Proteins were quantified with a Pierce™ BCA Protein Assay Kit following the manufacturer's protocol and analyzed on a SpectraMax i3. Protein lysate (50 μ g) were solubilized in Laemmli buffer containing 5% β -mercaptoethanol (250 mM Tris pH 6.8, 10% SDS, 5% beta-mercaptoethanol, 0.02% bromophenol blue, 30% Glycerol) and boiled for 5 minutes at 95 °C. Samples were resolved by SDS-PAGE with a Bio-Rad Mini-Protean TGX 10% gel for 2 hours at 100 V in running buffer (25 mM Tris, 190 mM glycine, 0.1% SDS). Proteins were transferred to a 0.2 μ M PVDF membrane using a Trans-Blot Turbo Transfer Pack with a Trans-Blot Turbo Transfer System at 27 V for 7 minutes. Following transfer, membranes were first blocked in blocking buffer (5% Bovine serum albumin (BSA) in TBST (20 mM Tris-HCl pH 8, 150 mM NaCl, 0.1% Tween-20)) for 1 hour at room temperature and subsequently incubated with the the primary antibody diluted in blocking buffer (see **Table 25** for antibody dilutions) at 4 °C overnight. Afterwards, the membrane was incubated with the secondary immunoglobulin/HRP diluted in washing buffer (see **Table 25** for dilution) for 1 hour at room temperature. Washing was performed with TBST, protein bands were visualized with Immobilon Western Chemiluminescent HRP Substrate and detected by a LAS-4000 Image Analyzer (Fujifilm/Raytek).

Table 25 List of antibodies used to detect proteins by Western blot

Protein	Antibody	Antibody name	Dilution	Company	Cat. no.
Cas9	1 st	Anti-Cas9	1:2000	Abcam	ab204448
	2 nd	Goat anti-rabbit	1:10000	Agilent technologies	P0448
ALK	1 st	Rabbit ALK (D5F3®) XP® antibody	1:1000	Cell Signalling	3633
	2 nd	Goat anti-rabbit	1:10000	Agilent technologies	P0448
pALK	1 st	Rabbit Phospho-ALK (Tyr1604) antibody	1:1000	Cell Signalling	3341
	2 nd	Goat anti-rabbit	1:10000	Agilent technologies	P0448
STAT3	1 st	Rabbit STAT3 antibody	1:1000	Cell Signalling	4904S
	2 nd	Goat anti-rabbit	1:10000	Agilent technologies	P0448
STAT1	1 st	Rabbit STAT1 antibody	1:1000	Cell Signalling	9172
	2 nd	Goat anti-rabbit	1:10000	Agilent technologies	P0448
pSTAT3	1 st	Rabbit Phospho-STAT3 (Tyr705) antibody	1:1000	Cell Signalling	9145
	2 nd	Goat anti-rabbit	1:10000	Agilent technologies	P0448
pSTAT1	1 st	Rabbit Phospho-STAT1 (Tyr701) antibody	1:1000	Cell Signalling	14994
	2 nd	Goat anti-rabbit	1:10000	Agilent technologies	P0448
STAT5A	1 st	Mouse STAT5A (4H1) antibody	1:1000	Cell Signalling	4807
	2 nd	Goat anti-mouse	1:10000	Agilent technologies	P0161
pSTAT5A	1 st	Rabbit Phospho-STAT5 (Tyr694) antibody	1:1000	Cell Signalling	9359
	2 nd	Goat anti-rabbit	1:10000	Agilent technologies	P0448
α -Tubulin	1 st	Mouse anti- α -Tubulin	1:10000	Sigma Aldrich	T9026
	2 nd	Goat anti-mouse	1:10000	Agilent technologies	P0161

2.14 sgRNA cloning

To clone individual sgRNAs into lenti sgRNA(MS2)_zeo/lenti sgRNA(MS2)_puro, guide sequences (Table 26) were designed with the Cas9 activator tool³⁶⁰ and synthesized at Sigma Aldrich. They included a 4-bp overhang for the forward (CACC) and complementary reverse (AAAC) oligos to enable cloning into the BsmB-I site of the lentiviral construct. On-target scoring was performed using the "Rule Set 2" method²⁹². The Microsoft implementation of the scoring model used was Azimuth 2.0. Off-target sites were evaluated using the Cutting Frequency Determination score.

Table 26 Oligonucleotides used to generate dsDNA fragments containing the 20 bp target sequence NT is a scrambled 20 bp sequence that is predicted to not target any region of the human genome. **Gray nucleotides** indicate the overhangs while black nucleotides represent the target sequence.

Gene	sgRNA	Forward ssDNA element	Reverse ssDNA element
ARHGEF9	1	CACCgCGCAAGCGCCCGCAGTCGCT	AAACAGCGACTGCGGGCGCTTGCGc
	2	CACCgGGCGGGTATGTCTAGTGGCTC	AAACGAGCCACTGACATACCCGCCc
BCL10	1	CACCgAGGTACTGACAAGCCCAGAC	AAACGTCTGGGCTTGTCTAGTACCTc
	2	CACCgGCAGGGTCTGGGAAAAGGGG	AAACCCCCTTTTCCCAGACCCTGCc
CRK	1	CACCgACGCGCTCCCTGCCCGAGGG	AAACCCCTCGGGCAGGGAGCGCGTc
	2	CACCgGGCTGCCGGGAAGGGGCCCG	AAACCGGGCCCCTTCCCAGCAGCCc
EREG	1	CACCgGGTGCTGCGAACTTTATACT	AAACAGTATAAAGTTCGCAGCACCc
	2	CACCgGAGCCCCTCCCGGGCCCTAA	AAACTTAGGGCCCAGGGGGCTCcc
FOS	1	CACCgAAACGTCACGGGCTCAACCA	AAACTGGTTGAGCCCGTGACGTTTc
	2	CACCgGGCGCCAGAGGGGTGGCGCG	AAACCGCGCCACCCTCTGGCGCCc
NR4A2	1	CACCgCAGCGCGGCGATTGGCGGCG	AAACGCCGCCAATCGCCGCGCTGc
	2	CACCgGGCCAGGAGTCCAGGGAGCG	AAACCGCTCCCTGGACTCCTGGCCc
PLEKHG6	1	CACCgCAGTAATGAGGGCTGAGTAA	AAACTTACTCAGCCCTCATTACTGc
	2	CACCgGGGCGGGGCGCCGCGGGGG	AAACCCCCGCGGGCGCCCCGCCc
PRKACA	1	CACCgTGCGGGGGCGTACAGACAG	AAACCTGTCTGTGACGCCCCCGCAc
	2	CACCgGGCCTAGCCAATGAGCGGC	AAACGCCGCTCATTGGCCTAGGCCc
PSD2	1	CACCgGGGACGGACGGCAGGAGGGA	AAACTCCCTCCTGCCGTCCGTCCCc
	2	CACCgGGAGCGGAGCCGTGAGCTGG	AAACCCAGTCTACGGCTCCGCTCCc
PTGES	1	CACCgCTGCAGGAAAGCACAAAGT	AAACACTTTTGTGCTTTCCCTGCAGc
	2	CACCgGGGCGGTGCTGGCTGCAGGA	AAACTCCTGCAGCCAGCACCCGCCc
RORC	1	CACCgCCCCAGTGCTTCTGGACTG	AAACCAGTCCAGAAGCACTGGGGGc
	2	CACCgGTTTAAGCTCTGCACCACAC	AAACGTGTGGTGCAGAGCTTAAACc
	3	CACCgGGGAGGGGCGAGCCAATCGTA	AAACTACGATTGGCTGCCCTCCCc
	4	CACCgCCCCAAGGGGTGCAGTGAGT	AAACTCACTGCAACCCTTGGGc
SAM4A	1	CACCgCTCCCCCTTCTTGCAGCTT	AAACAAGCTGCAAGAAGGGGGAGc
	2	CACCgGATGGTGATTTCGGCGTCC	AAACGGACGCGGAAATCACCATCcc
SPDEF	1	CACCgTATAATGGGAAATCAGGCC	AAACGGCCTGATTTCCCATTATAc
	2	CACCgTTTGTTTCAAGTAAATAAGGA	AAACTCCTTATTTACCTGAACAAAc
UBIAD1	1	CACCgGCCGCGGCGCGGGCTGGAC	AAACGTCCAGCCCGCGCCGCGGGc
	2	CACCgCCGCCCTCCAGCCACCCTC	AAACGAGGGTGGGCTGGAGGGCGGc
YAP1	1	CACCgGGCGAGTTTCTGTCTCAGTC	AAACGACTGAGACAGAACTCGCCc
	2	CACCgCAAACGCCAAAATAAAGTT	AAACAACCTTTAGTTTTGGCGTTTg
ABC1	1	CACCgGGATAAGTTTGGGTGGAGGA	AAACTCCTCCACCCAACTTATCCc
	2	CACCgCACTAATCAGTAAAACCCA	AAACTGGGTTTTCACTGATTAGTGc
NMP1	1	CACCgCTGCGCAGACTCTTGGCGGG	AAACCCCGCAAGAGTCTGCGCAGc
	2	CACCgTGGAAAGCACGCGTGCGCAC	AAACGTGCGCACGCGTGTCTTCCAc
	3	CACCgCCGGCGCGCTTGGAGGGAG	AAACTCCCCTCAAGCGCGCCGGc
MYC	1	CACCgGGTGGGGAGGAGACTCAGCC	AAACGGCTGAGTCTCTCCCCACCc
	2	CACCgGAACCCGGGAGGGGCGCTTA	AAACTAAGCGCCCCTCCCGGGTTc
MKNK1	1	CACCgGGCGTGACAGGGAAGAGGCG	AAACCGCCTCTTCCCTGTCAGCCc
	2	CACCgGAGCTGCGCCTGCGCCCTGA	AAACTCAGGGCGCAGGCGCAGCTCcc
IL10RA	1/49	CACCgTAGCGCCCCAGGACAGCCTC	AAACGAGGCTGTCTGGGGCGCTAc
	2/50	CACCgGCCCCAGGCGGTAGCCCTGT	AAACACAGGGCTACCGCCTGGGGCcc

Gene	sgRNA	Forward ssDNA element	Reverse ssDNA element
	3/72	CACCgGGACAGTGGTTCCTCCCGTCCG	AAACCGGACGGGGAACCACTGTCCc
P2RY6	1	CACCgGGCAGCAATGAGCAGAAGCA	AAACTGCTTCTGCTCATTGCTGCCc
	2	CACCgACTCCAGAGAAGCCAGGAGA	AAACTCTCTGGCTTCTCTGGAGTc
SH2D2A	1	CACCgATCTGTGTCACTCTGTGTTT	AAACAAACACAGAGTGACACAGATc
	2	CACCgTGAAGGTCAGGCAGCAGTAA	AAACTTACTGCTGCCTGACCTTCAc
HELZ2	1	CACCgCAGCTCGGCCCTCCGCTGCGA	AAACTCGCAGCGGGGGCCGAGCTGc
	2	CACCgCTGCTCGCTGGCGCTTCCCG	AAACCGGGAAGCGCCAGCGAGCAGc
NT		CACCgGGTCCCTCAGGGTGCAACTT	AAACAAGTTGCACCCTGAGGGACCc
GPR161	1	CACCgGGCCGCAGGGGAGGGGCGCG	AAACCGCGCCCTCCCCTGCGGCCc
	2	CACCgTGCGCTTGCTTTGGAGAGC	AAACGCTCTCCAAAGCAAGGCGCAc
ADORA2A	1	CACCgTCACTGCAACCTCCACCTCC	AAACGGAGGTGGAGTTGACAGTGAc
	2	CACCgCCCAGCTACTCGGGAGGCTG	AAACCAGCCTCCCGAGTAGCTGGGc
PGBD1	1	CACCgAGTGACCTGGGCGGGCAGG	AAACCCTGCCCGCCAGGTCACTc
	2	CACCgATGGCCTGGGGTCCGCGCG	AAACCCGCGGACCCAGGCCCATc
BDNF	1	CACCgGATTCATTTTTTTGTGTTGG	AAACCCAACACAAAAAATGAATCc
	2	CACCgTGTGCGGTGGGGAGAGGAGG	AAACCTCTCTCCCACCGCACAc
CLYBL	1	CACCgGAAGGAGGGCGTGGCTGGCG	AAACCGCCAGCCACGCCCTCTTCc
	2	CACCgGTCTAAGCCCTGGCCGGGA	AAACTCCCGGCCAGGGCTTAGGACc
COPZ2	1	CACCgACGGGCCCCGAGGAAAGGG	AAACCCCTTTCTCGGGGCCCGTc
	2	CACCgGATGGGGGAGAACGAGCAAG	AAACCTTGCTCGTTCTCCCCATCc
EGR4	1	CACCgCAGGTGGGAAGCGCATCTAC	AAACGTAGATGCGCTTCCACCTGc
	2	CACCgGCCTCACCGGGCCGACCGTC	AAACGACGGTCGGCCCGGTGAGGCc
EML2	1	CACCgCTCCCGATCCAGTTCTTT	AAACAAAGAACCTGGGATCGGGAGc
	2	CACCgGGGAGAGTGGTTGAGAACA	AAACTGTTCTCAACCAGTCTCCCCc
ETV1	1	CACCgGGGATTTACGGTCTGTTAT	AAACATAACGAGCCACTAAATCCCCc
	2	CACCgGGTTACCCTGACTACCCGTC	AAACGACGGGTATCCAGGTAACCCc
FAIM2	1	CACCgGCGCTGCGGAGCAACCCAG	AAACCTGGGGTTGCTCCGACGCGCc
	2	CACCgTCCCGGGGGAGGGCTAAGGG	AAACCCCTTAGCCCTCCCCCGGAc
FOXP1	1	CACCgGCGCCCCGGCCCCCTCCGCG	AAACCGCGGAGGGGGCCGGGGCGCc
	2	CACCgGTGTGGGGCGCGCGCGCGCG	AAACCGCCGCGCGCGCCCCACAc
MFSD2A	1	CACCgCTCCTAGCAATCCGAGAAGC	AAACGCTTCTCGATTGCTAGGAGc
	2	CACCgGCTTGGAGAACGTGGCTCGG	AAACCCGAGCCACGTTCTCCAAGCc
NIN	1	CACCgGGCCCGCGCGGCTCAGGCAG	AAACCTGCCTGAGCCGCGCGGGCCc
	2	CACCgGGCGGGCGCTCGGAGCGGGA	AAACTCCCGCCGAGCGCCCGCCc
NKX2-4	1	CACCgCGTCACAGGCTCAGCTGCCG	AAACCGGCAGCTGAGCCTGTGACGc
	2	CACCgGTCTGTCTGTAACCTGGCGC	AAACGCGCCAGGTTTACGACAGAc
NPY	1	CACCgAGGGGCGGGAAGTGCGGGT	AAACACCCGCCACTTCCCGCCCTc
	2	CACCgCGGGAGGGTTGGGGTGTGGG	AAACCCACACCCCAACCCTCCCGc
PIK3CD	1	CACCgGATGATGCCCTCTAGCGGT	AAACACCGCTAGAGGGGCATCATCc
	2	CACCgGGAAAAACAACAGTCTCTCC	AAACGGAGGACCTGTTGTTTTTCCc
PIM1	1	CACCgCGGACTGGGCGACTCCCT	AAACAGGGGAGTCGCCAGTCCCGc
	2	CACCgGGGAGCAGGGCTGCCGGGC	AAACGCCCGCAGCCCTGCTCCCCc
PRRX2	1	CACCgGGATGGAACAGACAAAACA	AAACTGTTTTGTGCTTTTCCATCCc
	2	CACCgTGGGTGGGAGGGTGAAGGG	AAACCCCTTACCCTCCCAACCCAc
RRAS	1	CACCgGGACACTTAAGGAGGGGAGC	AAACGTCCCCCTCCTTAAGTGTCCc
	2	CACCgCGGGAATTCCGAATGAGGCG	AAACCGCCTCATTCCGAATTCCCCc
SAGE1	1	CACCgCTCAAGGCGGATGGAAGGAA	AAACTTCTTCCATCCGCCTTGAGc
	2	CACCgTGGGAGTGATGCTCATGGGG	AAACCCCATGAGCATCACTCCCAc
SEMA4A	1	CACCgCAGTATAACCAGCCTAGCAG	AAACCTGCTAGGCTGGTTATACTGc
	2	CACCgGTGACATGATGGAGAGGCAG	AAACCTGCCTCTCCATCATGTCACc
SLC7A3	1	CACCgGGCTTTGCAAAAAGGATTGCG	AAACCGCAATCCTTTTGCAAAGCCc
	2	CACCgTGAGGATGGGACGCAGTCTC	AAACGAGACTGCGTCCCATCCTCAc
SSBP3	1	CACCgGAGCCGCTGCCTGCTCCTGC	AAACGCAGGAGCAGGCAGCGGCTCc
	2	CACCgTGCCGCGGCCGGCGCTGTCA	AAACTGACAGCGCCGGCCGCGGCAc
SURF2	1	CACCgGGCTGGGACGGGTGAGCGC	AAACGCGCTACCCGTCCAGCCc
	2	CACCgGTTGCAGCTGGGGTGGCGG	AAACCCCGCAGCCCCAGCTGCAACc
UTF1	1	CACCgAGGACCCGGCGGGCGGGGCG	AAACCGCCCCGCGCGGGGTCTc
	2	CACCgAGGGTCCGTCTGGCGCTG	AAACCAGCGCCAGGACCGACCCCTc
IL10	1/86	CACCgAAAGGGGACAGAGAGGTGA	AAACTCACCTCTGTCCCCCTTc
	2/87	CACCgTGGCTTTTTAATGAATGAAG	AAACCTTCATTCATTAATAAAGCCAc

First, dsDNA fragments were generated to be used as the inserts to be ligated into the lenti sgRNA(MS2)_zeo/lenti sgRNA(MS2)_puro backbone vector. Therefore, each oligonucleotide mix (**Table 27**) was phosphorylated and annealed in a thermocycler using the following conditions: 37 °C for 30 min; 95 °C for 5 min; and ramped down to 25 °C at 5 °C/min.

Table 27 Phosphorylation and annealing of single-stranded sgRNA oligonucleotides

Component	Amount (μL)	Final concentration
Forward sgRNA	1	10 μM
Reverse sgRNA	1	10 μM
T4 Ligation buffer, 10x	1	1x
T4 PNK	0.5	N/A
Nuclease-free water	6.5	N/A
Total	10	

After the thermocycler run, the annealed dsDNA was diluted 1:10 and the Golden Gate assembly reaction for each sgRNA was set-up as described in **Table 28** with cycle conditions specified in **Table 29**. The ligated products were transformed into NEB High Efficiency Stable Competent *E. coli* using the manufacturer's protocol. The constructs were then extracted from bacteria with the QIAprep Spin Plasmid Kit, plasmid DNA was quantified using a Nanodrop 1000 (ThermoFisher) and the sequence verified by standard Sanger sequencing using a U6_promoter_F oligonucleotide (Sigma-Aldrich) 5'-AATGGACTATCATATGCTTACCG-3' at the DNA Sequencing Facility service (University of Cambridge).

Table 28 Golden Gate assembly

Component	Start conc.	Amount [μL]	Final conc.
T4 Ligase buffer (NEB, cat. no.: B0202S)	10x	2.5	1x
DTT (ThermoFisher, cat. no.: 707265ML)	10 mM	2.5	1 mM
BSA	2 mg/mL	1.25	0.1 mg/mL
Annealed sgRNA	1 μM	1	0.04 μM
lenti sgRNA(MS2)_zeo (Addgene, cat. no.: 70183)	N/A	N/A	1 ng/μL
BsmB1 (NEB, cat. no.: R05805)	10,000 U/mL	1	10 U
T4 DNA Ligase (NEB, cat. no.: M0202S)	40,000 U/mL	1	N/A
Nuclease-free water		N/A	
Total		25	

Table 29 PCR cycle conditions used for Golden Gate assembly

Cycle number	Condition
1-15	37 °C for 5 min, 20 °C for 5 min

2.15 Genome-scale Cas9 transcriptional activation screen

2.15.1 Genome-scale Cas9 transcriptional activation screen design

For genome-scale Cas9 transcriptional activation screens, a three plasmid (**Figure 8B-D**) system – human CRISPR activation library v1 – was used²⁷¹.

This library is based on a dCas9-VP64 fusion protein (**Figure 8B**) that recruits transcriptional complexes to the TSS of target transcripts as well as an altered sgRNA (**Figure 8D**) to recruit accessory transcriptional co-activators (MS2-p65-HSF1) (**Figure 8C**) to synergistically interact with the

transcriptional complex. Specifically, a hairpin aptamer that selectively binds to the MS2 phage protein was appended to the tetraloop and stem loop no. 2 regions²⁸⁵. Then a separate vector (**Figure 8C**) was constructed to express MS2 protein fused to the p65 transcription factor and HSF1. This allows for additional recruitment of transcriptional activators to the TSS, leading to >500-fold enhanced overexpression in targeted mRNA levels compared to dCas9-VP64 alone²⁷¹.

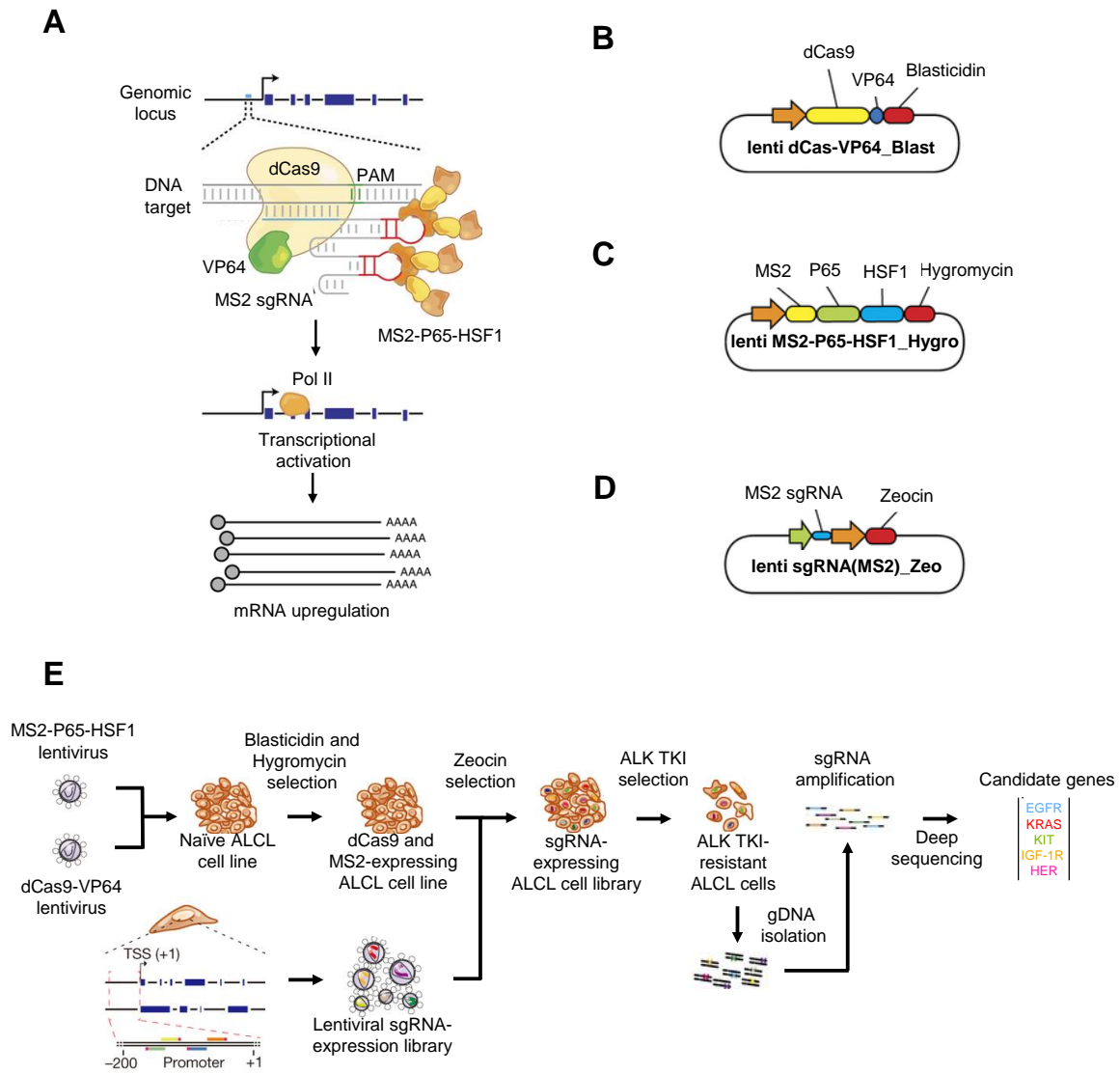


Figure 8 The genome-scale Cas9 transcriptional activation screen employed to identify bypass resistance mechanisms to ALK TKIs

(A) Programmable transcriptional activation can be achieved using dCas9 and activation domains (e.g., VP64/p65/HSF1) to recruit transcriptional machinery to the transcription start site of the desired gene target, resulting in upregulation of the target transcript. PAM: protospacer adjacent motif, Pol II: RNA polymerase II. (B-D) The vector-system used for the genome-scale Cas9 transcriptional activation screen. The library (lenti sgRNA(MS2)_Zeo) must be combined with additional SAM effectors in a 3-vector format. Blast: Blasticidin, Hygro: Hygromycin, Zeo: Zeocin. (E) Genome-scale Cas9 transcriptional activation screens begin with the construction of a plasmid library encoding the effector protein and sgRNAs. SAM libraries target the 200-bp region upstream of the transcription start site of 23,430 human RefSeq coding isoforms with 3 sgRNAs per isoform. These plasmid libraries are packaged into lentivirus and then transduced into the cell type of interest to generate stably expressing lines for the screen, along with an accessory transcriptional activator complex. A selection pressure –e.g. the ALK TKI crizotinib– is applied and genomic DNA is harvested. Surviving sgRNA sequences (coloured bars) are amplified from genomic DNA and then analyzed by deep sequencing to identify candidate genes. Figure modified from Jung et al., 2017²⁸⁶.

2.15.2 Generation of dCas9 and MS2 expressing cell lines

To conduct genome-scale Cas9 transcriptional activation screens, cell lines stably expressing lenti dCAS-VP64_Blast and lenti MS2-P65-HSF1_Hygro were engineered (Figure 8E)²⁷¹. Briefly, the lentiviral plasmids were individually packaged into lentiviruses and subsequently used for viral transduction in cell lines. First, the expression plasmids were co-transfected into log-phase 293FT cells with second-generation lentiviral packaging plasmids – psPAX2 and pMD2.G at a ratio of 1:1:1 with TransIT-293 in OptiMEM reduced serum medium at 32 °C. After 24 hours the medium was replaced with fresh Dulbecco's Modified Eagle Medium supplemented with 10% FBS, DNase I, 20 mM HEPES pH 7.4 and 5 mM MgCl₂. Viral supernatant was collected 48 and 72 hr post-transfection, pooled, centrifuged at 360 x g for 5 min, with the resulting supernatant filtered and stored at -80 °C if not used directly.

Afterwards, cells were first transduced with viral particles of lenti dCAS-VP64_Blast at a multiplicity of infection (MOI) of < 0.7 then selected in blasticidin S HCl (see Table 30 for concentration) 24 hr post viral transduction for seven days to completion (defined as 0% survival in uninfected cells). Then lenti MS2-P65-HSF1_Hygro particles at an MOI of < 0.7 were applied and stable cells were selected in hygromycin B (see Table 30 for concentration) 24 hr post viral transduction for seven days to completion.

Table 30 Antibiotic concentrations that were used for the selection of the transduced cell lines
(* indicates the presence/absence of the pathognomonic translocation t(2;5)(p32;q35) and/or of the fusion gene NPM-ALK.

Cell line	Diagnosis	t(2;5) NPM-ALK*	Hygromycin	Blasticidin	Zeocin	Puromycin
DEL	ALCL	cryptic t(2;5) NPM-ALK	200 µg/mL	10 µg/mL	100 µg/mL	500 ng/mL
Karpas 299	ALCL (refractory, terminal)	t(2;5) NPM-ALK	200 µg/mL	10 µg/mL	100 µg/mL	1 µg/mL
SU-DHL-1	ALCL	t(2;5) NPM-ALK	125 µg/mL	5 µg/mL	80 µg/mL	1 µg/mL
SUP-M2	ALCL (refractory)	t(2;5) NPM-ALK	200 µg/mL	10 µg/mL	100 µg/mL	1 µg/mL
Mac-2A	ALCL, cutaneous (terminal)	N/A	125 µg/mL	10 µg/mL	100 µg/mL	1 µg/mL
SHSY5Y	NB	N/A	300 µg/mL	10 µg/mL	750 µg/mL	1 µg/mL
CHLA-20	NB	N/A	300 µg/mL	10 µg/mL	300 µg/mL	1 µg/mL

2.15.3 Transformation, amplification and preparation of lentiviral sgRNA libraries

Aliquots (~1000 ng (50 ng/µl)) of the Human CRISPR Activation Library v1 (SAM - 3 plasmid system) were acquired. Each library (100 ng) was transformed into ElectroMAX Stbl4 Competent Cells via electroporation with the Gene Pulser II Electroporation System according to the protocol supplied with the Stbl4 cells. This process was carried out with 4 replicate reactions. Cells were recovered in SOC Outgrowth Medium and cultured for 1.5 hours at 30 °C before being plated onto ampicillin lysogeny broth (LB) agarose bioassay dishes, which were incubated overnight at 30 °C. The bacterial colonies were then harvested, and the CRISPR plasmid libraries were isolated using the EndoFree Plasmid Maxi Kit. To prepare lentivirus libraries, log-phase HEK293FT cells were seeded at ~50% confluence the day before transfection in reduced (5%) FBS supplemented DMEM to obtain ~80% confluence for transfection. For each T175 flask, 18 µg of sgRNA plasmid library, 16 µg of psPAX2, and 10 µg of

pMD2.G were incubated in 4.5 mL of Opti-MEM/TransIT-293 (110 μ L of TransIT-293) for 15 minutes at room temperature. 60 hours after transfection, the media was collected and centrifuged at 500 x g at 4 °C for 15 minutes to remove the cellular debris. Aliquots of the supernatant were stored at –80 °C.

2.15.4 Transduction of ALCL cell lines using lentiviral CRISPR libraries

To determine optimal virus volumes for achieving a MOI of 0.3, trial infections to determine the effective MOI were set up using ALCL cell lines (specifically DEL, SUP-M2 and K299). Briefly, 1 million cells per well were seeded into a 6-well plate in 10% FBS RPMI 1640. Afterwards, the virus libraries, mixed with fresh media, were added to the cells. Each well received different volumes of viruses (10 μ l up to 500 μ l) along with a mock (no virus) transduction control. Cells were incubated with the virus for 24 hours and cells from each well were then split into 2 wells in a 6-well plate. One well received 100 μ g/mL of zeocin depending on the cell type (**Table 30**). After 5 days, when no viable cells remained in the no-transduction control duplicate wells incubated with zeocin, viable cells were counted following trypan blue exclusion. The effective MOI was calculated as the average cell count from the triplicate wells incubated with zeocin divided by the average cell count from the triplicates with no selection reagent. The virus volume yielding a MOI of 0.3 was selected to be scaled up for the screens. The virus transduction protocol for the actual screens was scaled up to 20 million cells per T175 flask with a total of 500 million cells being transduced.

Stable DEL/SUP-M2/K299 SAM cells were infected with the library at a MOI of 0.3 and a ratio of at least 500 cells/sgRNA were then incubated with zeocin (100 μ g/mL) for 7 days. Two separate infections were performed and for each condition 500 cells/sgRNA were collected as input control. The remaining cell pools were subsequently cultured with crizotinib (120/150/300 nM for DEL/SUP-M2/K299) or DMSO for 14 days and harvested for DNA extraction.

2.15.5 Preparation of HiSeq libraries for the screen readout

Frozen cell pellets were lysed and their gDNA was extracted with the QIAamp DNA Blood Maxi Kit. PCR of the virally integrated guides was performed on gDNA at the equivalent of 500 cells per guide using Herculase II Fusion DNA Polymerase (**Table 31**). Oligonucleotides included the Illumina adapters, staggered region and the barcodes (**Table 32**). The amount of input gDNA for each sample to achieve 500 x coverage of the SAM library was calculated to be approximately 230 μ g DNA per replicate, assuming 6.6 μ g of gDNA is the yield of 1 million cells. Therefore, 23 parallel 100 μ l PCR reactions with 10 μ g of input genomic DNA in each reaction were completed in an ABI Veriti Thermal Cycler in a single-step reaction of 24 cycles (**Table 33**).

Table 31 PCR amplification of virally integrated guides

Component	Amount per reaction (μ l)	Final concentration
UltraPure water	61	
5 x Buffer	20	1x
100% DMSO	2	2%
100 mM dNTP	1	1 mM
10 μ M F Primer Mix	2.5	0.25 μ M
10 μ M R Primer	2.5	0.25 μ M
Herculase II Fusion DNA Polymerase	1	N/A
1 μ g/mL gDNA	10	0.1 μ g/mL

Table 32 Oligonucleotides used for HiSeq library preparation

All forward oligonucleotides were mixed at equal molar concentrations, introducing artificial diversity to the library from the varied staggered sequences, then used with one reverse primer (unique 8 bp molecular barcode) per sample. **Illumina P5 adaptor**, **Illumina P7 adaptor**, **sequencing forward**, **sequencing reverse**, **stagger (varied) sequence**, **index barcode**, **priming site**. A maximum of nine samples were run on one flow cell.

Primer	Sequence
F1	AATGATACGGCGACCACCGA GATCTACACTCTTTCCCTACACGACGCTCTTCCGATCT TAAGTAGAGGCTT TATATATCTTGTGGAAAGGACGAAACACC
F2	AATGATACGGCGACCACCGA GATCTACACTCTTTCCCTACACGACGCTCTTCCGATCT ATCATGCTTAGCT TTATATATCTTGTGGAAAGGACGAAACACC
F3	AATGATACGGCGACCACCGA GATCTACACTCTTTCCCTACACGACGCTCTTCCGATCT GATGCACATCTGC TTTATATATCTTGTGGAAAGGACGAAACACC
F4	AATGATACGGCGACCACCGA GATCTACACTCTTTCCCTACACGACGCTCTTCCGATCT CGATTGCTCGACG CTTTATATATCTTGTGGAAAGGACGAAACACC
F5	AATGATACGGCGACCACCGA GATCTACACTCTTTCCCTACACGACGCTCTTCCGATCT TCGATAGCAATTC GCTTTATATATCTTGTGGAAAGGACGAAACACC
F6	AATGATACGGCGACCACCGA GATCTACACTCTTTCCCTACACGACGCTCTTCCGATCT ATCGATAGTTGCT TGCTTTATATATCTTGTGGAAAGGACGAAACACC
F7	AATGATACGGCGACCACCGA GATCTACACTCTTTCCCTACACGACGCTCTTCCGATCT GATCGATCCAGTT AGGCTTTATATATCTTGTGGAAAGGACGAAACACC
F8	AATGATACGGCGACCACCGA GATCTACACTCTTTCCCTACACGACGCTCTTCCGATCT CGATCGATTTGAG CCTGCTTTATATATCTTGTGGAAAGGACGAAACACC
F9	AATGATACGGCGACCACCGA GATCTACACTCTTTCCCTACACGACGCTCTTCCGATCT ACGATCGATACAC GATCGCTTTATATATCTTGTGGAAAGGACGAAACACC
F10	AATGATACGGCGACCACCGA GATCTACACTCTTTCCCTACACGACGCTCTTCCGATCT ACGATCGATGGT CCAGAGCTTTATATATCTTGTGGAAAGGACGAAACACC
R1	CAAGCAGAAGACGGCATACGAGATGAAGAAGTGTGACTGGAGTTCAGACGTGTGCTCTTCCGATCT GCCA AGTTGATAACGGACTAGCCTT
R2	CAAGCAGAAGACGGCATACGAGATCGTTACCA GTGACTGGAGTTCAGACGTGTGCTCTTCCGATCT GCCA AGTTGATAACGGACTAGCCTT
R3	CAAGCAGAAGACGGCATACGAGATGTCTGATGTGACTGGAGTTCAGACGTGTGCTCTTCCGATCT GCCA AGTTGATAACGGACTAGCCTT
R4	CAAGCAGAAGACGGCATACGAGATTTACGCACGTGACTGGAGTTCAGACGTGTGCTCTTCCGATCT GCCA AGTTGATAACGGACTAGCCTT
R5	CAAGCAGAAGACGGCATACGAGATTTGAATAGGTGACTGGAGTTCAGACGTGTGCTCTTCCGATCT GCCA AGTTGATAACGGACTAGCCTT
R6	CAAGCAGAAGACGGCATACGAGATTCCTTGGTGTGACTGGAGTTCAGACGTGTGCTCTTCCGATCT GCCA AGTTGATAACGGACTAGCCTT
R7	CAAGCAGAAGACGGCATACGAGATACAGGTATGTGACTGGAGTTCAGACGTGTGCTCTTCCGATCT GCCA AGTTGATAACGGACTAGCCTT
R8	CAAGCAGAAGACGGCATACGAGATAGGTAAGGTGACTGGAGTTCAGACGTGTGCTCTTCCGATCT GCC AAGTTGATAACGGACTAGCCTT
R9	CAAGCAGAAGACGGCATACGAGATAACAATGGGTGACTGGAGTTCAGACGTGTGCTCTTCCGATCT GCCA AGTTGATAACGGACTAGCCTT

Table 33 PCR cycle conditions used to amplify the sgRNAs' guide sequence region and to append the Illumina (HiSeq) compatible adapters and barcodes

Cycle number	Denature	Anneal	Extend
1	95 °C, 20 sec	N/A	N/A
2-25	95 °C, 20 sec	60 °C, 20 sec	72 °C, 40 sec
26	N/A	N/A	72 °C, 3 min

PCR products from all 23 reactions were pooled, purified using the Zymo DNA Clean and Concentrator-5 kit and a small amount of sample separated on a 2% agarose in 1 x Tris-acetate-EDTA (TAE) gel at 100 V for 2.5 hours to confirm the removal of excess primers. The isolated amplicons were then quantified by qPCR reactions using the KAPA Library Quantification Kit, fragments were analyzed using the 2100 BioAnalyzer System and the 2200 Tape Station, mixed at equal molar concentrations and submitted for HiSeq High Output v4 on 1 x 100 bp mode with 10% PhiX spike at the Bauer Core (Harvard University).

2.16 Genome-scale Cas9 mini knockout screen

2.16.1 Genome-scale Cas9 knockout screen design

For CRISPR-Cas9 based knockout, the Cas9–sgRNA complex is targeted to a specific sequence in the coding region of a gene and cleaves both strands of the DNA^{273,274} (**Figure 9A**). The DNA double-strand break is repaired by NHEJ, an error-prone pathway introducing insertion or deletion mutations that can lead to frameshifts²⁷⁵ and a PTC in the expressed transcript, resulting in NMD of the mRNA and aberrant peptide products that are degraded²⁷⁶.

For genome-scale Cas9 knockout screens, a one plasmid system – human lentiCRISPR library v2– was used²⁸⁸ (**Figure 9B-C**).

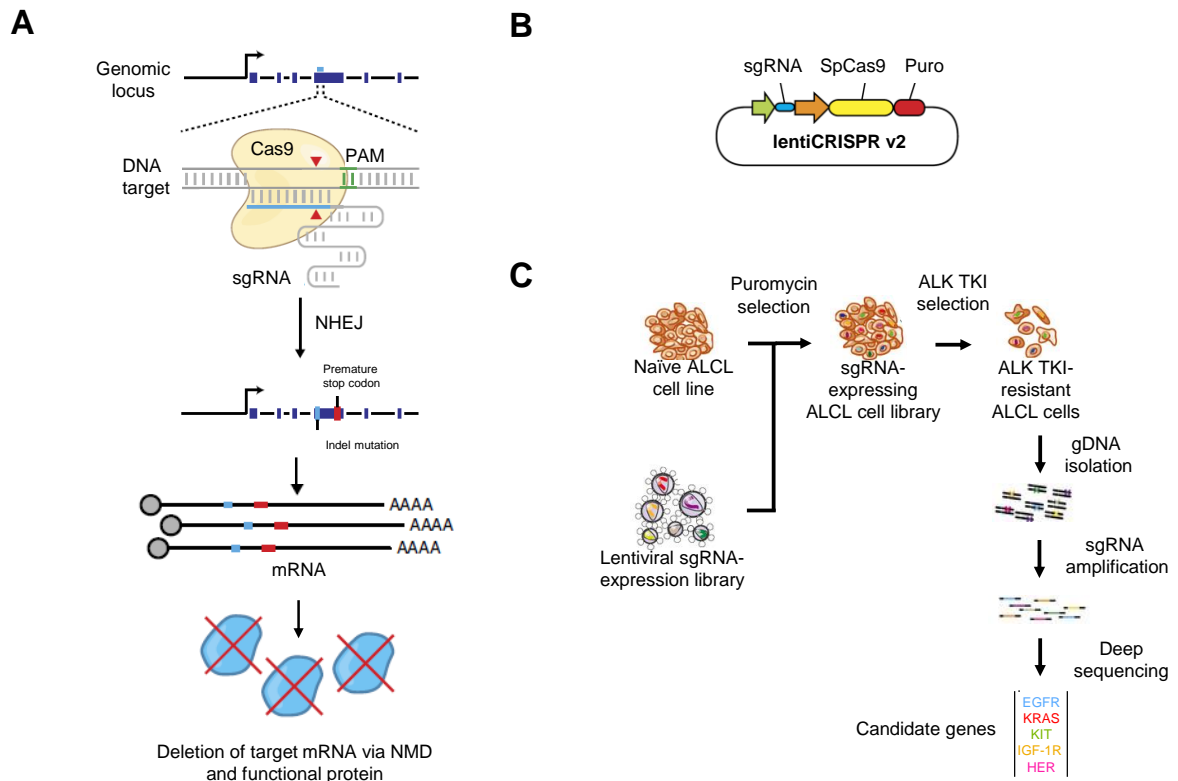


Figure 9 The genome-scale Cas9 knockout screen employed to identify bypass resistance mechanisms to ALK TKIs

(A) Knockout is accomplished by targeted indel formation at a genomic site complementary to the sgRNA. An indel can result in a frameshift, causing early termination, and either production of non-functional protein or non-sense-mediated decay (NMD) of the mRNA transcript. NHEJ, non homologous end joining. PAM: protospacer adjacent motif, (B) Vector-system used for the genome-scale Cas9 knockout screen. (C) Genome-scale Cas9 knockout screens begin with the construction of a plasmid library encoding the effector protein and sgRNAs. These plasmid libraries are packaged into lentivirus particles and then transduced into the cell type of interest to generate stably expressing lines for the screen. A selection pressure –e.g. the ALK TKI crizotinib– is applied and genomic DNA is harvested. Surviving sgRNA sequences (coloured bars) are amplified from genomic DNA and then analyzed by deep sequencing to identify candidate genes. Figure modified from Jung et al., 2017²⁸⁶.

2.16.2 CRISPR Mini Knockout Screen

A CRISPR targeted knockout screen was performed using a mini screen library (**Table 34**) based on the commercially available GeCKO v2 A or B libraries as described previously²⁸⁸.

Table 34 sgRNAs cloned for the CRISPR Mini Knockout Screen

Oligonucleotides used to generate dsDNA fragments containing the 20 bp target sequence that were cloned into lentiCRISPR v2. Grey nucleotides indicate the overhangs. NT = non-targeting. UID = unique ID for Addgene # 1000000048.

Gene	sgRNA	UID	Forward ssDNA element	Reverse ssDNA element
<i>ADORA2A</i>	1	HGLibA_01012	CACCgTCTGGCGGAAGTTCGCGGATA	AAACTATCCGCGAGTTCGCCAGAc
	2	HGLibA_01013	CACCgCTCCTCGGTGTACATCACGG	AAACCCGTGATGTACACCGAGGAGc
	3	HGLibA_01014	CACCgCGTGGCTGCGAATGATCTTG	AAACCAAGATCATTGCGAGCCACGc
	4	HGLibB_01010	CACCgCTCCACCGTGTACACCCG	AAACCGGTGTACATCACGGTGGAGc
	5	HGLibB_01011	CACCgTAGCCATTGGCCCTCCGCTC	AAACGAGCGGAGGCCAATGGCTAc
	6	HGLibB_01012	CACCgGAAGGGATTACAACCGAAT	AAACATTCCGTTGTGAATCCCTTCc
<i>MYC</i>	1	HGLibA_30663	CACCgAACGTTGAGGGGCATCGTCG	AAACCGACGATGCCCTCAACGTTc
	2	HGLibA_30664	CACCgGCCGTATTTCTACTGCGACG	AAACCGTCGCGAGTAGAAATACGGCc
	3	HGLibA_30665	CACCgTGCGTAGTTGTGCTGATGTG	AAACCACATCAGCACAACACTACGCa
	4	HGLibB_30621	CACCgACAACGTCCTGGAGCGCCAG	AAACCTGGCGTCCAAGACGTTGTc
	5	HGLibB_30622	CACCgCGCCGTCGTTGTCTCCCGA	AAACTCGGGGAGACAACGACGGCGc
	6	HGLibB_30623	CACCgTCGCTTACCAGAGTCGCTGC	AAACGCAGCGACTCTGGTAAGCGAc
<i>GPR161</i>	1	HGLibA_19956	CACCgCCCCTCGGCTGGAATCCGTG	AAACCACGGATTCCAGCCGAGGGGc
	2	HGLibA_19957	CACCgCTATGGCTTCATCTCCGCG	AAACCGCGGAAGATGAAGCCATAGc
	3	HGLibA_19958	CACCgCACAGTCGTATCGTGGAGG	AAACCCTCCACGATGACGACTGTGc
	4	HGLibB_19928	CACCgCACGTGCCATGAGCCAGTG	AAACCACTGCGCTCAGGCGTGTGc
	5	HGLibB_19929	CACCgAGAGACTCCACGTCCCGCTC	AAACGAGCGGGACGTTGGAGTCTCTc
	6	HGLibB_19930	CACCgCCCACACCTCACTGCGCTCA	AAACTGAGCGCAGTGAGGTGTGGGc
<i>HELZ2</i>	1	HGLibA_21125	CACCgGACGGGCGCAGGCCCCCT	AAACAGGGGGGCCGTGCGCCCGTCc
	2	HGLibA_21126	CACCgGCCGTGCGCCCGTCGCCATC	AAACGATGGCGACGGGCGCACGGCc
	3	HGLibA_21127	CACCgGGAGTGGTCCGGCGCACGC	AAACGCGTGCGCCGGACCCACTCCc
	4	HGLibB_21097	CACCgCAACCAGCCCTGATGTACC	AAACGGTACATCAGGGCGTGTGc
	5	HGLibB_21098	CACCgTCCGCTCACCTCAGAGTGA	AAACTCCAATCTGAGGTGAGCGGAc
	6	HGLibB_21099	CACCgGCTCCACAGCCTGCGTGC	AAACGCGCACGCAGGCTGTGGAGCc
<i>IL10</i>	1	HGLibA_22943	CACCgGTTGTTAAAGGAGTCTTGC	AAACGCAAGGACTCCTTTAACAAc
	2	HGLibA_22944	CACCgAGCGCCGTAGCCTCAGCCTG	AAACCAGGCTGAGGCTACGGCGCTc
	3	HGLibA_22945	CACCgTTCACATGCGCCTTGATGTC	AAACGACATCAAGGCGCATGTGAa
	4	HGLibB_22912	CACCgCACCTTAAAGTCTCCAGCA	AAACTGCTGGAGGACTTTAAGGTGc
	5	HGLibB_22913	CACCgTCGTATCTTATTGTCATGT	AAACACATGACAATGAAGATACGAc
	6	HGLibB_22914	CACCgGAAGATGTCAAACACTCACTCA	AAACTGAGTGAGTTTGACATCTTCc
<i>IL10RA</i>	1	HGLibA_22946	CACCgTTCGGCGCCGCACATACAGC	AAACGCTGTATGTGCGGCGCCGAa
	2	HGLibA_22947	CACCgGGTCACTGCGGTAAGGTCAT	AAACATGACCTTACCGCAGTGACCc
	3	HGLibA_22948	CACCgGTATGAGATTGCCATTGCGA	AAACTGCGAATGGCAATCTCATAc
	4	HGLibB_22915	CACCgTGGGTAGCTGAATCTCCCG	AAACCGGGAAGATTGAGTACCCAc
	5	HGLibB_22916	CACCgCAGGAGCCCACTCATAGC	AAACGCTATGAAGTGGCGCTCTGc
	6	HGLibB_22917	CACCgTGACGGTCCAGTTGGAGTGC	AAACGCACTCCAAGTGGACCGTCAc
<i>IL10RB</i>	1	HGLibA_22949	CACCgACTTATTGTGTTCAAGTTCG	AAACCGAACTTGAACACAATAAGTc
	2	HGLibA_22950	CACCgTTAGCCATTATTGGACCCCC	AAACGGGGTCCAATAATGGCTAAc
	3	HGLibA_22951	CACCgCTTTCACAGCTCAGTACCTA	AAACTAGTACTGAGCTGTGAAAGc
	4	HGLibB_22918	CACCgCTTCTGATCGGAACAAGC	AAACGCTTTGTTCCGATCAGGAAGc
	5	HGLibB_22919	CACCgTGAGAAATCACATCCGTCA	AAACTGACGGAATGTGATTTCTAc
	6	HGLibB_22920	CACCgTTGAGAATGAATACGAAACT	AAACAGTTTCGTATTCTCTCAAc
<i>MKNK1</i>	1	HGLibA_29341	CACCgGGAGACGCTGTATCAGTGTG	AAACGACACTGATACAGCGTCTCCc
	2	HGLibA_29342	CACCgTCGGAGTAGGGTGTTCGAG	AAACCTCGAAACACCCTACTCCGAc
	3	HGLibA_29343	CACCgGGCACCCTGAACCTTTGGCAT	AAACATGCCAAAGTTCAAGGTGCCc
	4	HGLibB_29300	CACCgGAACCCCTTCCCATCGCAGA	AAACTCTGCGATGGGAAGGGTTCc
	5	HGLibB_29301	CACCgCCTCTGTCCACATCTGCGA	AAACTCGCAGATGGTGACAGGAGGc
	6	HGLibB_29302	CACCgGGAGCCTATGCCAAAGTTCA	AAACTGAACCTTTGGCATAGGCTCCc
<i>P2RY6</i>	1	HGLibA_34890	CACCgCGGACGGCGAAGTCGCCAAA	AAACTTTGGGCACTTCGCCTGCCGc
	2	HGLibA_34891	CACCgGCCAGCACCGCCGAATACAC	AAACGTGTATTGCGCGGTGCTGGCc
	3	HGLibA_34892	CACCgAAACGGCGCGTGCCTTTGT	AAACACAAAGGCACGCGGCCGTTTc
	4	HGLibB_34844	CACCgCGGCGCTCGAGCGCACTGCC	AAACGGCAGTGCCTGACGCGGGCc
	5	HGLibB_34845	CACCgTCACCCAGAAAGTTCGCG	AAACGCGGAACCTTCTTCTGGGTGAc
	6	HGLibB_34846	CACCgTCGCCGGCGGAACCTTCTCT	AAACAGAAGAAGTTCGCGCGGCGAc
<i>PGBD1</i>	1	HGLibA_36215	CACCgCCTGGAGATGAGCTGATCCG	AAACCGGATCAGCTCATCTCCAGGc
	2	HGLibA_36216	CACCgCACTTCAGGGTGGTTATCCC	AAACGGGATAACCACCCTGAAGTGc

Gene	sgRNA	UID	Forward ssDNA element	Reverse ssDNA element
	3	HGLibA_36217	CACCgTGGCCTTACTCATCGGACTG	AAACCAGTCCGATGAGTAAGGCCAc
	4	HGLibB_36168	CACCgACAGGACATGCACCCAATGG	AAACCCATTGGGTGCATGTCTGTc
	5	HGLibB_36169	CACCgCACATCTGAGTCTGACTCGG	AAACCCGAGTCAGACTCAGATGTGc
	6	HGLibB_36170	CACCgTGCTGTGTTTAAACCCAGTC	AAACGACTGGGTTAAACACAGGCCAc
RORC	1	HGLibA_41780	CACCgGCCTCTTACCCCGTGAGGCT	AAACAGCCTCACGGGGTAAGAGGCCc
	2	HGLibA_41781	CACCgGTGATCCCTTGCAAAATCTG	AAACCAGATTTTGCAAGGGATCACc
	3	HGLibA_41782	CACCgAAGTCGTCTGGGATCCACTA	AAACTAGTGGATCCCAGACGACTTc
	4	HGLibB_41728	CACCgAGAGACAGCACCAGCCCTCA	AAACTGAGGCTCGGTGCTGTCTCTc
	5	HGLibB_41729	CACCgTATCACCTGTGAGGGGTGCA	AAACTGCACCCCTCACAGGTGATAc
	6	HGLibB_41730	CACCgACTCACCTTGACCCCTCAC	AAACGTGAGGGGTGCAAGGTGAGTc
SH2D2A	1	HGLibA_43888	CACCgGGTGCGGTTCCAGCGAGAGCG	AAACCGCTCTCGCTGAACCGCACCCc
	2	HGLibA_43889	CACCgTCACCTGTAAGTCAGCACGA	AAACTCGTCTGACTTACAGGTGAc
	3	HGLibA_43890	CACCgTGCGGGTCATGTCTGTGATC	AAACTCACCTGTAAGTCAGCACGAc
	4	HGLibB_43835	CACCgACCTCCGGGTGATGAAGCCA	AAACTGGCTTCATCACCCGGAGGTc
	5	HGLibB_43836	CACCgCACTACCAGCAGTAGCCCC	AAACGGGCTACACTGCGGTGAGTc
	6	HGLibB_43837	CACCgGGCTTGTTCCAGAAGACCC	AAACGGGTCTTCTGGAACCAAGCCc
NT	1	HGLibA_64384	CACCgACGGAGGCTAAGCGTCGCAA	AAACTTGCGACGCTTAGCCTCCGTc
	2	HGLibA_64386	CACCgATCGTTTTCCGCTAACGGCG	AAACCGCCGTTAAGCGGAAACGATc
	3	HGLibA_64387	CACCgGTAGGCGCGCCGCTCTCTAC	AAACGTAGAGAGCGGCGCGCCTACc
	4	HGLibA_64399	CACCgCGACTAACCGGAAACTTTTT	AAACAAAAAGTTTCCGGTTAGTGCc
	5	HGLibA_64407	CACCgCTATCTCGAGTGGTAATGCG	AAACCGCATTACCACCTGAGATAGc
	6	HGLibA_64411	CACCgCGGACGACTCAACCTAGTC	AAACGACTAGGTTGAGTCGTGCGGc
	7	HGLibA_64420	CACCgCGTGGCCGGAACCGTCATAG	AAACCTATGACGGTTCCGGCCACGc
	8	HGLibA_64433	CACCgATCGTATCATCAGCTAGCGC	AAACGCGCTAGCTGATGATACGATc
	9	HGLibA_64440	CACCgCCGCTATTGAAACCGCCAC	AAACGTGGGCGGTTTCAATAGCGGc
	10	HGLibA_64443	CACCgTTCGCACGATTGCACCTTGG	AAACCCAAGGTGCAATCGTCCGAAc
	11	HGLibA_64447	CACCgTACGCTTGCGTTTAGCGTCC	AAACGGACGCTAAACGCAAGCGTAc
	12	HGLibA_64468	CACCgTCTGGCTTGACACGACCGTT	AAACAACGGTCTGTCAAGCCAGAc
	13	HGLibA_64470	CACCgAGCACGTAATGTCCGTGGAT	AAACATCCACGGACATTACGTGCTc
	14	HGLibA_64472	CACCgACTGCGGAGCGCCCAATATC	AAACGATATTGGGCGCTCCGCACTc
	15	HGLibA_64482	CACCgAAGAGTAGTAGACGCCCGGG	AAACCCCGGGCGTCTACTACTCTTc
	16	HGLibA_64484	CACCgCGGCTCGTTCTACGCACTGA	AAACTCAGTGGCTAGAACGAGCTCCc
	17	HGLibA_64510	CACCgATGCGCTTTAATCGCCGTTT	AAACGAAACGGGATTAAAGCGCATc
	18	HGLibA_64520	CACCgTGGAAATCGACTGTGCGCTT	AAACAAGCGCACAGTGCATTTCCAc
	19	HGLibA_64521	CACCgATTAGCCGTTGCCATATCAA	AAACTTGATATGGCAACGGCTAATc
	20	HGLibA_64534	CACCgTGACGCGATAGAGTTGGCTT	AAACAAGCCAACCTATCGCGTCAc
	21	HGLibA_64550	CACCgCGGCTTTGTGCCCGTAAGC	AAACGCTTACGGGCAACAAAGCCGc
	22	HGLibA_64557	CACCgCAGTGTCCGAGCGATATTTT	AAACAAAATATCGCTCGGACACTGc
	23	HGLibA_64563	CACCgACAGCGCTCTCGTGTACTAT	AAACATAGTACACGAGAGCGCTGTc
	24	HGLibA_64661	CACCgCCGGCAAGAACTATACTTG	AAACCAAGTATAGTTTCTTGCCGGc
	25	HGLibA_64663	CACCgCCGCTGTCTACTAATCTCA	AAACTGAGATTAGTGAGACAGCGGc
	26	HGLibA_64671	CACCgCAGACGGTTGGTAAGGACGC	AAACGCGTCTTACCAACCGTCTGc
	27	HGLibA_64674	CACCgCAGGTTTGCACGCTAGCTA	AAACTAGTATGCGTGCAAACTGc
	28	HGLibA_64689	CACCgCGTTGGCAGTAAACGCAACT	AAACAGTGTTCGCTTACCCCAACGc
	29	HGLibA_64724	CACCgTGGCGGCCAAACTTAAACAC	AAACGTGTTAAGTTTGGGCGGCCAc
	30	HGLibA_64735	CACCgGCCATTCTAGTCCCAGCATA	AAACTATGCCGGGACTAGAATGGCCc
	31	HGLibA_64744	CACCgATGCTGCAGCTTACGATCA	AAACTGATCGTAAAGCTGCAGCATc
	32	HGLibA_64746	CACCgACATACCCCCCTGGTTCAGA	AAACTCTGAACCAGGGGGTATGTc
	33	HGLibA_64797	CACCgTTCAATTCACCGAGGGCGCA	AAACTGCGCCCTCGGTGAATTGAAc
	34	HGLibA_64805	CACCgACCCATTGAGAGTCCGCTGA	AAACTCAGGCGACTCTCAATGGGTc
	35	HGLibA_64816	CACCgCTGCGTGTCTTGCTCGCATG	AAACCATGCGAGCAAGACACGCAGc
	36	HGLibA_64818	CACCgTGTCTTCGGATAGGCGGCTT	AAACAAGCCGCTATCCGAAGACAc
	37	HGLibA_64833	CACCgCTGGCCGAATCTCACTATGT	AAACACATAGTGAGATTGCGCCAGc
	38	HGLibA_64876	CACCgTTTTGACTCTAATCACCAGT	AAACACCGGTGATTAGAGTCAAAAc
	39	HGLibA_64946	CACCgGAACCGACTTGAAGGGGGCT	AAACAGCCCCCTTCAAGTCCGTTCCc
	40	HGLibA_64947	CACCgACTGAGTGGGTAACACGCAT	AAACATGCGTGTACTACCCACTAAGTc
	41	HGLibA_64950	CACCgCCTAAACTCAGACGCACTAC	AAACGTAGTGCCTGAGTTTAGGc
	42	HGLibA_64951	CACCgTACCCTGGATTGCTTGGCG	AAACCGCAAGGACAATCCAGGGTAc
	43	HGLibA_64965	CACCgGATCATAATCGCTTCAAGCA	AAACTGCTTGAAGCGATTATGATCc
	44	HGLibA_65069	CACCgGAACGTAGAAATTTCCATTT	AAACAAATGGGAATTTCTACGTTCCc
	45	HGLibA_65102	CACCgACGCATGCTTCCCAAAGCGT	AAACACGCTTTGGGAAGCATCCGTCc
	46	HGLibA_65134	CACCgGGCGTTAATTAACAGTTTTT	AAACAAAACAGTTTAAATTAACGCCc
	47	HGLibA_65198	CACCgGATTTTAGCTTAGGTCTTAC	AAACGTAAAGACCTAAGCTAAAATCCc
	48	HGLibA_65230	CACCgCTCCAGTACCAGTCAAGTTC	AAACGAACTGACTGGTACTGGGAGc
	49	HGLibA_65280	CACCgCCATTCACAAATCCCACTACA	AAACTGTAGTGGGATTGTGAATGGc
	50	HGLibA_65321	CACCgATCAAAGTGTCTGACTTATT	AAACAATAAGTCAGACACTTTGATc

The mini screen library consisted of 6 sgRNAs for each gene and 50 non-targeting sgRNAs. sgRNA cloning is described above. The lentiviral library was generated in HEK293T cells by seeding 5×10^6 cells in a 10 cm dish one day before transfection. For each dish, 15 μg of the targeted screen plasmid library was co-transfected with 5 μg of pMD2.G, 5 μg of pRSV-Rev and 5 μg of pCMVR8.74 in 600 μL of reaction buffer supplemented with 9 μL of Xfect™ Transfection Reagent. Supernatant containing virus was collected 60 hours after transfection and ultra-centrifuged at 24,000 rpm for 2 hours at 4 °C to concentrate the virus. Aliquots were stored at –80 °C. SUP-M2 derived TS and K299 cells were infected with the library at a MOI of 0.3 and a ratio of at least 500 cells/sgRNA and selected with puromycin (0.2-0.3 $\mu\text{g}/\text{mL}$) for 7 days. Separate infections were conducted for the GeCKO v2 A and B mini libraries. After 7 days, 500 cells/sgRNA were collected as the input control (D0), and genomic DNA was extracted with the Phenol/Chloroform protocol. The remaining cell pools, at a density of 500 cells/sgRNA, were subsequently cultured with crizotinib (80 nM for TS, 100 nM for K299) or DMSO for 14 days and harvested for DNA extraction with the Phenol/Chloroform protocol. Amplification of the specific sgRNAs was performed in a 2-step PCR reaction. First, priming site to lentiCRISPR GeCKO v2 was added using v2Adaptor_F AATGGACTATCATATGCTTACCGTAACTTGAAAGTATTTTCG and v2Adaptor_R TCTACTATTCTTTCCCTGCACTGTTGTGGCGATGTGCGCTCTG in 13 separate 100 μL reactions with 10 μg genomic DNA per reaction as the input. Next, amplicons were pooled and a second PCR performed in a 100 μL reaction volume with 5 μL of input of the pooled first PCR reaction, each amplified with a reverse primer and forward primer (Table 35). The resulting amplicons were gel extracted. Products were tested for their concentration and specificity using High sensitivity D1000 ScreenTape and qPCR using the KAPA Library Quantification Kit. Libraries were pooled and sequenced using an Illumina NextSeq500 SE on 35bp mode with 150 cycles and with a 20% PhiX spike.

Table 35 Oligonucleotides used for HiSeq library preparation
Illumina P5 adaptor, **Illumina P7 adaptor**, **sequencing forward**, **sequencing reverse**, **stagger (varied) sequence**, **index barcode**, **priming site**. One forward oligonucleotide was used with one reverse primer per sample. A maximum of ten samples were run on one flow cell.

Primer	Sequence
F1	AATGATACGGCGACCACCGA <u>GATCTACACTCTTTCCCTACACGACGCTCTTCCGATCTTCTTGTGGAAAGGAC</u> GAAACACCG
F2	AATGATACGGCGACCACCGA <u>GATCTACACTCTTTCCCTACACGACGCTCTTCCGATCTATCTTGTGGAAAGGA</u> CGAAACACCG
F3	AATGATACGGCGACCACCGA <u>GATCTACACTCTTTCCCTACACGACGCTCTTCCGATCTGATCTTGTGGAAAGG</u> ACGAAACACCG
F4	AATGATACGGCGACCACCGA <u>GATCTACACTCTTTCCCTACACGACGCTCTTCCGATCTCGATCTTGTGGAAAG</u> GACGAAACACCG
F5	AATGATACGGCGACCACCGA <u>GATCTACACTCTTTCCCTACACGACGCTCTTCCGATCTTCGATCTTGTGGAAA</u> GGACGAAACACCG
F6	AATGATACGGCGACCACCGA <u>GATCTACACTCTTTCCCTACACGACGCTCTTCCGATCTATCGATCTTGTGGAA</u> AGGACGAAACACCG
R1	<u>CAAGCAGAAGACGGCATAACGAGATAAGTAGAGTGACTGGAGTTCAGACGTGTGCTCTTCCGATCTTCTACT</u> ATTCTTTCCCTGCACTGT
R2	<u>CAAGCAGAAGACGGCATAACGAGATACACGATCGTACTGGAGTTCAGACGTGTGCTCTTCCGATCTATCTAC</u> TATTCTTTCCCTGCACTGT
R3	<u>CAAGCAGAAGACGGCATAACGAGATCGCGCGGTGACTGGAGTTCAGACGTGTGCTCTTCCGATCTGATCT</u> ACTATTCTTTCCCTGCACTGT
R4	<u>CAAGCAGAAGACGGCATAACGAGATCATGATCGTACTGGAGTTCAGACGTGTGCTCTTCCGATCTCGATCT</u> ACTATTCTTTCCCTGCACTGT

2.17 Short-hairpin RNA (shRNA) Knockdown

pLKO.1-puro shRNA^{302,303} constructs targeting the gene of interest were constructed using the standard Broad Institute protocol³⁶¹. First, two oligonucleotides were synthesized to be annealed (**Table 36**). Using T4 DNA Ligase, the annealed dsDNA was then ligated into the pLKO.1-puro vector, which had been digested with AgeI-HF and EcoRI-HF. The ligated constructs were then transformed in NEB Stable Competent *E. coli* using the manufacturer's protocol, the plasmids isolated with the QIAprep Spin Miniprep Kit, plasmid DNA quantified using a Nanodrop 1000 and the sequence verified by standard Sanger sequencing using a LKO.1_F oligonucleotide 5'-GACTATCATATGCTTACCGT-3'.

Table 36 Oligonucleotides used to generate dsDNA fragments containing the target shRNA sequence that were cloned into pLKO.1-puro

All primers were synthesized by Sigma-Aldrich. Red (Sense), Blue (Loop), Antisense (Green), Black (Term).

Gene	#	Primer sequence (5' - 3')
STAT3	1	CCGGGCACAATCTACGAAGAATCAACTCGAGTTGATTCTTCGTAGATTGTGCTTTTT
	2	CCGGGCTGACCAACAATCCCAAGAACTCGAGTTCTTGGGATTGTTGGTCAGCTTTTT
PIM1	1	CCGGACATCCTTATCGACCTCAATCCTCGAGGATTGAGGTCGATAAGGATGTTTTT
	2	CCGGCATCCGCGTCTCCGACAACCTTCTCGAGAAGTTGTCGGAGACGCGGATGTTTTTTG

All pLKO.1-puro constructs were packaged into lentiviral particles by co-transfection of pLKO.1-puro vectors with psPax2 and pMD2.G into 293FT cells as described above. Viruses were harvested 60 hours after transfection and stored in -80 °C. ALCL cells were transduced with viral particles of pLKO.1-puro at an MOI of < 0.7 then incubated with puromycin (see **Table 30** for concentration) 24 hours post viral transduction for three days to completion (defined as 0% survival in uninfected cells).

2.18 Drug Synergy Experiments

For dose-response curves, cells were treated with log-scale concentrations of ALK inhibitors as previously described, in addition to fixed concentrations of AZD1208 as indicated. Potential synergy between ALK inhibitors and AZD1208 was evaluated by calculating the combination index (CI) based on the Bliss Independence model³⁶². The CI was calculated with the following equation: $CI = (E_a + E_b - (E_a * E_b)) / E_{ab}$, where E_a indicates the viability effect of drug A (ALK inhibitor) and E_b indicates the viability effect of drug B (AZD1208) and E_{ab} indicates the viability effect of the drug combination. $CI < 1$ indicates synergism, $CI = 1$ indicates additivity and $CI > 1$ indicates antagonism. For dose-response matrices, cells were treated with log-scale concentrations of each compound in 8x8 grids and the DMSO concentration was maintained at 0.3%. Cell viability was measured with CellTiter-Blue as previously described and data were normalized to the average of all untreated wells on the plate ($n = 17$). All synergy experiments were performed in technical triplicates.

2.19 Immunohistochemistry (IHC)

IHC was performed on FFPE sections with the conventional avidin–biotin–peroxidase method. Heat antigen retrieval was performed using citrate buffer pH 6.1 and endogenous peroxidases were quenched by incubating sections in 3% H₂O₂ in PBS for 10 minutes. First, sections were blocked using the Avidin/Biotin blocking kit. Then, the indicated primary antibodies were added in 1% BSA/PBS and incubated at 4°C overnight. Finally, slides were incubated with biotin-conjugated secondary antibodies

using the IDtect Super Stain System – Horseradish peroxidase (HRP) and developed using the AEC substrate kit. Next, the sections were washed with PBS 3 times between each step. The stained slides were mounted with Aquatex and assessed by an experienced pathologist (blindly in respect to clinicopathological parameters and patient outcome) for both the intensity and percentage of positively stained cells: 0 negative, 1+ weak, 2+ moderate and 3+ strong staining. Positive staining was considered if present in >1% of cells.

Table 37 Antibodies used to detect proteins by IHC

Antibody	Dilution	Company	Cat. no.
IL10RA antibody	1:100	Abcam	ab94811
IL10RB antibody	1:100	Abcam	ab106282
IL10 antibody	1:200	Abcam	ab34843

2.20 Chromatin Immunoprecipitation (ChIP) qPCR

ChIP-qPCR analysis for IL10, IL10RA, IL10RB and IRF4 was performed on 10×10^6 ALCL cells per sample using an anti-STAT3 (124H6) or anti-GFP antibody. Following treatment with 1000 nM crizotinib or DMSO for 3 hours in growth medium, 10×10^6 cells were fixed with 0.75% formaldehyde for 15 minutes with orbital shaking at room temperature. Subsequently, glycine was added to a final concentration of 125 nM and the reaction was incubated for 5 minutes at room temperature. Next, cells were washed twice with cold PBS, collected by centrifugation then flash frozen in dry ice/isopropanol and stored at -80 °C until use.

Cross-linked cell pellets were lysed in 650 μ L ChIP lysis buffer (50 mM HEPES-KOH pH7.5, 140 mM NaCl, 1 mM EDTA pH8, 1% Triton X-100, 0.1% sodium deoxycholate, 0.1% SDS) supplemented with cOmplete™ Mini EDTA-free protease inhibitor cocktail per 20×10^6 cells, followed by sonication for a total of 10 minutes with 30 seconds pulses on followed by 30 seconds off, with a Bioruptor® Pico in 15 mL polypropylene centrifuge tubes utilizing sonication beads. Immunoprecipitation reactions were performed by incubating the sonicated samples overnight with 3 μ g STAT3 (Cat#: 9139, Cell Signalling) or green fluorescent protein (GFP, Cat#: ab290, Abcam) antibodies at 4 °C. Next, antibodies and chromatin were captured using 50 μ L of Protein G Dynabeads per sample for 2 hours at 4 °C. Beads were first washed three times with low salt buffer (0.1% SDS, 1% Triton X-100, 2 mM EDTA, 20 mM Tris-HCL pH 8.0, 150 mM NaCl), followed by three washes with high salt buffer (0.1% SDS, 1% Triton X-100, 2 mM EDTA, 20 mM Tris-HCl pH 8.0, 500 mM NaCl), two washes with LiCl wash buffer (0.25 M LiCl, 1% NP-40, 1% Sodium Deoxycholate, 1 mM EDTA, 10 mM Tris-HCl pH 8.0) and two final washes with TE buffer (10 mM Tris pH 8.0, 1 mM EDTA). DNA was eluted in 200 μ L elution buffer (1% SDS, 100mM NaHCO₃), the RNA was then digested using 2 μ L RNase A (10 mg/mL) at 37 °C for 30 minutes, before cross-links were reversed following incubation at 65 °C for 2 hours with 2 μ L proteinase K (20 mg/mL).

De-crosslinked DNA was purified with a Zymo DNA Clean and Concentrator-5 kit. ChIP and input DNA were analyzed with SYBR-Green qPCR analysis performed using the QuantStudio™ 6 Flex Real-Time PCR System in accordance with the manufacturer's protocol using qPCR primers (**Table 38**) designed based on ChIP-seq dataset GSE117164.

Table 38 **ChIP-qPCR Sequencing Primers**

Gene	Forward primer sequence	Reverse primer sequence
IL10 TSS	CGGGAAACCTTGATTGTGGC	TTCACCTCTCTGTCCCCCTT
IL10RA TSS up	AGGTGCGAGAGACTGAGGAT	GGTTTCCCTTGCTTGCTTGAA
IL10RB TSS	GGTCGTGTGCTTGGAGGAAG	CCTCACCTGACACCAGCAG
Control region	ATTCCACCTTGTCCAGCCCT	GGTTTTATCCCTCTCCCGAC
IRF4	CTCTAAACACCGCGGAGAGG	CTTGCAGAGCGTGTAAACGG

2.21 Enforced IL10RA overexpression

For enforced IL10RA overexpression, ALCL cells were selected 24 hours after infection with lentivirus particles of pLX302 IL10RA-V5 puro or pLX302 control constructs with 1 µg/mL puromycin before being plated for an experiment.

2.22 mRNA sequencing

Libraries were prepared with the TruSeq Stranded mRNA kit protocol according to the supplier's recommendations. Each transcriptome library was sequenced on an Illumina NextSeq500 as paired-end 75 bp reads.

2.23 Bioinformatics analysis

2.23.1 ChIP-seq Data Analysis

ChIP-seq data were converted to the FASTQ format using the fastq-dump tool (v2.8.2; part of SRA toolkit). ChIP-seq reads were aligned to the human genome (hg19) or mouse genome (MM10) with Bowtie2 with settings 'end-to-end', 'very-sensitive', and 'no-unal'³⁴⁰. Reads with a mapping quality < 35 (samtools view q = 35) and PCR duplicates (samtools rmdup) were filtered with SAMtools³³⁹. Output BAM files were sorted using BEDTools³⁴¹ "sort" function and converted into BigWig track files using genomeCoverageBed followed by UCSC utility "bedgraphToBigWig"³⁴³. The genome browser tracks were visualized in IGV v2.3.92^{342,343}.

2.23.2 Survival Analysis

Survival analysis was conducted using the Kaplan-Meier method, with the p-value determined by a log-rank test. PFS was defined as the time to recurrence or relapse, or if a patient had died without recurrence, the time to death. OS was determined as cancer-specific death. Hazard ratio (HR) and multivariate analysis adjusting for clinical parameters including sex, age, disease stage, CNS involvement, MDD/MRD status and ALK-autoantibody status was determined through a Cox proportional hazards model using the "coxph" function in the survival package in R³³⁸.

In building Kaplan-Meier curves, thresholds for the binary classification of intensity levels were determined using the "surv_cutpoint" function, survival analysis was performed with the "survfit" function, and visualizations were obtained using the "ggsurvplot" function, all in the survminer package in R³³⁷.

2.23.3 CRISPR Overexpression Screen Deconvolution and Analysis

Raw FASTQ sequencing files were demultiplexed with bcl2fastq2 v2.2 allowing for 0 bases mismatch, then matched to the guide sequences from the library files using the Model-based analysis of genome-wide CRISPR/Cas9 knockout (MAGeCK) count function³²⁹. Per-sgRNA read counts were then subjected to MAGeCK-MLE analysis, modelling each experimental iteration as a separate batch, as suggested by principal component analysis. MAGeCK-VISPR was used for quality control and visualization, specifically to obtain p-values and to test false discovery rates (FDR). Corresponding gene IDs were mapped to corresponding gene symbols using the biomaRt package in R³³⁴. Due to the absence of NT guides in this library, an analysis to control the empirical false positive rate could not be performed.

2.23.4 CRISPR Mini Knockout Screen Deconvolution and Analysis

The sgRNA sequences from the mini library files were aligned to the FASTQ file of each sample using BLAST aligner, allowing for a maximum of 2 bases of mismatch. The number of uniquely aligned reads for each sgRNA were counted and the number of reads for each unique sgRNA for a given sample were RPM (Reads Per Million mapped reads) normalized. Boxplots were generated by R boxplot function based on the log₂ (RPM normalized sgRNA counts) value, showing the difference of sgRNA representation at different time points, without (vehicle = DMSO) and with crizotinib treatment. The box extends from the first to the third quartile with the whiskers denoting 1.5 times the interquartile range.

2.23.5 mRNA-Seq Data Analysis

Data were provided under the MAPPYACTS protocol. Raw paired-end FASTQ files were mapped against the human reference genome (GRCh38.p12) and GENCODE transcriptome annotation version v29³⁵¹ using Salmon³³⁰ (version 0.14.0) with the default parameters. Strand-specific transcript counts were converted into gene counts with the tximport package in R³³¹. Differential gene expression analysis and normalization were performed using the edgeR package in R³³².

2.23.6 Gene Set Enrichment Analysis (GSEA) and Gene Ontology (GO) Analysis

GSEA was performed with the fgsea package³³⁵ in R using pathway annotations from the Kyoto Encyclopedia of Genes and genomes (KEGG)³⁵². GO analysis was performed with the topGO package³³⁶ in R.

2.23.7 Gene Expression Analysis

Published gene expression data from T-cell lymphoma patients (GSE78513, GSE65823, GSE6338, GSE14879, GSE19069, GSE58445) and lymphoma cell lines (GSE107951, GSE6338, GSE14879, GSE19069, GSE6184, GSE94669) were analyzed to better understand the biological relevance of IL10RA. For GSE78513, GSE65823, GSE6338, GSE14879, GSE19069, GSE58445 and GSE107951, gene expression profiling was performed using the HG-U133-plus2.0 arrays (Affymetrix Inc., Santa Clara, CA). For GSE6184, gene expression profiling was performed using the HG-U133A Array (Affymetrix Inc., Santa Clara, CA). For GSE94669, gene expression profiling was performed using the Illumina HumanHT-12 V4.0 expression beadchip (Illumina Inc., San Diego, CA).

The final study consisted of 78 ALK+ ALCL and 48 ALK- ALCL, 159 PTCL-NOS, 110 AITL patients, and 12 reactive Lymphnodes; as well as 64 lymphoma cell lines, 5 ALL cell lines and 1 CLL cell line.

Raw CEL files were loaded with the GEOquery package³⁴⁴ and subsequently subject to quality control using the arrayQualityMetrics package³⁴⁶, both in R. Background correction, normalisation and expression calculation were performed using the rma method with the oligo package in R³⁴⁵.

Annotation of the transcript clusters was added using the AnnotationDbi package³⁴⁷ in R. The analysis of differential expression using a linear model as well as the correction for multiple testing were conducted using the limma package³⁴⁸ in R.

For GSE94669, the raw Illumina text files were loaded then quality assessment and low-level analysis performed with the beadarray package³⁴⁹ in R. Annotations were added using the illuminaHumanv4.db package³⁵⁰ in R.

2.23.8 Co-Expression Analysis

Data used for co-expression analyses between IL10RA and IL10 in different cancer types were obtained from the Human Protein Atlas RNA-seq datasets portal. Pearson correlation coefficients to quantify co-expression between genes were assessed using VST-transformed gene expression levels. The threshold for significant Pearson correlation between gene pairs was determined as the Pearson correlation coefficient associated with the 99th percentile among 5,000 random protein-coding/noncoding gene pairs.

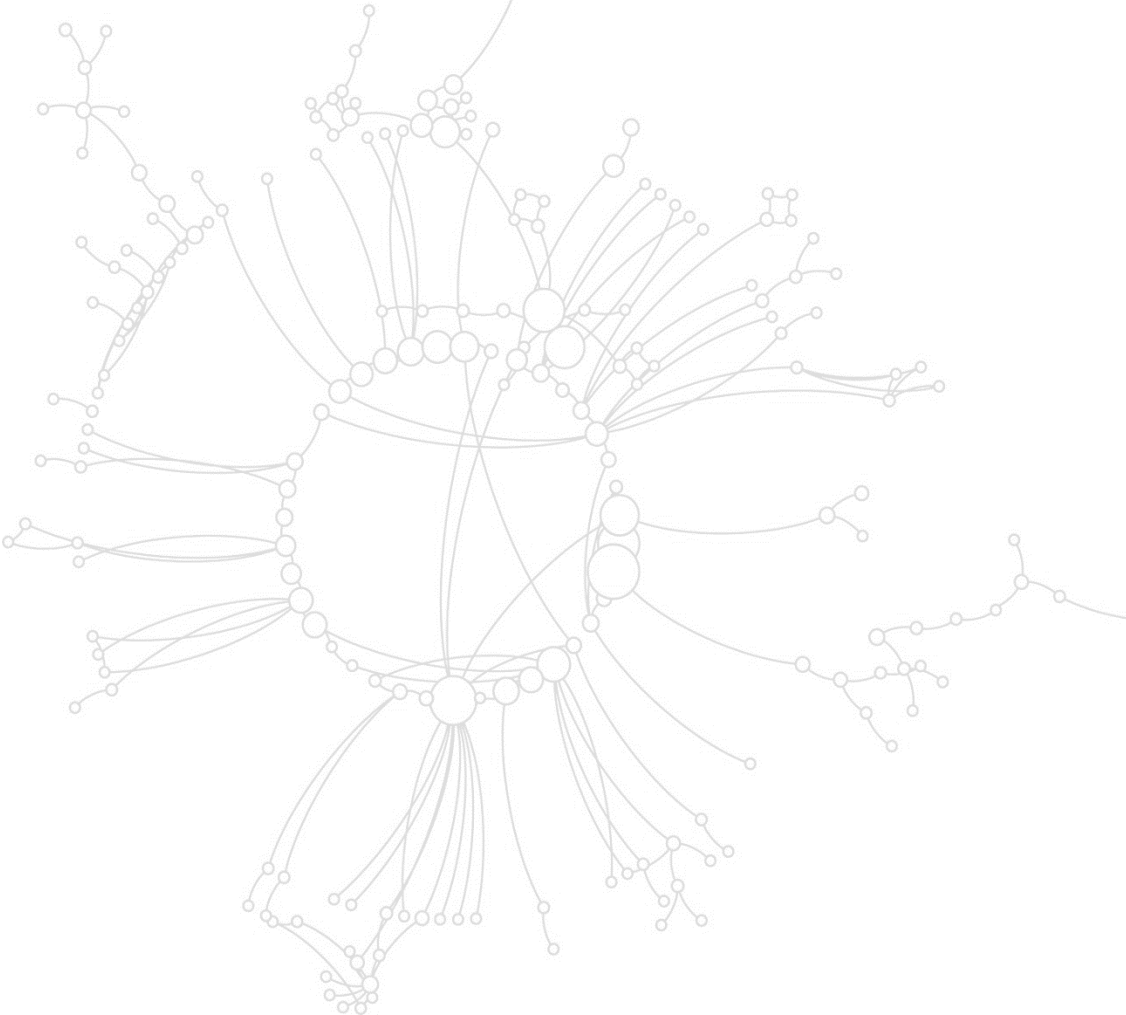
2.23.9 Analysis of Public Gene Expression Datasets

PIM1 was investigated by Kaplan-Meier EFS analysis with microarray data from primary NB patient cohorts using R2: Genomics Analysis and Visualization Platform (<http://r2.amc.nl>). The following cohorts were analysed: Kocak ($n = 476$) (accession: GSE45547)³⁶³ and SEQC ($n = 498$) (accession: GSE49710)³⁶⁴. The cut-off method was selected as 'scan' to determine the optimal threshold for each gene, and significance was assessed by the log-rank test. The p -values were corrected for multiple testing using the Bonferroni method. The HR was determined through a Cox proportional hazards model using the "coxph" function in the survival package in R³³⁸.

2.23.10 Waterfall Plot

The response to crizotinib/brigatinib/vehicle was determined by comparing tumour volume change at time t of study end point or censorship to its baseline: % tumour volume change = $\Delta\text{Vol} = ((V_t - V_{\text{baseline}}) / V_{\text{baseline}}) \times 100\%$. Tumour volumes were estimated using the modified ellipsoid formula: $V = ab^2/2$, where a and b ($a > b$) are length and width measurements. The study end point was reached once tumours reached 15 mm diameter in any direction or after 21 days of consecutive treatment. Mice were censored due to tumour ulceration, sudden death, self-mutilation, sickness or if mice remained tumour-free after 21 days of consecutive treatment.

CHAPTER 3 Bypass resistance landscape to crizotinib inhibition in ALK+ ALCL



3.1 Introduction

The first chemotherapy protocol was introduced to paediatric ALCL patients in the 1980s, but EFS and OS rates have scarcely improved and there is a clear need for new, less toxic and more effective therapies in the relapse setting²⁰. The NPM1-ALK fusion protein is the oncogenic driver in 75% of ALK+ ALCL²⁸. A chromosomal translocation gives rise to NPM1-ALK, leading to ectopic expression of this constitutively-active kinase, in turn up-regulating effectors of cell survival and proliferation, including the crucially important JAK/STAT pathway^{225,365}.

ALK is an ideal drug target particularly as endogenous expression is limited to neuronal cells during neonatal development¹⁰⁴. Therefore, three trials in the USA (COG-ANHL12P1, NCT01979536), France (AcSé CRIZOTINIB, NCT02034981) and Japan (UMIN000028075) have investigated the ALK/MET/ROS1 inhibitor crizotinib in paediatric ALK+ ALCL patients. Though the final results from these trials are yet to come, abrupt relapses following crizotinib discontinuation have been described^{126,127} suggesting that ALK inhibitors may have to be taken indefinitely and cases of crizotinib resistance have been reported¹³⁸. Preliminary results from the AcSé CRIZOTINIB trial showed that 5/15 patients progressed and that all cases of progression on crizotinib occurred during the first 3 months following treatment initiation¹²⁶.

An understanding of the molecular pathways enabling tumours to harbor primary drug resistance or to acquire resistance to targeted therapies is critical for precisely predicting patient responses and for the identification of additional targetable pathways to maximize clinical benefit²³⁸. The consensus gold standard for identifying ALK inhibitor resistance mechanisms involves WES coupled with RNA-seq of tumour tissues obtained from patients via multiple biopsies throughout their treatment²³⁸. Until now fewer than 130 paediatric ALCL patients (NCT01979536, n = 103; NCT02034981, n = 11; UMIN000028075, n = 10) have been treated with crizotinib in a clinical trial setting and the majority of these patients (all those recruited to NCT01979536) have not been re-biopsied at relapse due to ethical constraints and/or the health status of the patient.

However, defining a global landscape of resistance mechanisms requires matched presentation-relapse tumour specimens from a sufficiently large number of patients^{238 230,239}. For instance, the cataloguing of epidermal growth factor receptor (EGFR) inhibitor resistance in NSCLC patients with an incidence rate of 18,252 – 54,756 newly diagnosed cases per year in the USA is still incomplete with around 30% of relapsed patients currently presenting with ‘unknown’ resistance mechanisms^{228–230}. This problem is intensified for paediatric malignancies, such as ALK+ ALCL with an incidence rate of approximately 80 newly diagnosed and 16 relapse cases per year in children and adolescents in Europe²⁷. Such an extended discovery phase of resistance mechanisms leads to a deadly lag in the development of salvage therapeutic strategies. To counteract this, we employed genome-wide CRISPR overexpression and knockout screens combined with RNA-seq data from ALK inhibitor relapsed patient tumours to identify biological pathways involved in primary or acquired resistance to ALK-targeted therapy in ALK+ ALCL.

The data presented in this chapter of the thesis largely forms sections of a publication in *Blood* (Prokoph et al.)³⁰¹, which can be found in Appendix 1.

3.1.1 Aims

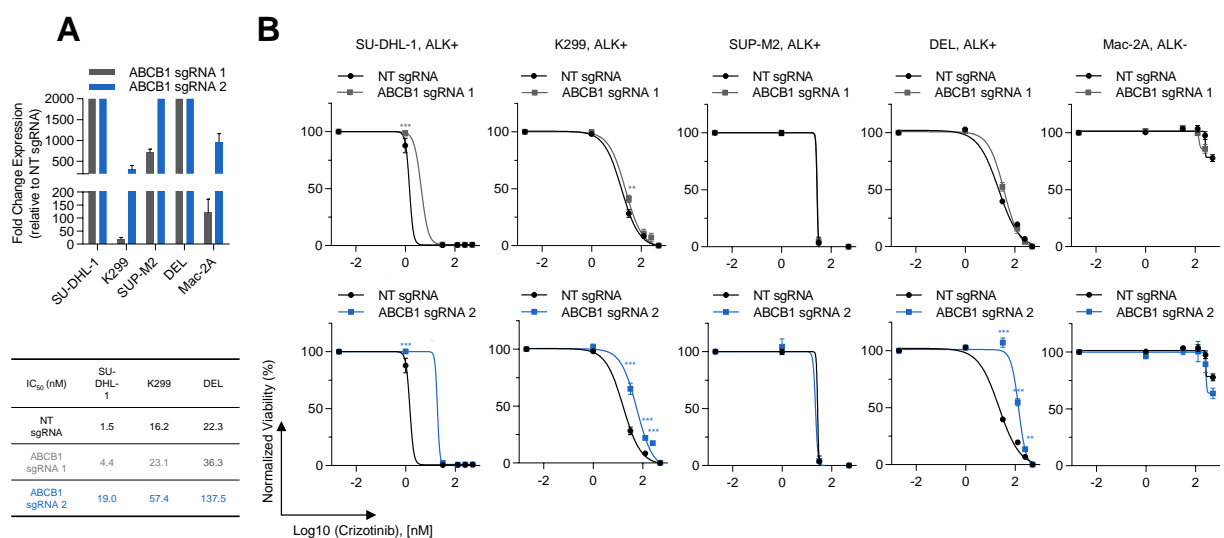
This chapter aims to:

- Validate CRISPR/dCas9-VP64 activity in the ALCL cell lines of interest
- Apply the validated CRISPR activation platform to screen for potential drivers of resistance to crizotinib inhibition using a genome wide sgRNA library
- Obtain a list of candidates that may induce resistance to crizotinib
- Perform individual validation assays for each of the candidate genes to confirm their capability to induce resistance to crizotinib
- Determine the overexpression levels of candidates in TKI resistant cell lines and an orthotopic xenograft model
- Determine which targets identified by the CRISPR screens are of potential clinical relevance by RNA-seq of ALK inhibitor relapse compared to sensitive patient tumours

3.2 Validation of the dCas9-VP64 induced overexpression phenotype

In order to comprehensively define potential mechanisms driving resistance to crizotinib in a high-throughput manner, we established a CRISPR-based overexpression system in ALCL cell lines^{271,286}. Transcriptional upregulation is achieved by directly fusing VP64 to catalytically inactive Cas9 (dCas9) and further recruiting the transcriptional activation domains p65 and HSF1, eventually recruiting the transcriptional machinery to the transcription start site (TSS) of the desired target genes.

Using this system, we first upregulated expression of the ATP binding cassette subfamily B member 1 (ABCB1) (**Figure 10A**), a transporter expressed in the liver and blood-brain barrier to efflux toxic agents³⁶⁶, that was previously shown to mediate crizotinib resistance in ALK+ NSCLC³⁶⁷. In doing so, we were able to increase the IC₅₀ of crizotinib for 3 of 4 ALK+ ALCL cell lines (SU-DHL-1/K299/DEL) but not for an ALK- ALCL cell line (Mac-2A) (**Figure 10B**), confirming that sensitivity to crizotinib can be readily manipulated.



(legend on next page)

Figure 10 ABCB1 overexpression induces resistance to crizotinib

(A) Fold change in expression levels of ABCB1 modulated by CRISPR overexpression for two sgRNAs in the indicated ALCL cell lines. Data are represented as means \pm SD of technical replicates, $n = 3$. **(B)** Overexpression of ABCB1 modified sensitivity to crizotinib in SUDHL-1, K299 and DEL, but not SUP-M2 or Mac-2A cell lines. Viability of the indicated ALCL cell lines based on normalized CellTiter-Blue fluorescence reads on exposure to increasing concentrations of crizotinib for 48 hours when expressing 1 of 2 of the indicated sgRNAs inducing overexpression of ABCB1. Data are represented as means \pm SD, $n = 3$. Two-sample t test: * $p < 0.05$. ** $p < 0.01$, *** $p < 0.001$. Reproduced from Prokoph et al.³⁰¹.

Next, to test the efficiency of the CRISPR overexpression system in ALCL cell lines, we used a panel of validated sgRNAs³⁰⁰ targeting the promoters of 15 genes, which were previously shown to lead to crizotinib resistance in EML4-ALK+ NSCLC²³². We found that the ability of most sgRNAs to achieve significant overexpression was highly cell line dependent. Specifically, we observed the highest activation of expression in SUP-M2 and DEL and the lowest in K299 cell lines (**Figure 11**).

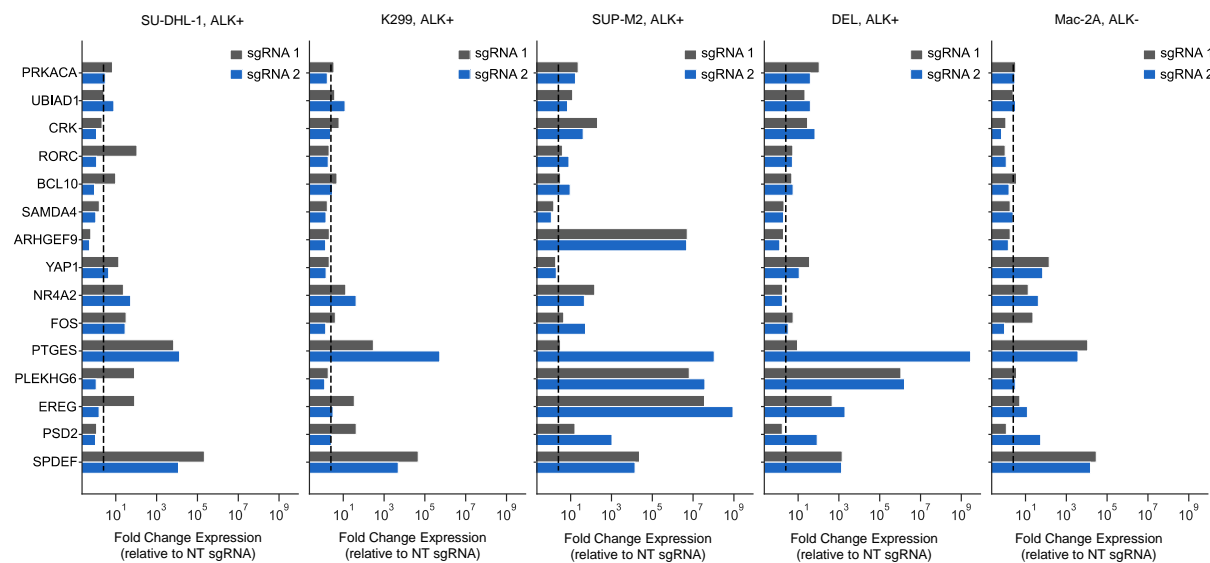


Figure 11 The dCas9-VP64-based CRISPR activation system induces overexpression of various genes in different ALCL cell lines

Fold change in expression levels modulated by CRISPR overexpression for two sgRNAs per gene versus non-targeting (NT) control sgRNA in ALCL cell lines. Data are represented as means of technical replicates, $n = 3$. An absolute log fold change of 2.5 is indicated by dashed lines. Reproduced from Prokoph et al.³⁰¹.

3.3 CRISPR Overexpression Screens Identify Genes Modulating Crizotinib Sensitivity in ALCL Cell Lines

To account for this inter-cell line variability, we applied our CRISPR-based overexpression platform to screen for potential drivers of resistance to crizotinib in three different ALCL cell lines using a genome wide sgRNA library containing 70,290 sgRNAs targeting 23,430 protein-coding genes²⁷¹ (**Figure 12A**). dCas9-VP64/MS2-P65-HSF1-expressing K299, DEL and SUP-M2 cells were transduced with the library and selected in zeocin for 7 days (day 0). For library screening, we exposed the selected cells to crizotinib or DMSO for 14 days (day 14). Genomic DNA was isolated from the cells on days 0 and 14, and deep-sequenced to measure read counts for each sgRNA. Following treatment, changes in abundance of each sgRNA were assessed using the MAGeCK count function³²⁹ and analyzed for quality control (**Figure 12B-D**). We identified a host of genes enriched in cells exposed to crizotinib compared

to D0, including genes with known relevance to ALCL disease biology, such as STAT3^{225,365}, RORC³²¹, MYC³⁶⁸ and IRF4^{321,368,369} (**Figure 12E**).

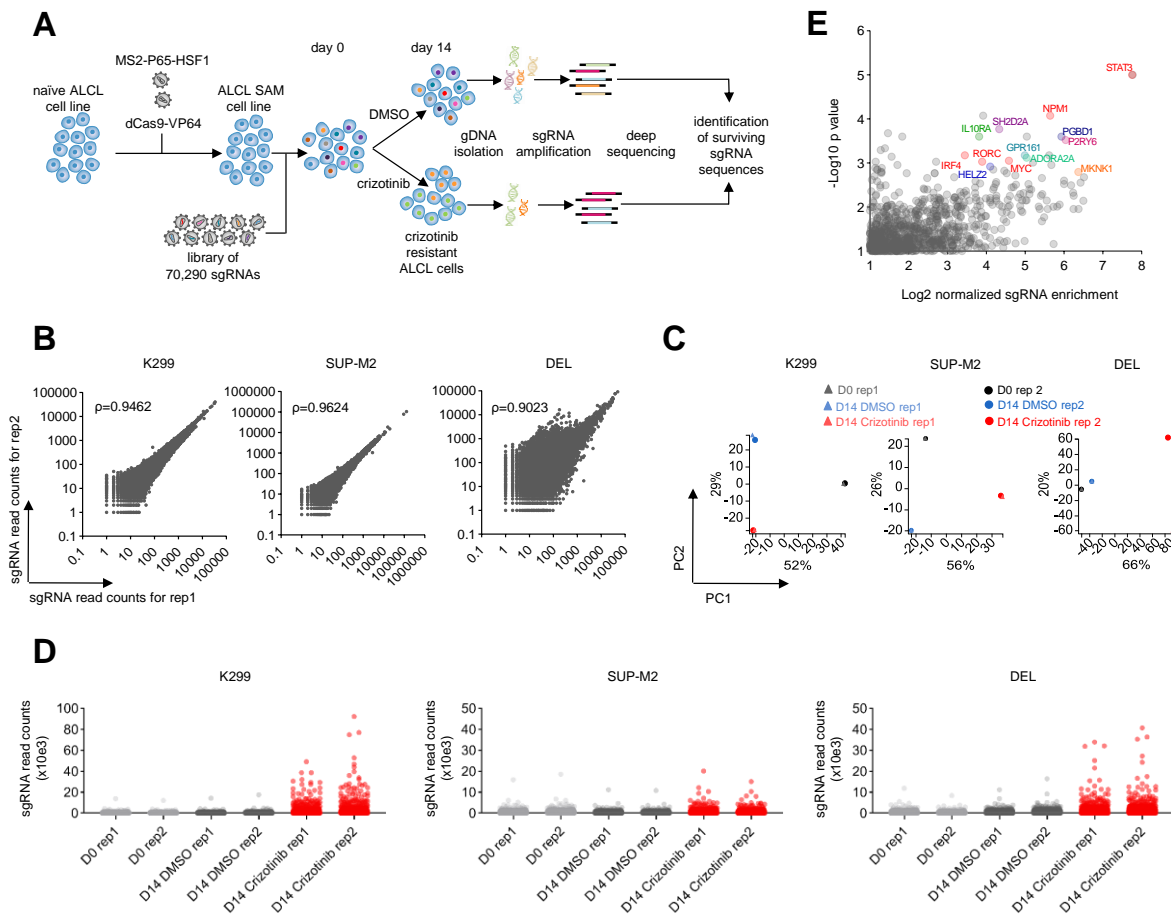


Figure 12 CRISPR Overexpression Screens Identify Genes Modulating Crizotinib Sensitivity in ALCL Cell Lines

(A) Schematic of the CRISPR-dCas9-based overexpression screen for the identification of genes whose activation modifies sensitivity to crizotinib in ALCL cell lines: Transcriptional activation is achieved by fusing/recruiting catalytically inactive Cas9 (dCas9) to transcriptional activation domains (VP64/p65, HSF1) to recruit the transcriptional machinery to the transcription start site of the desired target genes. As a first step a SAM (synergistic activation mediator) complex composed of catalytically inactive Cas9 (dCas9) fused to the transcriptional activator VP64 and further activation domains (p65, HSF1) are transduced into ALCL cell lines to generate stably expressing lines for the screen. Afterwards ALCL cell lines are transduced with the sgRNA library and selected with zeocin for 7 days (day 0). Next, crizotinib/DMSO selection pressure is applied, and genomic DNA is harvested on day 0 and after 14 days of treatment. The sgRNA regions are amplified from genomic DNA and then analyzed by next-generation sequencing followed by statistical analyses to identify candidate genes. (B) Correlation of sgRNA read counts across separate infection replicates for the indicated ALCL cell lines. ρ , Spearman correlation coefficient. (C) Principle Component (PC) analysis of sgRNA read counts across the sequencing libraries for the indicated ALCL cell lines. D = day, rep = separate infection replicate. (D) Distributions of sgRNA read counts across the CRISPR overexpression sequencing library for the indicated ALCL cell lines. D = day, rep = separate infection replicate. (E) Global changes in sgRNA representation of genes before and after 14 days of treatment with (120/150/300 nM for DEL/SUP-M2/K299) crizotinib, detected in at least two of the three ALCL cell lines tested. Reproduced from Prokoph et al.³⁰¹.

STAT3, a well-known downstream mediator of NPM1-ALK^{225,365}, was the most significantly enriched gene in all three CRISPR overexpression screens (**Figure 12E**, **Figure 13A**), thereby confirming the validity of this approach. In addition, NPM1 was also significantly enriched in the screens (**Figure 12E**, **Figure 13B**). Transcription of NPM1-ALK is driven by the NPM1 promoter³. It is therefore likely that

overexpression of NPM1 could mediate sensitivity to ALK inhibition by driving overexpression of NPM1-ALK. Indeed, sgRNA-mediated overexpression of NPM1 in 3 ALK+ ALCL cell lines confirmed co-overexpression of NPM1 and NPM1-ALK in these cell lines (**Figure 13C**). These data are consistent with previous studies that show overexpression of EML4-ALK or NPM1-ALK as a resistance mechanism to ALK TKIs in ALK+ NSCLC and ALCL respectively^{210,226,327,370,371}.

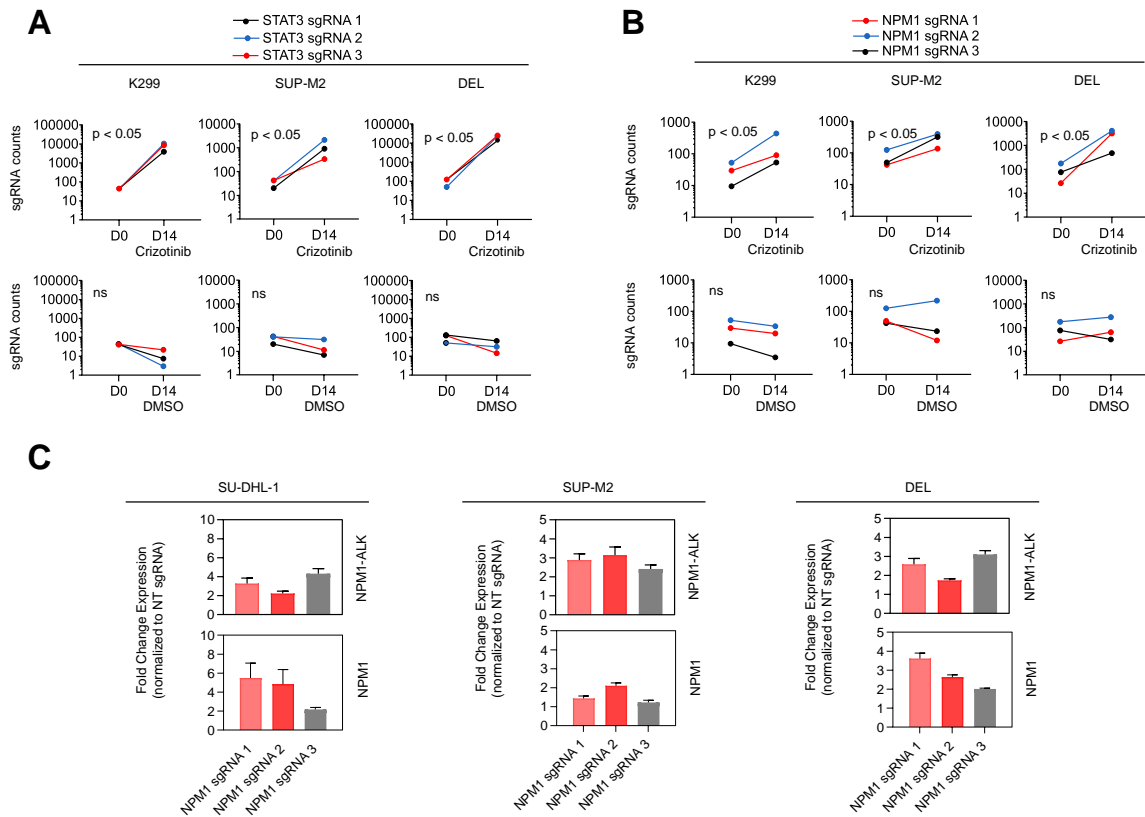


Figure 13 CRISPR Overexpression Screens Identified STAT3 and NPM1 to Modulate Crizotinib Sensitivity in ALCL Cell Lines

(A) Read counts of sgRNAs targeting STAT3 before and after a 14-day incubation with crizotinib (upper panel, 120/150/300 nM for DEL/SUP-M2/K299) or DMSO (lower panel) in the indicated ALCL cell lines. Data are presented as means, n = 2. The p values were calculated using a Wilcoxon matched pairs signed rank test. D = day. **(B)** Read counts of sgRNAs inducing overexpression of NPM1 before and after a 14-day incubation with crizotinib (upper panel, 120/150/300 nM for DEL/SUP-M2/K299) or DMSO (lower panel) in the indicated ALCL cell lines. Data are presented as means, n = 2. The p values were calculated using a Wilcoxon matched pairs signed rank test. D = day. **(C)** Fold change in expression levels of NPM1 (bottom panel) and NPM1-ALK (top panel) expression level for each of the 3 sgRNAs inducing overexpression of NPM1 versus non-targeting (NT) control sgRNA in ALCL cells. Data are represented as means \pm SD, n = 3. Reproduced from Prokoph et al.³⁰¹.

3.4 Validation of candidate genes identified in the screen

3.4.1 Overexpression-based validation of Candidate Genes Modulating ALK TKI Sensitivity in ALCL Cell Lines

We selected the 10 most significantly enriched genes that were shared between at least two ALK+ ALCL cell lines for further validation (**Figure 12E, Table 39**). First, we overexpressed these genes as well as NPM1 (positive control), using 2 sgRNAs per gene, in the 3 ALCL cell lines previously employed for the screens as well as additional ALK+ (SU-DHL-1) and ALK- (Mac-2A) cell lines. After confirming overexpression levels, growth inhibition in the presence of crizotinib was assessed (**Figure 14**).

Table 39 Candidate genes and their relevance in ALCL and other cancers
 To the best of our knowledge this information is currently publicly not available (N/A).

Gene	Protein	Relevance in ALCL disease biology	Role in cancer progression/treatment resistance
<i>IL10RA</i>	Interleukin-10 receptor subunit alpha	Merkel and colleagues ³⁷² showed that knockdown of IL10RA with shRNA in K299 cells led to increased cell death.	Béguelin et al. ³⁷³ identified that IL10RA is amplified in 21% of DLBCLs and its expression is a predictor for patient survival.
<i>GPR161</i>	G-protein coupled receptor 161	N/A	Feigin et al. ³⁷⁴ identified that GPR161 overexpression in Triple-negative breast cancer (TNBC) correlates with poor prognosis by promoting cell proliferation.
<i>ADORA2A</i>	Adenosine receptor A2a	N/A	Merighi et al. ³⁷⁵ summarized the role of ADORA2A in cancer progression and therapy resistance, as well as presented clinical candidates that are tested as single agents or in combination with immunotherapeutic agents.
<i>P2RY6</i>	P2Y purinoceptor 6	N/A	Wilson et al. ²³² identified P2RY6 as a putative resistance driver in crizotinib resistant ALK+ NSCLC
<i>MKNK1</i>	MAP kinase-interacting serine/threonine-protein kinase 1	N/A	Xie et al. ³⁷⁶ , Hou et al. ³⁷⁷ and Dreas et al. ³⁷⁸ summarized the role of MKNK1 in cancer including mantle cell lymphoma, chronic lymphocytic leukemia (CLL) and DLBCL ³⁷⁹ .
<i>RORC</i>	Nuclear receptor ROR-gamma	Mathas and colleagues ³²¹ have shown that pharmacological inhibition of RORC as single treatment leads to a reduction in cell viability that is significantly enhanced when RORC inhibitors (SR2211, SR1903 or GSK805) are used in combination with crizotinib. Ng et al. ³¹² performed CRISPR knockout screens in ALCL cell lines and confirmed RORC as vulnerability in ALK+ and ALK-ALCL.	Wilson et al. ²³² identified RORC as a putative resistance driver in crizotinib resistant ALK+ NSCLC
<i>PGBD1</i>	PiggyBac transposable element-derived protein 1	N/A	N/A
<i>SH2D2A</i>	SH2 domain-containing protein 2A	N/A	N/A
<i>HELZ2</i>	Helicase with zinc finger domain 2	N/A	N/A
<i>MYC</i>	Myc proto-oncogene protein	Lenz and colleagues ³⁶⁸ have shown that MYC is essential for ALCL survival, as both knockdown of MYC and pharmacologic inhibition of MYC signaling were toxic to ALCL cell lines. Ng et al. ³¹² performed CRISPR knockout screens in ALCL cell lines and confirmed MYC as vulnerability in ALK+ and ALK-ALCL.	Lyapichev et al. ³⁸⁰ identified that MYC expression was associated with a shorter overall survival in ALK+ ALCL.

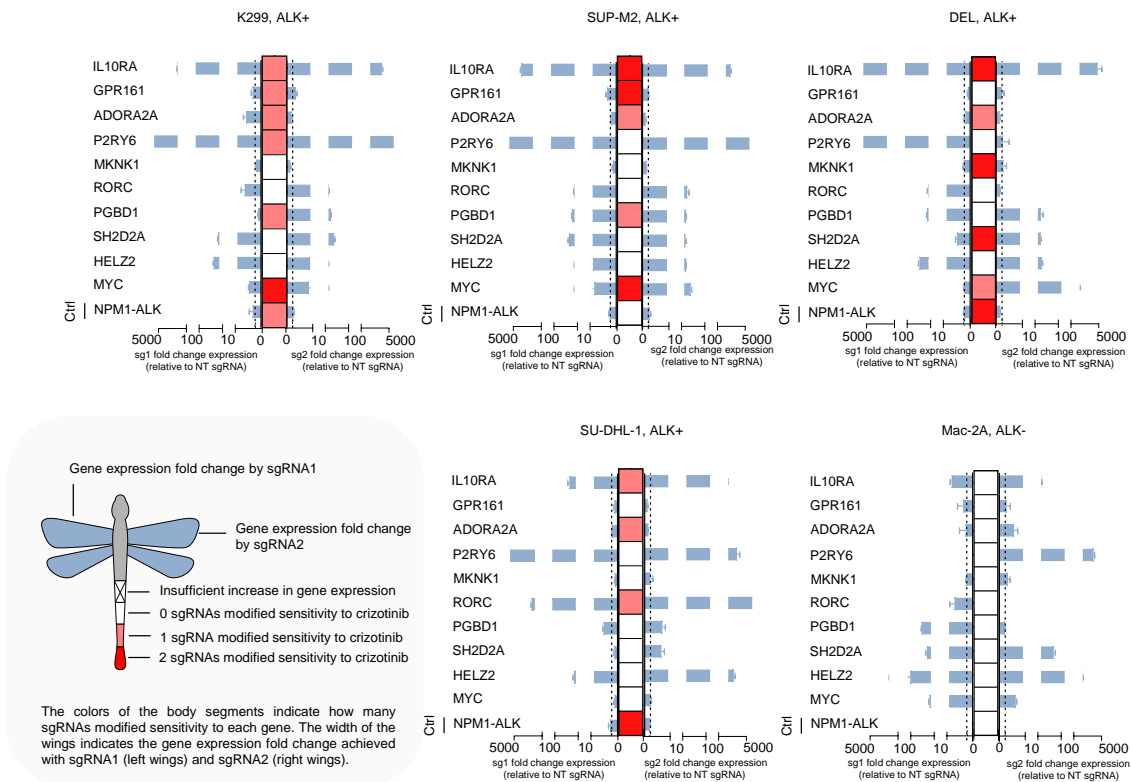


Figure 14 Overexpression of candidate genes identified from the SAM screen induce resistance to crizotinib

Dragonfly plots of crizotinib efficacy measurements in the indicated ALCL cell lines expressing sgRNAs targeting the indicated genes based on normalized CellTiter-Blue fluorescence reads following 48 hours of treatment with crizotinib. Six-point dose response curve experiments were performed as described in Figure 10B. An sgRNA was defined as modifying the sensitivity to crizotinib treatment when the difference between the sgRNA to non-targeting (NT) control sgRNA in a two-sample t test was $p \leq 0.05$. Data are represented as means, $n = 3$. Fold change of expression levels (blue-gray) modulated by CRISPR overexpression for two sgRNAs relative to non-targeting (NT) control sgRNA was determined at baseline. Data are represented as means \pm SD of technical replicates, $n = 3$. Ctrl = control. Reproduced from Prokoph et al.³⁰¹.

The most consistent targets, modifying crizotinib sensitivity in all ALK positive cell lines were IL10RA and ADORA2A (Figure 15).

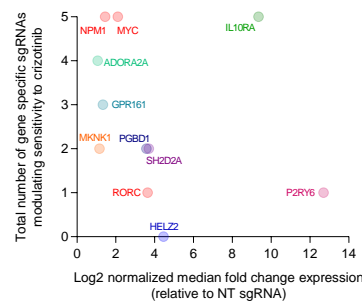


Figure 15 Overexpression-based validation of candidate genes

Fold change of expression levels of the CRISPR screen candidate genes modulated by CRISPR overexpression for two sgRNAs relative to non-targeting (NT) control sgRNA in 4 ALK+ ALCL cell lines (K299/DEL/SUP-M2/SU-DHL-1) plotted against the total number of gene specific sgRNAs that modified sensitivity to crizotinib in 48-hour CellTiter-Blue assays. Reproduced from Prokoph et al.³⁰¹.

3.4.2 Knockout-based validation of Candidate Genes Modulating ALK TKI Sensitivity in ALCL Cell Lines

We next reasoned that if overexpression of a gene would decrease sensitivity to crizotinib, then knockout of the same gene should increase sensitivity to crizotinib. To address this, we first analyzed a publicly available CRISPR knockout screen dataset³¹² by Ng et al. of 5 ALK+ and 1 ALK- ALCL cell line. While *MYC* and *RORC* were identified as vulnerabilities in ALK+ ALCL, knockout of the other 8 gene hits did not induce cell death.

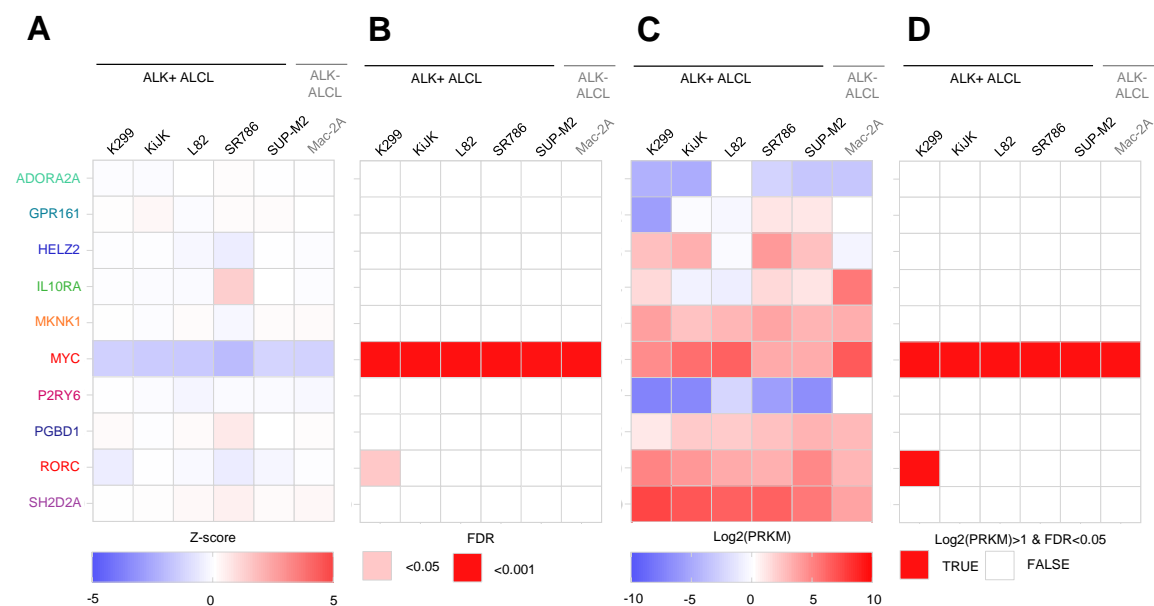


Figure 16 CRISPR knockout screen dataset by Ng et al. identifies *MYC* and *RORC* as vulnerabilities in ALK+ and ALK- ALCL

(A) Genes ranked by Z-score. (B) Corresponding false-discovery rate (FDR) q-values. (C) Corresponding gene expression level; RPKM, reads per kilobase of transcript, per million mapped reads. (D) Combined gene expression levels and FDRs identify vulnerabilities as true or false.

Having established that *ADORA2A*, *GPR161*, *HELZ2*, *IL10RA*, *MKNK1*, *P2RY6*, *PGBD1* and *SH2D2A* are non-essential genes in ALK+ ALCL, we next performed a mini CRISPR knockout screen in two ALCL cell lines targeting the same 10 candidate genes. K299/SUP-M2 cells were transduced with a GeCKO v2 mini library containing 6 sgRNAs per gene plus 50 NT sgRNAs and selected with puromycin for 7 days (day 0) before exposure to crizotinib or DMSO for 14 days (day 14) and processing as previously conducted for the activation screen (Figure 17A). Knockout of *IL10RA*, *P2RY6* and *PGBD1* rendered cells more sensitive to crizotinib in all SUP-M2, but not K299, cell lines (Figure 17B-C).

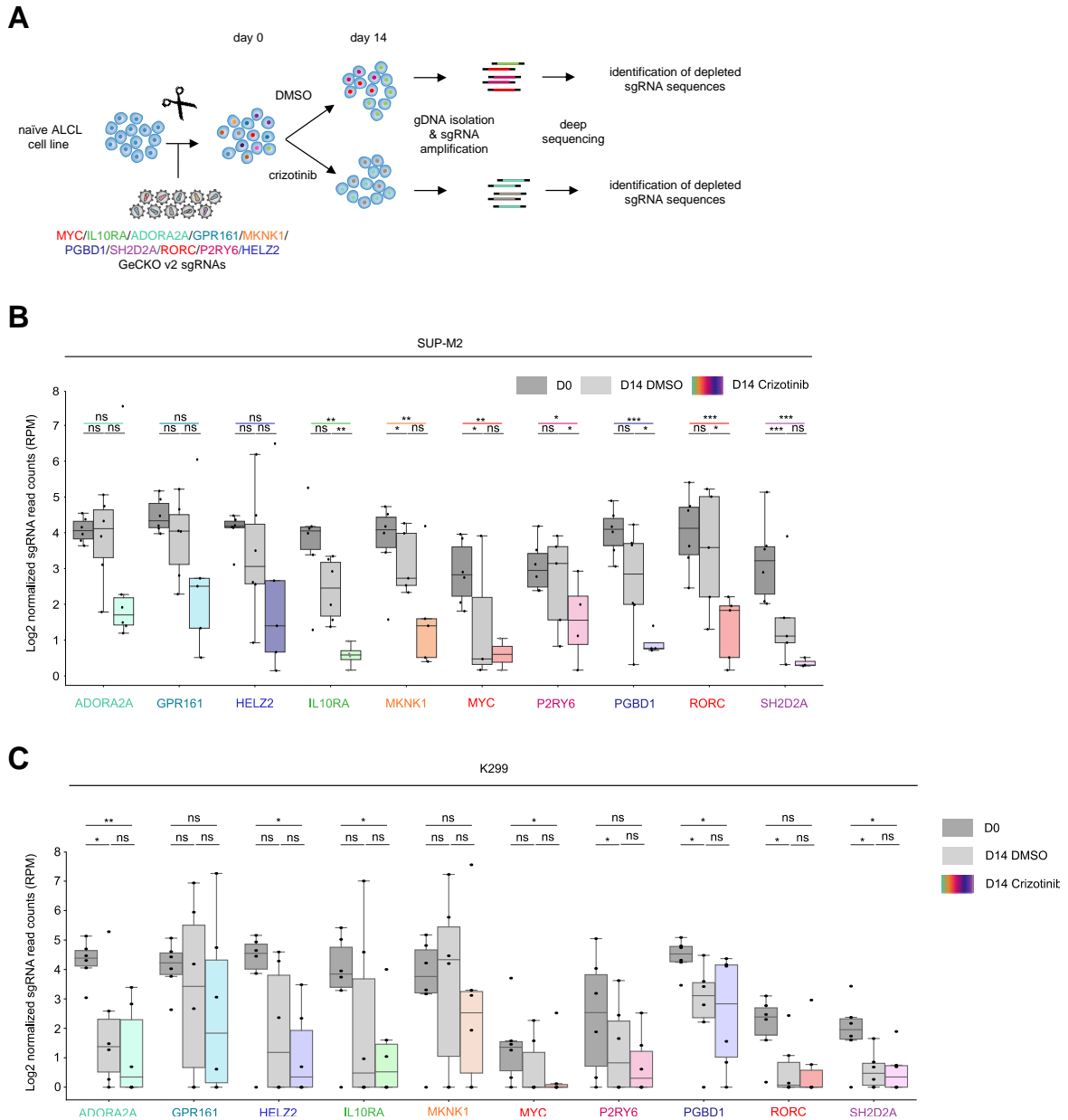


Figure 17 Knockout-based analysis

(A) Schematic of the CRISPR-Cas9-based mini knockout screen for the identification of genes whose knockout modifies sensitivity to crizotinib in ALCL cell lines. A crizotinib/DMSO selection pressure is applied, and genomic DNA is harvested on day 0 and after 14 days of treatment. The sgRNA regions are amplified from genomic DNA and then analyzed by next-generation sequencing followed by statistical analyses. (B-C) Read counts of 6 sgRNAs targeting the indicated genes before and after a 14-day incubation with DMSO or (80 nM for SUP-M2, 100 nM for K299) crizotinib in the indicated ALCL cell lines. Data are represented as boxplot with individual points representing each sgRNA ($n = 6$). Unpaired t test: * $p < 0.05$, ** $p < 0.01$, *** $p < 0.001$. RPM = Reads Per Million mapped reads. Reproduced from Prokoph et al.³⁰¹.

3.4.3 Validation of Candidate Genes Modulating ALK TKI Sensitivity in Resistant ALCL Cell Lines

In parallel, the same 10 candidate genes were analyzed for their expression levels in cells that had been chronically exposed to ALK TKIs (crizotinib, alectinib, brigatinib or lorlatinib) to render them resistant, and were compared with transcript levels in parental (treatment naïve) cells (**Figure 18**). Among the genes assessed, IL10RA was overexpressed in 30% of resistant cell lines (4/12). This suggests that upregulation of IL10RA is a common mechanism of resistance in ALCL cell lines. Interestingly, overexpression of IL10RA was largely mutually exclusive with overexpression of NPM1-ALK (**Figure 18**).

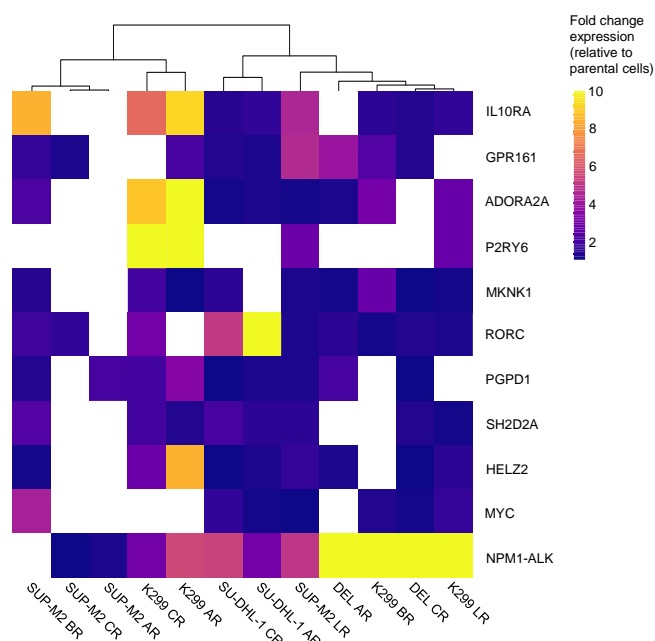


Figure 18 Hit validation in resistant ALCL cell lines

Fold change expression of the indicated genes in crizotinib resistant (CR), alectinib resistant (AR), brigatinib resistant (BR) and lorlatinib resistant (LR) ALCL cell lines compared to parental cell lines. Genes with a fold change expression of > 2 were classified as overexpressed in resistant compared to parental cell lines. White indicates downregulated genes. Data are represented as means, n = 3. Reproduced from Prokoph et al.³⁰¹.

3.4.4 Validation of Candidate Genes Modulating ALK TKI Sensitivity in a Resistant Orthotopic ALCL Cell Line Xenograft Model

Next, we analyzed publically available RNA-seq data³²⁸ of lorlatinib-resistant tumours compared to vehicle control treated tumours from cell line-derived orthotopic xenografts (**Figure 19A-B**). HELZ2 and IL10RA were upregulated in 3 lorlatinib-resistant tumours compared to 3 vehicle control treated tumours from cell line-derived orthotopic xenografts (**Figure 19B**).

Specifically, IL10RA was significantly upregulated in 3/10 lorlatinib-resistant tumours compared to 3 vehicle control treated tumours from cell line-derived orthotopic xenografts³²⁸ (**Figure 19C**).

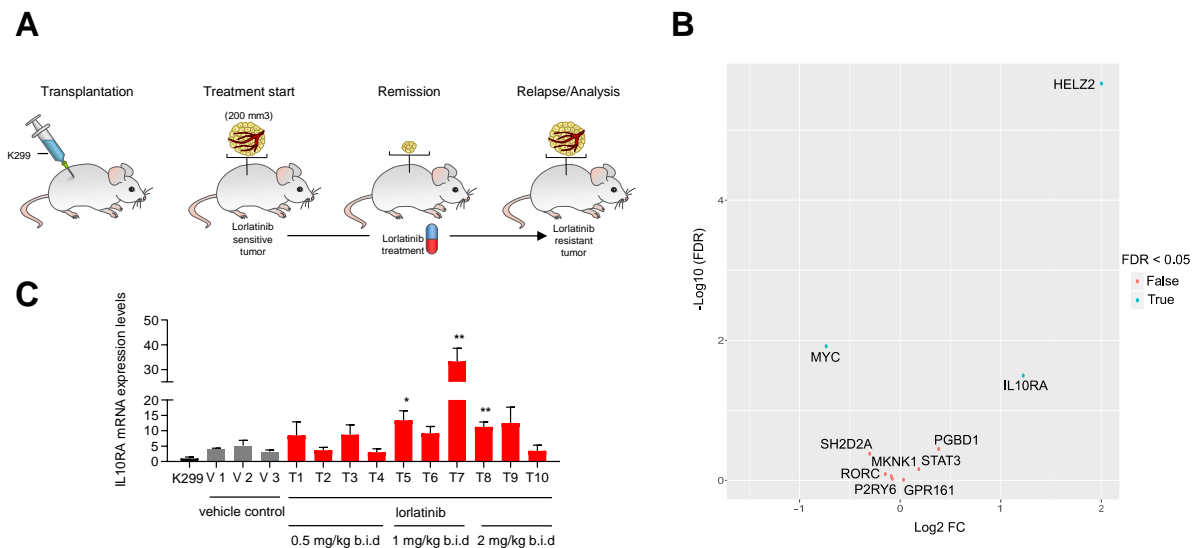


Figure 19 Hit validation in a resistant orthotopic ALCL cell line xenograft model
(A) Schematic of orthotopic xenograft treatment. K299 cells were injected subcutaneously and vehicle control or lorlatinib treatment initiated once tumours reached an average size of 200 mm³. **(B)** Volcano plot summarizing the global changes in gene expression levels between lorlatinib resistant tumours (T1, T5, T7) and vehicle control treated tumours (V1-3). Red: genes enriched in the lorlatinib resistant tumours vs vehicle control treated tumours. Blue: genes depleted in the lorlatinib resistant tumours vs vehicle control treated tumours. **(C)** mRNA expression levels of IL10RA normalized to GAPDH and relative to K299 cells in lorlatinib resistant tumours (T1-T10) compared to vehicle control treated tumours (V1-3). b.i.d.: orally, twice a day. Data are represented as means \pm SD of technical replicates, n = 3. Welch two sample t test: *p < 0.05. **p < 0.01, ***p < 0.001. Reproduced from Prokoph et al.³⁰¹.

3.4.5 Validation of Candidate Genes Modulating ALK TKI Sensitivity in ALCL Patients

To determine which targets identified by the screen are of potential clinical relevance, we analyzed data obtained from samples of resistant tumours from 4 patients with ALK+ ALCL recruited to the MAPPYACTS trial (NCT02613962), who had relapsed on ALK TKIs or chemotherapy (**Figure 20A**, **Table 17**). Patient 2 was treated with the standard ALCL99 chemotherapy protocol but progressed at 6 months following treatment initiation at which point crizotinib treatment was started, which only lasted for 2 months due to disease progression and then a biopsy was taken. Patient 1, having a more complex treatment history, had been treated with the ALCL99 chemotherapy protocol and remained in remission for 34 months until progression at which point multiple sequential therapies including crizotinib and lorlatinib were administered with short-term responses. The biopsy of this case was taken at the time of relapse on lorlatinib treatment while patients 3 and 4 were biopsied at the time of relapse from standard ALCL99 chemotherapy (**Figure 20A**). In contrast to patients 1 and 2, patients 3 and 4 responded to crizotinib and hence were classified as ALK TKI sensitive patients.

In order to identify resistance drivers and associated pathways that might play a role in clinical resistance to ALK TKIs, we performed RNA-seq to compare gene expression profiles between ALK+ ALCL tumours with acquired resistance to ALK TKIs compared to those that relapsed on standard ALCL99 chemotherapy but were ALK TKI sensitive (**Figure 20B-C**). Using GSEA, we identified positive enrichment for autoimmune disease signaling pathways including autoimmune thyroid disease, type I diabetes mellitus, systemic lupus erythematosus and asthma pathways in the ALK TKI sensitive compared to the ALK TKI resistant patient tumours. As expected, the T cell receptor pathway was

enriched in ALK TKI sensitive patients³⁸¹ (**Figure 20D, Table 17**). In agreement, the genes enriched in ALK TKI sensitive patients show specific gene ontology (GO) features such as T cell activation and differentiation (**Figure 20E**). Using GSEA, we identified positive enrichment for focal adhesion in ALK TKI resistant compared to ALK TKI sensitive patient tumours (**Figure 20D**). In agreement, the genes enriched in ALK TKI resistant patients showed GO features such as biological adhesion and cell adhesion (**Figure 20E**). Cell-cell adhesion is required for tissue invasion and metastasis of a tumour – one of the hallmarks of cancer²⁵¹. Interestingly, Ott et al. developed a dual ALK and focal adhesion kinase (FAK) inhibitor, which they successfully validated in cell line xenografts of ALK+ ALCL and NSCLC³⁸². Since FAK plays a role in cell-extracellular matrix signaling events as well as cell-cell junction regulation³⁸³, in future work FAK inhibitors could be tested in ALK inhibitor resistant settings.

Notably, while the global gene expression profiles of both ALK TKI sensitive patients (patients 3 and 4) clustered together, the ALK TKI resistant patients (patients 1 and 2) did not (**Figure 20F**).

To further investigate this difference in clustering, we determined whether any of the resistant patients had developed mutations in the ALK kinase domain. Patient 1 harbored a missense mutation (ALK L1196M, COSM99137) near the adenosine triphosphate (ATP)–binding pocket, which has previously been shown to mediate resistance to crizotinib in ALK+ NSCLC²²⁷, most likely accounting for the rapid relapse within 1 month of crizotinib initiation (**Table 17, Figure 20A**). In contrast, whilst we confirmed the presence of the NPM1-ALK rearrangement at crizotinib relapse for patient 2, no ALK mutation was detected. As expected, neither of the patients that relapsed after the standard ALCL99 chemotherapy (patients 3 and 4) had an ALK mutation at relapse (**Table 17**). These data allowed us to compare presumed ALK mutation-driven resistance (patient 1) to ALK mutation-independent resistance (patient 2).

We therefore integrated our RNA-seq analysis with the CRISPR overexpression screen results (**Figure 20G**). Of the 10 candidate genes identified by the CRISPR screens, 6/10 genes (PGBD1, GPR161, HELZ2, MKNK1, IL10RA and RORC) were more highly expressed in the ALK wild-type tumour of patient 2 compared to the ALK^{L1196M} tumour of patient 1 (**Figure 20G**). Of the 6 more highly expressed genes, IL10RA was selected for further analysis as it showed the highest expression levels among the 5 genes in tumours from both patients 1 and 2.

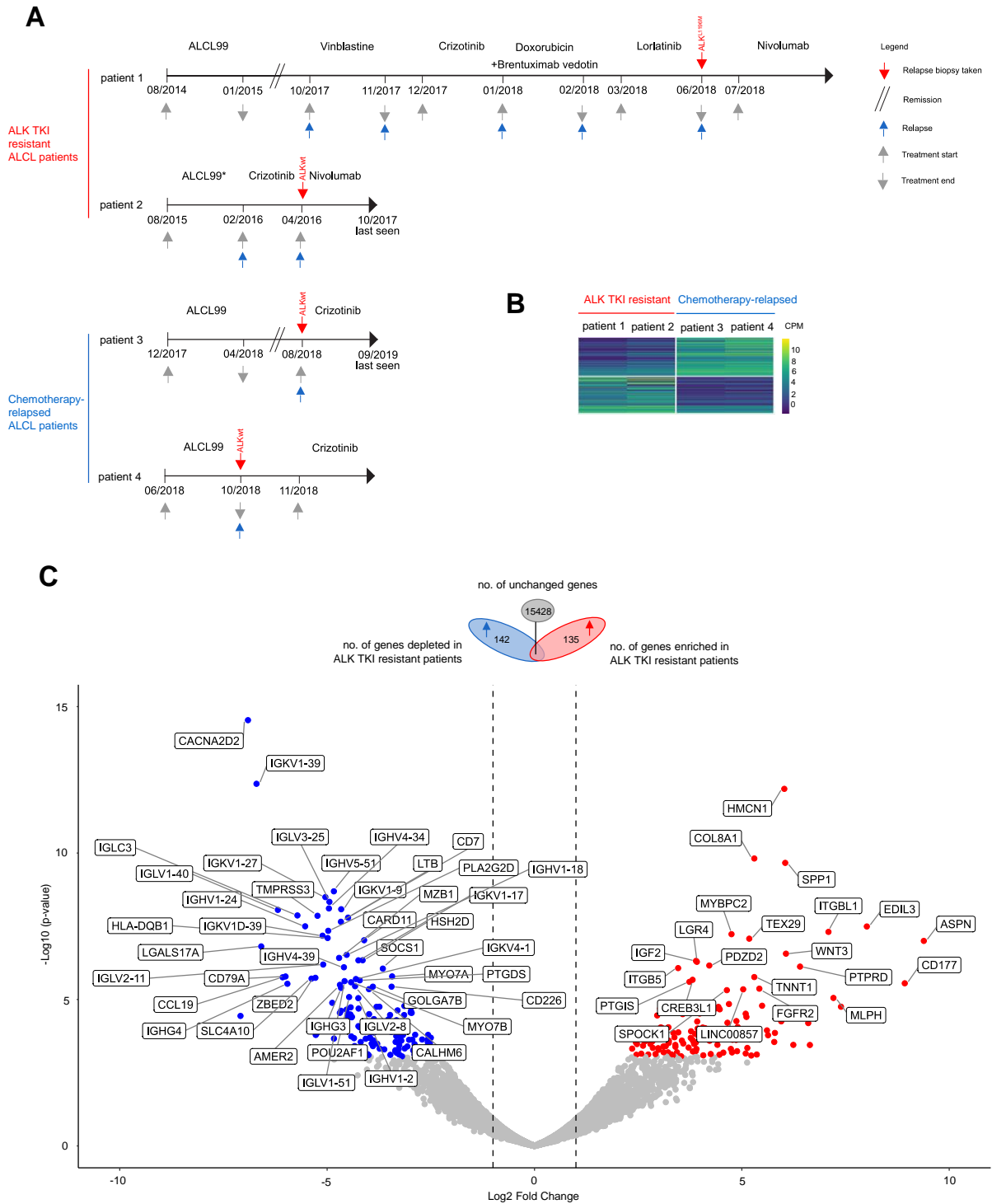


Figure 20 Validation of Candidate Genes Modulating ALK TKI Sensitivity in ALCL Patients
(A) Schema of the treatment history of ALK+ ALCL patients who relapsed on ALK targeted therapy (patients 1 and 2) or chemotherapy (patients 3 and 4). ALCL99* patient was treated according to ALCL99 recommendations for patients with central nervous system involvement as specified in Williams et al.⁹⁹. **(B)** Unsupervised clustering of RNA-seq data from chemotherapy-relapsed (patient 3, patient 4) and ALK TKI resistant (patients 1 and 2) patients. CPM = counts per million. **(C)** Top panel: Venn diagram of genes unchanged (gray) or differentially expressed genes (blue/red) between chemotherapy-relapsed (patients 3 and 4) and ALK TKI (patients 1 and 2) resistant patients. Bottom panel: Volcano plot summarizing the global changes in gene expression levels between chemotherapy-relapsed (patients 3 and 4) and ALK TKI resistant (patients 1 and 2) patients. Red: genes enriched in the ALK TKI resistant patient vs chemotherapy-relapsed patients. Blue: genes depleted in the ALK TKI resistant patient vs chemotherapy-relapsed patients. An absolute log fold change of 1 is indicated by dashed lines. Reproduced from Prokoph et al.³⁰¹.

(figure continued on next page)

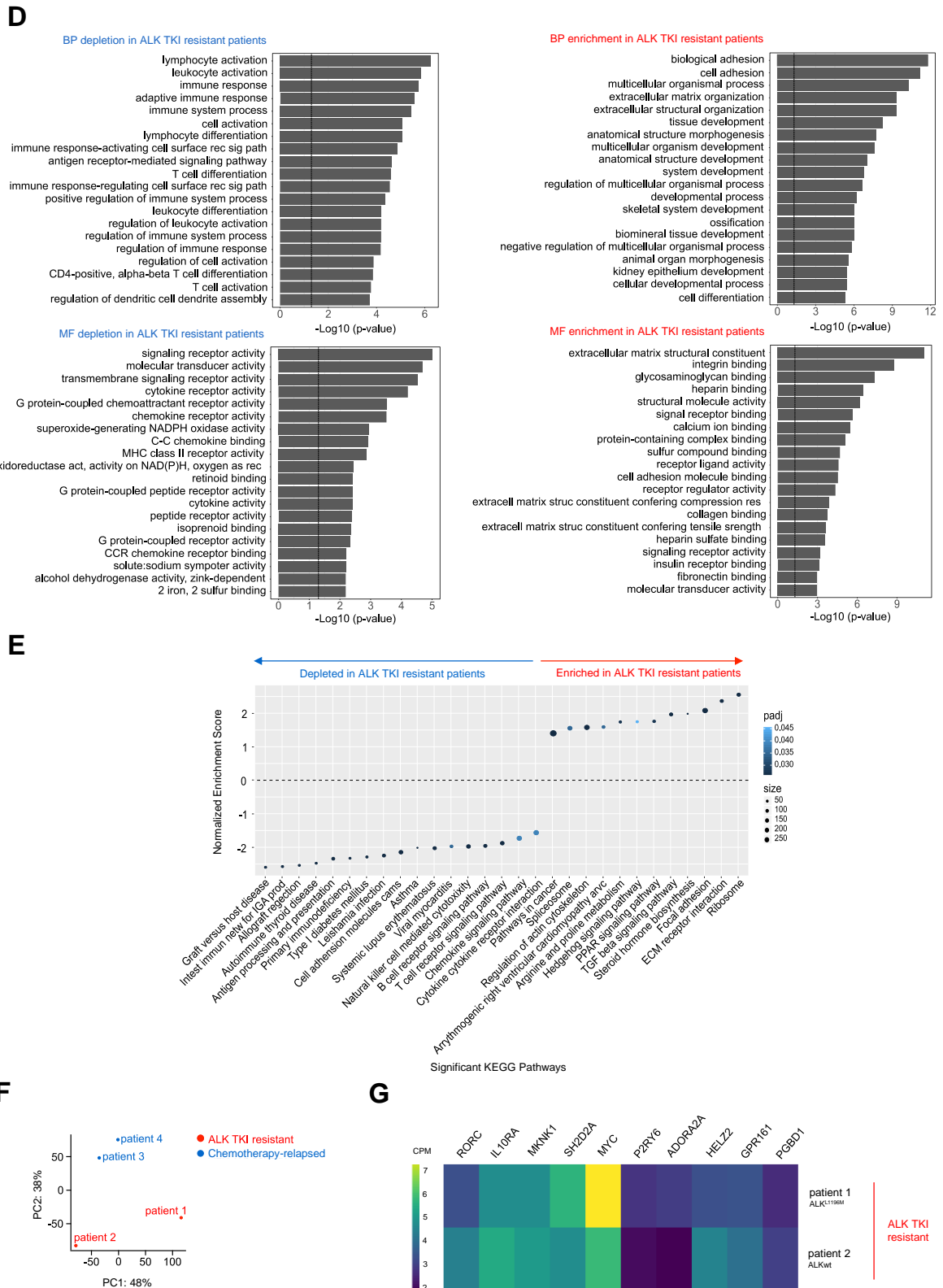


Figure 20 Validation of Candidate Genes Modulating ALK TKI Sensitivity in ALCL Patients
(D) Gene ontology analysis of differential gene expression between chemotherapy-relapsed and ALK TKI resistant patients. BP = biological process; MF = molecular function. **(E)** Summary of GSEA of genes ranked by fold change in differential gene expression between chemotherapy-relapsed and ALK TKI resistant patients annotated KEGG pathways. **(F)** Principal component (PC) analysis of gene expression levels across the 4 ALCL patient samples. **(G)** Candidate genes identified by the CRISPR screens are analyzed for differential expression between ALK TKI resistant patients with wild-type or mutated ALK. CPM = counts per million. Reproduced from Prokoph et al.³⁰¹.

3.5 Discussion

In the relapse setting, patients with ALK-rearranged ALCL are commonly treated with ALK inhibitors including crizotinib^{63,117} and the second-generation inhibitors ceritinib³⁸⁴ and alectinib⁶⁷. Two patient groups can be identified: Patients who i) achieved a CR and ii) present with disease progression during the first few months after treatment initiation. An understanding of the mechanisms leading to drug resistance in the second group is essential for designing therapeutic strategies to improve efficacy and prevent relapse. Previous work on ALK-rearranged NSCLC suggests that the most common mechanisms of resistance to ALK inhibition involve bypass signaling through functionally-related pathways³⁸⁵.

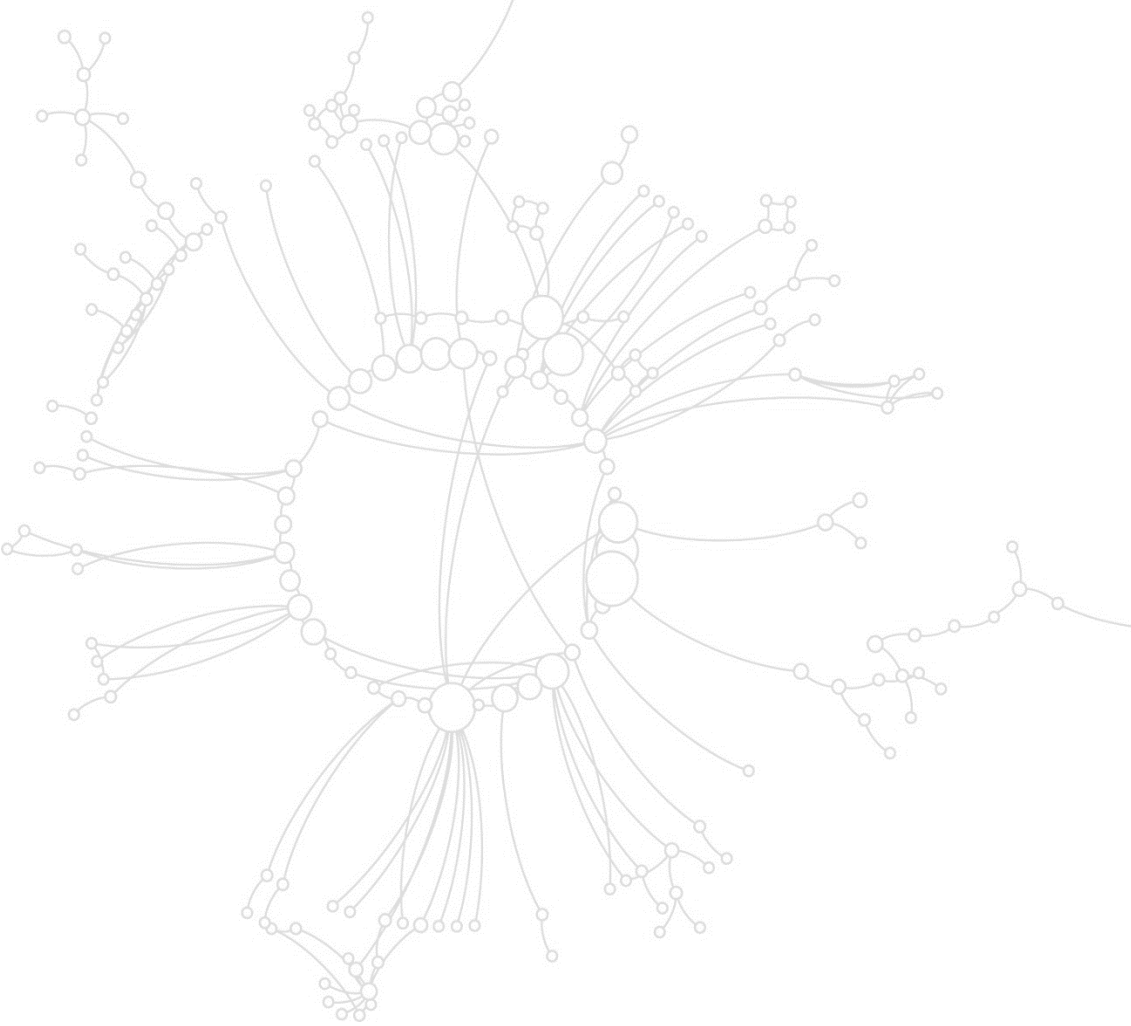
Here we present findings from a systematic large-scale functional study of resistance to ALK inhibition in NPM1-ALK+ ALCL, with the aim to inform future therapeutic approaches that prevent relapse or provide salvage options. We conducted the screens in three cell lines to enhance physiological relevance and avoid fundamental caveats of specific cell line models, such as the distinct genetic backgrounds and consequently cell line-specific resistance mechanisms inherently present in each cell line model.

Our CRISPR activation screens identified several new targets but were biased by the fold change gene expression achieved for a particular gene and sgRNA. While we have accounted for fold change gene expression in our validation process by excluding genes, which were not sufficiently overexpressed by either of the 2 tested sgRNAs (out of the 6 sgRNAs utilized in the CRISPR activation screens). We were not able to account for the level of overexpression due to the following reasons: Firstly, we do not know which level of overexpression for a specific gene – given that this gene can induce resistance - is sufficient to modify sensitivity to a drug. For example, *P2RY6* was the most highly overexpressed gene in all 4 ALK+ ALCL cell lines, but its overexpression only induces resistance in K299. Secondly, if one accounts for the level of fold change gene expression, then genes that are more highly expressed than needed to modify sensitivity to a drug are discriminated against.

To narrow down targets identified in the screen to those which may be clinically relevant, results were compared to RNA-seq data of relapse biopsy specimens of 2 ALCL patients resistant to ALK TKIs.

A target identified by the screen was STAT3, a prime candidate being activated in inflammatory cells by a number of cytokines and previously shown to be central to ALCL biology downstream of NPM1-ALK activity^{225,365}. Together with detection of the STAT3 target genes *MYC* and *IRF4* by the screen, these data were suggestive of a potential NPM1-ALK bypass track which could be activated by a protein upstream of STAT3 and independent of NPM1-ALK. Indeed, IL10RA, a cell surface receptor usually upstream of STAT3, was also consistently detected and validated as mediating decreased sensitivity to crizotinib. Importantly, we also show that IL10RA overexpression decreases cell sensitivity to other ALK TKIs besides crizotinib including lorlatinib, alectinib and brigatinib. Given that IL10RA can mediate activation of STAT3 activity on ligand binding together with IL10RB, we further investigated the role of IL10RA in the following chapter.

**CHAPTER 4 IL10RA Modulates ALK TKI
Sensitivity in ALK+ ALCL**



4.1 Introduction

The Interleukin 10 receptor (IL10R) was discovered by Ho et al. in 1993 on the basis of its specific binding of interleukin 10 (IL10)³⁸⁶. IL10R is structurally related to the interferon receptor (INFR) family and is mainly expressed by hematopoietic cells including B cells, T cells, natural killer cells, monocytes, and macrophages^{386,387}. In its functional form the IL10R is a tetramer, consisting of two IL10RA polypeptide chains and two interleukin 10 receptor subunit beta (IL10RB) chains³⁸⁷. Signaling most likely proceeds by JAK/STAT activation (**Figure 21**). Binding of the IL10 homodimer, to both extracellular domains of IL10RA, induces phosphorylation of janus kinase 1 (JAK1) and tyrosine kinase 2 (TYK2). Following this, two intracellular domain tyrosine residues (Y446 and Y496) in the IL10RA chains, act as temporary docking sites for the latent transcription factor STAT3. STAT3 is then phosphorylated by JAK1 and TYK2, and translocates to the nucleus, controlling the expression of downstream genes by binding STAT-binding-elements (SBE) motifs^{387–391}. SBE motifs can be found in the promoter region of different genes³⁸⁸. Besides IL10-induced activation of STAT3, other STAT proteins have been reported to be involved in IL10 signaling, such as STAT1 and STAT5^{389,392}.

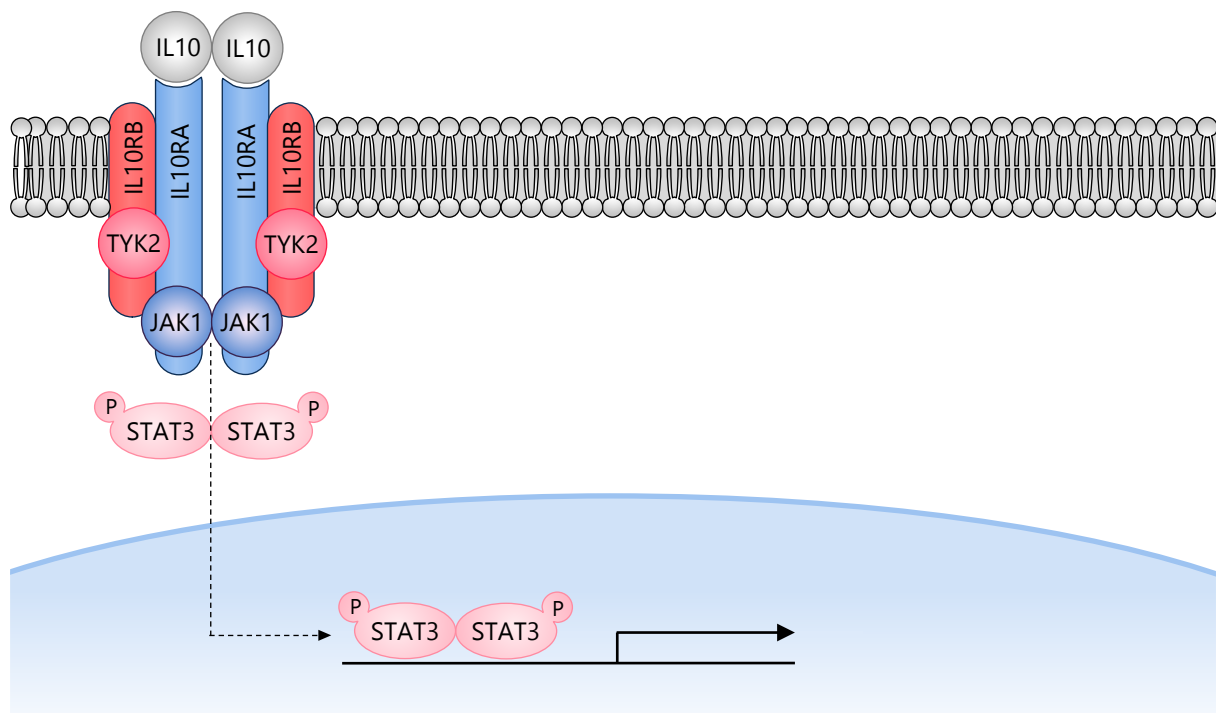


Figure 21 Schematic of the IL10 signalling pathway

IL10 signaling has previously been shown to play a crucial role in ALCL. For example, IL10 benefits ALCL cells directly by enhancing their viability and indirectly by suppressing the immune response³⁹³. In addition, IL10 is already known to be one of the most abundant cytokines secreted by ALCL cell lines³⁷² and is prevalent in the peripheral blood of children with ALCL³⁹⁴. Moreover, knockdown of IL10RA in the ALK⁺ cell line K299 resulted in reduced cell growth³⁷², whereas the roles and functions of IL10RA in drug resistance have not yet been fully elucidated.

In the previous chapter we show that overexpression of IL10RA, the IL10R-specific subunit, decreases sensitivity to ALK inhibitors in ALCL cell lines, whereas knockdown of IL10RA increases sensitivity to

crizotinib in ALCL cell lines. These results were further confirmed in ALK inhibitor resistant cell lines and in a cell line-derived orthotopic xenograft model. Furthermore, RNA-seq performed on a relapse biopsy of an ALK inhibitor-resistant ALCL patient with wild-type NPM1-ALK showed higher expression of IL10RA compared to an ALK inhibitor-resistant ALCL patient that harbored an ALK L1196M mutation at relapse, suggesting these results may be translationally relevant. Hence, we further investigated the mechanism of how overexpression of IL10RA modifies sensitivity to ALK inhibition.

The majority of the work presented in this chapter forms the basis of a publication in *Blood* (Prokoph et al.)³⁰¹, which can be found in Appendix 1.

4.1.1 Aims

This chapter aims to:

- Determine the IL10RA expression levels in ALCL patient tumour tissue
- Determine the effect of IL10RA overexpression on sensitivity to alectinib, brigatinib and lorlatinib
- Determine the effect of IL10RA overexpression on apoptosis
- Validate on-target effects of the CRISPR-based overexpression tool by reversing the resistant phenotype against IL10RA
- Identify ALCL context-specific downstream effector(s) of IL10RA responsible for the inhibition of apoptosis in ALCL cells in response to ALK inhibitors
- Determine whether IL10RA expression is predictive of clinical responses to standard chemotherapy in paediatric ALCL patients

4.2 IL10RA is Expressed in ALCL in an NPM1-ALK-Independent Manner

The IL10R is a tetrameric cell surface protein composed of 2 A and 2 B subunits that bind IL10 leading to activation of JAK1/TYK2 and STAT3. To characterize the importance of IL10/IL10R signaling in ALCL, we measured the expression levels of IL10RA and IL10RB by immunostaining of T-cell lymphoma tissue microarrays (TMAs) from adult patients (**Table 18, Table 19, Table 20**). We determined that IL10RA was expressed in 100% of ALK+ ALCLs, 92% of ALK- ALCLs, 43% AITL and 30% of PTCL-NOS (**Figure 22A-B**). In contrast, IL10RB was in general expressed at a higher level in ALCL than other peripheral T cell lymphomas but there was no difference in the percentage of tumour cells positive for this protein (**Figure 22B**). We further confirmed IL10RA and IL10RB expression by immunostaining of TMAs⁸⁰ comprising an independent cohort of 92 paediatric ALK+ ALCL patients (**Figure 22C, Table 15, Table 13, Table 14**) that were recruited onto three paediatric ALCL trials (NHL-BFM90/NHL-BFM95/NCT00006455). These data are consistent with existing gene expression data^{314–319} from 75 ALK+ ALCL compared to 40 ALK- ALCL patients, 160 PTCL-NOS patients, 100 AITL patients and 12 reactive lymph nodes from healthy donors (**Figure 22D**).

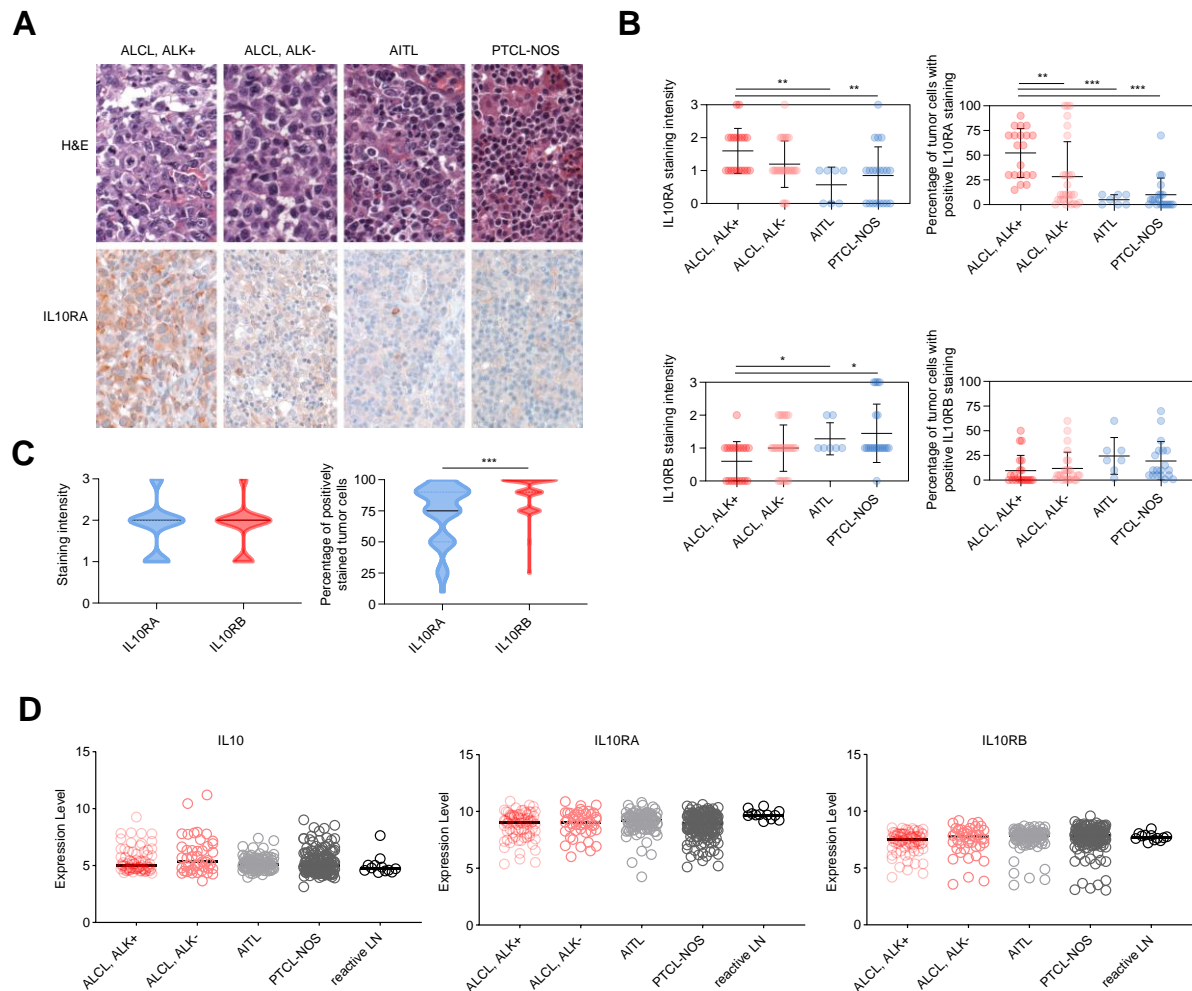


Figure 22 IL10RA is Expressed in ALCL Patient Tumour Tissue

(A) Representative hematoxylin and eosin staining with corresponding IL10RA IHC staining performed on tissue microarrays from different human T cell lymphoma subtypes: ALK+ and ALK- ALCL, angioimmunoblastic T-cell lymphoma (AITL) and peripheral T-cell lymphoma not otherwise specified (PTCL-NOS). **(B)** Intensity of staining or percentage of tumour cells expressing IL10RA or IL10RB determined by IHC of a tissue microarray (TMA) of formalin fixed paraffin embedded (FFPE) T cell lymphoma patient samples: n (ALK+ ALCL) = 25, n (ALK- ALCL) = 25, n (AITL) = 7, n (PTCL-NOS) = 21. Data are represented as means \pm SD. Welch two sample t test: *p < 0.05. **p < 0.01, ***p < 0.001. **(C)** Intensity of staining or percentage of tumour cells expressing IL10RA (n=92) or IL10RB (n=89) determined by IHC of a TMA of FFPE paediatric ALK+ ALCL patient samples. Data are presented as a violin plot with means indicated. Welch two sample t test: *p < 0.05. **p < 0.01, ***p < 0.001. **(D)** Microarray data (GSE58445, GSE6338, GSE65823, GSE78513, GSE14879, GSE19069) were analyzed for IL10, IL10RA and IL10RB expression in ALK+ ALCL (n = 75), ALK- ALCL (n = 45), PTCL-NOS (n = 160, peripheral T-cell lymphomas not otherwise specified), AITL (n = 100, angioimmunoblastic T-cell lymphomas) patients compared to reactive lymph nodes (LN, n = 12). Reproduced from Prokoph et al.³⁰¹.

To examine if IL10 signaling is represented in ALCL cell lines, we analyzed existing microarray data^{316-318,320,321} of a panel of lymphoma cell lines, including ALK+ and ALK- ALCL cell lines compared to other T- and B-cell lymphoma cell lines as well as normal T-cell controls (**Figure 23A-B**). In agreement with the patient data above, ALK+ ALCL cell lines showed robust mRNA expression of IL10RA, IL10RB and IL10.

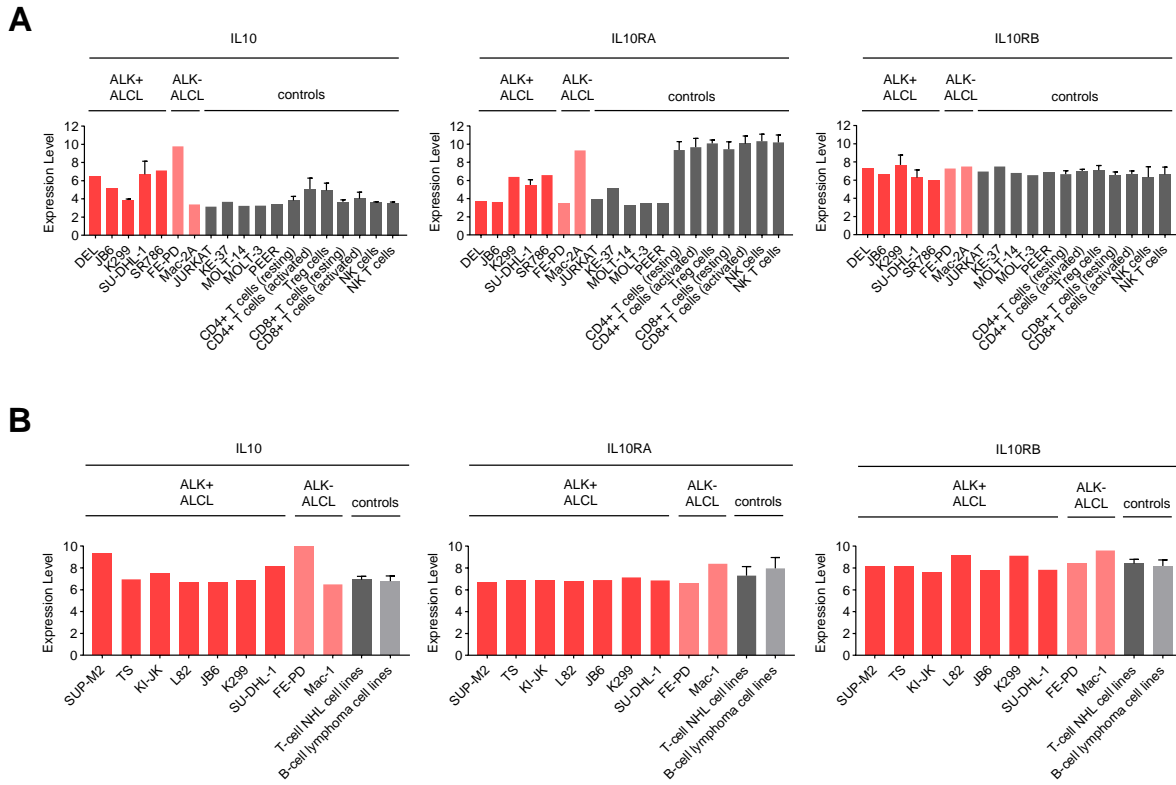


Figure 23 IL10 signaling is represented in ALCL cell lines

(A) Microarray data (GSE6338, GSE107951, GSE14879, GSE19069) were analyzed for IL10, IL10RA and IL10RB expression in ALK+ ALCL (n = 5) and ALK- ALCL (n = 2) cell lines compared to other lymphoma cell lines (n = 5), CD8+T cells, CD4+T cells, Treg cells, NK cells and NK T cells. **(B)** Microarray data (GSE94669) were analyzed for IL10, IL10RA and IL10RB expression in ALK+ ALCL (n = 7) and ALK- ALCL (n = 2) cell lines compared to other T cell (n = 3; H9, HuT78, HH) and B cell (n = 48) lymphoma cell lines. Reproduced from Prokoph et al.³⁰¹.

To determine whether IL10R signaling is mediated by NPM1-ALK, we examined whether IL10RA, IL10RB and IL10 expression were directly controlled by NPM1-ALK activity. Knockdown of ALK with an inducible shRNA led to decreased IL10, but not IL10RA nor IL10RB mRNA expression (**Figure 24A**), which is in agreement with existing microarray data³²² of ALK shRNA transduced ALCL cell lines (**Figure 24B**). Consistent with this, crizotinib inhibition of NPM1-ALK activity also resulted in decreased IL10, but not IL10RA or IL10RB mRNA expression (**Figure 24C**). Again, our results are in agreement with existing microarray data³²² from ALK TKI treated compared to untreated ALCL cell lines (**Figure 24D**). Hence, transcription of IL10RA is independent of NPM1-ALK expression and activity, suggesting IL10RA is a prime candidate for bypass signaling in response to ALK inhibition.

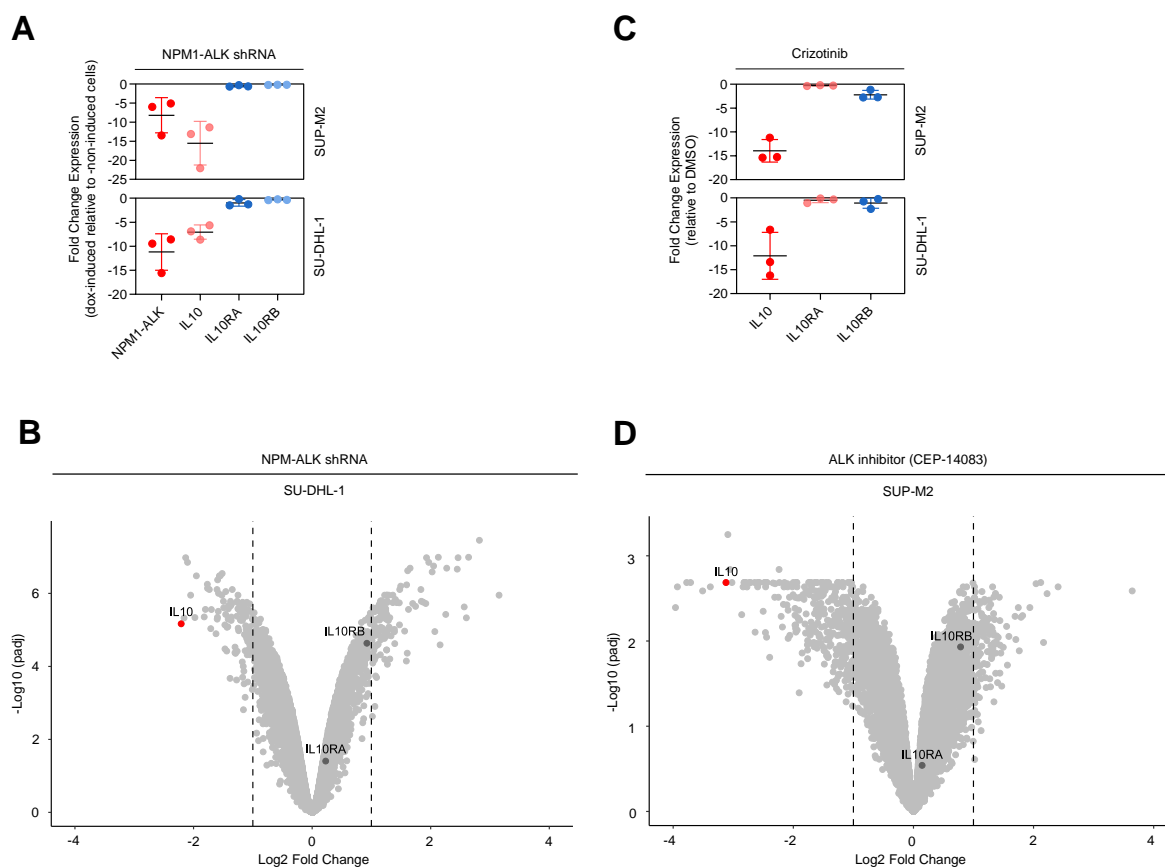


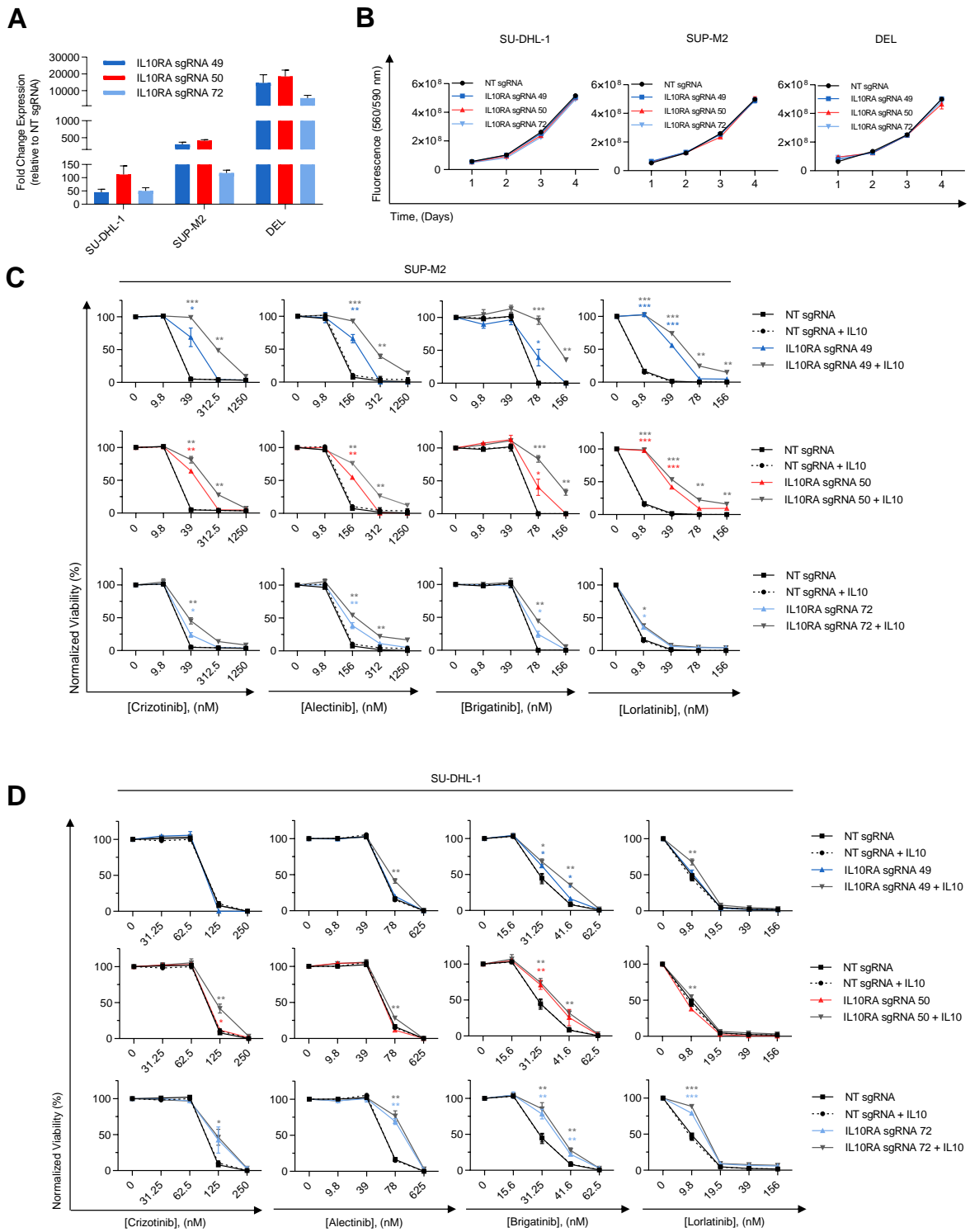
Figure 24 **Transcription of IL10RA is independent of NPM1-ALK expression and activity**
(A) Fold change in IL10, IL10RA and IL10RB mRNA expression levels in SUP-M2 derived TS or SU-DHL-1 cell lines transduced with a doxycycline dependent ALK shRNA. Doxycycline-induced cells were compared to non-induced cells and were normalized to GAPDH. Data are represented as means \pm SD, $n = 3$. **(B)** Microarray data (GSE6184) were analyzed for IL10, IL10RA and IL10RB expression changes with or without ALK shRNA induction in SU-DHL-1 cells. Volcano plot summarizing the global changes in gene expression of ALK shRNA transduced ALCL cell lines with or without doxycycline induction. Red: downregulated, Dark gray: unchanged. **(C)** Fold change in IL10, IL10RA and IL10RB mRNA expression levels in crizotinib treated (300 nM for 6 hours) ALCL cell lines normalized to GAPDH and relative DMSO control. Data are represented as means \pm SD, $n = 3$. **(D)** Microarray data (GSE6184) were analyzed for IL10, IL10RA and IL10RB expression changes after 6 hours treatment with 300 nM ALK inhibitor (CEP-14083) or DMSO treatment in SUP-M2 derived TS cells. Volcano plot summarizing the global changes in gene expression of SUP-M2 derived TS cells after 6 hours treatment with 300 nM CEP-14083 or DMSO. Red: downregulated, Dark gray: unchanged. Reproduced from Prokoph et al.³⁰¹.

4.3 IL10RA Overexpression Modulates Sensitivity to ALK Inhibition

To further characterize the effects of elevated IL10RA expression on ALK TKI induced cytotoxicity, we expressed 3 different sgRNAs activating IL10RA expression in 3 ALK+ ALCL cell lines (SU-DHL-1/SUP-M2/DEL) (**Figure 25A**). Expression of each sgRNA resulted in decreased crizotinib sensitivity especially on supplementation of IL10 (**Figure 25C-E**). As expected, the majority of these sgRNAs also promoted decreased sensitivity to the second generation ALK TKIs alectinib, brigatinib and lorlatinib.

To investigate how IL10RA overexpression may be enabling cell survival in the presence of ALK TKIs, we assessed cell proliferation and apoptosis. None of the three IL10RA-targeting sgRNAs promoted proliferation in the absence of crizotinib (**Figure 25B**), suggesting that cell survival is not facilitated by increased proliferation. On the other hand, most IL10RA sgRNAs were able to prevent apoptosis to some extent when cells were treated with crizotinib (**Figure 25F**), all three IL10RA-targeting sgRNAs

demonstrated a significant ability to diminish apoptosis in the presence of crizotinib particularly when IL10 was supplemented to the growth media (**Figure 25G**).



(legend on next page)

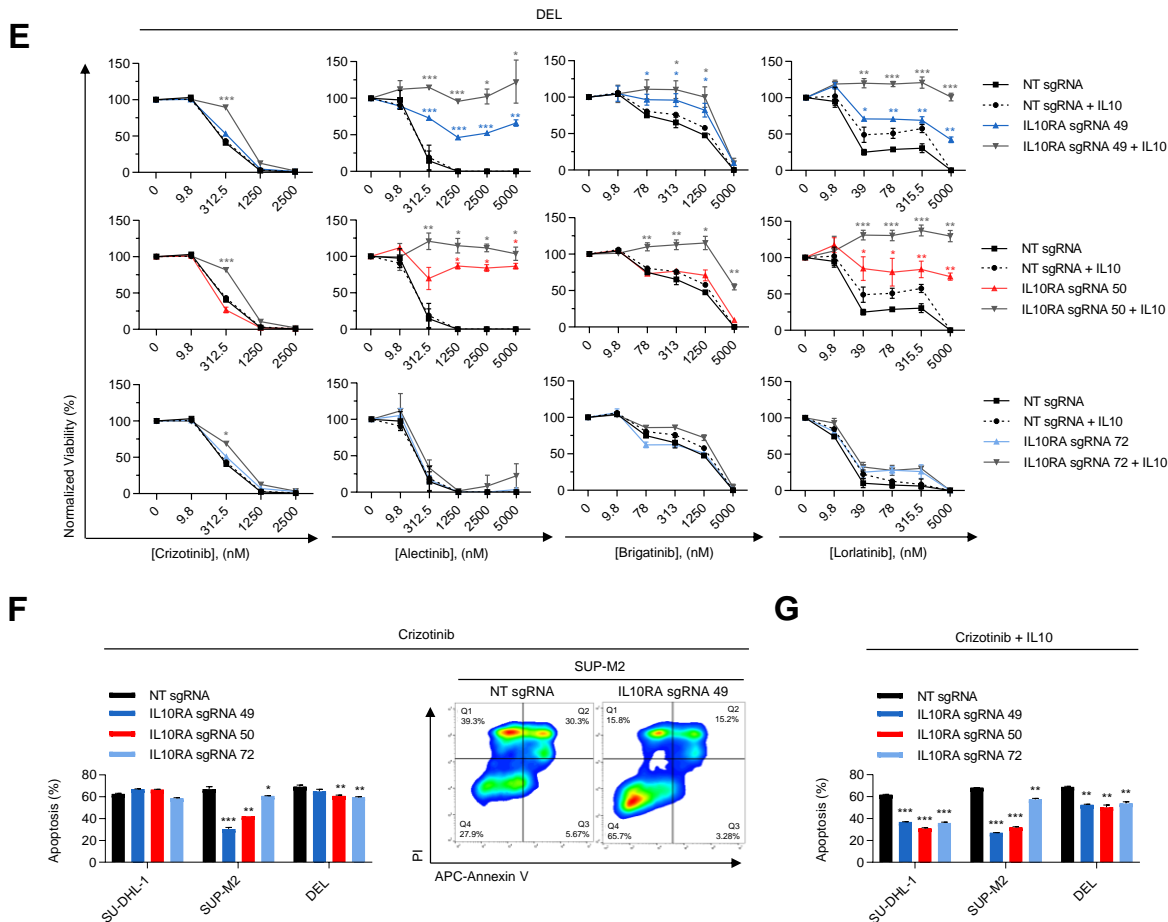
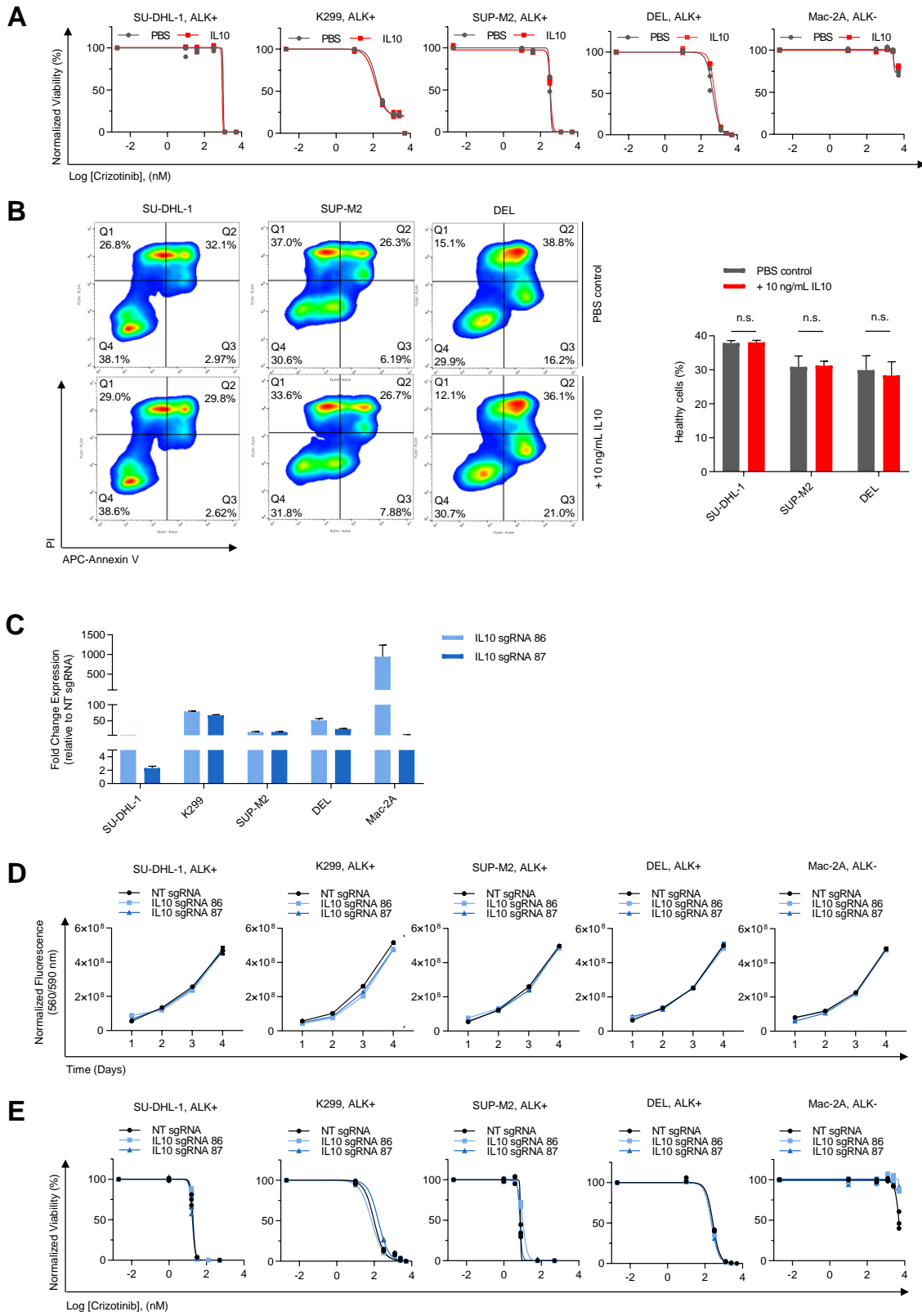


Figure 25 IL10RA Overexpression Modulates Sensitivity to ALK Inhibition
(A) Fold change in expression levels of IL10RA for each of the 3 sgRNAs targeting IL10RA versus non-targeting (NT) control sgRNA in the indicated ALCL cell lines. Data are represented as means \pm SD, $n = 3$. **(B)** Proliferation of ALCL cell lines expressing sgRNAs inducing overexpression of IL10RA over 4 days (D1–D4). Data are represented as means \pm SD, $n = 3$. Welch two-sample t test: * $p < 0.05$, ** $p < 0.01$, *** $p < 0.001$. **(C–E)** Viability of (C) SUP-M2, (D) SU-DHL-1 or (E) DEL cells based on normalized CellTiter-Blue reads on exposure to increasing concentrations of crizotinib, alectinib, brigatinib or lorlatinib for 48 hours when expressing 1 of 3 of the indicated sgRNAs inducing overexpression of IL10RA in the presence or absence of 10 ng/mL IL10. Data are represented as means \pm SD, $n = 3$. Welch two-sample t test: * $p < 0.05$, ** $p < 0.01$, *** $p < 0.001$. **(F)** Modulation of apoptosis upon expression of sgRNAs inducing overexpression of IL10RA in the indicated ALCL cell line. The percentage of apoptotic cells is determined by annexin V and propidium iodide (PI) staining of ALCL cells treated with 125 (SU-DHL-1), 312.5 (SUP-M2) or 1250 (DEL) nM crizotinib for 48 hours. Data are represented as means \pm SD of technical replicates, experiments performed independently three times. Welch two sample t test: * $p < 0.05$, ** $p < 0.01$, *** $p < 0.001$. Right panel: Representative flow cytometry plots of annexin V/PI staining intensities corresponding to IL10RA sgRNA promoting survival versus non-targeting (NT) control sgRNA in SUP-M2 cells. **(G)** Modulation of apoptotic response upon expression of sgRNAs inducing overexpression of IL10RA in the indicated ALCL cell lines. The percentage of apoptotic cells is determined by annexin V and propidium iodide (PI) staining of ALCL cells treated with 125 (SU-DHL-1), 312.5 (SUP-M2) or 1250 (DEL) nM crizotinib in the presence of 10 ng/mL IL10 for 48 hours. Data are represented as means \pm SD of technical replicates, experiments performed independently three times. Welch two sample t test: * $p < 0.05$, ** $p < 0.01$, *** $p < 0.001$. Reproduced from Prokoph et al.³⁰¹.

Since these data hint towards the possibility that IL10RA-mediated crizotinib resistance is dependent on IL10, we next assessed whether IL10 overexpression alone could drive crizotinib resistance. Neither decreased crizotinib sensitivity nor a reduction in apoptosis was observed in ALK+ and ALK- ALCL cell lines when the growth media was supplemented with IL10 (**Figure 26A-B**). Consistent with this observation, overexpression of two different IL10-targeting sgRNAs in the same ALCL cell lines (**Figure 26C**) neither promoted proliferation in the absence of crizotinib (**Figure 26D**), nor increased survival in

the presence of crizotinib (**Figure 26E**). This observation highlights the fact that expression of IL10RA is the limiting factor for IL10 signaling in these cell lines.



(legend on next page)

Figure 26 IL10 Overexpression does not Modulate Sensitivity to ALK Inhibition

(A) Viability of the indicated ALCL cell lines based on normalized CellTiter-Blue fluorescence reads on exposure to increasing concentrations of crizotinib for 48 hours in the presence or absence of 10 ng/mL IL10. Data are represented as means \pm SD of technical replicates, $n = 3$; experiment performed independently three times. Welch two-sample t test: * $p < 0.05$. ** $p < 0.01$, *** $p < 0.001$. **(B)** Left panel: Representative distributions of annexin V and propidium iodide co-staining intensities of the indicated ALCL cells treated with 1250 (DEL), 312.5 (SUP-M2), 156.25 (SU-DHL-1) nM crizotinib with or without 10 ng/mL IL10 for 48 hours as determined by flow cytometry. Right panel: The percentage of healthy cells as determined by annexin V and propidium iodide (PI) staining of ALCL cells treated with 125 (SU-DHL-1), 312.5 (SUP-M2), 1250 (DEL) nM crizotinib with or without 10 ng/mL IL10 for 48 hr. Data are represented as means \pm SD, $n = 3$. Welch two sample t test: * $p < 0.05$. ** $p < 0.01$, *** $p < 0.001$. **(C)** Fold change in expression levels of IL10 modulated by CRISPR overexpression for two sgRNAs relative to non-targeting (NT) control sgRNA in the indicated ALCL cell lines. Data are represented as means \pm SD of technical replicates, $n = 3$. **(D)** Proliferation of unchallenged ALCL cells expressing sgRNAs inducing overexpression of IL10. Proliferation was quantified over 4 days (D1–D4). Data are represented as means \pm SD, $n = 3$. Welch two-sample t test: * $p < 0.05$. ** $p < 0.01$, *** $p < 0.001$. **(E)** Viability of the indicated ALCL cell lines based on normalized CellTiter-Blue fluorescence reads on exposure to increasing concentrations of crizotinib for 48 hours when expressing 1 of 3 of the indicated sgRNAs inducing overexpression of IL10. Data are represented as means \pm SD of technical replicates, $n = 3$; experiment performed independently three times. Welch two-sample t test: * $p < 0.05$. ** $p < 0.01$, *** $p < 0.001$. Reproduced from Prokoph et al.³⁰¹.

Next, we overexpressed IL10RA with a puromycin selectable plasmid³¹¹ and could confirm the results achieved with sgRNA mediated CRISPR overexpression (**Figure 27A-D**). Plasmid-based IL10RA overexpression was induced in ALCL cell lines (**Figure 27A**), which was able to desensitize ALCL cell lines to crizotinib treatment (**Figure 27B**) and rescue the phosphorylation of STAT3 in the presence of crizotinib (**Figure 27D**). Furthermore, the addition of the STAT3 inhibitor stattic^{395–397} resensitized IL10RA overexpressing cells to crizotinib inhibition (**Figure 27C**).

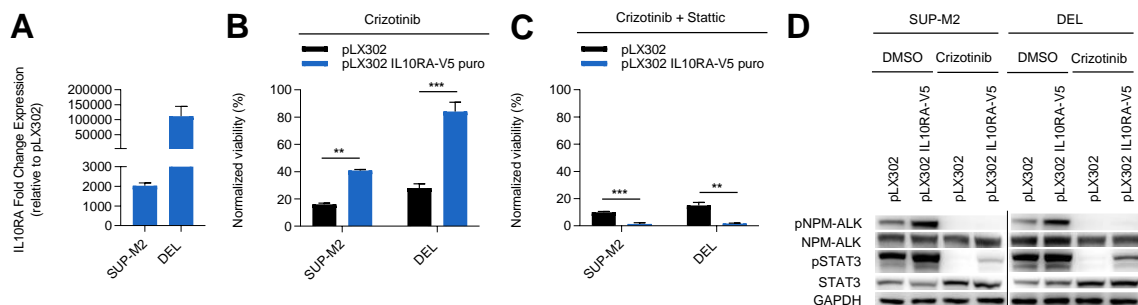


Figure 27 Plasmid-based IL10RA Overexpression Modulates Sensitivity to Crizotinib Inhibition

(A) Fold change in expression levels of IL10RA in the indicated ALCL cell lines after transfection with pLX302 IL10RA-V5 puro versus pLX302 control plasmid. Data are represented as means \pm SD, $n = 3$. **(B)** Viability of ALCL cells based on normalized CellTiter-Blue fluorescence reads on exposure to 312.5 nM crizotinib for 48 hours when expressing pLX302 IL10RA-V5 puro versus pLX302 control plasmid. Data are represented as means \pm SD, $n = 3$. Welch two-sample t test: * $p < 0.05$. ** $p < 0.01$, *** $p < 0.001$. **(C)** Viability of ALCL cells based on normalized CellTiter-Blue fluorescence reads on exposure to 312.5 nM crizotinib and 2500 nM (SUP-M2) or 3000 nM (DEL) stattic for 48 hours when expressing pLX302 IL10RA-V5 puro versus pLX302 control plasmid. Data are represented as means \pm SD, $n = 3$. Welch two-sample t test: * $p < 0.05$. ** $p < 0.01$, *** $p < 0.001$. **(D)** Western blot analysis of differential JAK/STAT signaling activation in the indicated ALCL cells when expressing pLX302 IL10RA-V5 puro versus pLX302 control plasmid. Cells were treated with DMSO or 1000 nM crizotinib for 1 hour. This blot is representative of three independent experiments. Lines indicate different blots. Reproduced from Prokoph et al.³⁰¹.

4.4 Knockout of IL10RA/IL10RB/IL10 further sensitizes ALCL cells to ALK inhibition

To understand if inhibition of any component of the IL10/IL10R complex would render cells sensitive to crizotinib treatment, we carried out a CRISPR-Cas9-based knockout of IL10, IL10RA and IL10RB in K299/SUP-M2 cells as described above using 6 sgRNAs per gene (**Figure 17A**) of which we validated 2 sgRNAs targeting IL10RA for their knockout efficiency (**Figure 28B**). We found sgRNAs targeting IL10, IL10RA and IL10RB significantly depleted in SUP-M2 cells that were treated with crizotinib for 14 days (D14 Crizotinib) in comparison to DMSO treatment (D14 DMSO) (**Figure 28A**). This is in agreement with a publicly available CRISPR knockout screen dataset by Ng et al.³¹² on 5 ALK+ and 1 ALK- ALCL cell lines that confirms that neither IL10RA, nor IL10 or IL10RB were found to be essential genes in the absence of ALK inhibition (**Figure 28C-F**). This suggests that the IL10R signaling pathway is not essential for the survival of ALCL cell lines, but becomes essential when ALCL cell lines are exposed to crizotinib. However, sgRNAs targeting IL10 were significantly depleted in K299 cells that were treated with crizotinib or DMSO in comparison to input control cells, suggesting that K299 cells are dependent on IL10 even without being challenged with crizotinib (**Figure 28A**). Moreover, in contrast to SUP-M2 cells, we did not find sgRNAs targeting IL10, IL10RA and IL10RB significantly depleted in K299 cells that were treated with crizotinib for 14 days (D14) in comparison to DMSO treatment (**Figure 28A**).

4.5 STAT3 is Activated Independently of NPM1-ALK through the IL10/IL10R Signaling Pathway on Crizotinib Inhibition

We next explored the mechanism by which IL10RA mediates resistance to ALK inhibition. Oncogenic ALK-fusions activate several signaling pathways, with STAT3 representing a key downstream effector^{225,365}. In agreement with previous publications^{395,398}, ALK inhibition through crizotinib treatment led to a complete loss of STAT3 phosphorylation (**Figure 29A**).

Activation of JAK/STAT signaling is also highly cytokine-dependent in lymphoid cells, with IL10 being a prominent activator³⁷³. To determine whether this also applies in ALCL, IL10RA overexpression was induced in ALCL cell lines using three different sgRNAs, which was able to rescue the phosphorylation of STAT3, but not STAT1, in the presence of crizotinib (**Figure 29A**). This indicates that IL10RA overexpression can mediate STAT3 phosphorylation independently of NPM1-ALK activity and that this mechanism can successfully reverse the effects of crizotinib-mediated inhibition on STAT3 activity.

To understand how transcriptional targets of STAT3 are affected by IL10RA overexpression, we examined their expression levels by RT-qPCR. Consistent with this, overexpression of IL10RA led to increased mRNA levels of the known STAT3 target genes including MYC, IRF4 and CD30 in crizotinib-treated cells (**Figure 29B**). These data are in keeping with the CRISPR overexpression screen results whereby sgRNA mediated overexpression of both MYC and IRF4 enabled cell survival in the presence of crizotinib (**Figure 12E**).

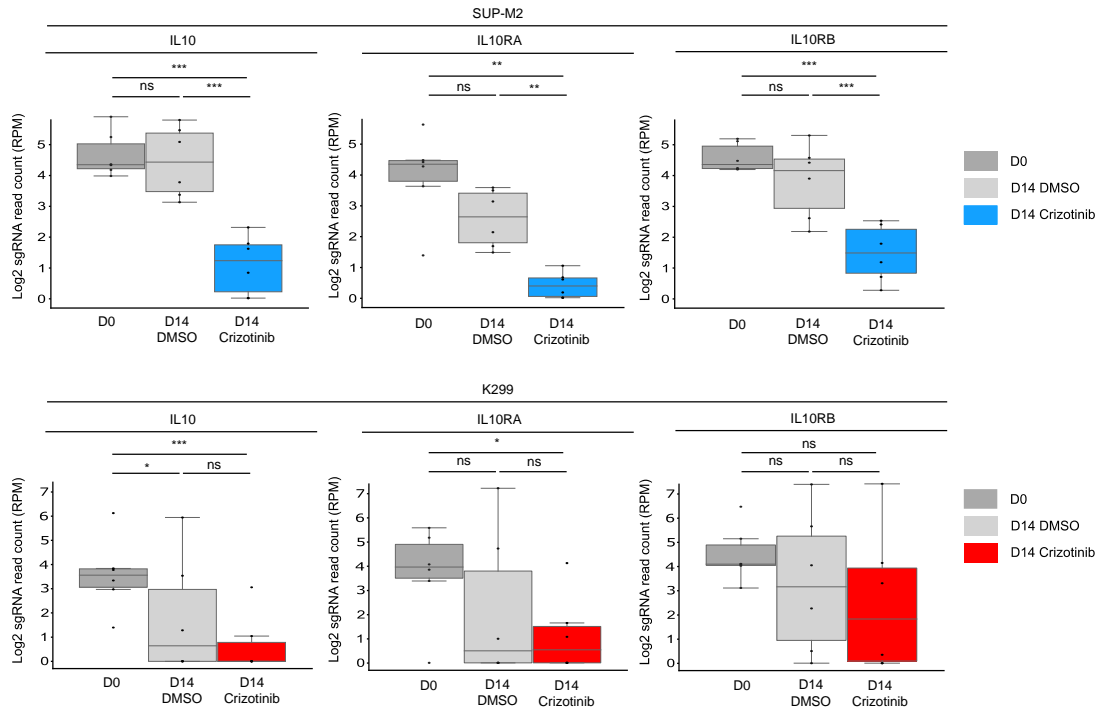
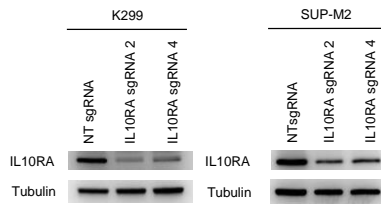
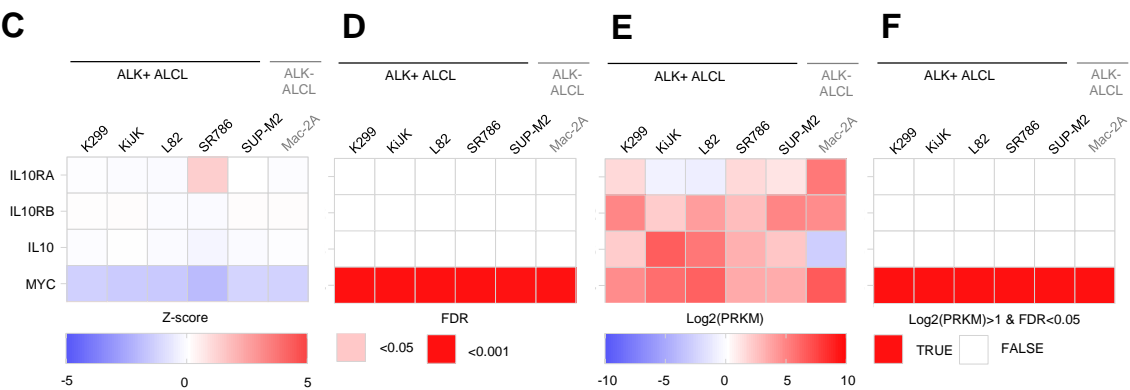
A**B****C**

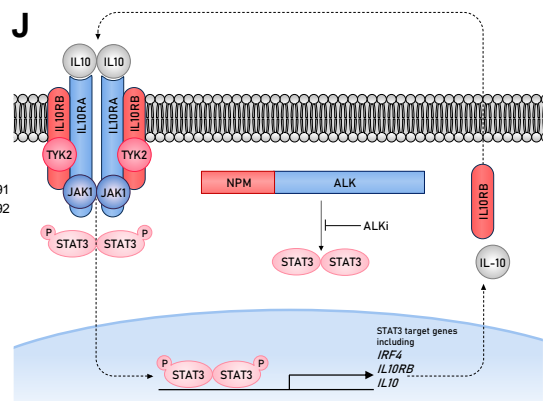
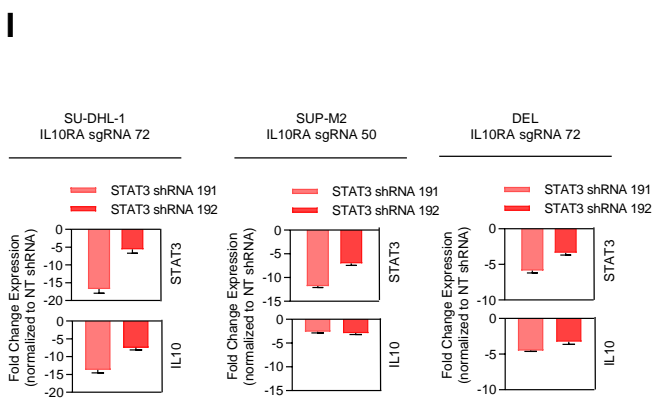
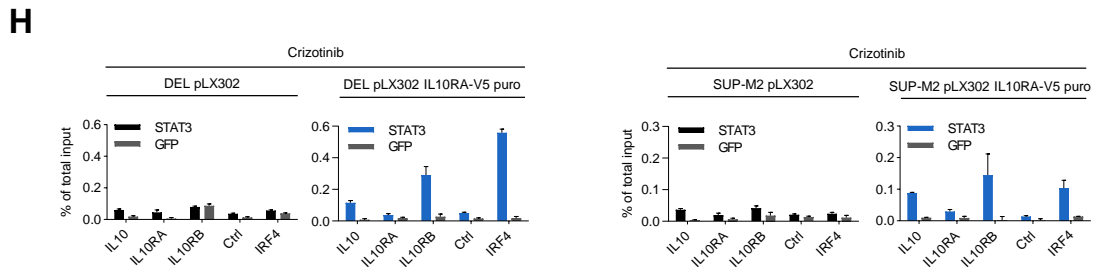
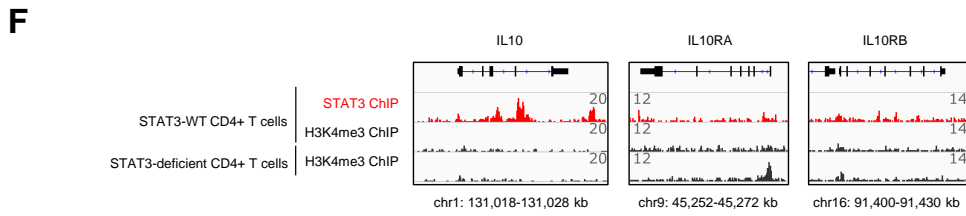
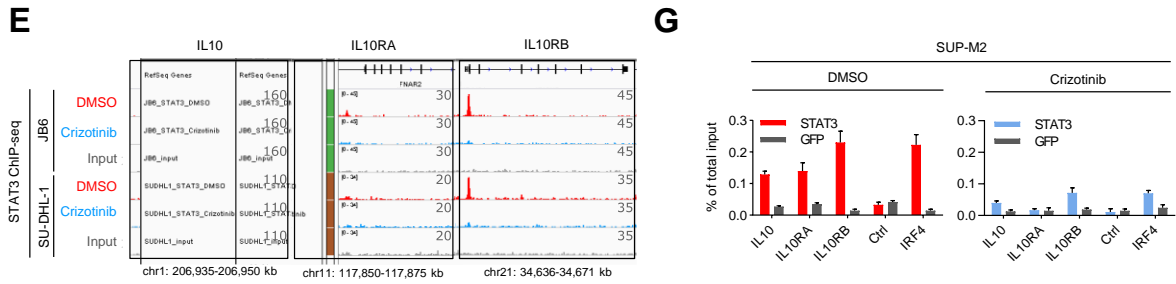
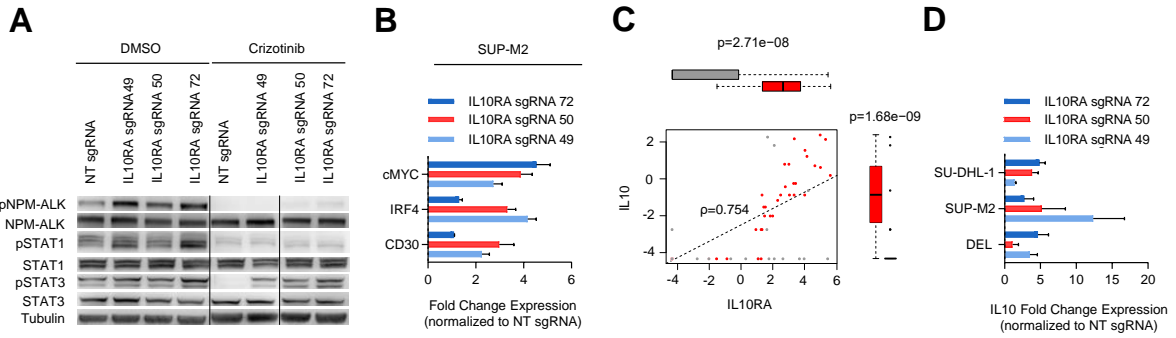
Figure 28 CRISPR-based knockout of IL10RA/IL10RB/IL10 is not lethal, but sensitizes ALCL cell lines to ALK inhibition

(A) Read counts of 6 sgRNAs targeting *IL10/IL10RA/IL10RB* before and after a 14-day incubation with DMSO or (80 nM for SUP-M2, 100 nM for K299) crizotinib in the indicated ALCL cell lines. Data are represented as boxplot with individual points representing each sgRNA ($n = 6$). Unpaired t test: * $p < 0.05$, ** $p < 0.01$, *** $p < 0.001$. RPM = Reads Per Million mapped reads. (B) Western blot analysis of the indicated ALCL cell lines upon expression of sgRNAs inducing knockout of IL10RA versus non-targeting (NT) control sgRNA. Cells were harvested 7 days after infection. Tubulin was used as a loading control. This blot is representative of two independent experiments. Reproduced from Prokoph et al.³⁰¹. (C-F) The CRISPR knockout screen dataset³¹² by Ng et al. identifies that *IL10RA*, *IL10* and *IL10RB* are non essential genes in ALK+ and ALK- ALCL in the absence of ALK inhibition. *MYC* served as the positive control. (C) Genes ranked by Z-score. (D) Corresponding false-discovery rate (FDR) q-values. (E) Corresponding gene expression level; RPKM, reads per kilobase of transcript, per million mapped reads. (F) Combined gene expression level and FDR identifies vulnerabilities as true or false.

We also observed a strong correlation between IL10RA and IL10 mRNA expression levels across publicly available Human Protein Atlas RNA-seq datasets (Spearman $\rho = 0.754$, $p < 1.68e-9$) (**Figure 29C**) and an overexpression of IL10RA led to an increase in IL10 mRNA expression in crizotinib treated cells (**Figure 29D**). These results suggest that when IL10RA is expressed in ALK+ ALCL, it may function by creating an autocrine positive feedback loop via activation of STAT3.

To investigate if STAT3 might directly regulate the transcription of *IL10*, *IL10RA* and *IL10RB* genes, we analyzed publicly available ChIP-seq data of two ALCL cell lines treated with crizotinib/DMSO³⁰⁴ and compared them to existing STAT3 ChIP-seq data on mouse CD4+ T cells³¹³. We found STAT3 binding upstream of the TSSs of *IL10/IL10RA/IL10RB* in both ALCL cell lines (**Figure 29E**), but not in naïve CD4+ T cells (**Figure 29F**). Strikingly, when ALK activity was inhibited by crizotinib the STAT3 binding was abrogated (**Figure 29E**). In addition, using IRF4 as a positive control we validated several STAT3 peaks by ChIP followed by quantitative PCR (ChIP–qPCR) using a STAT3-specific antibody, confirming STAT3 binding to the TSSs of *IL10/IL10RA/IL10RB* in SUP-M2 cells (**Figure 29G**). Furthermore, we confirmed that IL10RA overexpression rescued STAT3 binding to the TSS of *IL10/IL10RB/IRF4* in the presence of crizotinib (**Figure 29H**). Consistent with this, STAT3 depletion was found to diminish the expression of IL10 mRNA in ALCL cell lines expressing sgRNAs targeting IL10RA (**Figure 29I**).

Thus, our data support a model whereby increased expression of IL10RA promotes upregulation of the IL10 ligand, ultimately reversing crizotinib-mediated inhibition of STAT3 phosphorylation. This mechanism promotes cellular survival and resistance to ALK TKI treatment in ALK+ ALCL (**Figure 29J**).



(legend on next page)

Figure 29 STAT3 is Activated Independently of NPM1-ALK through the IL10/IL10R Signaling Pathway on Crizotinib Inhibition

(A) Western blot analysis of differential JAK/STAT signaling activation in response to individual NT sgRNA control or IL10RA sgRNA overexpression in SUP-M2 cells treated with DMSO or 1000 nM crizotinib for 1 hour. This blot is representative of three independent experiments. Lines indicate different blots. (B) Fold change in transcript level of the indicated STAT3 target genes relative to GAPDH and relative to NT sgRNA in SUP-M2 cells expressing sgRNAs targeting IL10RA and treated with 1000 nM crizotinib for 1 hour. Data are represented as means \pm SD, n = 3. (C) Correlation between IL10RA and IL10 mRNA expression levels in the Human Protein Atlas RNA-seq datasets, including non-transformed (red) and cancer (gray) cell lines. ρ , Spearman correlation coefficient. (D) Fold change in IL10 mRNA expression levels in crizotinib treated ALCL cell lines expressing sgRNAs inducing expression of IL10RA. Data are represented as means \pm SD, n = 3. (E) STAT3 ChIP-seq tracks near the *IL10/IL10RB/IL10RA* loci in ALCL cell lines treated for 3 hours with crizotinib (300 nM) or DMSO. (F) STAT3 ChIP-seq validation by ChIP-qPCR of the *IL10/IL10RA/IL10RB* and *IRF4* TSS in SUP-M2 cells treated for 3 hours with crizotinib (1000 nM) or DMSO. Data are represented as means \pm SD of technical replicates; experiment was performed independently three times. *IRF4* served as a positive control. (G) STAT3 and H3K4me3 ChIP-seq tracks near the *IL10*, *IL10RA* and *IL10RB* loci in STAT3 wild type (WT) or STAT3-deficient mouse CD4+CD44-CD62L+ T cells. (H) STAT3 ChIP-qPCR of the *IL10/IL10RA/IL10RB* and *IRF4* TSS in the indicated ALCL cell lines when expressing pLX302 IL10RA-V5 puro versus pLX302 control plasmid treated for 3 hours with crizotinib (1000 nM). Data are represented as means \pm SD of technical replicates; experiment was performed independently three times. (I) Fold change in expression levels of STAT3 and IL10 on STAT3 shRNA induction in the indicated ALCL cell lines compared to non-targeting (NT) control shRNA and simultaneous expression of sgRNAs inducing overexpression of IL10RA. Data are represented as means \pm SD, n = 3. (J) Model summarizing the mechanism by which IL10RA overexpression leads to ALK TKI resistance. Reproduced from Prokoph et al.³⁰¹.

4.6 High Expression of IL10RA at Diagnosis is not Predictive of Clinical Outcome for Patients Treated with Standard Chemotherapy

To determine whether IL10RA is an ALK TKI-specific resistance driver in ALK+ ALCL, we evaluated IL10RA protein expression levels in ALK+ ALCL patients treated with standard ALCL99 chemotherapy (n = 97, **Table 15**, **Table 13**, **Table 14**).

To determine whether high IL10RA protein expression levels at diagnosis confer chemotherapy resistance, we analyzed IL10RA expression levels in tumour samples collected before treatment initiation, and divided chemotherapy-treated patients into “relapse” and “no relapse” cases. Patients who showed no evidence of disease for over 10 years after chemotherapy were classified as “no relapse” cases and patients with disease recurrence within 10 years were considered “relapse” cases (**Figure 30A**). Samples from cancer patients who relapsed after standard ALCL99 chemotherapy did not show significantly higher IL10RA protein expression levels at diagnosis compared to patients that remained in remission (**Figure 30B**). Furthermore, IL10RA expression had no influence on EFS or OS in patients treated with chemotherapy (**Figure 30C-F**). Collectively, these results indicate that IL10RA expression does not correlate with response or resistance to standard ALCL99 chemotherapy. Whether IL10RA overexpression because of ALK TKI therapy re-sensitizes tumour cells to chemotherapy, and furthermore if co-treatment with an ALK TKI and chemotherapy could overcome resistance remains to be determined.

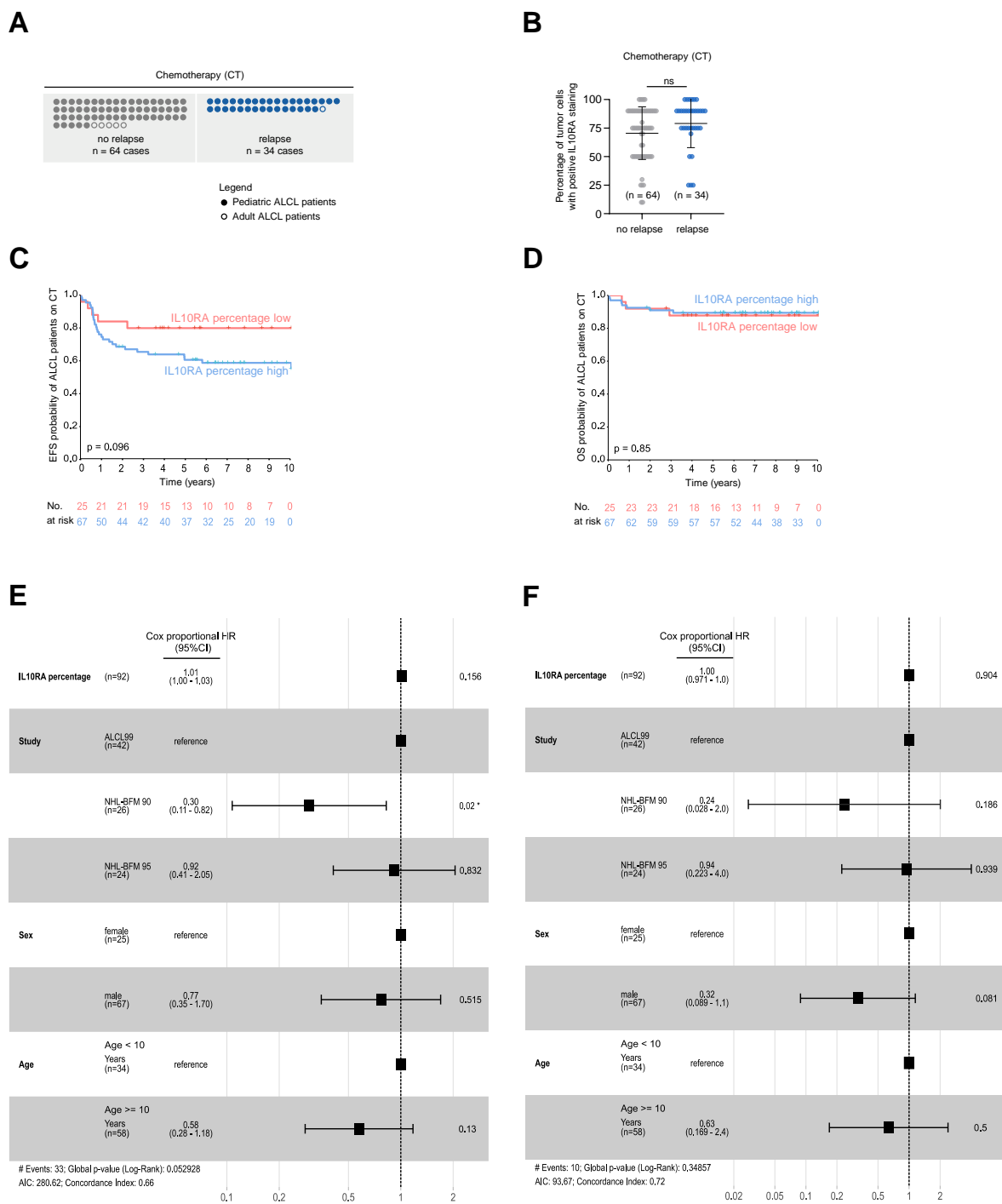


Figure 30 Initial High Expression of IL10RA is not Predictive of Clinical Outcome for Patients Treated with Chemotherapy

(A) Schematic summary of diagnostic biopsy specimens of ALK+ ALCL patient tumours analyzed by IHC. Numbers of standard ALCL99 chemotherapy treated patients that presented with a “relapse” or “no relapse” are indicated below each chart. (B) Percentage of tumour cells expressing IL10RA in diagnostic biopsy specimens of patients presented in (A) (n = 98) that were treated with standard ALCL99 chemotherapy. Individual quantifications are plotted with means ± SD indicated. (C,D) Paediatric patients (n = 92) treated with standard ALCL99 chemotherapy as part of the NHL-BFM90, NHL-BFM95 and ALCL99 trials were divided into two groups (low < 50%, high ≥ 50%) according to the percentage of tumour cells expressing IL10RA and the difference in median (C) EFS or (D) OS (log-rank test) was analyzed using the Kaplan–Meier estimator. P value determined by Cox proportional HR and the 95% CI is shown. pts, patients. (E,F) Forest plot assessing the effects of the indicated clinical parameter on (E) EFS or (F) OS. P values determined by Cox proportional HR with 95% CI are shown. Reproduced from Prokoph et al.³⁰¹.

4.7 Discussion

Among PTCLs, ALCL has been associated with the highest level of IL10 expression³⁹⁹. In addition, IL10 together with IL22 are known to be the most abundant cytokines secreted by ALCL cell lines³⁷² and their expression is mediated by NPM1-ALK^{393,400}. Both cytokines form autocrine loops to activate the IL10R (IL10RA/IL10RB) and the IL22R (IL22RA1 or IL22RA2/IL10RB)⁴⁰¹, respectively, that ultimately mediate a pro-proliferative effect via JAK/STAT signaling pathway activation^{393,400}. Although this illustrates that both cytokines and their receptors play a pivotal role in ALCL, only IL10RA, the IL10R specific subunit, was detected in the CRISPR overexpression screen. Furthermore, our study provides evidence that IL10RA and IL10RB expression are independent of NPM1-ALK expression, while IL22RA1 expression has been shown to be induced by NPM1-ALK⁴⁰⁰. Thus, we reasoned that IL10R subunits can be highly expressed even in the presence of crizotinib-mediated ALK inhibition, representing a bypass signaling pathway.

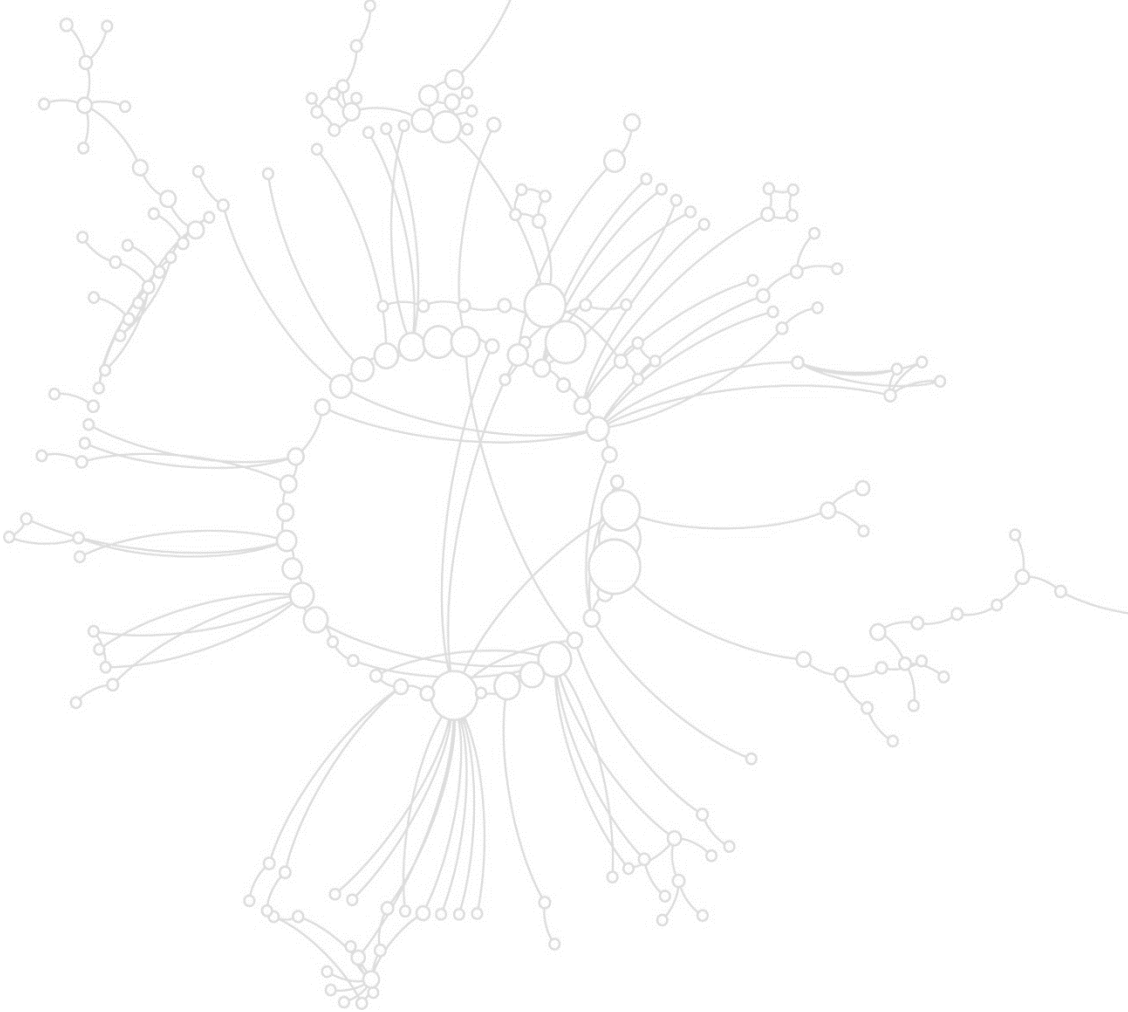
In future work it will be interesting to investigate how IL10RA overexpression is achieved. This could be either through decreased recycling of IL10RA or its increased transcription, perhaps driven by a transcription factor such as CEBPB, whose activity is not affected by ALK inhibition³⁰⁴. However, it is also possible that tumour cell sub-clones with higher IL10RA expression levels already exist and are selected with ALK TKI therapy.

Interestingly, two lorlatinib-resistant samples carrying an ALK L1196M mutation (patient 1 and mouse xenograft T5) showed high levels of IL10RA expression, suggesting that IL10 signaling might cooperate with mutant NPM1-ALK to provide a drug resistance phenotype, thus allowing expansion of an otherwise lorlatinib-sensitive NPM1-ALK mutant tumour.

IL10 binding results in autophosphorylation of the IL10RA subunit, which in turn leads to the activation of Janus kinase 1 (JAK1) or non-receptor tyrosine-protein kinase (TYK2). The activation of these two kinases further gives rise to the downstream activation of STAT family members⁴⁰², with IL10 preferentially signaling via STAT3³⁹³. Our data demonstrate that crizotinib inactivates STAT3 signaling by inhibiting NPM1-ALK-induced phosphorylation, whereas IL10RA expression leads to phosphorylation of STAT3 accounting for renewed signal transduction downstream of STAT3. Therefore, STAT3, pan-JAK or TYK2 inhibitors are rational candidates for combination with ALK TKIs to overcome or prevent therapy resistance^{372,403}. Although targeting STAT3 has proven difficult⁴⁰⁴, the STAT3 antisense oligonucleotide AZD9150 may potentially provide another effective option⁴⁰⁵. Alternatively, several pan-JAK or TYK2 inhibitors have been successfully validated in ALCL cell lines as efficacious single agents³⁷².

Furthermore, our results indicate that IL10RA expression does not correlate with response or resistance to standard chemotherapy, suggesting that resistance mechanisms, such as elevated IL10RA expression developing as a consequence of single agent crizotinib therapy, could be overcome by a combination of ALK-targeted therapy with chemotherapy. Hence, a combination of crizotinib with chemotherapy could prevent ALK-inhibitor resistance-specific relapse.

CHAPTER 5 Brigatinib is effective in a PDX of crizotinib-resistant ALK+ ALCL



5.1 Introduction

The relapse rate for paediatric ALK+ ALCL reaches 50% independent of the chemotherapy regimen^{20,52,72,406,407}. Unfortunately, shorter time to relapse is the strongest predictor for a subsequent relapse with approximately 50% of children who had progression during frontline therapy experiencing progression again during reinduction⁹⁸. In addition, three-year OS for patients after CNS relapse is 48.7%¹⁰⁰. The rarity of the disease combined with the fact that re-biopsy at relapse is not a routine procedure has meant that genomic and expression analysis of relapse and refractory ALK+ ALCL has not been extensively conducted. Beyond a recent study by Lobello et al., which compared tumour samples at diagnosis *versus* relapse in 4 adult patients and identified *TP53* as well as *EPHA5* mutated clones as possible drivers of relapse^{84,408}, little knowledge exists regarding the drivers of chemo-relapse in paediatric ALK+ ALCL.

The ALK inhibitor crizotinib has been trialled as a salvage therapy in paediatric ALK+ ALCL patients that relapsed from chemotherapy^{63,64,66,70,117}, but preliminary results from the AcSé CRIZOTINIB trial showed 5/15 patients progressed¹²⁶. Until now fewer than 130 paediatric ALK+ ALCL patients (NCT01979536, n = 103; NCT02034981, n = 11; UMIN000028075, n = 10) have been treated with crizotinib in a clinical trial setting. None of the 103 patients recruited to NCT01979536 have been re-biopsied at relapse due to ethical constraints and/or the health status of the patient. Of the 11 paediatric patients recruited to NCT02034981, several remained in complete remission or went on to receive a SCT and were therefore not re-biopsied¹²⁶. Therefore, our current knowledge of ALK-dependent resistance mechanisms is based so far on just 4 patients. Gambacorti Passerini et al. amplified the kinase domain of NPM1-ALK from peripheral blood samples from two adult ALK+ ALCL patients and identified the presence of ALK^{Q1064R}, ALK^{I1171N} and ALK^{M1328I} through deep sequencing after crizotinib relapse¹²⁸. In addition, in section 3.4.5, we recently identified an ALK^{L1196M} mutation by WES of tumour tissue from a crizotinib and lorlatinib resistant paediatric ALK+ ALCL patient, while a further crizotinib resistant paediatric ALK+ ALCL patient did not have an ALK mutation nor a NPM1-ALK amplification hinting towards the possibility of an existing bypass resistance mechanism³⁰¹.

Beside those three studies, mechanistic investigations into treatment regimens for relapsed disease have been focused on cell line-based models mostly established from tumour cells obtained from the diagnostic biopsy of patients (COST, DEL, Ki-JK, SU-DHL-1)²⁵⁷ and cell lines or cell line xenografts chronically exposed to ALK TKIs to render them resistant^{217,301,326–328,358,371,395,409,410–412}. However, *in vitro* culture conditions may cause rapid phenotypic and genotypic divergence of patient-derived cells from the originating tumour⁴¹³, and mouse xenografts utilising these cell lines have demonstrated limited predictive power in translational research^{414,415}. PDX models have evolved as powerful pre-clinical tools; by maintaining the heterogeneity of patient tumours, PDX models allow for more clinically-relevant insights into responses to treatment and development of therapy resistance⁴¹⁶. For instance, the Paediatric Preclinical Testing Program of the National Cancer Institute has shown improved prediction of clinical response with PDX models as opposed to cell line xenografts⁴¹⁷. Immunodeficient mice including athymic nude mice, severe combined immunodeficiency (SCID), nonobese diabetic (NOD)-SCID, and recombination-activating gene 2 (Rag2)-knockout mice have been used to establish xenograft models⁴¹⁸. The use of NOD/SCID mice with interleukin-2 receptor subunit gamma (IL2RG)

mutations (NSG) has proven to be effective across a range of cancers including those of lymphoid origin⁴¹³. However, the replacement of human stromal components by murine elements as well as the lack of interaction between immune cells and tumour cells are major disadvantages²⁴⁹.

Although transgenic mouse models would provide these tumour-stroma-immune interactions, they are not of human origin⁴¹³. In addition, the development of genetically engineered mouse models representing ALK+ ALCL has been challenging. Transgenic murine models which express NPM1-ALK driven by *vav*⁴¹⁹/*CD2*⁴²⁰ promoters or conditionally express ALK using the tetracycline system driven by the *EμSRα* promoter⁴²¹ developed B-cell lymphomas.. Chiarle et al. developed a murine model which expressed NPM1-ALK under the CD4 promoter, therefore restricting NPM1-ALK to T cells⁴²². This model still did not fully mimic ALK+ ALCL, with largely thymic-restricted tumours although cells did express CD30⁴²². A *cre-Ick* promoter chimeric model produced thymic T-cell lymphomas with CD30 expression^{423,424}. However, this model relies on *ex vivo* retroviral transduction; accordingly new mice have to be generated for each study with this model⁴²⁴. The closest ALCL mimic to date was developed in the Turner lab again expressing NPM1-ALK from the T cell specific CD4 promoter, but backcrossed to the class I-restricted Ova-specific T-cell receptor (TCR) transgenic line OT1⁴²⁵. As in human ALCL, tumours arising in these mice lack cell surface expression of the TCR complex. However, NPM1-ALK is expressed at all stages of thymocyte development and is therefore not exclusive to CD4 single positive T cells. In addition, tumours arising in these mice variably express CD4, CD8 or CD4 in combination with CD8⁴²⁵. Therefore, until the use of humanized PDX models becomes cost-effective, the use of PDXs in NSG mice offers the best platform for discovery and testing of targeted therapies for tumours showing poor responses to multi-agent chemotherapy and allogeneic SCT.

The first PDX model of paediatric ALK+ ALCL was developed by Kadin and colleagues²⁵⁶. Here we add to this by developing a unique PDX and cell line resource from ALK+ ALCL patients at or before CNS relapse compromising a subgroup of patients with unmet clinical need where no models currently exist to the best of our knowledge^{256,312}.

5.1.1 Aims

This chapter aims to:

- Establish PDXs of liquid biopsy samples obtained from crizotinib resistant and chemotherapy relapsed/refractory ALCL patients.
- Establish cell lines from the PDX tumours
- Determine whether the PDX model that was established from a crizotinib resistant patient maintains its crizotinib resistance *in vivo*
- Determine whether the crizotinib resistant PDX model and/or cell line is sensitive to second generation ALK inhibitors

5.2 Patient treatment history and sample collection

Two paediatric ALK+ ALCL patient experienced relapse/refractory disease during frontline ALCL99 chemotherapy (**Figure 31A, Table 16**). Patient 1 further progressed with CNS involvement on vinblastine treatment combined with intravenous and intrathecal chemotherapy. This is in line with a previous publication, which reported that shorter time to relapse was the strongest predictor of subsequent relapse⁹⁸. Since this treatment was poorly tolerated and only an incomplete response achieved, the patient commenced crizotinib treatment alongside intrathecal chemotherapy, achieving a complete remission (CR). The patient then received an allogenic SCT but progressed rapidly thereafter. The patient was re-treated with crizotinib until eventual progression, at which time we isolated mononuclear cells (MCs) from a bone marrow sample and injected them subcutaneously into NSG mice (**Figure 31B, MGS-A-x**). In line with a previous publication, which reported a three-year OS after CNS relapse of 48.70% for paediatric ALK+ ALCL patients¹⁰⁰, the patient sadly passed away 13 months after diagnosis.

Patient 2 commenced crizotinib treatment with intrathecal chemotherapy due to continued refractory disease, despite treatment including ALCL99 chemotherapy (**Figure 31A, Table 16**). We isolated MCs from a pleural effusion sample obtained early in the disease course, before crizotinib initiation, and injected them subcutaneously into NSG mice to establish a PDX model (**Figure 31B, MTK-A-x**). Unfortunately, despite excellent initial response to crizotinib, with CR confirmed on imaging seven weeks after initiation, Patient 2 relapsed with aggressive isolated CNS involvement shortly afterwards and sadly died despite further intensive conventional intravenous chemotherapy (**Figure 31A**).

5.3 Brigatinib is effective in a PDX of crizotinib-resistant ALK+ ALCL

Tumours were established in the mice from the MCs within 3 months and were confirmed by IHC to be positive for ALK and CD30 expression (**Figure 31C**). Next, to test the response of PDX tumours to ALK inhibitors in a high-throughput manner, we established cell lines from the PDX tumours of patients 1 (MGS) and 2 (MTK) (**Figure 31B**). In line with the clinical characteristics of the patients (**Figure 31A, Table 16**), MGS was less sensitive to crizotinib as compared to MTK (**Figure 31D**). In addition, while MGS was also less sensitive to ceritinib, the second generation ALK inhibitors alectinib, brigatinib and lorlatinib were effective (**Figure 31D**).

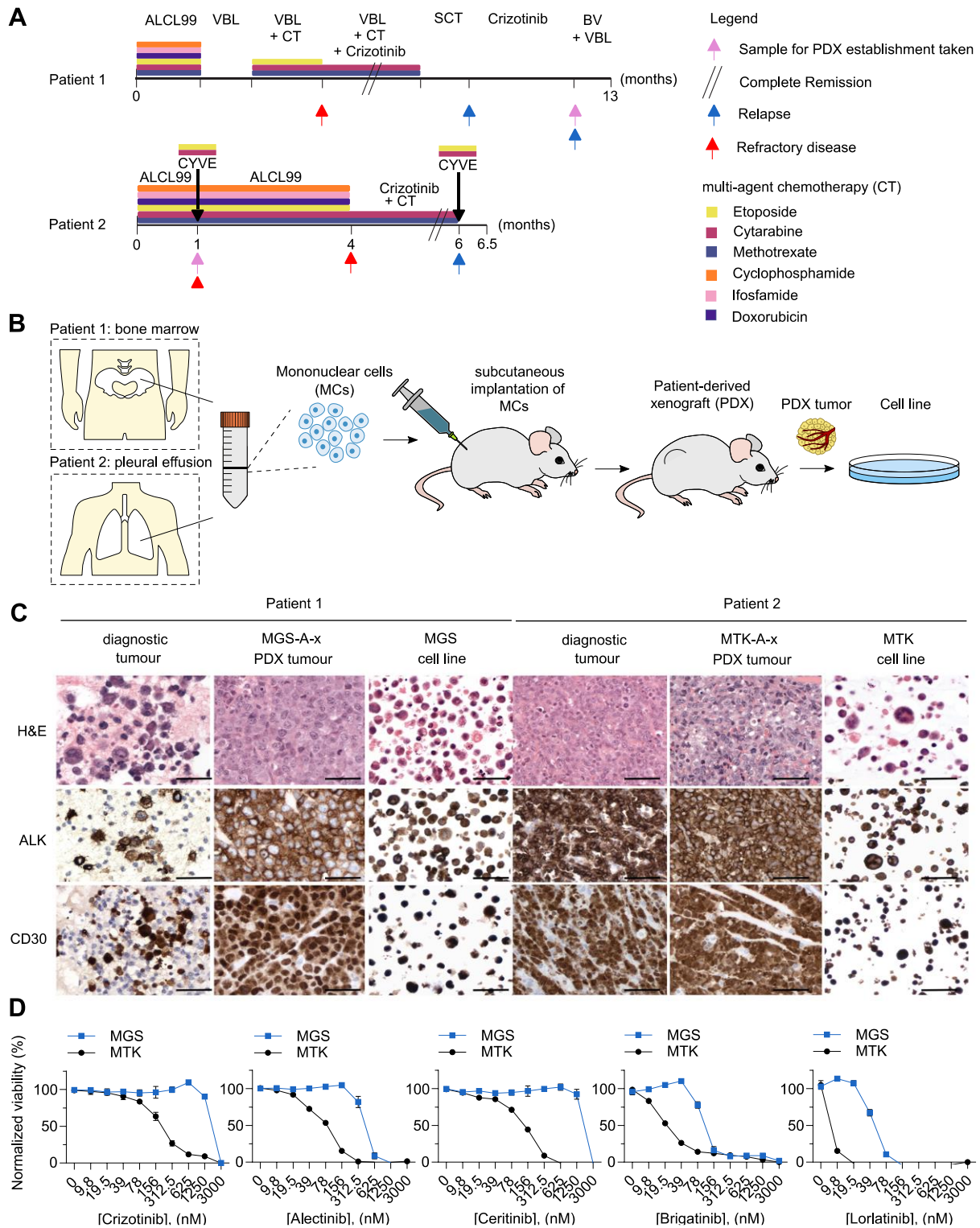


Figure 31 Established cell lines maintain crizotinib responsiveness of the original tumour
(A) Schema of the treatment history of the ALK+ ALCL patient with refractory disease on ALCL99 chemotherapy (Patient 2) or on ALCL99 chemotherapy and ALK targeted therapy (Patient 1). BV = Brentuximab vedotin, VBL = vinblastine. See Table 16 for further patient details. **(B)** Schema of the PDX and cell line generation. Mononuclear cells (MCs) were isolated from bone marrow (Patient 1) or pleural effusion (Patient 2) samples and injected subcutaneously into NSG mice to establish a PDX model of ALK+ ALCL. Cell lines were established from the PDX tumours. **(C)** Representative haematoxylin and eosin staining (400 \times) with corresponding ALK and CD30 IHC (400 \times) performed on sections of the diagnostic tumour compared with the PDX tumour (passage ≤ 3) and the corresponding established cell line (passage ≤ 10). **(D)** Viability of indicated cell lines based on normalized CellTiter-Blue fluorescence reads on exposure to increasing concentrations of ALK inhibitors for 48 hours. Data are means \pm SD of technical replicates. Reproduced from Prokoph & Matthews et al. (unpublished).

Since brigatinib is due to be tested in the next EICNHL trial (personal communication with Dr. Suzanne Turner) and crizotinib has been trialled^{63,64,66,70,117} in paediatric ALK+ ALCL patients that relapsed from chemotherapy (NCT00939770, NCT01606878, NCT01979536, NCT02304809, UMIN000028075, ITCC053) we selected the two ALK inhibitors for *in vivo* investigation (**Figure 32**).

Tumour-bearing MGS-A-x NSG mice were treated daily by oral gavage with either vehicle (PBS, 10% DMSO), crizotinib (100 mg/kg), or brigatinib (25 mg/kg). To better simulate an advanced disease stage, we started treatment when tumours reached 400 mm³ in volume.

The ALK inhibitor concentrations used were based on the findings of previous *in vivo* studies carried out by the European Medicines Agency⁴²⁶. The crizotinib dose used converts to a human equivalent dose of 301,8 mg/m² using conversion formulars based on Freireich *et al.*⁴²⁷ and assuming a child weight of 20 kg and a mouse weight of 0.033 kg, as recommended by the FDA⁴²⁸. This dose is comparable to 165 mg/m² used in the ongoing AcSé trial¹²⁶ (NCT02034981), COG-ANHL12P1 trial (NCT01979536) and the completed COG-ADVL0912 trial (NCT00939770). Mice were euthanized once tumours reached 15 mm in any direction. The study was stopped after 21 days of consecutive treatment.

Brigatinib led to a reduction in the mean tumour volume compared to the baseline level, and relative to either vehicle or crizotinib treatment (**Figure 33A**). While 5/8 mice that were treated with brigatinib showed a CR, 7/8 mice that were treated with crizotinib presented with tumour progression (**Figure 33B**). Survival analysis showed a significant increase in EFS for animals treated with brigatinib relative to vehicle (HR 0.07, $p = 0.0179$), but not for animals treated with crizotinib relative to vehicle (HR 1.09, $p = 0.882$) (**Figure 33C**), where an event was defined as a tumour reaching 15 mm in any one direction. Brigatinib was well-tolerated, with no significant decrease in body weight or lethal toxicity observed compared to either vehicle ($p = 0.4263$) or crizotinib ($p = 0.6407$, **Figure 33D**).

5.4 Discussion

There are two ways in which PDX models can be used to investigate treatment-resistant cancer: (i) PDX models can be derived from patient samples at the time of treatment resistance or (ii) PDX models can be developed from pretreatment tumour samples and resistance can be modelled in the PDX via artificial exposure to the drug⁴²⁹. Here we successfully established two PDX models from liquid biopsies of multi-agent chemotherapy-refractory (Patient 2, MTK-A-x), and both multi-agent chemotherapy-refractory and crizotinib resistant (Patient 1, MGS-A-x) paediatric ALK+ ALCL patients.

PDX models have been shown to retain the drug-sensitivity of the engrafted patient tumour, although PDX models of melanoma^{430,431} and lung adenocarcinoma²⁴² became sensitive after xenografting due to the imposed 'drug holiday'. While this may suggest that treatment-resistant PDXs should be propagated under the continuous selective pressure of treatment, this might on the other hand lead to the selection of subclones ultimately resulting in genetic differences between the PDX tumour and the original patient tumour⁴²⁹. Here, we show that although the MGS-A-x PDX model was established under a 'drug holiday' it retained the crizotinib-resistance profile of the corresponding patient tumour.

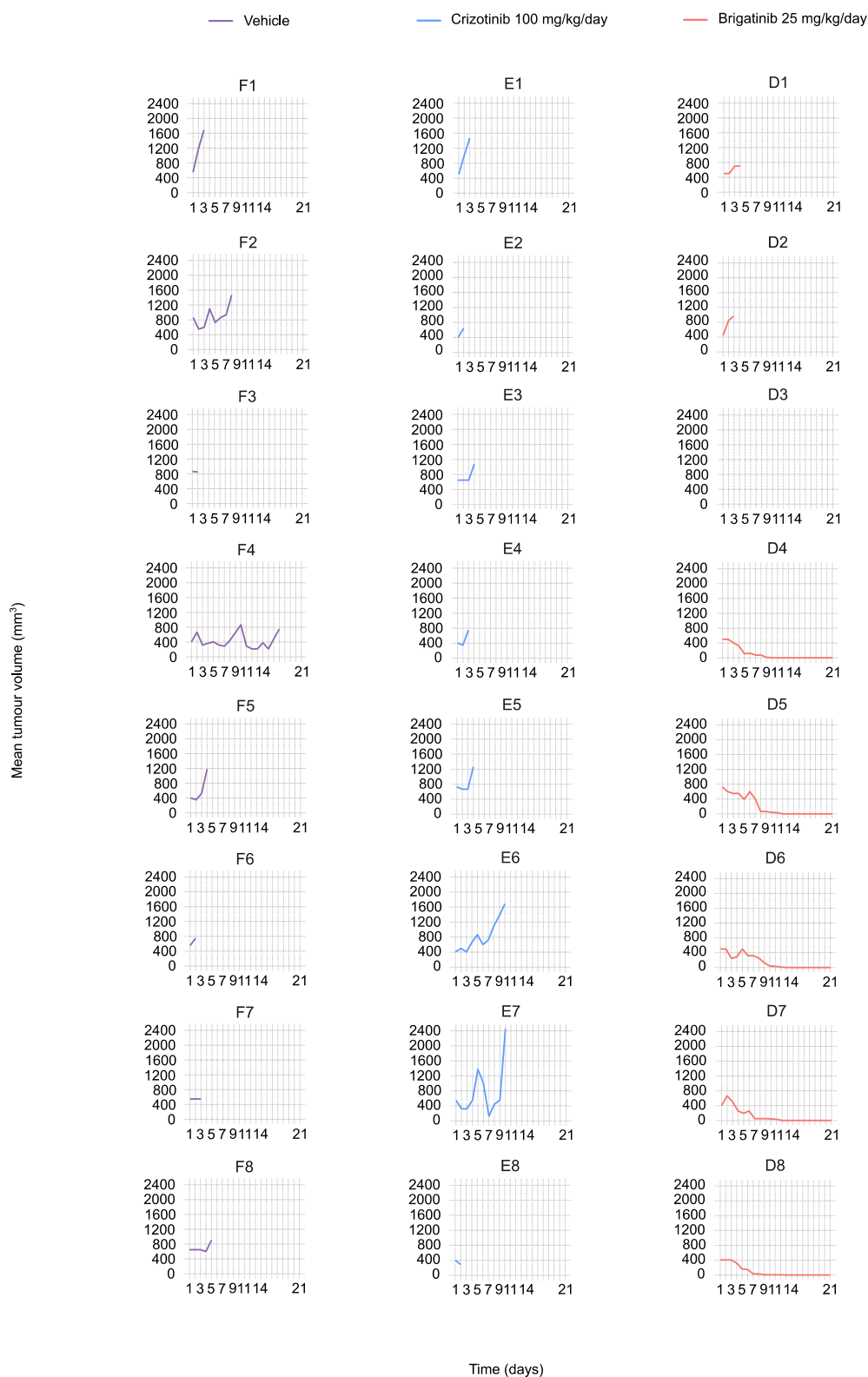


Figure 32 Tumour volume over time in MGS-A-x PDX mice

Tumour volume over time in MGS-A-x PDX mice administered with brigatinib (25 mg/kg; $n = 8$; mice D1-D8), crizotinib (100 mg/kg; $n = 8$; mice E1-8) or vehicle (PBS, 10% DMSO; $n = 8$; mice F1-F8) daily by oral gavage once tumours reached 400 mm³ in volume. Tumours were measured daily with manual calipers and tumour volumes estimated using the modified ellipsoid formula: $V = ab^2/2$, where a and b ($a > b$) are length and width measurements. Mice were euthanized once tumours reached the ethical limit of 15 mm in any direction. The study was stopped after 21 days of consecutive treatment. Mice were censored (*) due to tumour ulceration (mice E2, F5), sudden death (mice D3), self-mutilation (E8), sickness (D1) or if mice remained tumour-free after 21 days of consecutive treatment (D4-8). Modified from Prokoph & Matthews et al. (unpublished).

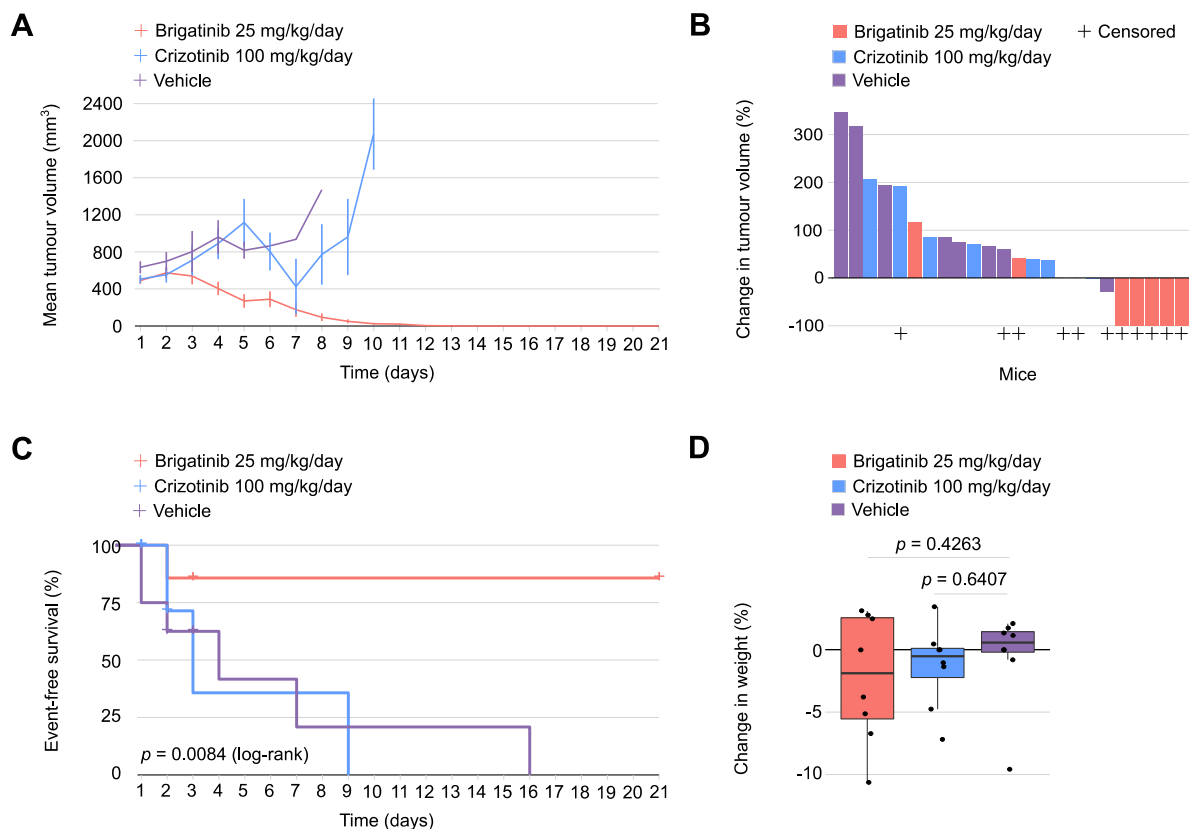


Figure 33 Brigatinib is effective in the treatment of a PDX of crizotinib-resistant ALK+ ALCL
(A) Tumour volume over time in MGS-A-x PDX mice administered with vehicle (PBS, 10% DMSO; $n = 8$), crizotinib (100 mg/kg; $n = 8$) or brigatinib (25 mg/kg; $n = 8$) daily by oral gavage once tumours reached 400 mm³ in volume. Tumours were measured daily with manual calipers and tumour volumes estimated using the modified ellipsoid formula: $V = ab^2/2$, where a and b ($a > b$) are length and width measurements. Mice were euthanised once tumours reached 15 mm in any direction. The study was stopped after 21 days of consecutive treatment. Data points represent mean \pm SEM. **(B)** Percentage change of the tumour volume at the study endpoint against the baseline for individual tumour-bearing MGS-A-x mice ($n = 8$) represented as bars according to each treatment specified in (A). The study end point was reached once tumours reached 15 mm diameter in any direction or after 21 days of consecutive treatment. **(C)** Kaplan–Meier event-free survival according to each treatment group specified in (A) for tumour-bearing MGS-A-x mice, where survival is defined as the time taken for tumours to reach 15 mm diameter. The study endpoint was reached once tumours reached 15 mm diameter in any direction or after 21 days of consecutive treatment. P value determined by Cox proportional HR: Brigatinib vs vehicle (HR 0.07, $p = 0.0179$), crizotinib vs vehicle (HR 1.09, $p = 0.882$). See Figure 32 for MGS-A-x PDX mice that were censored. **(D)** MGS-A-x mouse body weight at the experiment end-point relative to the baseline per treatment group specified in (A). Data are represented as box plots with individual points representing each mouse ($n = 8$). P -values were determined by two-sample t-test. Modified from Prokoph & Matthews et al. (unpublished).

We utilised immunodeficient NSG mice for PDX establishment. Despite the importance of an absent immune system to enable tumour engraftment, this is also one of the major limitations of NSG mouse models given the important role the tumour microenvironment (TME) plays in cancer. It will be necessary for ALK+ ALCL PDX models to possess a human immune system to facilitate the study of immune-cancer cell interactions and preclinical assessment of cancer immune therapies for the following reasons. Firstly, the anti-CD30 antibody armed with the antimicrotubule agent monomethyl auristatin E (MMAE) - BV – may be introduced as a frontline treatment either in combination with crizotinib (NCT02729961) or with the ALCL99 chemotherapy backbone (NCT01979536). Both multi-agent chemotherapy^{432,433,434,435} and ALK inhibitors^{436,437} have been shown to have immune stimulatory potential. Secondly, Nivolumab is being investigated as a treatment option for ALK+ ALCL patients that have failed both chemotherapy and ALK inhibitor treatment (NCT03703050).

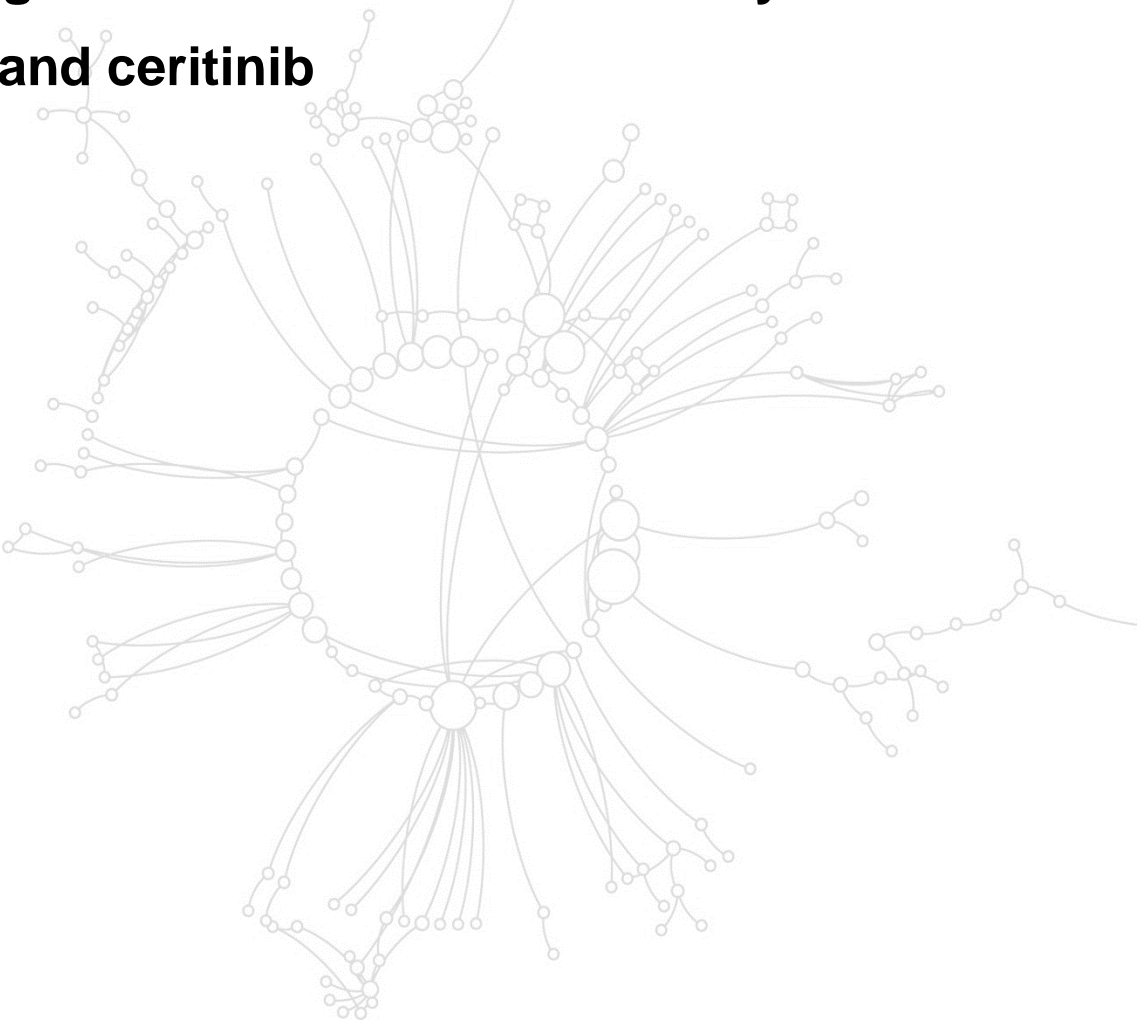
Humanized mice are immunocompromised mice in which a competent human immune system has been introduced. They can be developed by transplantation of (i) total peripheral blood from human healthy donors or patients, (ii) transplantation of tumour-infiltrating lymphocytes into immunodeficient mice or (iii) the transplant of CD34-positive human hematopoietic stem cells or precursors, either alone or in combination with additional human immune tissues into immunodeficient mice^{429,438}. However, they are not in common use as they are highly expensive.

Therefore, until the use of humanized PDX models becomes cost-effective, we propose MGS-A-x as a model of a multi-agent chemotherapy-refractory and crizotinib-resistant paediatric ALK+ ALCL to examine responses to novel therapies and the development of therapeutic resistance.

We established the PDX via subcutaneous injection of MCs isolated from a bone marrow sample of a patient after CNS relapse and this sub-group of patients comprises the most difficult to treat cases with the 3-year OS for patients after CNS relapse being 48.7%¹⁰⁰. Therefore, as a next step in the validation process of the PDX model, it will be important to test whether metastasis can be detected in the brain of the MGS-A-x mice. Subcutaneous PDX models are known to rarely metastasize⁴³⁹. Hence, IV injections could be attempted in the future.

In vivo investigation of MGS-A-x showed that second generation ALK inhibitor brigatinib led to a reduction in the mean tumour volume relative to crizotinib treatment. In future work, it will be interesting to investigate the genetic and/or transcriptomic reasons why MGS-A-x shows resistance to crizotinib, but sensitivity to brigatinib. Most likely, MGS-A-x harbours an ALK mutations, which renders ALK+ ALCL tumour cells resistant to crizotinib, but not brigatinib. Based on published ALK-dependent resistance mechanisms in ALK+ NSCLC, L1152P/R²¹⁴, C1156Y²¹⁴, F1174V/C/L^{214,218}, G1123S, F1127L or 1151Tins^{214,210,223} are possible ALK mutations likely to be detected. Hence, the FDA-approved second generation ALK inhibitor brigatinib could represent a treatment option for crizotinib-resistant ALK+ ALCL patients harbouring this ALK mutation.

**CHAPTER 6 Overexpression of PIM1 in
ALK+ malignancies decreases sensitivity to
brigatinib and ceritinib**



6.1 Introduction

Deriving from precursor cells of the sympathetic nervous system, NB is the most common and deadly extracranial solid tumour in children^{440,441}. NB presents at various sites along the sympathoadrenal axis, most commonly in the adrenal medulla or paraspinal ganglia⁴⁴². Characterized by heterogeneous biological and clinical features ranging from spontaneous regression to aggressive treatment-resistant disease, NB is often referred to as a 'clinical enigma'. While low- and intermediate-risk forms of NB are highly curable, over half of patients with high-risk disease suffer relapse and five-year survival is 40–50%⁴⁴³. Therefore, novel treatment strategies aimed at providing long-term disease remission are urgently sought.

ALK is the most commonly mutated gene in NB, where gain-of-function mutations in the kinase domain are found in 8-10% of cases overall^{177,444} (**Figure 4B**). An additional 2-3% of patients harbor focal amplification of *ALK*, and this feature correlates with poor survival^{177,444,445}. Given the plethora of interest in the development of ALK inhibitors in NSCLC, the assessment of these compounds in ALK-driven NB quickly followed (**Table 7**). Numerous recent studies have demonstrated the efficacy of ALK inhibitors against ALK-driven NB cell lines and PDXs^{446–448}. Several of these studies have documented the *de novo* resistance of the ALK^{F1174L} mutation to crizotinib and ceritinib, and have devised combinatorial treatment strategies to enhance efficacy^{221,446,449–451}.

In patients with ALK+ NSCLC, acquired resistance has been shown to arise with first, second and third-generation ALK inhibitors, presenting a major challenge in the long-term use of these compounds⁴⁵². The most common mechanisms of resistance to ALK inhibition in NSCLC are reported to involve bypass signaling through functionally-related pathways³⁸⁵.

To identify mechanisms of resistance to ALK inhibitors in ALK-driven NB that involve bypass signaling, Liam C. Lee and Ricky M. Trigg conducted genome-wide CRISPR overexpression screens²⁷¹ in the NB cell lines SH-SY5Y (ALK^{F1174L}) and CHLA-20 (ALK^{R1275Q}) under treatment with brigatinib or ceritinib for 14 days (**Figure 8E**). They identified putative resistance genes, of which the serine/threonine-protein kinase *PIM1* was chosen for further investigation.

PIM1 is a stress-response kinase with two isoforms being produced from alternative start codons⁴⁵³. *PIM1* expression is normally regulated by a wide variety of cytokines, including those involved in JAK-STAT and NF-κB pathways^{454–456}. Several oncogenic pathways have been identified as *PIM1* targets⁴⁵⁷ including three pathways that facilitate inhibition of apoptosis⁴⁵⁷. Specifically, *PIM1* phosphorylates the pro-apoptotic protein BCL2 associated agonist of cell death (BAD), thereby decreasing its interaction with the anti-apoptotic proteins B-cell lymphoma 2 (BCL2) and B-cell lymphoma extra-large (BCL-XL)⁴⁵⁸. In addition, *PIM1* phosphorylates apoptosis signal-regulating kinase 1 (ASK1), which reduces its kinase activity. Inactivation of ASK1 leads to reduced phosphorylation of Jun N-terminal kinase (JNK) and p38, which in turn results in reduced caspase 3 activation⁴⁵⁹. Finally, *PIM1* phosphorylates proline-rich Akt substrate of 40 kDa (PRAS40) inducing dissociation of PRAS40 from the mTOR complex (mTORC), thereby upregulating mTOR and unbound PRAS40 activity^{460,461}.

PIM1 expression has been associated with resistance to chemotherapy^{462–464} as well as molecularly targeted agents^{465,466}, but not previously for NB. Hence, we further investigated if overexpression of *PIM1* modifies sensitivity to ALK inhibition in ALK-related malignancies including NB and ALCL.

The data presented in this chapter of the thesis form sections of a publication in *Nature Communications* (Trigg, Lee & Prokoph et al.)³⁰⁰, which can be found in Appendix 1.

6.1.1 Aims

This chapter aims to:

- Perform individual validation assays for each of the 25 candidate genes to confirm their capability to induce resistance to ceritinib and brigatinib in SH-SY5Y/CHLA-20 cells
- Determine whether PIM1 expression is predictive of OS in NB patients
- Determine the clinical utility of pharmacologic inhibition of PIM1 alone or in combination with ALK inhibitors
- Validate on-target effects of the CRISPR-based overexpression tool by reversing the resistant phenotype with RNAi against PIM1
- Determine the effect of PIM1 overexpression on sensitivity of ALK+ ALCL cell lines to brigatinib and ceritinib

6.2 Validation of candidate resistance genes in ALK-driven NB cells exposed to ALK inhibitors identified in a genome-wide CRISPR-Cas9 overexpression screen

A genome wide sgRNA library containing 70,290 sgRNAs targeting 23,430 protein-coding genes²⁷¹ was used for an overexpression screen conducted by Liam C. Lee and Ricky M. Trigg. SH-SY5Y/CHLA-20 cells were transduced with the sgRNA library, selected in zeocin for 7 days (day 0) and then cultured for 14 days (day 14) with brigatinib, ceritinib or DMSO, maintaining > 500 cells per sgRNA. Genomic DNA was extracted from cells at days 0 and 14, and deep sequencing conducted to identify enriched sgRNAs (**Figure 8E**). The read counts of two biological replicates were normalized for each sgRNA and candidate resistance genes were defined as those targeted by at least two sgRNAs showing >1.5-fold enrichment in ALK inhibitor-treated cells relative to DMSO treated cells³⁰⁰.

Afterwards, all 25 candidates identified from the genome-wide CRISPR-Cas9 overexpression screens were functionally validated by transducing SH-SY5Y/CHLA-20 cells with two enriched sgRNAs individually and by assessing their response to brigatinib or ceritinib (**Figure 34**). First, levels of gene overexpression were assessed for all candidate genes by RT-qPCR (**Figure 34A,D**). Of the sgRNAs targeting 25 different genes, 76% (38/50) induced a significant increase in the ED₅₀ concentration for both brigatinib and ceritinib in SH-SY5Y ($p < 0.05$) (**Figure 34B-C**), and 24 genes were validated. Similar data were obtained for the CHLA-20 cell line (**Figure 34E-F**), while MET was the top-ranking resistance gene. Five druggable genes were identified that may be amenable to either direct targeting (*PIM1*, *PIK3CD* and *MET*) or indirect targeting (*KRAS* and *MYC*). Given substantial evidence in the literature that *PIM1* mediates resistance to standard chemotherapy^{462–464} as well as molecularly targeted agents^{465,466} and that high expression of *PIM1* is a poor prognostic indicator in multiple cancers^{467–469}, this gene was explored further.

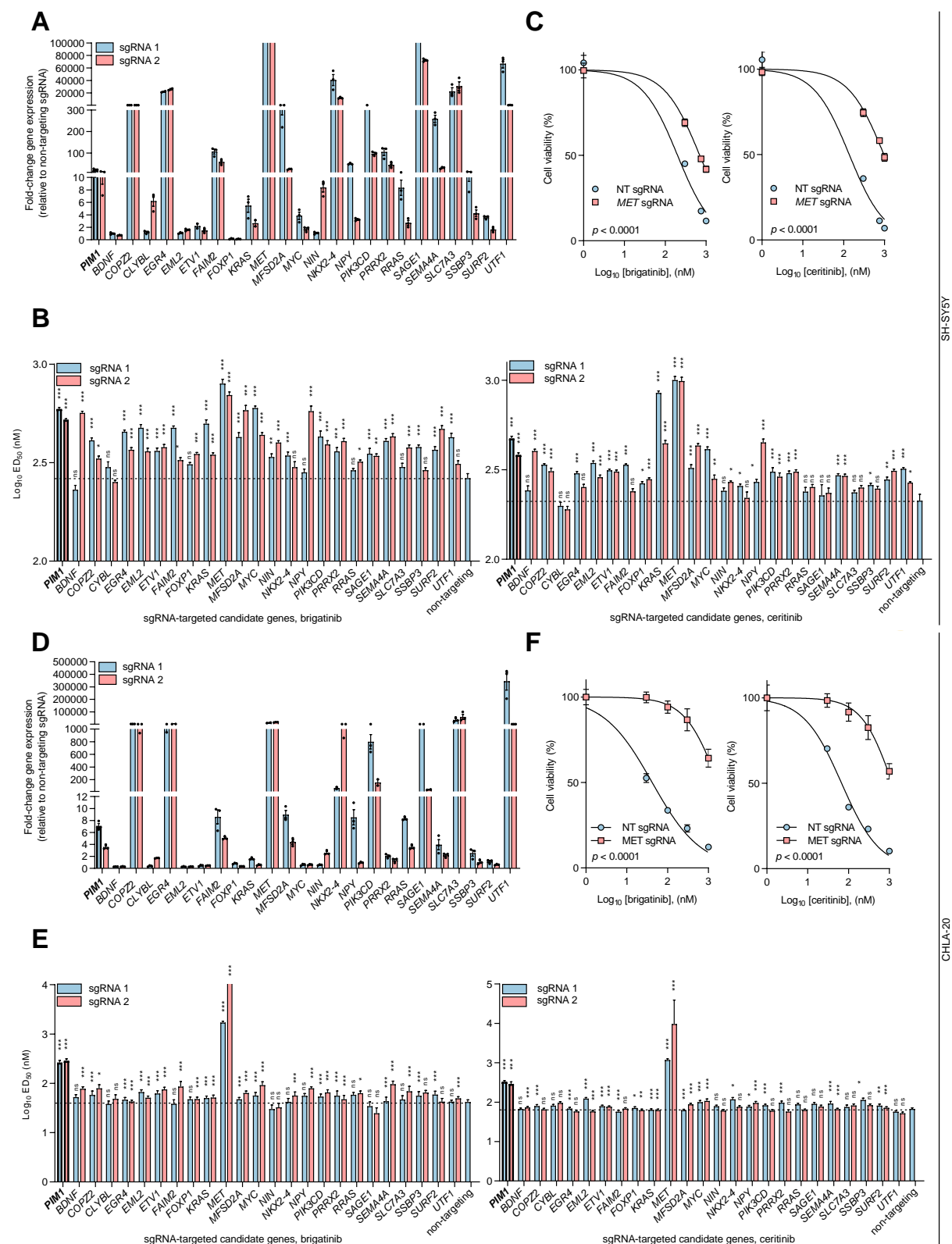


Figure 34 Validation of CRISPR dCas9 overexpression screen hits in SH-SY5Y and CHLA-20 cells
(A, D) RT-qPCR based gene expression in SH-SY5Y/CHLA-20 cells transduced with sgRNAs targeting candidate resistance inducing genes. Data were normalized to cells treated with NT sgRNA. Data represent mean \pm SEM of technical triplicates. **(B, E)** Log₁₀ transformed ED₅₀ values from 96-hour dose response curves of (B) SH-SY5Y or (E) CHLA-20 cells treated with brigatinib or ceritinib five days post transduction with sgRNA molecules targeting each indicated candidate gene, ns = not significant, * $p < 0.05$, ** $p < 0.001$, *** $p < 0.0001$ (one-way ANOVA). Data points represent mean SD of triplicates. **(C, F)** Representative 96-hour dose response curves of (C) SH-SY5Y or (F) CHLA-20 cells transduced with MET or non targeting sgRNAs. Data were analyzed for significance by one-way ANOVA. Data represent means \pm SEM of technical triplicates. Reproduced from Trigg, Lee & Prokoph et al.³⁰⁰.

6.3 PIM1 inhibition enhances the sensitivity of high-risk aberrant ALK-expressing NB to ALK inhibition regardless of MYCN status

6.3.1 High expression of PIM1 in NB is associated with advanced, high risk disease independent of MYCN amplification

Recently, Brunen *et al.*⁴⁷⁰ identified PIM kinases as potential therapeutic targets in *NF1* wild-type NB and demonstrated that high PIM expression is associated with poorer OS in NB patients. In support of PIM1 as a prognostic biomarker, we found its high expression to be significantly associated with worse OS in an independent cohort of NB patients ($n = 498$) (**Figure 35A**)³⁶⁴. Interestingly, *PIM1* transcript level serves as a prognostic biomarker independent of *MYCN* status in this cohort (**Figure 35B-D**). However, as reported by Brunen *et al.*⁴⁷⁰, we also found *MYCN* amplification to be a stronger predictor of poor prognosis than *PIM1* (**Figure 35A-B**).

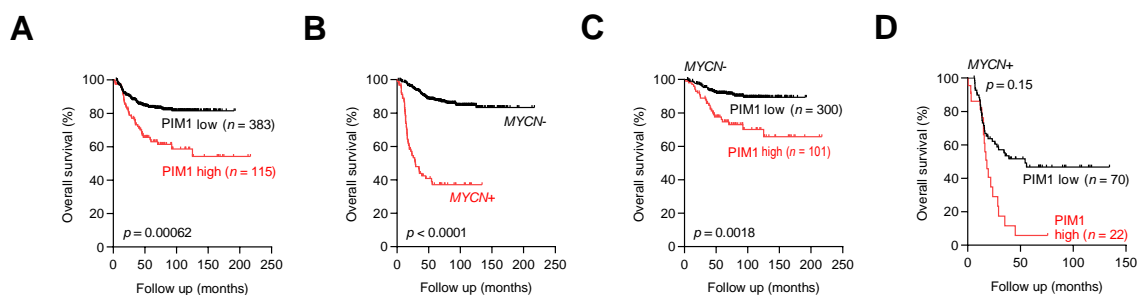


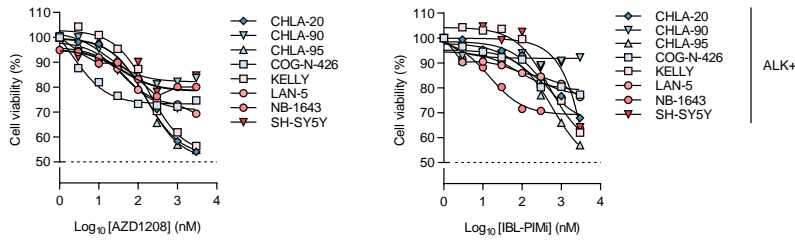
Figure 35 High expression of PIM1 in NB is associated with advanced, high risk disease independent of MYCN amplification

(A-D) NB patients ($n = 498$) were divided into two groups according to (A) PIM 1 expression, (B) MYCN amplification status, (C) PIM1 expression in MYCN- patients or (D) PIM1 expression in MYCN+ patients and the difference in median OS (log-rank test, Bonferroni corrected) was analyzed using the Kaplan–Meier estimator. Reproduced from Trigg, Lee & Prokoph *et al.*³⁰⁰.

6.3.2 Inhibition of PIM1 alone lacks potency in ALK-expressing NB but enhances the efficacy of ALK inhibitors

The activity of the pan-PIM inhibitor AZD1208⁴⁷¹ (with greatest potency for PIM1) was then determined in ALK-driven NB cell lines by 72-hour dose-response assays (**Figure 36A-B**). Consistent with data reported by Brunen *et al.*⁴⁷⁰, cell lines were relatively insensitive to AZD1208⁴⁷¹ at clinically-relevant concentrations, with predicted ED_{50} values exceeding $10 \mu\text{M}$ in 8/8 NB cell lines expressing a range of ALK mutants (**Figure 36A**). Similar results were noted in response to treatment with IBL-PiMi, another small-molecule pan-PIM kinase inhibitor in preclinical development (**Figure 36B**), suggesting that pharmacological inhibition of PIM kinases alone is not a viable therapeutic strategy. The response of ALK- NB cell lines to AZD1208 and IBL-PiMi was likewise analyzed and a similar response was observed, indicating that the response to PIM inhibitors is independent of ALK status (**Figure 36C-D**).

A



B

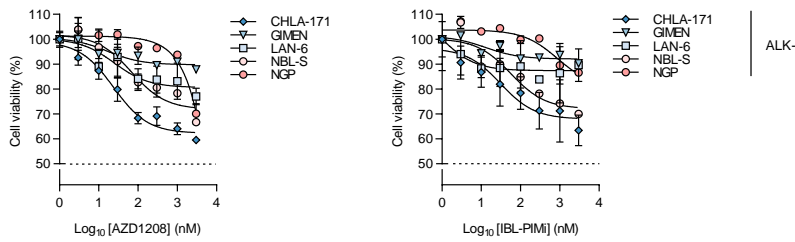


Figure 36 Response of ALK+ and ALK- NB cell lines to PIM inhibition

(A, B) 72-hour dose-response assays for (A) ALK+ or (B) ALK- NB cell lines treated with AZD 1208 or IBL-PIMI. Data represent means +/- SEM of technical triplicates. Reproduced from Trigg, Lee & Prokoph et al.³⁰⁰.

Recent human dose-escalation studies have displayed general tolerability for the PIM inhibitor AZD1208⁴⁷¹, which prompted the assessment of combined ALK and PIM1 inhibition in our study. To this end, cell viability following 72 hours exposure to AZD1208 in combination with brigatinib or ceritinib in KELLY (MYCN-amplified) cells using dose-response matrices in a log-scale format was analysed. The drug interactions were characterized using the Bliss Independence model³⁶². A wide range of Bliss combination index (CI) values were determined across the concentration ranges for both ALK inhibitors, but for the most part CI values were <1, indicative of mild synergy between ALK and PIM inhibition (Figure 37).

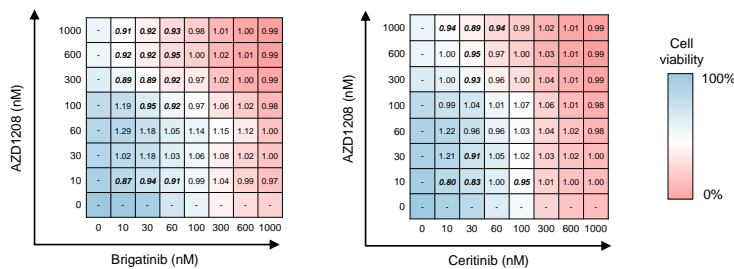


Figure 37 ALK inhibitors and AZD1208 exhibit mild synergism in KELLY cell lines

Heat maps representing the viability of KELLY cell lines based on normalized CellTiter-Blue fluorescent reads on exposure to log scale (0, 1, 3, 10, 30, 100, 300, 1000, 3000 nM) concentrations of AZD1208 and ALK inhibitors (brigatinib, ceritinib) for 72 hours. Drug doses used span upon and below the publicly available EC50 values of the individual drugs used⁴⁴⁶. Numbers indicate the Bliss combination index (CI) values for each dose pair. The Bliss independence model³⁶² was used to calculate CI values. $CI = (Ea + Eb - (Ea * Eb)) / Eab$, where Ea indicates the viability effect of drug A (ALK inhibitor), Eb indicates the viability effect of drug B (AZD1208) and Eab indicates the viability effect of the drug combination. CI < 1 indicates synergism, CI = 1 indicates additivity and CI > 1 indicates antagonism. Synergistic dose combinations (threshold ≤ 0.95) are shown in italic. Data points are representative of two independent experiments. Reproduced from Trigg, Lee & Prokoph et al.³⁰⁰.

6.3.3 Knockdown of PIM1 sensitizes NB cells to ALK inhibitors

As AZD1208 is a pan-PIM kinase inhibitor, KELLY (MYCN-amplified) cells were transduced with a PIM1-targeting shRNA to confirm the specificity of the potentiation effects described above. We achieved an approximate 50% reduction in PIM1 expression as confirmed by RT-qPCR (**Figure 38A**). PIM1 knockdown increased the sensitivity of cells to brigatinib and ceritinib, indicated by a significant decrease in ED₅₀ concentrations after 72 hours of treatment ($p < 0.0005$) (**Figure 38B**).

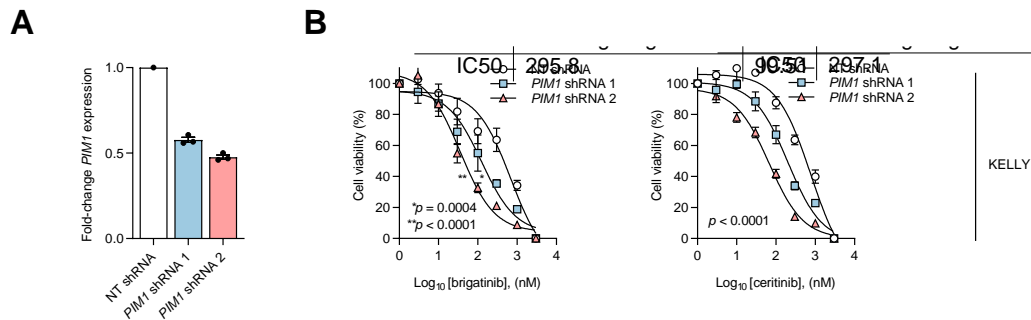


Figure 38 Knockdown of PIM1 sensitizes NB cells to ALK inhibitors (A) Analysis of PIM1 levels by RT-qPCR in KELLY cells with shRNA-mediated knockdown of PIM1. NT=non-targeting. RT-qPCR data represents the means + SD of triplicate experiments. (B) 72-hour dose-response assays following brigatinib or ceritinib exposure in KELLY cells treated with PIM1-targeting and non-targeting (NT) shRNA. Data points represent the mean of triplicate experiments. ED₅₀ values were compared by an unpaired Student's t-test. Reproduced from Trigg, Lee & Prokoph et al.³⁰⁰.

6.4 Overexpression of PIM1 in ALK+ ALCL cell lines decreases sensitivity to ALK inhibitors

Given that a strong synergistic effect was previously shown on simultaneous inhibition of ALK and PIM kinases in ALK+ ALCL cell lines⁴⁷², overexpression of *PIM1* was induced and sensitivity to ALK inhibitors monitored in ALK+ ALCL cell lines. K299 and SU-DHL-1 cells were transduced to express the dCas9-VP64/MS2-P65-HSF1 components whose activity was confirmed (**Figure 11**) before assessing their responses to brigatinib or ceritinib upon overexpression of *PIM1*. Indeed, overexpression of *PIM1* led to drug resistance, evidenced by significant increases in the brigatinib ED₅₀ ($p < 0.01$) and ceritinib ED₅₀ ($p < 0.001$) (**Figure 39**). Therefore, *PIM1* is a potential ALK inhibitor-resistance driver in ALCL and is worthy of further exploration.

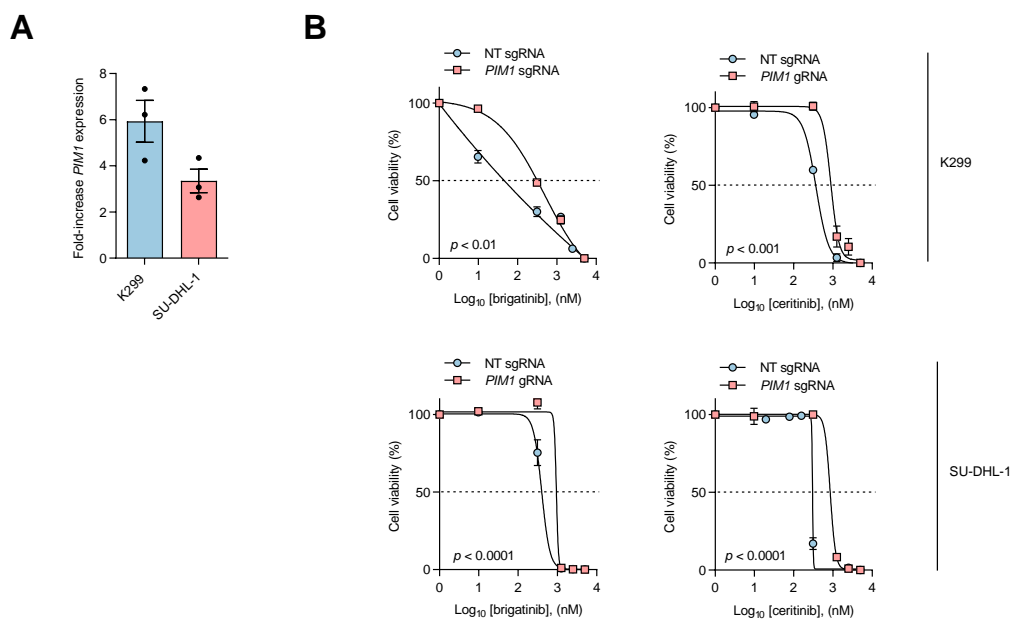


Figure 39 Overexpression of PIM1 in ALK+ ALCL cell lines decreases sensitivity to ALK inhibitors
(A) Expression of *PIM1* in K299 and SU-DHL-1 cells 5 days post-transduction with *PIM1*-targeted sgRNA relative to NT sgRNA, as determined by RT-qPCR. Data points represent the mean \pm SEM of triplicate experiments. **(B)** 48-hour dose-response assay of brigatinib or ceritinib in K299 and SU-DHL-1 cells treated with *PIM1*-targeting and NTsgRNA. Data points represent the mean \pm SEM of triplicate experiments. ED₅₀ values were compared by unpaired Student's *t*-test. Reproduced from Trigg, Lee & Prokoph et al.³⁰⁰.

6.5 Discussion

This work has expanded on the findings of previous publications investigating ALK inhibitor resistance mechanisms in NB^{446,473,474}; AXL activation was identified by a phospho-proteomic assay in NB cell lines rendered resistant to ALK inhibitors through continuous exposure to increasing concentrations of drugs⁴⁷³, whereas *MYCN* overexpression was noted as a resistance mechanism in another study⁴⁴⁶. Of note, neither *MYCN* nor *AXL* were among the resistance driver candidates identified. This may be due to insufficient overexpression of *MYCN* or *AXL* induced by the CRISPR-dCas9-VP64 platform as variable overexpression levels were observed for different genes. Ultimately, the *in vitro* studies conducted to date are potentially predictive of resistance mechanisms in patients but until more children with NB have been treated with ALK inhibitors and biopsy material is taken for study at relapse, CRISPR screens, whilst having their caveats offer the best approach for global, unbiased screening for resistance mechanisms. Among the validated genes mediating sensitivity to ALK inhibition in the two tested NB cells were genes known to mediate resistance in other ALK+ malignancies. Activation of MET has previously been shown to confer resistance to alectinib in ALK+ NSCLC⁴⁷⁵. Two are known to be activated downstream of ALK, namely *KRAS* and *PIK3CD*. Copy number gain and mutational activation of *KRAS* at codon 12 has been shown to confer resistance to crizotinib and ceritinib in ALK+ NSCLC^{234,370}. Similarly, mutational activation of *PIK3CA* is reported as a resistance mechanism to alectinib and ceritinib in these patients^{216,243}. Interestingly, we identified a resistance gene (*MFS2A*)⁴⁷⁶ encoding a sodium-dependent transporter of fatty acids expressed in brain endothelium, in both SH-SY5Y and CHLA-20 cells treated with brigatinib or ceritinib, most likely functioning as an efflux pump for ALK inhibitors although this remains to be investigated further.

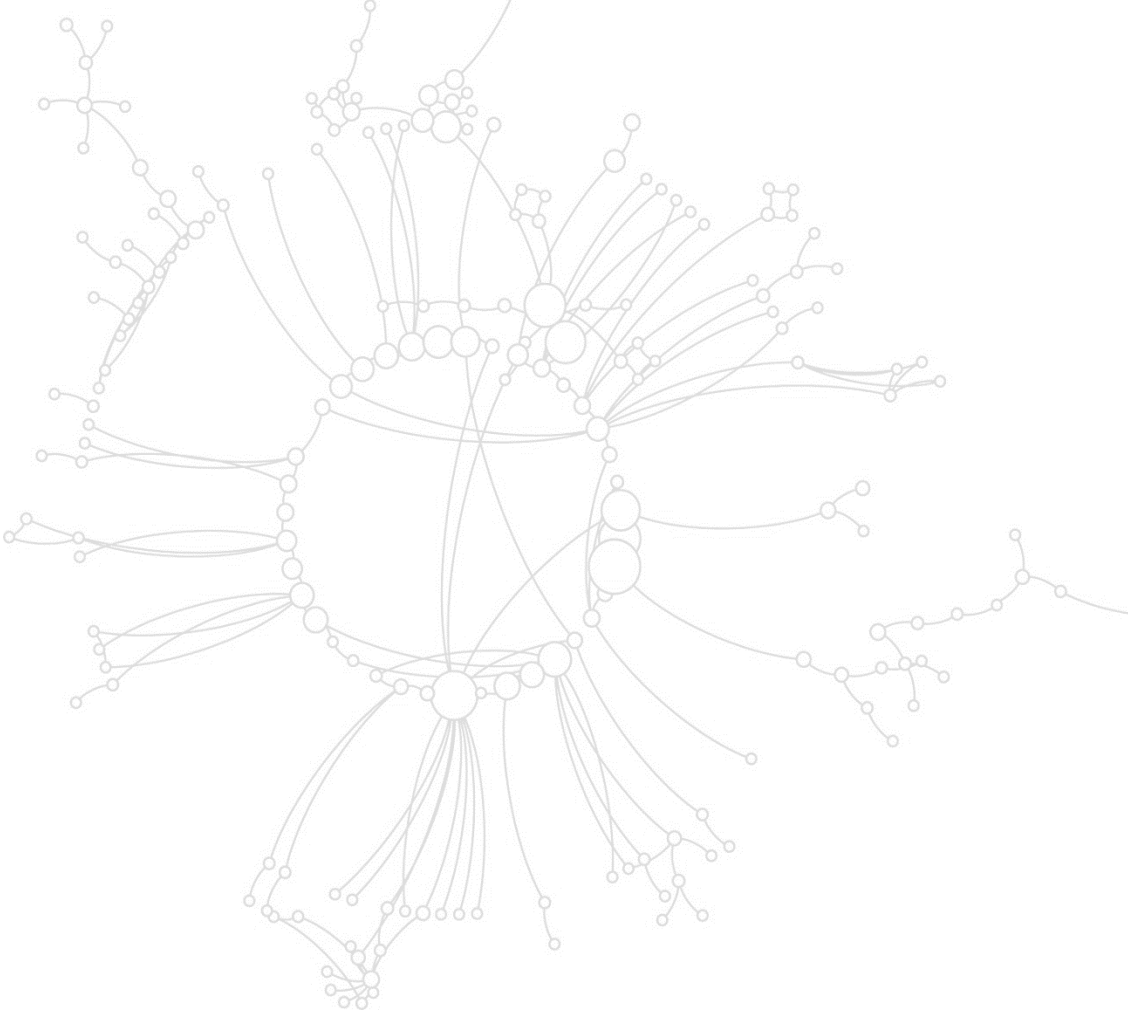
MET was the only putative resistant gene common to all ALK inhibitors. Given that crizotinib is a potent inhibitor of *MET*⁴⁷⁵ and can overcome ALK inhibitor resistance driven by activation of *MET* in NSCLC⁴⁷⁷, we chose to focus instead on *PIM1* whereby high *PIM1* gene expression levels were found to be associated with advanced, high-risk disease and poor survival outcomes on analysis of published datasets^{363,364}.

In addition to validating *PIM1* as a resistance gene in NB cell lines, we sought to determine whether *PIM1* induces resistance to ALK inhibition in another ALK-driven paediatric cancer, namely ALCL. Of the transgenic mice expressing *PIM1* and *MYC* under control of the immunoglobulin heavy chain enhancer that were cross-bred, the double transgenic mice developed T-lymphomas around birth. This established the oncogenic nature of *PIM1* and its cooperation with *MYC* in the formation of lymphoid tumours⁴⁷⁸. Indeed, overexpression of *PIM1* in ALK+ ALCL cell lines decreased sensitivity to brigatinib and ceritinib, consistent with results published previously demonstrating robust synergy between a small-molecule pan-PIM inhibitor and crizotinib in ALCL cell lines⁴⁷². Therefore, further studies investigating the potential for combined PIM and ALK inhibition in other ALK+ malignancies are warranted.

We assessed the *in vitro* responses of both ALK-driven and ALK-negative NB cells to several small-molecule pan-PIM kinase inhibitors and found that cells were relatively insensitive after 72 hours of exposure. However, knockdown of *PIM1* by RNAi sensitized cells to ALK inhibition and the combination of ALK inhibitors with AZD1208 demonstrated mild synergy. Therefore, our data suggest that *PIM1* induces resistance to ALK inhibitors in NB cell lines and demonstrate the potential for combined pharmacological inhibition of ALK and *PIM1* in patients with ALK-driven, high-risk NB.

However, the mechanism of how overexpression of *PIM1* modifies sensitivity to ALK inhibition remains to be determined. Published studies on *PIM1* overexpression in other cancer types provide possible suggestions. Studies of hematological malignancies⁴⁷⁹, gastric cancer⁴⁸⁰ and head and neck cancer⁴⁸¹ have demonstrated that aberrant expression of *PIM1* was associated with poor survival. *PIM1* overexpression associated with LN metastasis, histology and poor clinical outcome in both lung adenocarcinoma and squamous cell carcinoma⁴⁸², while it appeared to be a favorable prognostic factor in pancreatic cancer⁴⁸³. Furthermore, *PIM1* has emerged as a driver of drug resistance in various cancer types^{478,484} including T-cell lymphomas (TCLs) and EBV positive lymphomas^{485,486}, DLBCL⁴⁶⁶, acute myeloid leukemia (AML)^{463,487}, breast cancer^{488,489}, prostate cancer⁴⁹⁰ and ovarian cancer⁴⁹¹. More specifically, three studies on lung adenocarcinoma⁴⁹², prostate cancer⁴⁹⁰ and adult T-cell leukemia (ATL)⁴⁹³ found that *PIM1* is a central mediator of STAT3 signaling, two studies on chronic lymphocytic leukaemia (CLL)⁴⁹⁴ and myeloproliferative neoplasms⁴⁹⁵ found that *PIM1* triggered mTOR pathway activity, three studies on lung adenocarcinoma⁴⁹², breast cancer⁴⁸⁹ and prostate cancer⁴⁹⁶ found that *PIM1* potentiated PI3K/AKT signaling and one study on lung adenocarcinoma⁴⁹² found that *PIM1* potentiated RAS/ERK signaling. Furthermore, *PIM1* overexpression in TCLs⁴⁸⁵ and ovarian cancer⁴⁹⁷ lead to upregulation of *MYC*. In addition, *PIM1* affected NF- κ B signaling in the ABC subtype of DLBCL⁴⁶⁶ and in prostate cancer⁴⁹⁰, while phosphorylation of *MET* was observed in lung adenocarcinoma⁴⁹² and prostate cancer⁴⁹⁶. Future investigations will tell which pathways are involved in mediating ALK inhibitor resistance in ALK-driven, high-risk NB.

CHAPTER 7 Detection and clinical significance of anti-ALK autoantibodies



7.1 Introduction

7.1.1 Humoral Immune Response against ALK in ALK+ ALCL

While ALK is highly expressed in the nervous system during embryogenesis^{3,498}, it is almost absent in developed tissues except in a few neurons within the CNS and in the spinal cord⁴⁹⁹. Aberrant expression of tumour antigens that are not expressed in healthy tissue can induce the production of autoantibodies⁵⁰⁰. Therefore, Karen Pulford and colleagues investigated whether a humoral immune response against ALK in ALK+ ALCL patients exists⁸⁸. An immunoperoxidase labelling technique for NPM1-ALK transfectants (section 2.4) was used as a detection method. All analyzed (100%; 11/11 patients) ALK+ ALCL patients, but not healthy controls (n=5), had detectable anti-ALK antibodies specific for the oncoantigen⁸⁸. In a subsequent analysis by the same group, the presence of anti-ALK autoantibodies in ALK+ ALCL patients was further confirmed at different time points after diagnosis⁸⁹. These results were confirmed by an independent group, which detected anti-ALK autoantibodies in ALK+ ALCL patients (>80%, 25/28 patients)⁹⁰. Importantly, patients who presented with higher anti-ALK antibodies antibody levels prior to and after chemotherapy treatment, had a trend toward a reduced relapse risk⁹⁰. These results raised the possibility that the favorable prognosis of ALK+ ALCL could be contributed to the activation of the immune system⁸⁸.

This spurred an investigation into the clinical significance of anti-ALK autoantibody titres in a larger patient cohort. In a combined effort, Woessmann and Pulford analyzed anti-ALK autoantibodies in 95 paediatric ALK+ ALCL patients that were recruited onto comparable short-pulse chemotherapy trials (NHL-BFM90³³/NHL-BFM95⁹⁴) prior to treatment initiation. They confirmed that >90% of the ALK+ ALCL patients had measurable anti-ALK autoantibody titers at diagnosis compared to 1/99 controls⁹¹. They further categorized patients into low ($\leq 1/750$), intermediate ($1/750$ to $< 1/60,750$) and high ($\geq 1/60,750$) anti-ALK autoantibody titre groups. Interestingly, the magnitude of the antibody response inversely correlated with relapse risk⁹¹. The cumulative incidence of relapse was $11 \pm 6\%/31 \pm 8\%/63 \pm 10\%$ for patients in the high/intermediate/low titre group⁹¹.

Next, Woessmann and colleagues combined anti-ALK autoantibody titre and MDD³⁹. This way ALK+ ALCL patients could be stratified into three biological risk groups (bRG): high risk (bHR): MDD-positive and antibody titre $\leq 1/750$, low risk (bLR): MDD negative and antibody titre $> 1/750$, intermediate risk (bIR): all remaining patients. PFS was 28%, 68% and 93% for bHR, bIR and bLR, respectively. Five year OS was 71%, 83% and 98% for bHR, bIR and bLR³⁹.

Finally, a systematic analysis of the course of anti-ALK autoantibody titres during treatment was performed in 122 paediatric ALK+ ALCL patients that were recruited onto comparable short-pulse chemotherapy studies (NHL-BFM95⁹⁴/Associazione Italiana di Ematologia e Oncologia Pediatrica (AIEOP) LNH-97⁹⁵/ALCL99²⁸/NHL-BFM 2012 registry)⁹². The EFS of paediatric ALK+ ALCL patients with anti-ALK autoantibody titres of $> 1/750$ at the end of therapy was $93 \pm 5\%$ compared to $65 \pm 5\%$ for patients with anti-ALK autoantibody titres below this cut-off⁹². They further categorized paediatric ALK+ ALCL patients according to the decrease in the anti-ALK autoantibody titre from diagnosis to the end of therapy: patients with very low initial titres ($\leq 1/250$), patients who showed a titre-decrease of maximal

two dilution steps (≤ 2) or patients who showed a titre-decrease of more than two dilution steps (> 2). 10-year EFS was $52 \pm 9\%$, $91 \pm 5\%$ or $70 \pm 6\%$ for patients in the $\leq 1/250$, ≤ 2 or > 2 group⁹².

7.1.2 Humoral Immune Response against ALK in ALK+ NSCLC

As ALK rearrangement and ALK upregulation have been described in other cancers, ALK might serve as an embryonal tumour-associated antigen in other ALK+ malignancies. The first indication was published by Chiarle and colleagues who demonstrated that ALK vaccination is not only effective in preventing disease relapse in a murine tumour model of NPM1-ALK+ ALCL, but also in a murine tumour model of EML4-ALK+ NSCLC^{142,501}. One year later, a pilot study showed the presence of ALK autoantibodies in the sera of 13/21 ALK+ NSCLC patients⁵⁰². This observation was confirmed in an independent study that detected anti-ALK autoantibodies in 9/53 ALK+ NSCLC patients, but not in 0/38 ALK- NSCLC patients⁵⁰³. The first study⁵⁰² utilized an immunoperoxidase labelling technique for NPM1-ALK transfectants (section 2.4) as the detection method, while the second study⁵⁰³ developed an enzyme-linked immunosorbent assay (ELISA) to measure anti-ALK autoantibody levels in a mixed population of treatment-naïve and ALK inhibitor/chemotherapy treated patients and detected anti-ALK autoantibodies in 62%⁵⁰² and 17%⁵⁰³ of ALK+ NSCLC patients, respectively. Although highly variable, these data indicate that an ALK-specific immune response exists in a fraction of ALK+ NSCLC patients with possible prognostic application. Although statistically not significant, ALK+ NSCLC patients with higher anti-ALK autoantibody levels showed a trend towards more favorable OS outcomes⁵⁰³. However, whether the presence of anti-ALK autoantibodies in ALK+ NSCLC patients confers a more favorable prognosis warrants further investigation.

7.1.3 Aims

This chapter aims to:

- Develop a protein microarray assay to determine circulating anti-ALK autoantibody levels in serum, plasma, and frozen whole blood
- Cross-validate the newly developed protein microarray with the old immunoperoxidase labelling technique for NPM1-ALK transfectants using samples from treatment-naïve paediatric ALK+ ALCL enrolled onto the ALCL-99 (NCT00006455) trial

7.2 A pipeline to quantify ALK autoantibody titres in ALK+ malignancies

Circulating ALK antibody titres have so far been evaluated using an immunoperoxidase labelling technique for NPM1-ALK transfectants. However, the assay is labour-intensive, difficult to standardize amongst multiple labs and subjective in interpretation leading to false positive results. Therefore, in collaboration with Cambridge Life Sciences, a protein microarray assay was developed that can be fully automated (**Figure 40**). The printing of the teflon mask and the functionalization of the glass slides were outsourced. The antigen spotting took place at Cambridge Life Sciences. The analysis of microarray slides was optimized for both an automated slide processor commonly available in hospitals and for manual handling in research laboratories.

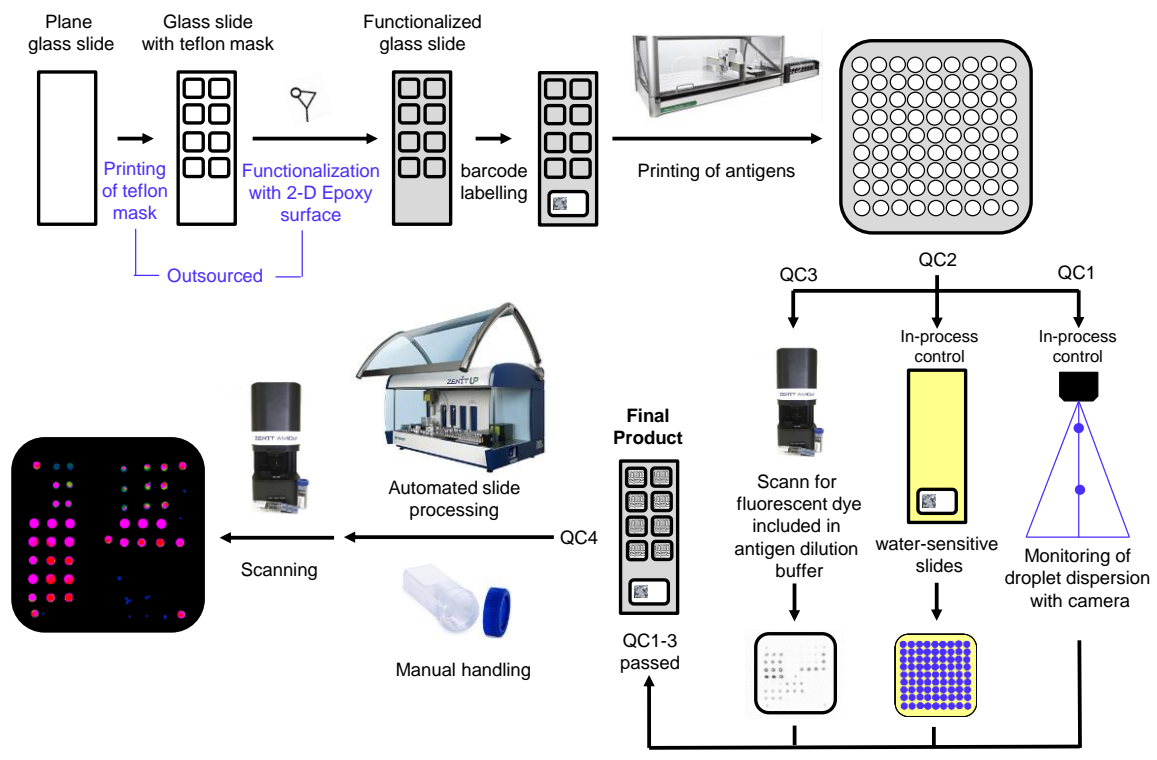


Figure 40 Production, quality control (QC) and processing of microarray slides

Glass slides are masked with Teflon, the surface is functionalized for antigen binding with a 2-D Epoxy surface and labelled. Antigens are spotted with a picolitre droplet dispenser. In-process controls monitor the angle of the droplet dispersion before and after each individually dispensed antigen (QC1), and the successful spotting with water-sensitive slides that turn from yellow to blue (QC2). After the droplets are dispensed, the even distribution of the antigens is confirmed by scanning for a fluorescent dye that was included in the antigen dilution buffer (QC3). Two slides out of each print run are processed (QC4) either with an automated slide processor (e.g. ZENIT UP) or handled manually and scanned for fluorescent intensity (e.g. with a Zenit AmiDot reader) before the final product is used to evaluate patient samples.

7.2.1 2D-Epoxy is the best slide activation chemistry for antigen binding

As a first step in the optimization process, 2-dimensional (2D)-Epoxy, 3-dimensional (3D)-Epoxy, 3D-N-Hydroxy succinimide (NHS), 2D-Aldehyde and 3D-Aldehyde functionalized glass slides were evaluated for their ability to form covalent bonds with DyLight550 conjugated human IgG that was used as a detection antibody in the final assay set-up (**Figure 41**). 2D-Epoxy surfaces showed the best binding properties (**Figure 41C**) for coupling of biochemical species via nucleophilic groups such as amines, thiols and hydroxyl groups via formation of a covalent bond (**Figure 41B**). Additionally, Epoxy surfaces show better stability than NHS and Aldehyde surfaces as they are stable to temperatures of 40 °C and to humid conditions rendering them ideal for commercial production of slides. Unspecific binding to surfaces with printed PBS blank (data not shown) occurred for 3D slides. Therefore, 2D-Epoxy slides were chosen for further optimization.

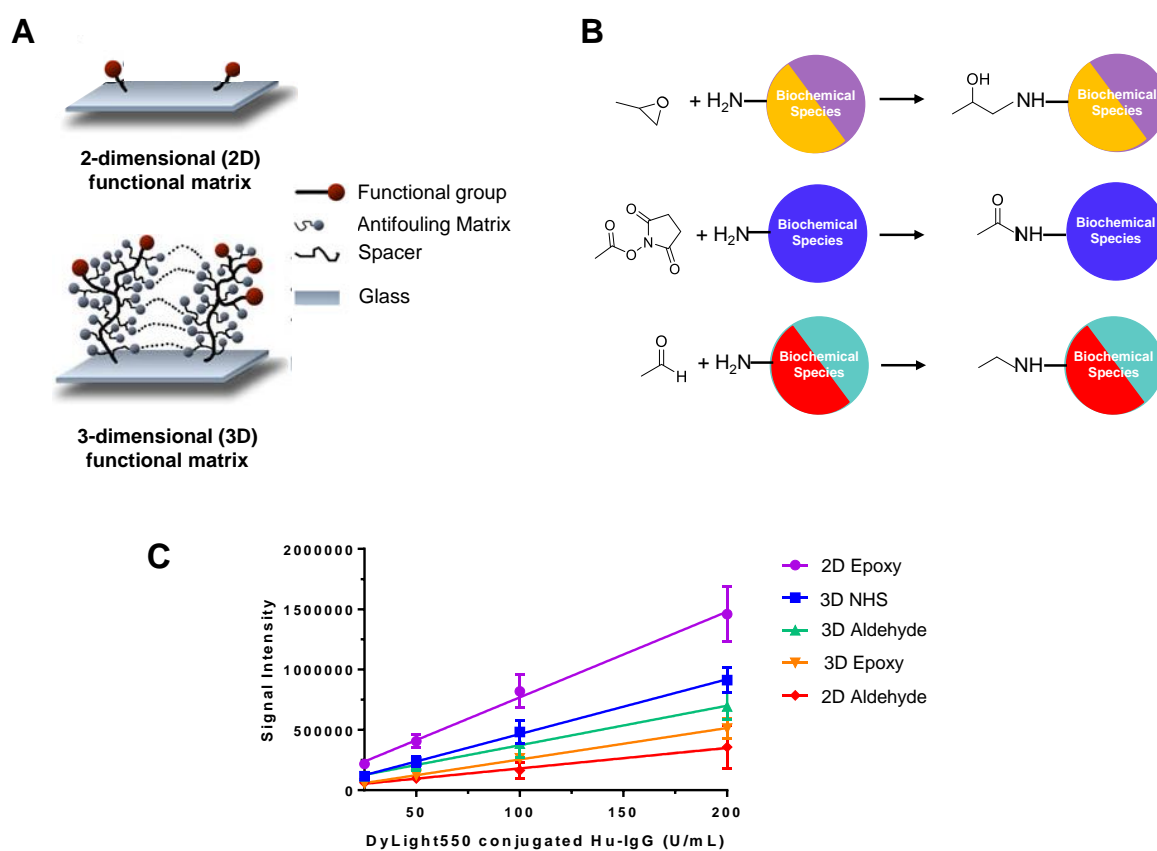


Figure 41 Effect of slide activation chemistry

(A) A cartoon demonstrating the 2-dimensional (2D) and 3-dimensional (3D) functional matrices that were tested. **(B)** Visual representation of the Epoxy (violet, orange), NHS (blue) and Aldehyde (green, red) functional groups that were tested. **(C)** Increasing concentrations of DyLight550 conjugated Hu-IgG were printed on 2D-Epoxy, 3D-Epoxy, 3D-NHS, 2D-Aldehyde, and 3D-Aldehyde functionalized glass slides. Coupling properties were evaluated via the signal intensity of the printed antigen.

7.2.2 A reduced teflon mask increases the signal intensity

For evaluation of slide activation chemistry, glass slides without a mask (**Figure 42A**) were utilized. Next, a Teflon mask was introduced so that the slides could be processed with an automated slide processor. First, we tested a full mask. However, we observed a 3-fold decrease in signal intensity (**Figure 42B**) that might have occurred due to interference of the Teflon mask with the functionalization of the surface with 2D-Epoxy. Therefore, a reduced mask was designed leading to increased signal intensity as compared to the use of a full mask (**Figure 42B**).

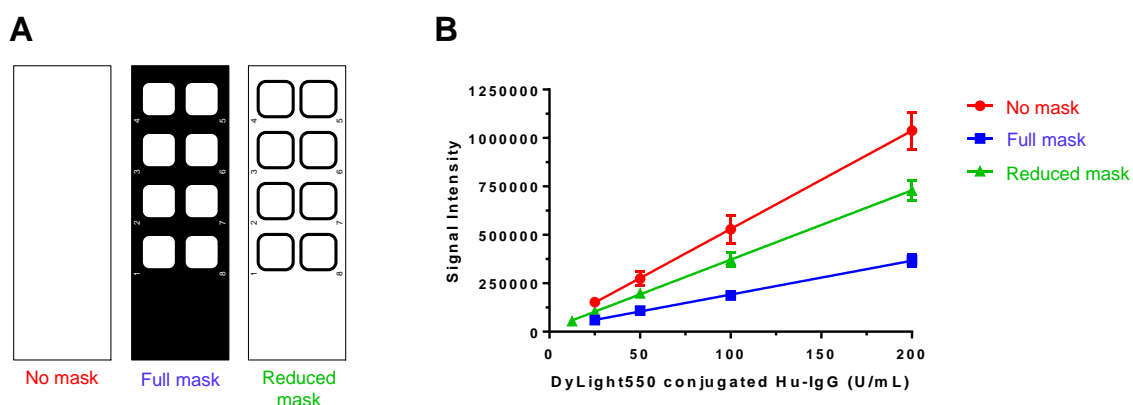


Figure 42 Effect of the Teflon mask

(A) The illustrated Teflon masks needed for automated processing of glass slides were coated with a 2D-Epoxy surface and analysed for their assay performance. (B) Effect of the Teflon mask on the signal intensity of DyLight550 conjugated human IgG.

7.2.3 Evaluation of ALK and control proteins

Damm-Welk et al. showed that sera or plasma from ALK+ NSCLC patients stained both EML4-ALK and NPM1-ALK transfectants, and sera or plasma from ALK+ ALCL patients reacted to NPM1-ALK, TPM3-ALK and full-length-ALK transfected COS cells⁵⁰². In addition, epitopes within the intracytoplasmic domain of ALK recognized by ALK autoantibodies have been described in sera or plasma from nine ALK+ NSCLC⁵⁰³ and 129 ALK+ ALCL⁵⁰⁴ patients. Collectively, these results suggest that anti-ALK autoantibodies target the ALK-portion of the fusion proteins⁵⁰². Hence, we used commercially available full-length ALK protein for the microarray. Full-length ALK protein is insoluble at concentrations utilized in the microarray assay (data not shown), therefore an ALK protein with an uncleaved GST-tag was purchased.

Besides ALK-GST, several control proteins were chosen (**Figure 43A**). GST protein was used to detect unspecific binding of autoantibodies. Anti-human IgG was spotted as a positive control that binds all human IgG antibodies. Human IgG was utilized for use in standard curve measurements. DyLight550 conjugated IgG served as a recognition spot for the scanner during QC3 (**Figure 40**) before slides were processed and incubated with the detection antibody.

To investigate the ability of the microarray to detect ALK autoantibodies in patient samples, we measured sera from two ALK+ ALCL patients (**Figure 43B**) that had previously tested positive using the immunoperoxidase labelling technique of NPM1-ALK transfectants. Unspecific binding was not observed for frozen whole blood or plasma from one healthy individual and serum from a pool of 100 healthy individuals. Therefore, as opposed to the immunoperoxidase labelling technique for NPM1-ALK transfectants, this assay enables the detection of ALK autoantibodies in not only serum and plasma but also frozen whole blood.

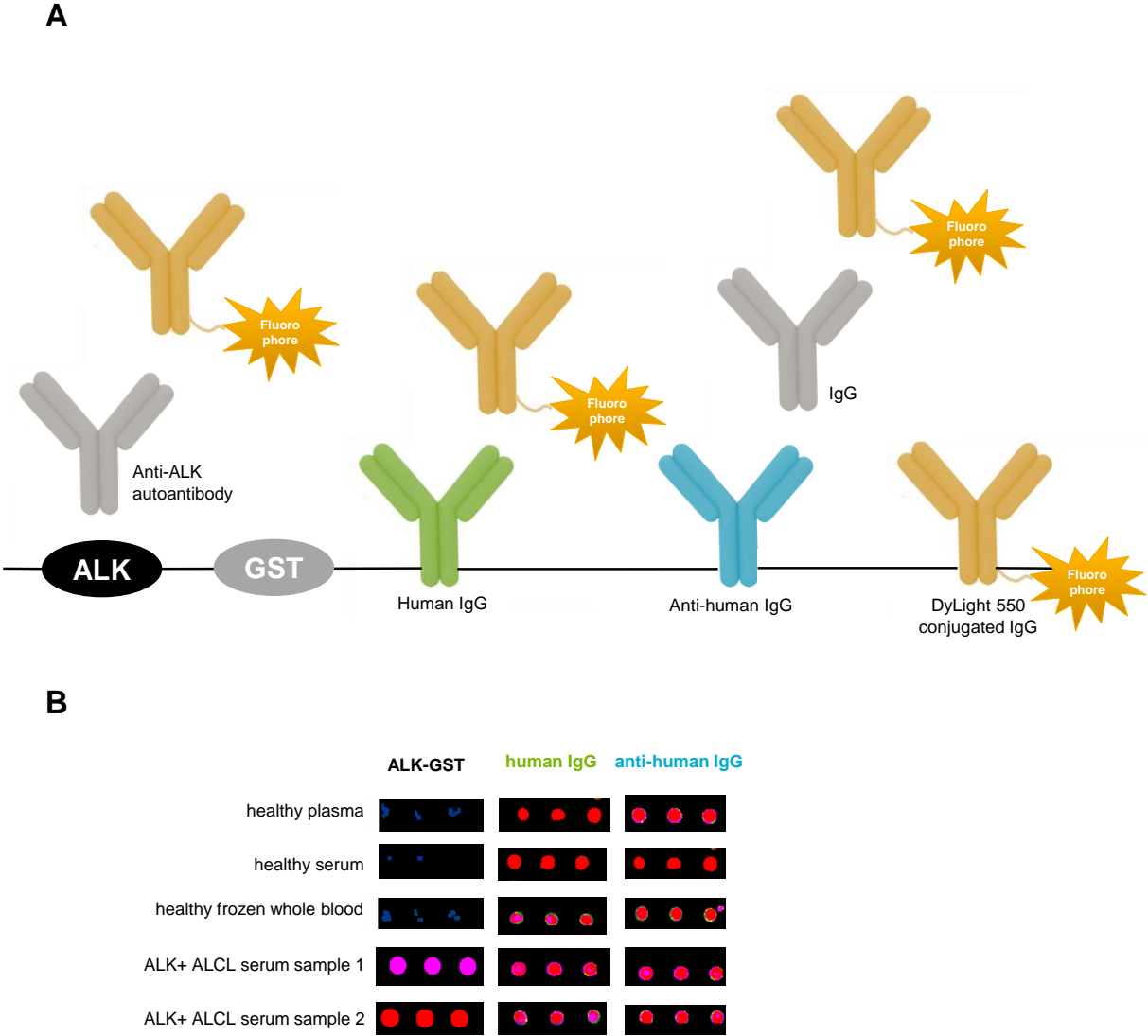


Figure 43 Antigens utilized in the microarray assay
(A) Autoantibodies specific for human ALK bind and are detected with DyLight 550 conjugated IgG. GST protein serves as a control for unspecific binding of circulating autoantibodies to the GST-tag of the ALK protein. Human IgG serves as a control to confirm activity of the secondary antibody and is utilized for a standard curve. Anti-human IgG detects whether saturating levels of patient samples are used. **(B)** Binding of circulating autoantibodies in donor samples to the indicated antigens on the microarray.

7.2.4 Final slide layout

A final slide layout with 8 wells (**Figure 44**) was chosen to enable a high throughput analysis of clinical trial samples. However, in the future the number of wells could be adjusted to reflect the low incidence of ALK+ ALCL patients. Each well is able to accommodate 81 antigen spots (**Figure 44B-C**) with 29 spots being occupied by control antigens leaving space for 17 different antigens in triplicates.

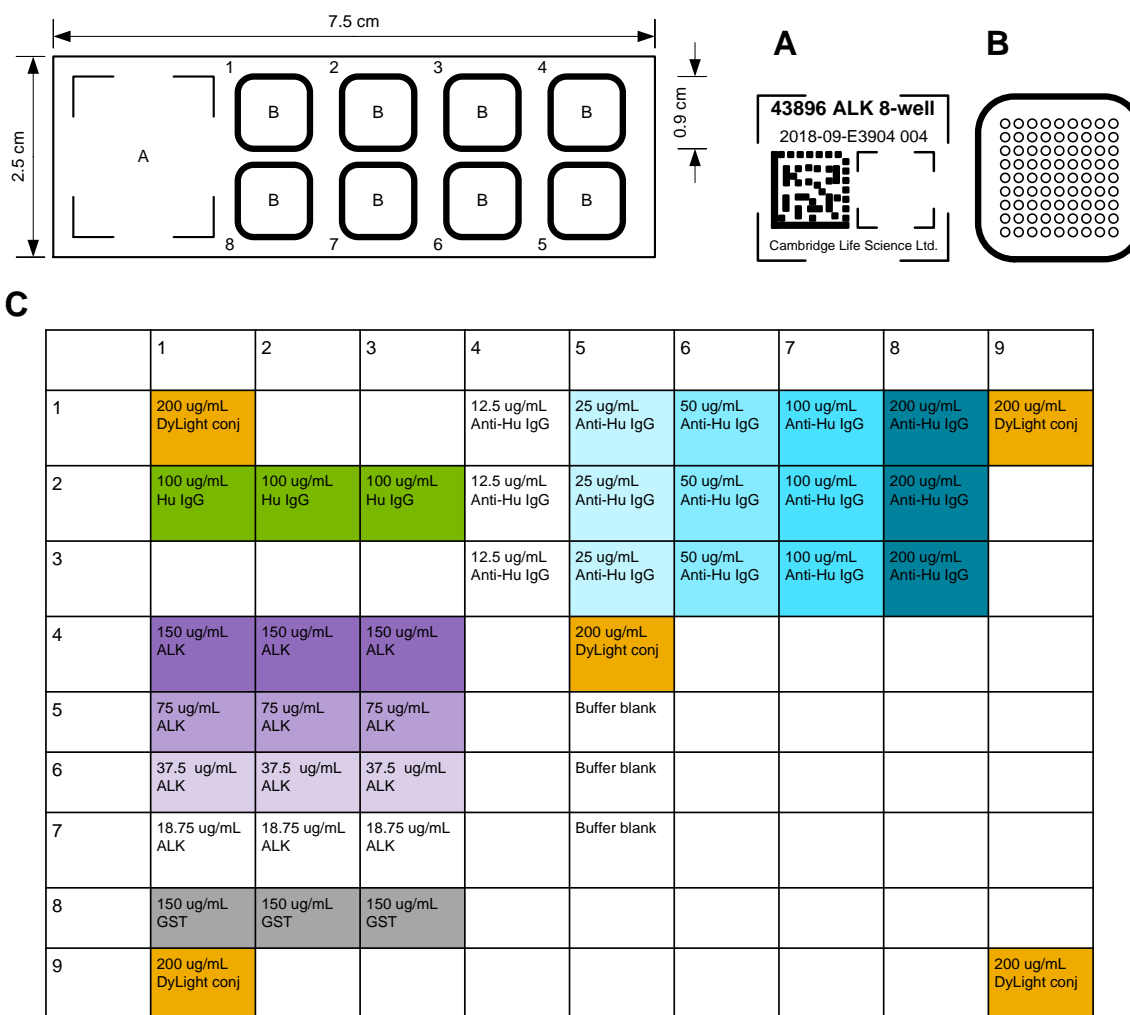


Figure 44 A typical slide layout

(A) Position of the barcode. **(B)** The pattern of 9x9 possible antigen spots per well. **(C)** The grid with antigen positions used in the final microarray indicated.

7.3 Protein microarray assay cross-validation

To cross-validate the microarray assay with the immunoperoxidase labelling technique we determined the presence of anti-ALK antibodies in plasma or serum samples of 93 paediatric ALK-positive ALCL patients at diagnosis. The patients were included in the ALCL-99 trial (NCT00006455)²⁸. The patient's treatment consisted of a cytoreductive prephase followed by six chemotherapy courses, as previously described³³. The patient cohort consisted of 57% male, 89.2% CNS negative and 41.9% MDD positive patients. The majority of patients showed no bone marrow (94.6%), bone (82.8%) or skin (81.7) involvement at diagnosis (**Table 40**).

Table 40 Baseline characteristics of Paediatric ALCL Patients Recruited to the ALCL99 Trial
MDD = Minimal disseminated disease.

Characteristic	Classification	Number of patients	% of total
Total		93	
Gender	Male	53	57
	Female	40	43
St Jude Stage	N/A	4	4.3
	I	6	6.5
	II	19	20.4
	III	59	63.4
	IV	5	5.4
Age	< 10 years	27	29
	>= 10 years	66	71
Histological subtype	Common	53	57
	Small cell, lymphohistiocytic, mixed, giant, not further classified	40	43
CNS	N/A	9	9.7
	negative	83	89.2
	positive	1	1.1
Bone marrow	No	88	94.6
	Yes	5	5.4
Bone	No	77	82.8
	Yes	16	17.2
Skin	No	76	81.7
	Yes	17	18.3
MDD	N/A	18	19.4
	negative	36	38.7
	positive	39	41.9

ALK antibodies in plasma or serum were assessed using both an immunocytochemical approach (anti-ALK autoantibody titre) as well as the newly developed microarray approach (anti-ALK autoantibody concentration). Anti-ALK autoantibodies were detected in 92.4% (86/93) and 93.5% (87/93) of patients using the immunocytochemical approach and the microarray approach, respectively. We also observed a strong correlation ($\rho = 0.68$, Spearman) between anti-ALK autoantibody titre and anti-ALK autoantibody concentration levels across the paediatric ALK-positive ALCL patient cohort (**Figure 45**).

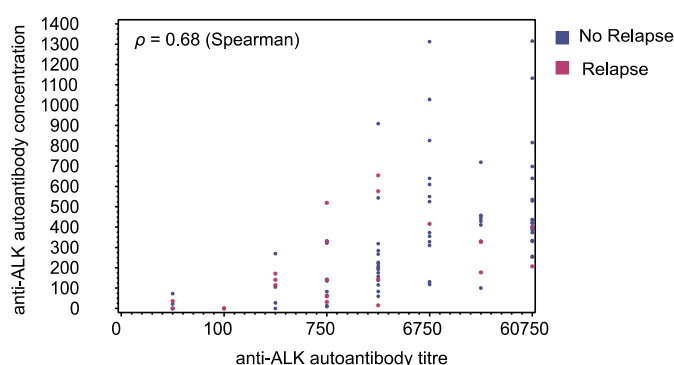


Figure 45 Correlation between anti-ALK autoantibody titre and anti-ALK autoantibody concentration levels in paediatric ALK-positive ALCL patients enrolled in the ALCL-99 trial
Patients that relapsed within 5 years following diagnosis are highlighted. ρ , Spearman correlation coefficient.

Twenty-eight patients (30%) mounted low or no autoantibody titres against ALK ($\leq 1/750$) and 65 patients (70%) presented intermediate or high titres ($> 1/750$). In comparison, 37 patients (40%) showed a low or no anti-ALK autoantibody concentration (≤ 200) and 56 patients (60%) had intermediate or high concentrations (> 200 , **Figure 46**). As previously reported^{91,39,92} for anti-ALK autoantibody titres, low anti-ALK autoantibody titres ($\leq 1/750$, $p < 0.0001$) and concentrations (≤ 200 , $p = 0.033$) were associated with a decreasing 5-year EFS (**Figure 46A**), but not with OS (**Figure 46B**). In agreement with previous reports^{91,39,92} on anti-ALK autoantibody titres, the anti-ALK autoantibody titres ($p = 0.0005$, Gray test) and concentrations ($p = 0.009$, Gray test) inversely correlated with the risk of relapse (**Figure 46C**).

Previous work reported minimal disseminated disease (MDD) detected by qualitative RT-PCR for NPM1-ALK in bone marrow or peripheral blood to confer a relapse risk of $\sim 50\%$ ^{73,79}. When the MDD and antibody titres were considered in combination, the following three subgroups of patients with different prognoses were identified: (1) a biological high risk (bHR) group defined by MDD-positivity and antibody titre $\leq 1/750$; (2) a biological low risk (bLR) group defined by MDD-negativity and an antibody titre $> 1/750$; (3) a biological intermediate risk (bIR) group including all other patients (MDD-negative/antibody titre $\leq 1/750$ or MDD-positive/antibody titre $> 1/750$)³⁹.

NPM-ALK transcripts, analyzed by RT-qPCR of bone marrow or peripheral blood, were available for 75 patients within our cohort (**Figure 47**). Utilizing the same risk stratification as for anti-ALK autoantibody titre tested patients, 48% (36/75) of patients were classified as bLR, 36% (27/75) as bIR and 17% (13/75) as bHR (**Figure 47C**) and relapse risk was significantly different ($p = 0.009$) for bLR (8.3%), bIR (18.5%) and bHR (62.2%) (**Figure 47C**).

When the MDD and antibody concentrations were considered in combination, the following three subgroups of patients with differing prognoses were identified: (1) a bHR group defined by MDD-positivity and antibody concentration ≤ 350 ; (2) a bLR group defined by MDD-negativity and an antibody concentration > 350 ; (3) a bIR group including all other patients (MDD-negative/antibody concentration ≤ 350 or MDD-positive/antibody concentration > 350). Utilizing the same risk stratification as Mussolin et al.³⁹, 48% (36/75) of patients were classified as bLR, 21% (16/75) as bIR and 31% (23/75) as bHR (**Figure 47C**). Relapse risk was significantly different ($p = 0.005$) for bLR (8.3%), bIR (12.5%) and bHR (47.8%) (**Figure 47C**). Hence, these data suggest that the anti-ALK autoantibody concentration could be used for the risk stratification of patients with ALK+ ALCL.

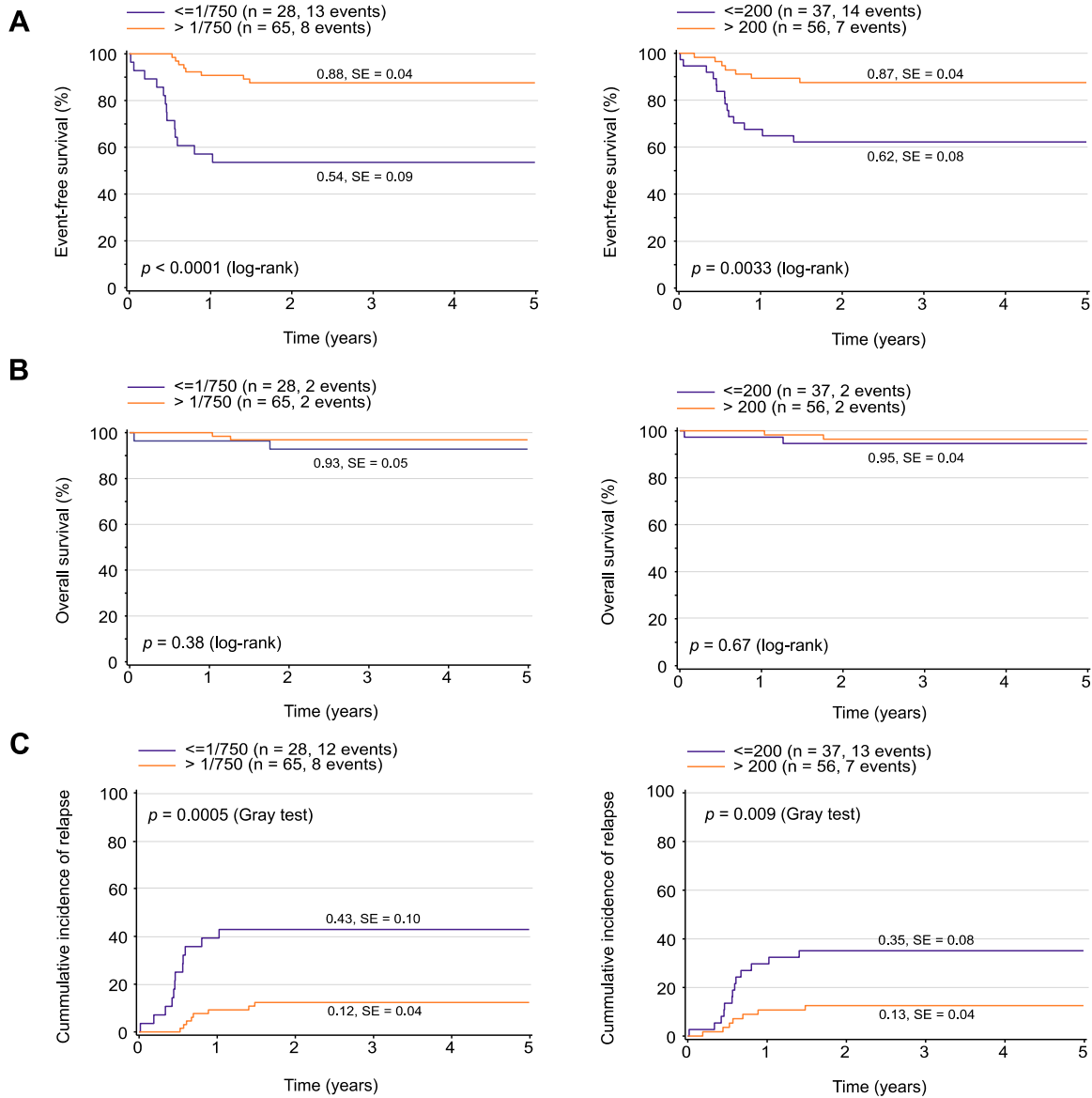


Figure 46 Outcomes of paediatric ALK+ ALCL patients according to the magnitude of the antibody response to ALK

(A,B) Paediatric patients (n = 93) treated with standard ALCL99 chemotherapy within the ALCL99 trial were divided into two groups according to the anti-ALK autoantibody titre (left) or the anti-ALK autoantibody concentration (right) and the difference in median (A) EFS or (B) OS (log-rank test) was analyzed using the Kaplan-Meier estimator. (C) Cumulative incidence of relapse in paediatric patients (n = 94) treated with standard ALCL99 chemotherapy within the ALCL99 trial that were divided into two groups according to the anti-ALK autoantibody titre (left) or the anti-ALK autoantibody concentration (right). P-values were determined by a Gray test.

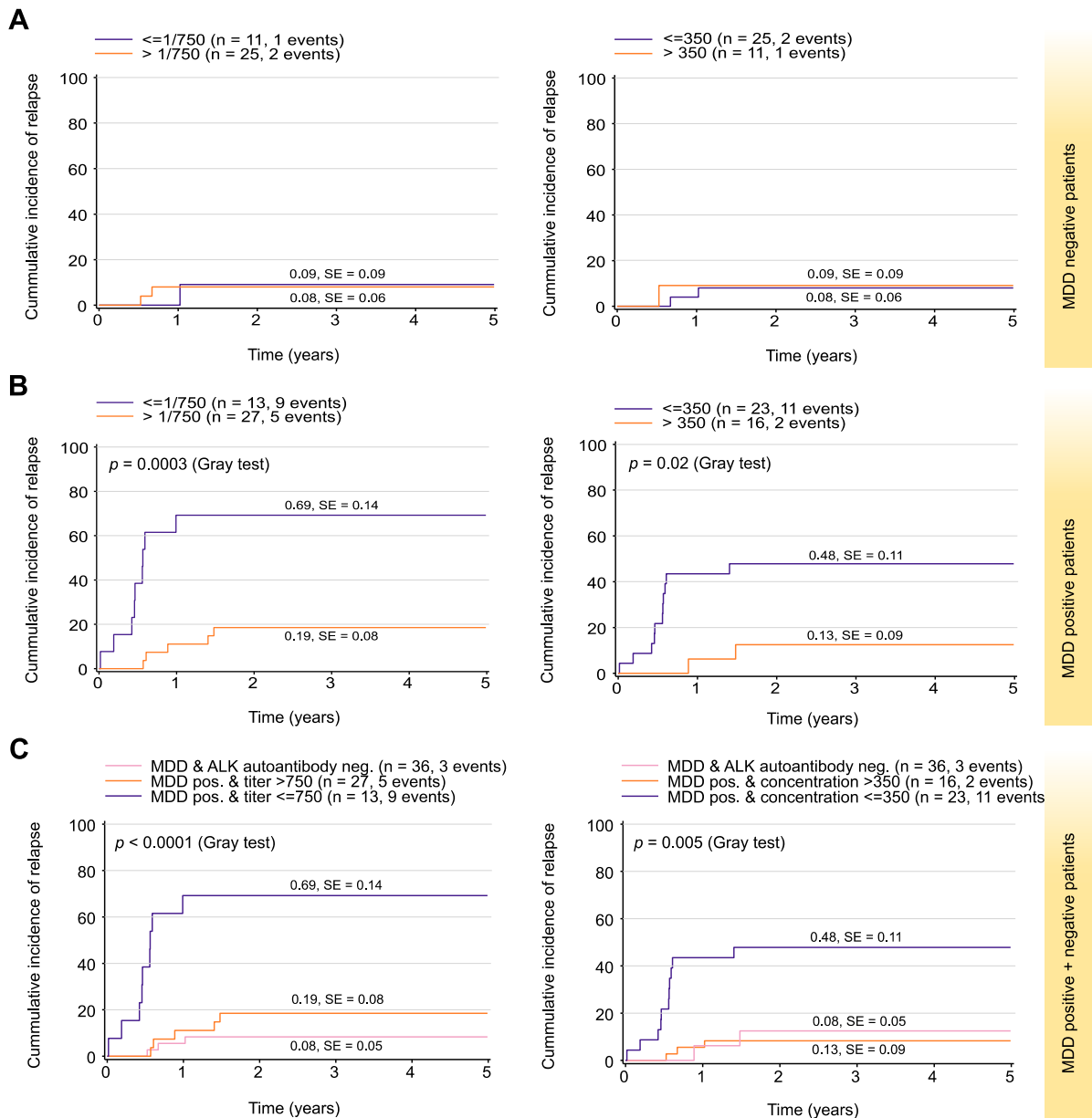


Figure 47 Outcomes of paediatric ALK+ ALCL patients according to the magnitude of the antibody response against ALK in combination with their minimal disseminated disease (MDD) status

(A) Cumulative incidence of relapse in MDD-negative paediatric patients ($n = 36$) treated with standard ALCL99 chemotherapy within the ALCL99 trial were divided into two groups according to the anti-ALK autoantibody titre (left) or the anti-ALK autoantibody concentration (right). P-values were determined by a Gray test. **(B)** The cumulative incidence of relapse in MDD-positive paediatric patients ($n = 40$) treated with standard ALCL99 chemotherapy within the ALCL99 trial were divided into two groups according to the anti-ALK autoantibody titre (left) or the anti-ALK autoantibody concentration (right). P-values were determined by a Gray test. **(C)** The cumulative incidence of relapse in paediatric patients ($n = 76$) treated with standard ALCL99 chemotherapy within the ALCL99 trial were divided into three groups according to the anti-ALK autoantibody titre (left) or the anti-ALK autoantibody concentration (right) combined with the MDD status and anti-ALK autoantibody titre or concentration of the patients. P-values were determined by a Gray test.

7.4 Discussion

Biomarkers that predict a patient's prognosis and/or response to therapy are informative in devising therapeutic protocols, particularly in this era of personalised medicine. Previous reports have described that the magnitude of the autoantibody response to the oncoantigen ALK is inversely correlated with lymphoma dissemination and relapse risk in ALK-positive ALCL, and that by combining MDD and antibody titer, patients could be stratified into three different groups with significantly different PFS probabilities^{39,91}. The present study validates that the preexisting antibody response to ALK correlates inversely with tumour dissemination and has prognostic value for patients with this malignancy. The automated assay we have developed could allow for a non-subjective assessment of this biomarker for incorporation into future ALCL clinical trials. However, whether this biomarker remains predictive when children with ALK+ ALCL are treated with targeted agents such as ALK inhibitors and anti-CD30 antibody therapy remains to be seen.

The increased risk of relapse in patients with low antibody titers against ALK did not translate into a significant difference in OS. One explanation for this may be the availability of an effective salvage therapy for most relapsing ALK+ ALCL patients⁴³⁵.

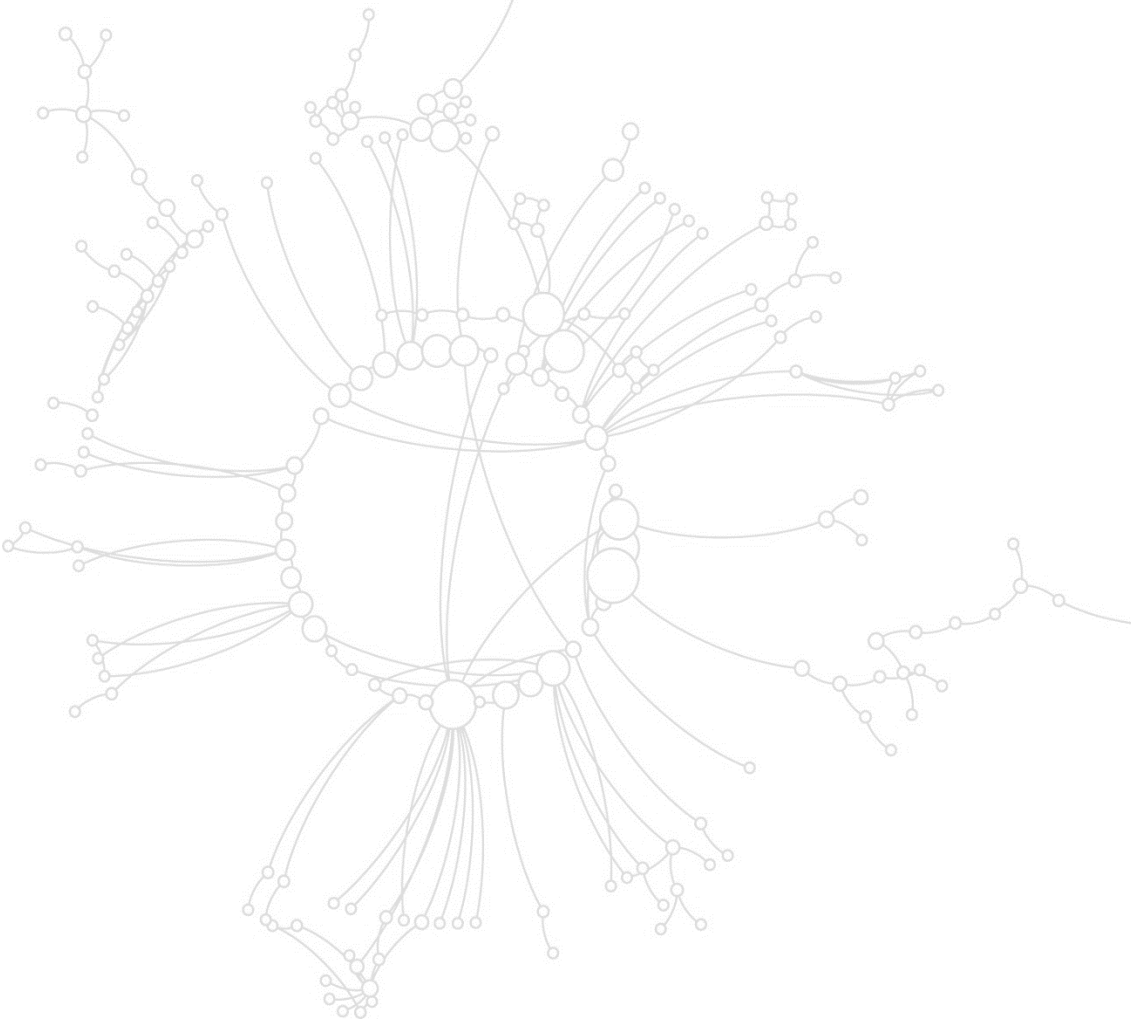
In addition, our data support published data^{88,89,91,90,39,92} that an immune response to ALK is implicated in the control of ALK+ ALCL. Together with the observation of ALK-specific cellular immune responses in patients undergoing multi-agent chemotherapy treatment⁹² and in long-term survivors of ALK+ ALCL⁸⁹, these data further support the idea of a specific immunostimulatory approach for the consolidation of remission in patients with ALK+ ALCL⁴³⁵. There is a growing body of evidence to support the potential development of an ALK targeting vaccine⁵⁰³; ALK ranked fourth in a list of 75 tumour antigens evaluated by the National Cancer Institute⁵⁰⁵.

The combination of a vaccination against ALK with either immune stimulatory multi-agent chemotherapy^{432,433,434,435} or ALK TKIs^{436,437} protected against relapse in murine models of ALK+ ALCL and ALK+ NSCLC, respectively^{142,501}. In support of this, anti-HER2 autoantibodies were found to suppress the activity of HER2 in HER2+ breast or ovarian cancer patients after vaccination with HER2 specific peptides^{435,506}. Therefore, vaccination to boost a pre-existing anti-ALK immune response for ALK+ ALCL or NSCLC patients with a pre-existing ALK immune response could provide a promising approach⁴³⁵ without the risks associated with unspecific immunostimulatory therapies like nivolumab¹³⁸, resistance-prone ALK inhibitor therapy¹²⁶ or in the case of ALCL highly toxic SCT and BV.

In addition, a direct anti-tumour effect of recombinant anti-ALK autoantibodies has been described in ALK-driven NB^{507,508} and glioblastoma⁵⁰⁹. These data suggest that recombinant anti-ALK antibodies might provide a therapeutic effect in other ALK+ cancer patients. While the anti-ALK antibody titre in ALK+ ALCL or NSCLC appears to be associated with the anti-tumour immune response^{435,142,140,89,510-512}, it is not clear whether they are functional against tumour cells⁴³⁵. Although, ALK fusion proteins in ALK+ ALCL and NSCLC patients are expressed exclusively intracellularly^{371,513-519}, future studies by Chiarle and Woessmann will shed light on this unanswered question.

Finally, as part of this chapter, we analyzed anti-ALK autoantibody titres in 124 ALK+ NSLCL patients recruited onto the ALEX trial (NCT02075840) as well as 103 ALK+ ALCL patients recruited onto the ANHL12P1 trial (NCT01979536), which will be made available once the trials have been completed.

CHAPTER 8 Discussion



8.1 Introduction

Throughout this thesis, genome wide CRISPR overexpression screens in ALK+ ALCL and ALK driven NB cell lines have yielded insights into potential mechanisms of ALK inhibitor resistance. Finally, the development of a paediatric ALK+ ALCL PDX model has allowed the *in vivo* investigation of brigatinib treatment in a chemotherapy-refractory and crizotinib-resistant setting.

In this chapter, potential future directions and the clinical implications of these findings are discussed in the context of the current literature.

8.2 The use of ALK inhibitors for the treatment of paediatric ALK+ ALCL

8.2.1 Crizotinib in combination with multi-agent chemotherapy could be used as a consolidation therapy before allogeneic SCT for paediatric ALK+ ALCL patients after relapse

Fortunately, paediatric ALK+ ALCL patients are relatively chemo-sensitive with an OS varying between 70-90% dependent on treatment duration, drugs used and their dosages (**Table 3**)^{31–33,42–44}. In addition, four independent retrospective analyses found that approximately 75% of relapsed patients reached a second remission by reinduction chemotherapy^{71,97,98,118}. The response rate was dependent on the time to relapse, with approximately 85% of children with relapse after completion of frontline therapy reaching a remission by any chemotherapy^{71,97,98,118}, but approximately 50% of children who experienced progression during frontline therapy undergoing progression again during reinduction⁹⁸. Fortunately, for this patient group, 5-year EFS and OS rates of 81% and 83%, respectively, can be achieved by allogeneic SCT⁹⁸.

Crizotinib and BV are targeted therapies inducing remission in up to 90% of patients with relapsed ALK+ ALCL^{63,115,117,126,128,520} that could offer an alternative to highly toxic multi-agent chemotherapy protocols, but there is no consensus as to whether these drugs should be administered as single agents, for how long and for which patients.

Our investigation into possible resistance mechanisms to ALK inhibitor treatment including crizotinib showed multiple options via which an ALK+ ALCL cell can acquire resistance to single agent ALK inhibitors^{301,521}. Specifically, our results indicate that IL10RA expression does not correlate with response or resistance to standard chemotherapy, suggesting that resistance mechanisms, such as elevated IL10RA expression developing as a consequence of single agent crizotinib therapy, could be overcome by a combination of ALK-targeted therapy with chemotherapy.

Single agent crizotinib could be used to induce second remission^{98,522} as already established in adult relapsed ALK+ ALCL patients before allogeneic SCT¹²⁸. However, while single agent crizotinib represents a low toxicity option⁹⁸, a combination of crizotinib with chemotherapy could be advisable to prevent ALK-inhibitor resistance-specific relapse if crizotinib has to be given for an extended time to achieve remission. This is especially important as CNS progression in crizotinib treated patients has been observed and CNS prophylaxis during re-induction therapy before SCT is highly recommended⁵²³. Low-risk patients defined by relapse at more than one year after initial diagnosis might better be treated with multi-agent chemotherapy for which many years of experience exists⁹⁸.

8.2.2 Brigatinib could offer a bridge to transplant for paediatric ALK+ ALCL patients after CNS relapse

Since the 5-year cumulative CNS relapse risk in paediatric ALK+ ALCL patients is only 4% and the 3-year OS for patients after CNS relapse is 48.7% with median survival being 23.5 months¹⁰⁰, this subgroup of patients comprises the most difficult to treat cases with the least treatment experience.

Early identification of ALK+ ALCL patients with a risk of CNS relapse is an important future goal that will enable tailored treatment strategies¹⁰⁰. For example, lorlatinib and brigatinib have shown promising results in ALK+ NSCLC but have not yet been sufficiently tested in the paediatric setting^{125,524}. The advantage of these ALK inhibitors over crizotinib and ceritinib is that they are able to cross the blood-brain-barrier and as such are active or preventive against CNS disease^{525–528}. In Japan, crizotinib is being trialled as a monotherapy for children with recurrent or refractory ALK+ ALCL (UMIN000028075) and in the USA, crizotinib is being investigated in combination with multi-agent chemotherapy (NCT01979536) and might therefore not present a viable option for patients with CNS involvement³⁶⁶. However, in Japan, alectinib (UMIN000016991)^{67–69} has been approved for children with recurrent or refractory ALK+ ALCL in 2020¹²⁴ and the EICNHL is planning to trial brigatinib in combination with the ALCL99 backbone (personal communication with Dr. Suzanne Turner) offering hope for paediatric ALK+ ALCL patients with CNS involvement at diagnosis or experiencing a CNS relapse. In addition, a first case report described the successful treatment of a girl, who suffered from a CNS relapse, with alectinib¹²⁵.

While limited to a CNS relapsed patient who achieved a CR during initial crizotinib treatment but relapsed after allogeneic SCT, our *in vivo* investigation indicates that brigatinib was effective in a PDX model of this CNS relapsed chemotherapy-refractory and crizotinib-resistant ALK+ ALCL patient. The investigation of brigatinib in clinical trials will have to prove whether this can be translated to the clinic.

8.3 The use of ALK inhibitors for the treatment of ALK-driven NB

Our investigation into possible resistance mechanisms against ALK inhibitor treatment including ceritinib and brigatinib highlighted multiple pathways through which ALK-driven NB cells can acquire resistance to single agent ALK inhibition³⁰⁰. Trigg et al. identified PIM1 overexpression as one of the main resistance mechanisms to ceritinib and brigatinib and further explored PIM1 as a therapeutic target after observing that its overexpression led to evasion of apoptosis^{300,529}. While treatment with the PIM1 inhibitor AZD1208 was not sufficient to kill ALK-driven NB cells, reduction of PIM1 mRNA sensitized NB cells to ALK inhibitors and combination of AZD1208 with ALK inhibitors showed mild synergism. To examine the clinical relevance of this drug combination, Trigg et al. employed two patient-derived models of high-risk NB harboring ALK^{F1245C} or ALK^{F1174L} mutations, respectively³⁰⁰. The authors observed a significant delay in tumour growth with the combination treatment relative to single-agent treatments in both models³⁰⁰. PIM inhibition sensitized both MYCN-amplified and wild-type, ALK-driven NB cells to ALK inhibitors *in vivo*. It has previously been shown that ALK and MYCN are part of a positive feedback loop whereby ALK regulates expression of MYCN through repression of HPB1⁵³⁰. However, Trigg et al. suggest that combined PIM1 and ALK inhibition is effective independent of MYCN status³⁰⁰.

Moreover, *PIM1* mRNA levels were significantly elevated in tumours treated with ceritinib relative to the vehicle at the experimental end-point, thus providing *in vivo* evidence of *PIM1* as a resistance gene³⁰⁰.

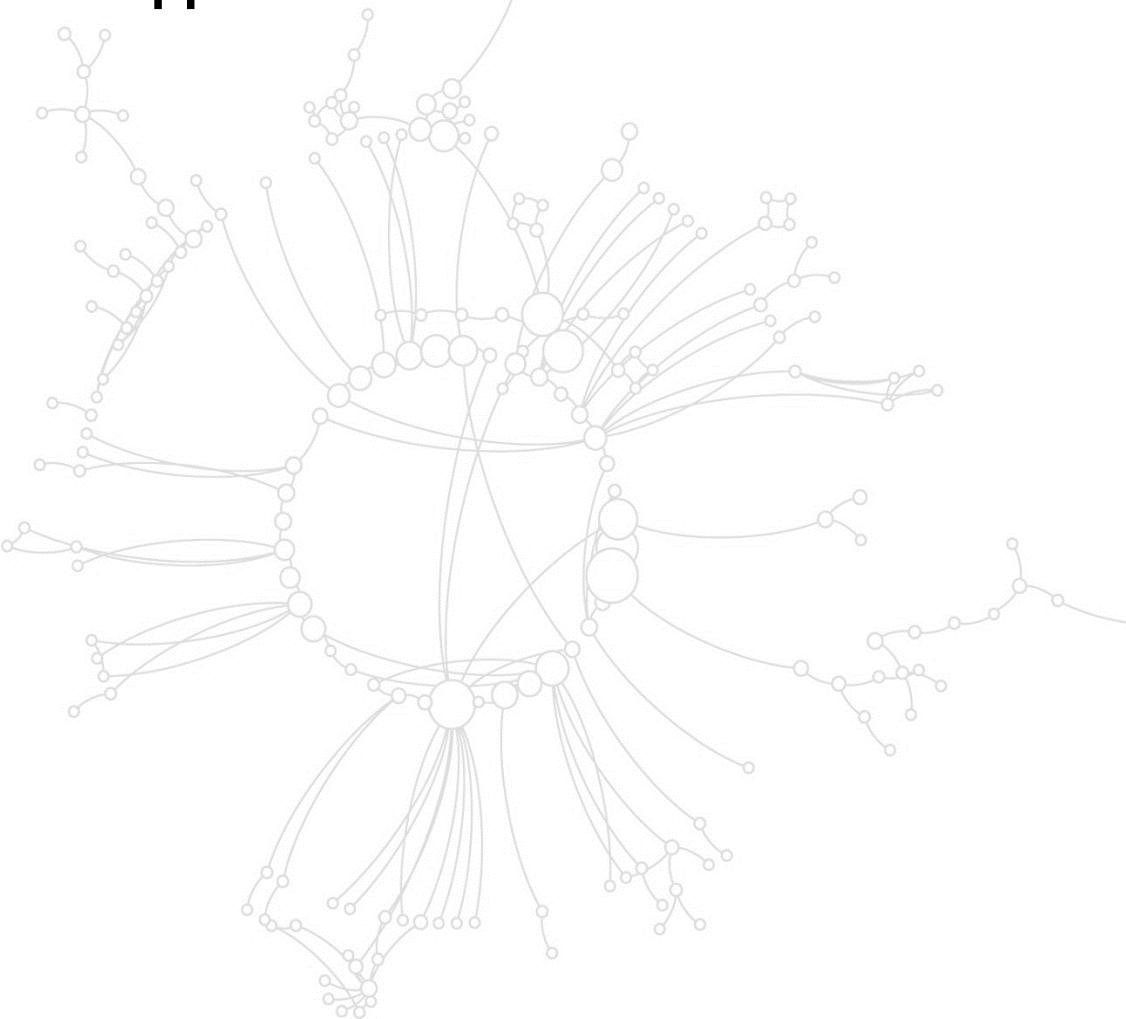
8.4 A collaborative approach to collate and integrate data will be crucial to making progress in the treatment of paediatric cancers

The low incidence of paediatric cancer cases has been a key factor in the limited collection of clinical and biological data, and the difficulties encountered in conducting clinical trials. Given this, utilizing *in vitro* screening of relatively uncommon paediatric tumours such as ALK+ ALCL and ALK-driven NB is currently the only approach to characterize ALK inhibitor resistance mechanisms. However, it remains unclear what proportion of clinical cases of ALK inhibitor resistance involve IL10RA in ALK+ ALCL or PIM1 in ALK-driven NB. Moreover, it remains to be elucidated what level of IL10RA expression in ALK+ ALCL or PIM1 expression in ALK-driven NB are needed *in vivo* for induction of these resistance mechanisms⁵³¹. In our studies, IL10RA and PIM1 were artificially overexpressed *in vitro* and in the case of IL10RA with or without IL-10 supplementation. Ultimately, further clinical samples of matched diagnostic and relapse tumours are required to assess the degree to which IL10RA or PIM1 overexpression represents a predominant resistance mechanism to the investigated or other ALK inhibitors. The full diversity of ALK-independent escape mechanisms also remains unknown⁵³¹; survival pathways other than IL10 signaling or PIM1-induced apoptosis evasion may exist and resistance could be induced by other gene candidates identified by our screening approach. This will require extensive functional follow-up studies with validation in patient tumours.

Additionally, Turner⁵³² and other groups^{533–560} have identified a distinct population of cells – called cancer stem cells⁵⁶¹, tumour-initiating cells⁵⁶², leukaemia-initiating cells⁵⁶¹ or tumour-propagating cells⁵⁶³ – within cell lines derived from haematopoietic (including ALK+ ALCL⁵³²) and solid tumours (including NB⁵⁶⁴) that by definitions of Clarke et al.⁵⁶⁵ and Nguyen et al.⁵⁶⁶ can be isolated and were shown to have self-renewal capacity⁵⁶¹. In future work it will be interesting to test whether the cancer stem cell population of ALK+ ALCL and NB cell lines overexpress IL10RA and PIM1, respectively, or other candidates identified by the screens.

Furthermore, the factors underlying the diversity of resistance mechanisms that develop in patients with the same cancer receiving the same treatment remain unclear. Considering the annual 300,000 European childhood cancer survivors, many are at risk of relapse and of the 35,000 newly diagnosed paediatric cancer cases in Europe each year many present with refractory disease (Pilot Project & Preparation Action Grant, European Commission). Therefore, several national clinical sequencing studies aimed at identifying treatment targets in children or adolescents are based on tumour biopsies taken at relapse/refractory disease⁴³⁹: Individualized Therapy for Relapsed Malignancies in Childhood (INFORM, Germany), Individualized Therapies for Children with Relapsed/Refractory Malignancies using Molecular Profiling (iTHER, The Netherlands), MAPPYACTS, Zero Childhood Cancer (ZERO, Australia), Precision Oncology for Young People Program (PROFYLE, Canada) and Pediatric Molecular Analysis for Therapy Choice (Pediatric MATCH, USA). Since paediatric cancers are rare diseases, going forward, a collaborative approach to collate and integrate the collected data will be crucial and must be compared to robust biological functional validation studies as described here.

CHAPTER 9 Appendix



9.1 Appendix 1: List of peer-reviewed papers and reviews

9.1.1 Primary research articles

- 10 Lobello C., Boris T., Bystry V., Radova L., Filip D., Marz M., Montes-Mojarro I.A., [Prokoph N.](#), Larose H., Liang H.C., Sharma G.G., Mogni L., Belada D., Kamaradova K., Fend F., Gambacorti-Passerini C., Merkel O., Turner S.D., Janikova A., Pospisilova S. (2020) [STAT3 and TP53 Mutations Associate with Poor Prognosis in Anaplastic Large Cell Lymphoma](#). *Leukemia*.
- 9 Forde S.D., Matthews J.D., Jahangiri L., Lee L.C., [Prokoph N.](#), Malcolm T.I.M., Giger O.T., Bell N., Blair H., O'Marcaigh A., Smith O., Kenner L., Bomken S., Burke G.A.A., Turner S.D. (2020) [Paediatric burkitt lymphoma patient-derived xenografts capture disease characteristics over time and are a model for therapy](#). *British Journal of Haematology*.
- 8 [Prokoph N.](#), Probst N.A., Lee L.C., Monahan J.M., Matthews J.D., Liang H-C., Bahnsen K., Montes-Mojarro I.A., Karaca-Atabay E., Sharma G.G., Malik V., Larose H., Forde S.D., Ducray S.P., Lobello C., Wang Q., Pospisilova S., Gambacorti-Passerini C., Burke G.A.A., Pervez S., Attarbaschi A., Janikova A., Parquement H., Landman-Parker J., Lambilliotte A., Schleiermacher G., Klapper W., Jauch R., Woessmann W., Vassal G., Kenner L., Merkel O., Mogni L., Chiarle R., Brugières L., Georger B., Barbieri I., Turner S.D. (2020) [IL10RA modulates crizotinib sensitivity in NPM1-ALK+ anaplastic large cell lymphoma](#). *Blood*. 136(14):1657-1669.
Cover page & Invited commentary by the editor: Hu G. & Feldman A.L. (2020) Drivers of crizotinib resistance in ALK+ ALCL. *Blood*. 136(14):1573-1575.
- 7 Larose H., [Prokoph N.](#), Matthews J.D., Schleder M., Högler S., Alsulami A.F., Ducray S.P., Nuglozeh E., Fazaludeen F.M.S., Elmouna A., Ceccon M., Mogni L., Gambacorti-Passerini C., Hoefler G., Lobello C., Pospisilova S., Janikova A., Woessmann W., Damm-Welk C., Zimmermann M., Fedorova A., Malone A., Smith O., Wasik M., Inghirami G., Lamant L., Blundell T.L., Klapper W., Merkel O., Burke G.A.A., Mian S., Ashankyty I., Kenner L., Turner S.D. (2020) [Whole Exome Sequencing reveals NOTCH1 mutations in Anaplastic Large Cell Lymphoma and points to Notch both as a key pathway and a potential therapeutic target](#). *Haematologica*.
- 6 Trigg R.*, Lee L.C.*, [Prokoph N.*](#), Jahangiri L., Reynolds P., Burke G.A.A., Probst N.A., Han M., Matthews J.D., Lim H.K., Manners E., Martínez Gonzalez S., Pastor Fernandez J., Blanco-Aparicio C., Merkel O., Garces de los Fayos Alonso I., Kodajova P., Tangermann S., Högler S., Luo J., Kenner L., Turner S.D. (2019) [The targetable kinase PIM1 drives ALK inhibitor resistance in high-risk neuroblastoma independent of MYCN status](#). *Nat Commun*. 10(1):5428. *joint first
Editors' choice: Malone J. (2019) A new hope for neuroblastoma treatment? *Science Transl. Med*. 11(523), eaaz9769.
- 5 Russell M., [Prokoph N.](#), Henderson N., Eketjäll S., Balendran C., Michaëlsson E., Fidock M., Hughes G. (2017) [Determining myeloperoxidase activity and protein concentration in a single assay: utility in biomarker and therapeutic studies](#). *Journal of Immunological Methods*. 449:76-79.
- 4 Fontaine F., Overman J., Moustaqil M., Mamidyala S., Salim A., Narasimhan K., [Prokoph N.](#), Robertson A.A.B., Lua L., Alexandrov K., Koopman P., Capon R.J., Sieracki E., Gambin Y., Jauch R., Cooper M.A., Zuegg J., Francois M. (2017) [Small molecule inhibitors of the Sox18 transcription factor](#). *Cell Chemical Biology*. 24(3):346-359.
- 3 [Prokoph N.](#), Ormö M., O'Mahony G., Hogner A., McPheat J., Karlsson U., Holmberg Schiavone L., Liu J. (2016) [Development of an ELISA assay for high throughput screening of Inhibitors of the CDK5-mediated PPARγ phosphorylation](#). *Assay Drug Dev Techn*. 14(4):261-72.
- 2 Klaus M.*, [Prokoph N.*](#), Wang X., Huang Y.-H., Girbig M., Srivastava Y., Hou L., Narasimhan K., Kolatkar P., Francois M., Jauch R. (2016) [Structure and decoy-mediated inhibition of the SOX18/Prox1-DNA interaction](#). *Nucleic Acids Res*. 44(8):3922-35. *joint first
- 1 Paul A.J., Schwab K., [Prokoph N.](#), Haas E., Handrick R., Hesse F. (2015) [Fluorescence dye-based detection of mAb aggregates in CHO culture supernatants](#). *Anal. Bioanal. Chem*. 407(16):4849-56.

9.1.2 Review article

- 1 [Prokoph N.*](#), Larose H.*, Lim M.S., Burke G.A.A., Turner S.D. (2018) [Treatment Options for Paediatric Anaplastic Large Cell Lymphoma \(ALCL\): Current Standard and beyond](#). *Cancers*. 10(4):99. *joint first

Reference List

1. Chiarle R, Voena C, Ambrogio C, Piva R, Inghirami G. The anaplastic lymphoma kinase in the pathogenesis of cancer. *Nat Rev Cancer*. 2008;8(1):11-23. doi:10.1038/nrc2291
2. Hallberg B, Palmer RH. Mechanistic insight into ALK receptor tyrosine kinase in human cancer biology. *Nat Rev Cancer*. 2013;13(10):685-700. doi:10.1038/nrc3580
3. Morris SW, Kirstein MN, Valentine MB, et al. Fusion of a kinase gene, ALK, to a nucleolar protein gene, NPM, in non-Hodgkin's lymphoma. *Science* (80-). 1994;263(5151):1281-1284. doi:10.1126/science.8122112
4. Lemmon MA, Schlessinger J. Cell Signaling by Receptor Tyrosine Kinases. *Cell*. 2010;141(7):1117-1134. doi:10.1016/j.cell.2010.06.011
5. Barreca A, Lasorsa E, Riera L, et al. Anaplastic lymphoma kinase in human cancer. *J Mol Endocrinol*. 2011;47(1):R11-R23. doi:10.1530/JME-11-0004
6. Trigg RM, Turner SD. ALK in Neuroblastoma: Biological and Therapeutic Implications. *Cancers (Basel)*. 2018;10(4). doi:10.3390/cancers10040113
7. Cessna MH, Zhou H, Sanger WG, et al. Expression of ALK1 and p80 in Inflammatory Myofibroblastic Tumor and Its Mesenchymal Mimics: A Study of 135 Cases. *Mod Pathol*. 2002;15(9):931-938. doi:10.1097/01.MP.0000026615.04130.1F
8. Passoni L, Longo L, Collini P, et al. Mutation-Independent Anaplastic Lymphoma Kinase Overexpression in Poor Prognosis Neuroblastoma Patients. *Cancer Res*. 2009;69(18):7338-7346. doi:10.1158/0008-5472.CAN-08-4419
9. Weissinger SE, Keil P, Silvers DN, et al. A diagnostic algorithm to distinguish desmoplastic from spindle cell melanoma. *Mod Pathol*. 2014;27(4):524-534. doi:10.1038/modpathol.2013.162
10. Salido M, Pijuan L, Martínez-Avilés L, et al. Increased ALK Gene Copy Number and Amplification are Frequent in Non-small Cell Lung Cancer. *J Thorac Oncol*. 2011;6(1):21-27. doi:10.1097/JTO.0b013e3181fb7cd6
11. Tuma RS. ALK Gene Amplified in Most Inflammatory Breast Cancers. *JNCI J Natl Cancer Inst*. 2012;104(2):87-88. doi:10.1093/jnci/djr553
12. Schoppmann SF, Streubel B, Birner P. Amplification but not translocation of anaplastic lymphoma kinase is a frequent event in oesophageal cancer. *Eur J Cancer*. 2013;49(8):1876-1881. doi:10.1016/j.ejca.2013.02.005
13. Murugan AK, Xing M. Anaplastic thyroid cancers harbor novel oncogenic mutations of the ALK gene. *Cancer Res*. 2011;71(13):4403-4411. doi:10.1158/0008-5472.CAN-10-4041
14. Wang Y-W, Tu P-H, Lin K-T, Lin S-C, Ko J-Y, Jou Y-S. Identification of oncogenic point mutations and hyperphosphorylation of anaplastic lymphoma kinase in lung cancer. *Neoplasia*. 2011;13(8):704-715. Accessed January 23, 2018. <http://www.ncbi.nlm.nih.gov/pubmed/21847362>
15. Mossé YP, Laudenslager M, Longo L, et al. Identification of ALK as a major familial neuroblastoma predisposition gene. *Nature*. 2008;455(7215):930-935. doi:10.1038/nature07261
16. Carén H, Abel F, Kogner P, Martinsson T. High incidence of DNA mutations and gene amplifications of the ALK gene in advanced sporadic neuroblastoma tumours. *Biochem J*. 2008;416(2):153-159. doi:10.1042/bj20081834
17. Armstrong F, Duplantier M-M, Trempat P, et al. Differential effects of X-ALK fusion proteins on proliferation, transformation and invasion properties of NIH3T3 cells. *Oncogene*. 2004;23(36):6071-6082. doi:10.1038/sj.onc.1207813
18. Soda M, Choi YL, Enomoto M, et al. Identification of the transforming EML4-ALK fusion gene in non-small-cell lung cancer. *Nature*. 2007;448(7153):561-566. doi:10.1038/nature05945
19. Ou S-HI, Kwak EL, Siwak-Tapp C, et al. Activity of Crizotinib (PF02341066), a Dual Mesenchymal-Epithelial Transition (MET) and Anaplastic Lymphoma Kinase (ALK) Inhibitor, in a Non-small Cell Lung Cancer Patient with De Novo MET Amplification. *J Thorac Oncol*. 2011;6(5):942-946. doi:10.1097/JTO.0b013e31821528d3
20. Prokoph N, Larose H, Lim M, Burke G, Turner S. Treatment Options for Paediatric Anaplastic Large Cell Lymphoma (ALCL): Current Standard and beyond. *Cancers (Basel)*. 2018;10(4):99. doi:10.3390/cancers10040099
21. Stein H, Gerdes J, Schwab U, et al. Identification of Hodgkin and sternberg-reed cells as a unique cell type derived from a newly-detected small-cell population. *Int J Cancer*. 1982;30(4):445-459. doi:10.1002/ijc.2910300411
22. Schwab U, Stein H, Gerdes J, et al. Production of a monoclonal antibody specific for Hodgkin and Sternberg-Reed cells of Hodgkin's disease and a subset of normal lymphoid cells. *Nature*. 1982;299(5878):65-67. doi:10.1038/299065a0
23. Delsol G, Al Saati T, Gatter KC, et al. Coexpression of epithelial membrane antigen (EMA), Ki-1, and interleukin-2 receptor by anaplastic large cell lymphomas. Diagnostic value in so-called malignant histiocytosis. *Am J Pathol*. 1988;130(1):59-70. <http://www.ncbi.nlm.nih.gov/pmc/articles/PMC1880552/>
24. Fischer P, Nacheva E, Mason DY, et al. A Ki-1 (CD30)-positive human cell line (Karpas 299) established from a high-grade non-Hodgkin's lymphoma, showing a 2;5 translocation and rearrangement of the T-cell receptor beta-chain gene. *Blood*. 1988;72(1):234-240. <http://www.bloodjournal.org/content/72/1/234.abstract>

25. Rimokh R, Magaud JP, Berger F, et al. A translocation involving a specific breakpoint (q35) on chromosome 5 is characteristic of anaplastic large cell lymphoma ('Ki-1 lymphoma'). *Br J Haematol.* 1989;71(1):31—36. doi:10.1111/j.1365-2141.1989.tb06270.x
26. Alessandri AJ, Pritchard SL, Schultz KR, Massing BG. A population-based study of pediatric anaplastic large cell lymphoma. *Cancer.* 2002;94(6):1830-1835. doi:10.1002/cncr.10396
27. Shiramizu B, Mussolin L, Woessmann W, Klapper W. Paediatric non-Hodgkin lymphoma - perspectives in translational biology. *Br J Haematol.* 2016;173(4):617-624. doi:10.1111/bjh.14009
28. Brugières L, Le Deley M-C, Rosolen A, et al. Impact of the Methotrexate Administration Dose on the Need for Intrathecal Treatment in Children and Adolescents With Anaplastic Large-Cell Lymphoma: Results of a Randomized Trial of the EICNHL Group. *J Clin Oncol.* 2009;27(6):897-903. doi:10.1200/JCO.2008.18.1487
29. Boi M, Zucca E, Inghirami G, Bertoni F. Advances in understanding the pathogenesis of systemic anaplastic large cell lymphomas. *Br J Haematol.* 2015;168(6):771-783. doi:10.1111/bjh.13265
30. Falini B, Pileri S, Zinzani PL, et al. ALK+ lymphoma: clinico-pathological findings and outcome. *Blood.* 1999;93(8):2697-2706.
31. Brugières L, Deley MC, Pacquement H, et al. CD30(+) anaplastic large-cell lymphoma in children: analysis of 82 patients enrolled in two consecutive studies of the French Society of Pediatric Oncology. *Blood.* 1998;92(10):3591-3598.
32. Rosolen A, Pillon M, Garaventa A, et al. Anaplastic large cell lymphoma treated with a leukemia-like therapy: report of the Italian Association of Pediatric Hematology and Oncology (AIEOP) LNH-92 protocol. *Cancer.* 2005;104(10):2133-2140. doi:10.1002/cncr.21438
33. Seidemann K, Tiemann M, Schrappe M, et al. Short-pulse B-non-Hodgkin lymphoma-type chemotherapy is efficacious treatment for pediatric anaplastic large cell lymphoma: a report of the Berlin-Frankfurt-Münster Group Trial NHL-BFM 90. *Blood.* 2001;97(12):3699-3706. doi:10.1182/blood.V97.12.3699
34. Cheson BD, Horning SJ, Coiffier B, et al. Report of an International Workshop to Standardize Response Criteria for Non-Hodgkin's Lymphomas. *J Clin Oncol.* 1999;17(4):1244. doi:10.1200/JCO.1999.17.4.1244
35. Cheson BD, Pfistner B, Juweid ME, et al. Revised response criteria for malignant lymphoma. *J Clin Oncol.* 2007;25(5):579-586. doi:10.1200/JCO.2006.09.2403
36. Cheson BD, Fisher RI, Barrington SF, et al. Recommendations for Initial Evaluation, Staging, and Response Assessment of Hodgkin and Non-Hodgkin Lymphoma: The Lugano Classification. *J Clin Oncol.* 2014;32(27):3059-3067. doi:10.1200/JCO.2013.54.8800
37. Cheson BD, Ansell S, Schwartz L, et al. Refinement of the Lugano Classification lymphoma response criteria in the era of immunomodulatory therapy. *Blood.* 2016;128(21):2489-2496. doi:10.1182/blood-2016-05-718528
38. NCI. NCI Dictionary of Cancer Terms. Accessed October 15, 2020. <https://www.cancer.gov/publications/dictionaries/cancer-terms>
39. Mussolin L, Damm-Welk C, Pillon M, et al. Use of minimal disseminated disease and immunity to NPM-ALK antigen to stratify ALK-positive ALCL patients with different prognosis. *Leukemia.* 2012;27(2):416-422. doi:10.1038/leu.2012.205
40. Le Tourneau C, Gan HK, Razak ARA, Paoletti X. Efficiency of new dose escalation designs in dose-finding phase I trials of molecularly targeted agents. *PLoS One.* 2012;7(12):e51039. doi:10.1371/journal.pone.0051039
41. Fukano R, Mori T, Fujita N, et al. Successful outcome with reduced-intensity condition regimen followed by allogeneic hematopoietic stem cell transplantation for relapsed or refractory anaplastic large-cell lymphoma. *Int J Hematol.* 2019;110(6):723-728. doi:10.1007/s12185-019-02748-1
42. Laver JH, Kravaka JM, Hutchison RE, et al. Advanced-Stage Large-Cell Lymphoma in Children and Adolescents: Results of a Randomized Trial Incorporating Intermediate-Dose Methotrexate and High-Dose Cytarabine in the Maintenance Phase of the APO Regimen: A Pediatric Oncology Group Phase III Trial. *J Clin Oncol.* 2005;23(3):541-547. doi:10.1200/JCO.2005.11.075
43. Lowe EJ, Sposto R, Perkins SL, et al. Intensive Chemotherapy for Systemic Anaplastic Large Cell Lymphoma in Children and Adolescents: Final Results of Children's Cancer Group Study 5941. *Pediatr Blood Cancer.* 2009;52(3):335-339. doi:10.1002/pbc.21817
44. Williams DM, Hobson R, Imeson J, Gerrard M, McCarthy K, Pinkerton CR. Anaplastic large cell lymphoma in childhood: analysis of 72 patients treated on The United Kingdom Children's Cancer Study Group chemotherapy regimens. *Br J Haematol.* 2002;117(4):812-820. doi:10.1046/j.1365-2141.2002.03482.x
45. Reiter A, Schrappe M, Parwaresch R, et al. Non-Hodgkin's lymphomas of childhood and adolescence: results of a treatment stratified for biologic subtypes and stage-a report of the Berlin-Frankfurt-Münster Group. *J Clin Oncol.* 1995;13(2):359-372. doi:10.1200/JCO.1995.13.2.359
46. Reiter A, Schrappe M, Tiemann M, et al. Successful treatment strategy for Ki-1 anaplastic large-cell lymphoma of childhood: a prospective analysis of 62 patients enrolled in three consecutive Berlin-Frankfurt-Münster group studies. *J Clin Oncol.* 1994;12(5):899-908. doi:10.1200/JCO.1994.12.5.899
47. Pillon M, Piglione M, Garaventa A, et al. Long-term results of AIEOP LNH-92 protocol for the treatment of pediatric lymphoblastic lymphoma: a report of the Italian Association of Pediatric Hematology and Oncology. *Pediatr Blood Cancer.* 2009;53(6):953-959. doi:10.1002/pbc.22162
48. Alexander S, Kravaka JM, Weitzman S, et al. Advanced Stage Anaplastic Large Cell Lymphoma in Children and Adolescents: Results of ANHL0131, a Randomized Phase III Trial of APO Versus a Modified Regimen with Vinblastine: A Report from the Children's Oncology Group. *Pediatr Blood Cancer.* 2014;61(12):2236-2242. doi:10.1002/pbc.25187

49. Sandlund JT, Pui CH, Roberts WM, et al. Clinicopathologic features and treatment outcome of children with large-cell lymphoma and the t(2;5)(p23;q35). *Blood*. 1994;84(8):2467-2471. <http://www.bloodjournal.org/content/84/8/2467.abstract>
50. Vecchi V, Burnelli R, Pileri S, et al. Anaplastic large cell lymphoma (Ki-1+/CD30+) in childhood. *Med Pediatr Oncol*. 1993;21(6):402—410. doi:10.1002/mpo.2950210603
51. Woessmann W, Seidemann K, Mann G, et al. The impact of the methotrexate administration schedule and dose in the treatment of children and adolescents with B-cell neoplasms: a report of the BFM Group Study NHL-BFM95. *Blood*. 2005;105(3):948-958. doi:10.1182/blood-2004-03-0973
52. Le Deley MC, Rosolen A, Williams DM, et al. Vinblastine in children and adolescents with high-risk anaplastic large-cell lymphoma: Results of the randomized ALCL99-vinblastine trial. *J Clin Oncol*. 2010;28(25):3987-3993. doi:10.1200/JCO.2010.28.5999
53. Attarbaschi A, Mann G, Rosolen A, et al. Limited stage I disease is not necessarily indicative of an excellent prognosis in childhood anaplastic large cell lymphoma. *Blood*. 2011;117(21):5616-5619. doi:10.1182/blood-2010-12-324012
54. Mori T, Fukano R, Saito A, et al. Analysis of Japanese registration from the randomized international trial for childhood anaplastic large cell lymphoma (ALCL99-R1). *Rinsho Ketsueki*. 2014;55(5):526—533. doi:DN/JST.JSTAGE/rinketsu/55.526
55. Wrobel G, Mauguen A, Rosolen A, et al. Safety assessment of intensive induction therapy in childhood anaplastic large cell lymphoma: report of the ALCL99 randomised trial. *Pediatr Blood Cancer*. 2011;56(7):1071—1077. doi:10.1002/pbc.22940
56. Oeffinger KC, Mertens AC, Sklar CA, et al. Chronic Health Conditions in Adult Survivors of Childhood Cancer. *N Engl J Med*. 2006;355(15):1572-1582. doi:10.1056/NEJMsa060185
57. Alexander S, Kravaka JM, Weitzman S, et al. Advanced stage anaplastic large cell lymphoma in children and adolescents: results of ANHL0131, a randomized phase III trial of APO versus a modified regimen with vinblastine: a report from the children's oncology group. *Pediatr Blood Cancer*. 2014;61(12):2236-2242. doi:10.1002/pbc.25187
58. Brentuximab Vedotin or Crizotinib and Combination Chemotherapy in Treating Patients With Newly Diagnosed Stage II-IV Anaplastic Large Cell Lymphoma. Accessed January 8, 2018. <https://clinicaltrials.gov/ct2/show/NCT01979536>
59. Ceritinib With Brentuximab Vedotin in Treating Patients With ALK-Positive Anaplastic Large Cell Lymphoma. Accessed January 8, 2018. <https://clinicaltrials.gov/ct2/show/NCT02729961>
60. Combination Chemotherapy Followed By Stem Cell Transplant in Treating Young Patients With Progressive or Relapsed Anaplastic Large Cell Lymphoma. Accessed January 10, 2018. <https://clinicaltrials.gov/ct2/show/NCT00317408>
61. Ifosfamide, Carboplatin, Etoposide, and SGN-30 in Treating Young Patients With Recurrent Anaplastic Large Cell Lymphoma. Accessed January 8, 2018. <https://clinicaltrials.gov/ct2/show/results/NCT00354107>
62. Study of Brentuximab Vedotin (SGN-35) in Pediatric Participants With Relapsed or Refractory (r/r) Systemic Anaplastic Large-Cell Lymphoma or Hodgkin Lymphoma. Accessed January 10, 2018. <https://clinicaltrials.gov/ct2/show/NCT01492088>
63. Mossé YP, Lim MS, Voss SD, et al. Safety and activity of crizotinib for paediatric patients with refractory solid tumours or anaplastic large-cell lymphoma: a Children's Oncology Group phase 1 consortium study. *Lancet Oncol*. 2013;14(6):472-480. doi:10.1016/S1470-2045(13)70095-0
64. Balis FM, Thompson PA, Mosse YP, et al. First-dose and steady-state pharmacokinetics of orally administered crizotinib in children with solid tumors: a report on ADVL0912 from the Children's Oncology Group Phase 1/Pilot Consortium. *Cancer Chemother Pharmacol*. 2017;79(1):181-187. doi:10.1007/s00280-016-3220-6
65. Crizotinib and Combination Chemotherapy in Treating Younger Patients With Relapsed or Refractory Solid Tumors or Anaplastic Large Cell Lymphoma. Accessed January 10, 2018. <https://clinicaltrials.gov/ct2/show/NCT01606878>
66. ClinicalTrials.gov. National Library of Medicine. Phase 2 Study Assessing Efficacy and Safety of Crizotinib in Patients Harboring an Alteration on ALK, MET or ROS1 (AcSé). Identifier: NCT02034981. Accessed March 20, 2019. <https://clinicaltrials.gov/ct2/show/NCT02034981>
67. Nagai H, Fukano R, Sekimizu M, et al. Phase II trial of CH5424802 (alectinib hydrochloride) for recurrent or refractory ALK-positive anaplastic large cell lymphoma: Study protocol for a non-randomized non-controlled trial. *Nagoya J Med Sci*. 2017;79(3):407-413. doi:10.18999/nagjms.79.3.407
68. UMIN-CTR Clinical Trial Information for UMIN000016991. Accessed January 8, 2018. https://upload.umin.ac.jp/cgi-open-bin/ctr_e/ctr_view.cgi?recptno=R000019718
69. UMIN-CTR Clinical Trial Information for UMIN000028075. Accessed January 8, 2018. https://upload.umin.ac.jp/cgi-open-bin/ctr/ctr_view.cgi?recptno=R000031711
70. ITCC-053 trial information, Netherlands trial register. Accessed January 10, 2018. <http://www.trialregister.nl/trialreg/admin/rctview.asp?TC=5584>
71. Brugières L, Quartier P, Le Deley MC, et al. Relapses of childhood anaplastic large-cell lymphoma: treatment results in a series of 41 children—a report from the French Society of Pediatric Oncology. *Ann Oncol*. 2000;11(1):53-58. doi:10.1023/A:1008352726155
72. Brugières L, Pacquement H, Le Deley M-C, et al. Single-Drug Vinblastine As Salvage Treatment for Refractory or Relapsed Anaplastic Large-Cell Lymphoma: A Report From the French Society of Pediatric Oncology. *J Clin Oncol*. 2009;27(30):5056-5061. doi:10.1200/JCO.2008.20.1764

73. Mussolin L, Pillon M, D'Amore ES, et al. Prevalence and clinical implications of bone marrow involvement in pediatric anaplastic large cell lymphoma. *Leukemia*. 2005;19(9):1643-1647. doi:10.1038/sj.leu.2403888
74. Damm-Welk C, Mussolin L, Zimmermann M, et al. Early assessment of minimal residual disease identifies patients at very high relapse risk in NPM-ALK-positive anaplastic large-cell lymphoma. *Blood*. 2014;123(3):334-337. doi:10.1182/blood-2013-09-526202
75. Burkhardt B, Zimmermann M, Oschlies I, et al. The impact of age and gender on biology, clinical features and treatment outcome of non-Hodgkin lymphoma in childhood and adolescence. *Br J Haematol*. 2005;131(1):39-49. doi:10.1111/j.1365-2141.2005.05735.x
76. Le Deley M-C, Reiter A, Williams D, et al. Prognostic factors in childhood anaplastic large cell lymphoma: results of a large European intergroup study. *Blood*. 2008;111(3):1560-1566. doi:10.1182/blood-2007-07-100958
77. Lamant L, McCarthy K, d'Amore E, et al. Prognostic impact of morphologic and phenotypic features of childhood ALK-positive anaplastic large-cell lymphoma: results of the ALCL99 study. *J Clin Oncol Off J Am Soc Clin Oncol*. 2011;29(35):4669-4676. doi:10.1200/JCO.2011.36.5411
78. Mussolin L, Le Deley M-C, Carraro E, et al. Prognostic Factors in Childhood Anaplastic Large Cell Lymphoma: Long Term Results of the International ALCL99 Trial. *Cancers (Basel)*. 2020;12(10). doi:10.3390/cancers12102747
79. Damm-Welk C, Busch K, Burkhardt B, et al. Prognostic significance of circulating tumor cells in bone marrow or peripheral blood as detected by qualitative and quantitative PCR in pediatric NPM-ALK-positive anaplastic large-cell lymphoma. *Blood*. 2007;110(2):670-677. doi:10.1182/blood-2007-02-066852
80. Abramov D, Oschlies I, Zimmermann M, et al. Expression of CD8 is associated with non-common type morphology and outcome in pediatric anaplastic lymphoma kinase-positive anaplastic large cell lymphoma. *Haematologica*. 2013;98(10):1547-1553. doi:10.3324/haematol.2013.085837
81. Suzuki R, Kagami Y, Takeuchi K, et al. Prognostic significance of CD56 expression for ALK-positive and ALK-negative anaplastic large-cell lymphoma of T/null cell phenotype. *Blood*. 2000;96(9):2993-3000. doi:10.1182/blood.V96.9.2993
82. Nasr MR, Laver JH, Chang M, Hutchison RE. Expression of anaplastic lymphoma kinase, tyrosine-phosphorylated STAT3, and associated factors in pediatric anaplastic large cell lymphoma: A report from the children's oncology group. *Am J Clin Pathol*. 2007;127(5):770-778. doi:10.1309/FNY8Y4H6PK1V2MGE
83. Larose H, Prokoph N, Matthews JD, et al. Whole Exome Sequencing reveals NOTCH1 mutations in anaplastic large cell lymphoma and points to Notch both as a key pathway and a potential therapeutic target. *Haematologica*. Published online April 23, 2020:haematol.2019.238766. doi:10.3324/haematol.2019.238766
84. Lobello C, Tichy B, Bystry V, et al. STAT3 and TP53 mutations associate with poor prognosis in anaplastic large cell lymphoma. *Leukemia*. Published online November 2020. doi:10.1038/s41375-020-01093-1
85. Schlette EJ, Medeiros LJ, Goy A, Lai R, Rassidakis GZ. Survivin expression predicts poorer prognosis in anaplastic large-cell lymphoma. *J Clin Oncol Off J Am Soc Clin Oncol*. 2004;22(9):1682-1688. doi:10.1200/JCO.2004.10.172
86. ten Berge RL, Meijer CJLM, Dukers DF, et al. Expression levels of apoptosis-related proteins predict clinical outcome in anaplastic large cell lymphoma. *Blood*. 2002;99(12):4540-4546. doi:10.1182/blood.v99.12.4540
87. Kalinova M, Krskova L, Brizova H, Kabickova E, Kepak T, Kodet R. Quantitative PCR detection of NPM/ALK fusion gene and CD30 gene expression in patients with anaplastic large cell lymphoma--residual disease monitoring and a correlation with the disease status. *Leuk Res*. 2008;32(1):25-32. doi:10.1016/j.leukres.2007.01.002
88. Pulford K, Falini B, Banham AH, et al. Immune response to the ALK oncogenic tyrosine kinase in patients with anaplastic large-cell lymphoma. *Blood*. 2000;96(4):1605-1607.
89. Ait-Tahar K, Cerundolo V, Banham AH, et al. B and CTL responses to the ALK protein in patients with ALK-positive ALCL. *Int J Cancer*. 2006;118(3):688-695. doi:10.1002/ijc.21410
90. Mussolin L, Bonvini P, Ait-Tahar K, et al. Kinetics of humoral response to ALK and its relationship with minimal residual disease in pediatric ALCL. *Leukemia*. 2009;23(2):400-402. doi:10.1038/leu.2008.184
91. Ait-Tahar K, Damm-Welk C, Burkhardt B, et al. Correlation of the autoantibody response to the ALK oncoantigen in pediatric anaplastic lymphoma kinase-positive anaplastic large cell lymphoma with tumor dissemination and relapse risk. *Blood*. 2010;115(16):3314-3319. doi:10.1182/blood-2009-11-251892
92. Mussolin L, Pillon M, Zimmermann M, et al. Course of anti-ALK antibody titres during chemotherapy in children with anaplastic large cell lymphoma. *Br J Haematol*. 2018;182(5):733-735. doi:10.1111/bjh.14864
93. Iijima-Yamashita Y, Mori T, Nakazawa A, et al. Prognostic impact of minimal disseminated disease and immune response to NPM-ALK in Japanese children with ALK-positive anaplastic large cell lymphoma. *Int J Hematol*. 2018;107(2):244-250. doi:10.1007/s12185-017-2338-6
94. Woessmann W, Oschlies I MG. Intensification with HD-MTX, HD-Arac/VP-16 did not improve the outcome of high risk pediatric ALCL - results from the trial NHL-BFM95. *J Pediatr Hematol Oncol*. Published online 2003:25:S4.
95. Pillon M, Gregucci F, Lombardi A, et al. Results of AIEOP LNH-97 protocol for the treatment of anaplastic large cell lymphoma of childhood. *Pediatr Blood Cancer*. 2012;59(5):828-833. doi:10.1002/pbc.24125
96. Mori T, Kiyokawa N, Shimada H, Miyauchi J, Fujimoto J. Anaplastic large cell lymphoma in Japanese children: retrospective analysis of 34 patients diagnosed at the National Research Institute for Child Health and Development. *Br J Haematol*. 2003;121(1):94-96. doi:10.1046/j.1365-2141.2003.04249.x

97. Woessmann W, Zimmermann M, Lenhard M, et al. Relapsed or Refractory Anaplastic Large-Cell Lymphoma in Children and Adolescents After Berlin-Frankfurt-Muenster (BFM)-Type First-Line Therapy: A BFM-Group Study. *J Clin Oncol*. 2011;29(22):3065-3071. doi:10.1200/JCO.2011.34.8417
98. Knörr F, Brugières L, Pillon M, et al. Stem Cell Transplantation and Vinblastine Monotherapy for Relapsed Pediatric Anaplastic Large Cell Lymphoma: Results of the International, Prospective ALCL-Relapse Trial. *J Clin Oncol Off J Am Soc Clin Oncol*. Published online July 2020:JCO2000157. doi:10.1200/JCO.20.00157
99. Williams D, Mori T, Reiter A, et al. Central nervous system involvement in anaplastic large cell lymphoma in childhood: Results from a multicentre European and Japanese study. *Pediatr Blood Cancer*. 2013;60(10):E118-E121. doi:10.1002/pbc.24591
100. Del Baldo G, Abbas R, Woessmann W, et al. Neuro-meningeal relapse in anaplastic large-cell lymphoma: incidence, risk factors and prognosis - a report from the European intergroup for childhood non-Hodgkin lymphoma. *Br J Haematol*. Published online July 2020. doi:10.1111/bjh.16755
101. Lowe EJ, Sposto R, Perkins SL, et al. Intensive chemotherapy for systemic anaplastic large cell lymphoma in children and adolescents: final results of Children's Cancer Group Study 5941. *Pediatr Blood Cancer*. 2009;52(3):335-339. doi:10.1002/pbc.21817
102. Fraga M, Brousset P, Schlaifer D, et al. Bone Marrow Involvement in Anaplastic Large Cell Lymphoma: Immunohistochemical Detection of Minimal Disease and Its Prognostic Significance. *Am J Clin Pathol*. 1995;103(1):82-89. doi:10.1093/ajcp/103.1.82
103. Damm-Welk C, Pillon M, Woessmann W, Mussolin L. Prognostic factors in paediatric anaplastic large cell lymphoma: role of ALK. *Front Biosci (Schol Ed)*. 2015;7:205-216.
104. Morris SW, Naeve C, Mathew P, et al. ALK, the chromosome 2 gene locus altered by the t(2;5) in non-Hodgkin's lymphoma, encodes a novel neural receptor tyrosine kinase that is highly related to leukocyte tyrosine kinase (LTK). *Oncogene*. 1997;14(18):2175-2188. doi:10.1038/sj.onc.1201062
105. Camidge DR, Bang Y-J, Kwak EL, et al. Activity and safety of crizotinib in patients with ALK-positive non-small-cell lung cancer: updated results from a phase 1 study. *Lancet Oncol*. 2012;13(10):1011-1019. doi:10.1016/S1470-2045(12)70344-3
106. FDA Approved Drug Products Information for Xalori. Accessed January 8, 2018. <https://www.accessdata.fda.gov/scripts/cder/daf/index.cfm?event=overview.process&appno=202570>
107. FDA Approved Drug Products Information for Zykadia. Accessed January 8, 2018. <https://www.accessdata.fda.gov/scripts/cder/daf/index.cfm?event=overview.process&appno=205755>
108. FDA Approved Drug Products Information for Alecensa. Accessed January 8, 2018. <https://www.accessdata.fda.gov/scripts/cder/daf/index.cfm?event=overview.process&appno=208434>
109. FDA Approved Drug Products Information for Alunbrig. Accessed January 8, 2018. <https://www.accessdata.fda.gov/scripts/cder/daf/index.cfm?event=overview.process&appno=208772>
110. Swerdlow, SH, Campo, E, Harris N. *WHO Classification of Tumours of Haematopoietic and Lymphoid Tissues*. 4th ed. International Agency for Research on Cancer; 2008.
111. Turner SD, Lamant L, Kenner L, Brugières L. Anaplastic large cell lymphoma in paediatric and young adult patients. *Br J Haematol*. 2016;173(4):560-572. doi:10.1111/bjh.13958
112. Kung Sutherland MS, Sanderson RJ, Gordon KA, et al. Lysosomal trafficking and cysteine protease metabolism confer target-specific cytotoxicity by peptide-linked anti-CD30-auristatin conjugates. *J Biol Chem*. 2006;281(15):10540-10547. doi:10.1074/jbc.M510026200
113. Francisco JA, Cerveny CG, Meyer DL, et al. cAC10-vcMMAE, an anti-CD30-monomethyl auristatin E conjugate with potent and selective antitumor activity. *Blood*. 2003;102(4):1458-1465. doi:10.1182/blood-2003-01-0039
114. Younes A, Bartlett NL, Leonard JP, et al. Brentuximab Vedotin (SGN-35) for Relapsed CD30-Positive Lymphomas. *N Engl J Med*. 2010;363(19):1812-1821. doi:10.1056/NEJMoa1002965
115. Pro B, Advani R, Brice P, et al. Brentuximab vedotin (SGN-35) in patients with relapsed or refractory systemic anaplastic large-cell lymphoma: Results of a phase II study. *J Clin Oncol*. 2012;30(18):2190-2196. doi:10.1200/JCO.2011.38.0402
116. Pro B, Advani R, Brice P, et al. Four-Year Survival Data from an Ongoing Pivotal Phase 2 Study of Brentuximab Vedotin in Patients with Relapsed or Refractory Systemic Anaplastic Large Cell Lymphoma. *Blood*. 2014;124(21):3095. <http://www.bloodjournal.org/content/124/21/3095.abstract>
117. Mossé YP, Voss SD, Lim MS, et al. Targeting ALK with crizotinib in pediatric anaplastic large cell lymphoma and inflammatory myofibroblastic tumor: A Children's Oncology Group study. *J Clin Oncol*. 2017;35(28):3215-3221. doi:10.1200/JCO.2017.73.4830
118. Mori T, Takimoto T, Katano N, et al. Recurrent childhood anaplastic large cell lymphoma: A retrospective analysis of registered cases in Japan. *Br J Haematol*. 2006;132(5):594-597. doi:10.1111/j.1365-2141.2005.05910.x
119. Zinzani PL, Sasse S, Radford J, Gautam A, Bonthapally V. Brentuximab vedotin in relapsed/refractory Hodgkin lymphoma: An updated review of published data from the named patient program. *Crit Rev Oncol / Hematol*. 2018;104:65-70. doi:10.1016/j.critrevonc.2016.04.019
120. Haggood G, Savage KJ. The biology and management of systemic anaplastic large cell lymphoma. *Blood*. 2015;126(1):17-25. doi:10.1182/blood-2014-10-567461
121. Woessmann W, Peters C, Lenhard M, et al. Allogeneic haematopoietic stem cell transplantation in relapsed or refractory anaplastic large cell lymphoma of children and adolescents--a Berlin-Frankfurt-Münster group report. *Br J Haematol*. 2006;133(2):176-182. doi:10.1111/j.1365-2141.2006.06004.x

122. Fukano R, Mori T, Kobayashi R, et al. Haematopoietic stem cell transplantation for relapsed or refractory anaplastic large cell lymphoma: A study of children and adolescents in Japan. *Br J Haematol.* 2015;168(4):557-563. doi:10.1111/bjh.13167
123. Woessmann, W ; Brugieres, L; Rosolen, A; Zimmermann, M; Attarbaschi, A; Mellgren, K; Williams, D; Uyttebroeck, A; Wrobel, G; Reiter A. Risk-adapted therapy for patients with relapsed or refractory ALCL - interim-results of the prospective EICNHL-Trial ALCL-relapse. *Br J Haematol.* 2012;159(74):41.
124. Fukano R, Mori T, Sekimizu M, et al. Alectinib for relapsed or refractory ALK-positive anaplastic large cell lymphoma: an open label phase 2 trial. *Cancer Sci.* Published online October 2020. doi:10.1111/cas.14671
125. Yang J, Li J, Gu W-Y, et al. Central nervous system relapse in a pediatric anaplastic large cell lymphoma patient with CLTC/ALK translocation treated with alectinib: A case report. *World J Clin cases.* 2020;8(9):1685-1692. doi:10.12998/wjcc.v8.i9.1685
126. Brugières L, Houot R, Cozic N, et al. Crizotinib in Advanced ALK+ Anaplastic Large Cell Lymphoma in Children and Adults: Results of the Acs© Phase II Trial. *Blood.* 2017;130(Suppl 1).
127. Gambacorti-Passerini C, Mussolin L, Brugieres L. Abrupt Relapse of ALK-Positive Lymphoma after Discontinuation of Crizotinib. *N Engl J Med.* 2016;374(1):95-96. doi:10.1056/NEJMc1511045
128. Gambacorti-Passerini C, Farina F, Stasia A, et al. Crizotinib in advanced, chemoresistant anaplastic lymphoma kinase-positive lymphoma patients. *J Natl Cancer Inst.* 2014;106(2):2-5. doi:10.1093/jnci/djt378
129. Study of Brentuximab Vedotin (SGN-35) in Pediatric Participants With Relapsed or Refractory (r/r) Systemic Anaplastic Large-Cell Lymphoma or Hodgkin Lymphoma. Accessed January 8, 2018. <https://clinicaltrials.gov/ct2/show/results/NCT01492088?sect=X4301256&view=record>
130. Vaklavas C, Forero-Torres A. Safety and efficacy of brentuximab vedotin in patients with Hodgkin lymphoma or systemic anaplastic large cell lymphoma. *Ther Adv Hematol.* 2012;3(4):209-225. doi:10.1177/2040620712443076
131. Yamamoto R, Nishikori M, Tashima M, et al. B7-H1 expression is regulated by MEK/ERK signaling pathway in anaplastic large cell lymphoma and Hodgkin lymphoma. *Cancer Sci.* 2009;100(11):2093-2100. doi:10.1111/j.1349-7006.2009.01302.x
132. Marzec M, Zhang Q, Goradia A, et al. Oncogenic kinase NPM/ALK induces through STAT3 expression of immunosuppressive protein CD274 (PD-L1, B7-H1). *Proc Natl Acad Sci U S A.* 2008;105(52):20852-20857. doi:10.1073/pnas.0810958105
133. Parry R V, Chemnitz JM, Frauwirth KA, et al. CTLA-4 and PD-1 Receptors Inhibit T-Cell Activation by Distinct Mechanisms. *Mol Cell Biol.* 2005;25(21):9543-9553. doi:10.1128/MCB.25.21.9543-9553.2005
134. Dong H, Strome SE, Salomao DR, et al. Tumor-associated B7-H1 promotes T-cell apoptosis: A potential mechanism of immune evasion. *Nat Med.* 2002;8(8):793-800. doi:10.1038/nm730
135. Curiel TJ, Wei S, Dong H, et al. Blockade of B7-H1 improves myeloid dendritic cell-mediated antitumor immunity. *Nat Med.* 2003;9(5):562-567. doi:10.1038/nm863
136. Chan TSY, Khong P-L, Kwong Y-L. Pembrolizumab for relapsed anaplastic large cell lymphoma after allogeneic haematopoietic stem cell transplantation: efficacy and safety. *Ann Hematol.* 2016;95(11):1913-1915. doi:10.1007/s00277-016-2764-1
137. Hebart H, Lang P, Woessmann W. Nivolumab for refractory anaplastic large cell lymphoma: A case report. *Ann Intern Med.* 2016;165(8):607-608. doi:10.7326/L16-0037
138. Rigaud C, Abbou S, Minard-Colin V, et al. Efficacy of nivolumab in a patient with systemic refractory ALK+ anaplastic large cell lymphoma. *Pediatr Blood Cancer.* Published online November 28, 2017:e26902. doi:10.1002/pbc.26902
139. Grigg C, Rizvi NA. PD-L1 biomarker testing for non-small cell lung cancer: truth or fiction? *J Immunother Cancer.* 2016;4:48. doi:10.1186/s40425-016-0153-x
140. Ait-Tahar K, Barnardo MCN, Pulford K. CD4 T-Helper Responses to the Anaplastic Lymphoma Kinase (ALK) Protein in Patients with ALK-Positive Anaplastic Large-Cell Lymphoma. *Cancer Res.* 2007;67(5):1898-1901. doi:10.1158/0008-5472.CAN-06-4427
141. Merkel O, Hamacher F, Sift E, Kenner L, Greil R. Novel Therapeutic Options in Anaplastic Large Cell Lymphoma: Molecular Targets and Immunological Tools. *Mol Cancer Ther.* 2011;10(7):1127-1136. doi:10.1158/1535-7163.MCT-11-0042
142. Chiarle R, Martinengo C, Mastini C, et al. The anaplastic lymphoma kinase is an effective oncoantigen for lymphoma vaccination. *Nat Med.* 2008;14(6):676-680. doi:10.1038/nm1769
143. Maris JM. Recent Advances in Neuroblastoma. *N Engl J Med.* 2010;362(23):2202-2211. doi:10.1056/NEJMra0804577
144. Brodeur GM. Neuroblastoma: biological insights into a clinical enigma. *Nat Rev Cancer.* 2003;3(3):203-216. doi:10.1038/nrc1014
145. Smith MA, Seibel NL, Altekruse SF, et al. Outcomes for Children and Adolescents With Cancer: Challenges for the Twenty-First Century. *J Clin Oncol.* 2010;28(15):2625-2634. doi:10.1200/JCO.2009.27.0421
146. Spix C, Pastore G, Sankila R, Stiller CA, Steliarova-Foucher E. Neuroblastoma incidence and survival in European children (1978–1997): Report from the Automated Childhood Cancer Information System project. *Eur J Cancer.* 2006;42(13):2081-2091. doi:10.1016/j.ejca.2006.05.008
147. Isaacs H. FETAL AND NEONATAL NEUROBLASTOMA: RETROSPECTIVE REVIEW OF 271 CASES. *Fetal Pediatr Pathol.* 2007;26(4):177-184. doi:10.1080/15513810701696890
148. Diede SJ. Spontaneous regression of metastatic cancer: learning from neuroblastoma. *Nat Rev Cancer.* 2014;14(2):71-72. doi:10.1038/nrc3656
149. Maris JM, Hogarty MD, Bagatell R, Cohn SL. Neuroblastoma. *Lancet.* 2007;369(9579):2106-2120.

- doi:10.1016/S0140-6736(07)60983-0
150. PDQ Pediatric Treatment Editorial Board. *Neuroblastoma Treatment (PDQ®): Health Professional Version.*; 2002.
 151. Park JR, Bagatell R, London WB, et al. Children's Oncology Group's 2013 blueprint for research: Neuroblastoma. *Pediatr Blood Cancer.* 2013;60(6):985-993. doi:10.1002/psc.24433
 152. Smith L, Minter S, O'Brien P, Kravaka JM, Medina AM, Lazarchick J. Neuroblastoma in an adult: case presentation and literature review. *Ann Clin Lab Sci.* 2013;43(1):81-84.
 153. Joshi S, R. A, L.R. L, Zulcic M, Ahn H, L. D. Novel Therapeutic Approaches for Neuroblastoma. In: *Neuroblastoma.* InTech; 2013. doi:10.5772/55451
 154. Pugh TJ, Morozova O, Attiyeh EF, et al. The genetic landscape of high-risk neuroblastoma. *Nat Genet.* 2013;45(3):279-284. doi:10.1038/ng.2529
 155. Mossé YP, Laudenslager M, Longo L, et al. Identification of ALK as a major familial neuroblastoma predisposition gene. *Nature.* 2008;455(7215):930-935. doi:10.1038/nature07261
 156. Janoueix-Lerosey I, Lequin D, Brugières L, et al. Somatic and germline activating mutations of the ALK kinase receptor in neuroblastoma. *Nature.* 2008;455(7215):967-970. doi:10.1038/nature07398
 157. Chen Y, Takita J, Choi YL, et al. Oncogenic mutations of ALK kinase in neuroblastoma. *Nature.* 2008;455(7215):971-974. doi:10.1038/nature07399
 158. George RE, Sanda T, Hanna M, et al. Activating mutations in ALK provide a therapeutic target in neuroblastoma. *Nature.* 2008;455(7215):975-978. doi:10.1038/nature07397
 159. Krause DS, Van Etten RA. Tyrosine kinases as targets for cancer therapy. *N Engl J Med.* 2005;353(2):172-187. doi:10.1056/NEJMra044389
 160. Klaus M, Prokoph N, Girbig M, et al. Structure and decoy-mediated inhibition of the SOX18/Prox1-DNA interaction. *Nucleic Acids Res.* 2016;44(8):3922-3935. doi:10.1093/nar/gkw130
 161. Lamant L, Pulford K, Bischof D, et al. Expression of the ALK Tyrosine Kinase Gene in Neuroblastoma. *Am J Pathol.* 2000;156(5):1711-1721. doi:10.1016/S0002-9440(10)65042-0
 162. Dirks WG, Fähnrich S, Lis Y, Becker E, MacLeod RAF, Drexler HG. Expression and functional analysis of the anaplastic lymphoma kinase (ALK) gene in tumor cell lines. *Int J Cancer.* 2002;100(1):49-56. doi:10.1002/ijc.10435
 163. Lee CC, Jia Y, Li N, et al. Crystal structure of the ALK (anaplastic lymphoma kinase) catalytic domain. *Biochem J.* 2010;430(3):425-437. doi:10.1042/BJ20100609
 164. Bresler SC, Weiser DA, Huwe PJ, et al. ALK mutations confer differential oncogenic activation and sensitivity to ALK inhibition therapy in neuroblastoma. *Cancer Cell.* 2014;26(5):682. doi:10.1016/J.CCELL.2014.09.019
 165. Sausen M, Leary RJ, Jones S, et al. Integrated genomic analyses identify ARID1A and ARID1B alterations in the childhood cancer neuroblastoma. *Nat Genet.* 2013;45(1):12-17. doi:10.1038/ng.2493
 166. Pugh TJ, Morozova O, Attiyeh EF, et al. The genetic landscape of high-risk neuroblastoma. *Nat Genet.* 2013;45(3):279-284. doi:10.1038/ng.2529
 167. Cheung N-K V. Association of Age at Diagnosis and Genetic Mutations in Patients With Neuroblastoma. *JAMA.* 2012;307(10):1062. doi:10.1001/jama.2012.228
 168. Carpenter EL, Mossé YP. Targeting ALK in neuroblastoma—preclinical and clinical advancements. *Nat Rev Clin Oncol.* 2012;9(7):391-399. doi:10.1038/nrclinonc.2012.72
 169. Zhu S, Lee J-S, Guo F, et al. Activated ALK Collaborates with MYCN in Neuroblastoma Pathogenesis. *Cancer Cell.* 2012;21(3):362-373. doi:10.1016/j.ccr.2012.02.010
 170. Schönherr C, Ruuth K, Kamaraj S, et al. Anaplastic Lymphoma Kinase (ALK) regulates initiation of transcription of MYCN in neuroblastoma cells. *Oncogene.* 2012;31(50):5193-5200. doi:10.1038/onc.2012.12
 171. Schleiermacher G, Javanmardi N, Bernard V, et al. Emergence of new ALK mutations at relapse of neuroblastoma. *J Clin Oncol.* 2014;32(25):2727-2734. doi:10.1200/JCO.2013.54.0674
 172. Eleveld TF, Oldridge DA, Bernard V, et al. Relapsed neuroblastomas show frequent RAS-MAPK pathway mutations. *Nat Genet.* 2015;47(8):864-871. doi:10.1038/ng.3333
 173. Padovan-Merhar OM, Raman P, Ostrovskaya I, et al. Enrichment of Targetable Mutations in the Relapsed Neuroblastoma Genome. *PLoS Genet.* 2016;12(12):e1006501. doi:10.1371/journal.pgen.1006501
 174. Bellini A, Bernard V, Leroy Q, et al. Deep Sequencing Reveals Occurrence of Subclonal ALK Mutations in Neuroblastoma at Diagnosis. *Clin Cancer Res.* 2015;21(21):4913-4921. doi:10.1158/1078-0432.CCR-15-0423
 175. Osajima-Hakomori Y, Miyake I, Ohira M, Nakagawara A, Nakagawa A, Sakai R. Biological Role of Anaplastic Lymphoma Kinase in Neuroblastoma. *Am J Pathol.* 2005;167(1):213-222. doi:10.1016/S0002-9440(10)62966-5
 176. Miyake I, Hakomori Y, Shinohara A, et al. Activation of anaplastic lymphoma kinase is responsible for hyperphosphorylation of ShcC in neuroblastoma cell lines. *Oncogene.* 2002;21(38):5823-5834. doi:10.1038/sj.onc.1205735
 177. De Brouwer S, De Preter K, Kumps C, et al. Meta-analysis of Neuroblastomas Reveals a Skewed ALK Mutation Spectrum in Tumors with MYCN Amplification. *Clin Cancer Res.* 2010;16(17):4353-4362. doi:10.1158/1078-0432.CCR-09-2660
 178. ClinicalTrials.gov. National Library of Medicine. Crizotinib in Treating Young Patients with Relapsed or Refractory Solid Tumors or Anaplastic Large Cell Lymphoma. Identifier: NCT00939770. Accessed March 20, 2019. <https://clinicaltrials.gov/ct2/show/NCT00939770>

179. ClinicalTrials.gov. National Library of Medicine. An Investigational Drug, Crizotinib (PF-02341066), Is Being Studied In Tumors, Except Non-Small Cell Lung Cancer, That Are Positive For Anaplastic Lymphoma Kinase (ALK). Identifier: NCT01121588. Accessed March 20, 2019. <https://clinicaltrials.gov/ct2/show/NCT01121588>
180. ClinicalTrials.gov. National Library of Medicine. Crizotinib and Combination Chemotherapy in Treating Younger Patients with Relapsed or Refractory Solid Tumors or Anaplastic Large Cell Lymphoma. Identifier: NCT01606878. Accessed March 20, 2019. <https://clinicaltrials.gov/ct2/show/NCT01606878>
181. ClinicalTrials.gov. National Library of Medicine. Phase I Study of LDK378 in Pediatric, Malignancies with a Genetic Alteration in Anaplastic Lymphoma Kinase (ALK). Identifier: NCT01742286. Accessed March 20, 2019. <https://clinicaltrials.gov/ct2/show/NCT01742286>
182. ClinicalTrials.gov. National Library of Medicine. Study of RDX-101 in Children with Recurrent or Refractory Solid Tumors and Primary CNS Tumors, With or Without TRK, ROS1, or ALK Fusions. Identifier: NCT02650401. Accessed March 20, 2019. <https://clinicaltrials.gov/ct2/show/NCT02650401>
183. ClinicalTrials.gov. National Library of Medicine. Next Generation Personalized Neuroblastoma Therapy (NEPENTHE). Identifier: NCT02780128. Accessed March 20, 2019. <https://clinicaltrials.gov/ct2/show/NCT02780128>
184. ClinicalTrials.gov. National Library of Medicine. Ensartinib in Treating Patients with Relapsed or Refractory Advanced Solid Tumors, Non-Hodgkin Lymphoma, or Histiocytic Disorders with ALK or ROS1 Genomic Alterations (A Pediatric MATCH Treatment Trial). I. Accessed March 20, 2019. <https://clinicaltrials.gov/ct2/show/NCT03213652>
185. ClinicalTrials.gov. National Library of Medicine. Study of Lorlatinib (PF-06463922). Identifier: NCT03107988. Accessed March 20, 2019. <https://clinicaltrials.gov/ct2/show/NCT03107988>
186. ClinicalTrials.gov. National Library of Medicine. Iobenguane I-131 or Crizotinib and Standard Therapy in Treating Younger Patients with Newly-Diagnosed High-Risk Neuroblastoma or Ganglioneuroblastoma. Identifier: NCT03126916. Accessed March 20, 2019. <https://clinicaltrials.gov/ct2/show/NCT03126916>
187. Shaw AT, Engelman JA. Ceritinib in ALK -Rearranged Non-Small-Cell Lung Cancer. *N Engl J Med*. 2014;370(26):2537-2539. doi:10.1056/NEJMc1404894
188. Khozin S, Blumenthal GM, Zhang L, et al. FDA Approval: Ceritinib for the Treatment of Metastatic Anaplastic Lymphoma Kinase-Positive Non-Small Cell Lung Cancer. *Clin Cancer Res*. 2015;21(11):2436-2439. doi:10.1158/1078-0432.CCR-14-3157
189. Allen CE, Laetsch TW, Mody R, et al. Target and Agent Prioritization for the Children's Oncology Group—National Cancer Institute Pediatric MATCH Trial. *JNCI J Natl Cancer Inst*. 2017;109(5). doi:10.1093/jnci/djw274
190. The International Agency for Research on Cancer, the World Health Organization. Accessed February 15, 2018. http://globocan.iarc.fr/Pages/fact_sheets_cancer.aspx
191. Torre LA, Bray F, Siegel RL, Ferlay J, Lortet-Tieulent J, Jemal A. Global cancer statistics, 2012. *CA Cancer J Clin*. 2015;65(2):87-108. doi:10.3322/caac.21262
192. Reade CA, Ganti AK. EGFR targeted therapy in non-small cell lung cancer: potential role of cetuximab. *Biologics*. 2009;3:215-224. Accessed January 23, 2018. <http://www.ncbi.nlm.nih.gov/pubmed/19707410>
193. Surveillance, Epidemiology, and End Results Program; National Cancer Institute. Accessed February 15, 2018. <https://seer.cancer.gov/statfacts/html/lungb.html>
194. Garber K. ALK, Lung Cancer, and Personalized Therapy: Portent of the Future? *JNCI J Natl Cancer Inst*. 2010;102(10):672-675. doi:10.1093/jnci/djq184
195. Jemal A, Clegg LX, Ward E, et al. Annual report to the nation on the status of cancer, 1975-2001, with a special feature regarding survival. *Cancer*. 2004;101(1):3-27. doi:10.1002/cncr.20288
196. Shaw AT, Yeap BY, Mino-Kenudson M, et al. Clinical Features and Outcome of Patients With Non-Small-Cell Lung Cancer Who Harbor EML4-ALK. *J Clin Oncol*. 2009;27(26):4247-4253. doi:10.1200/JCO.2009.22.6993
197. Kwak EL, Bang Y-J, Camidge DR, et al. Anaplastic Lymphoma Kinase Inhibition in Non-Small-Cell Lung Cancer. *N Engl J Med*. 2010;363(18):1693-1703. doi:10.1056/NEJMoa1006448
198. Bergethon K, Shaw AT, Ignatius Ou S-H, et al. ROS1 Rearrangements Define a Unique Molecular Class of Lung Cancers. *J Clin Oncol*. 2012;30(8):863-870. doi:10.1200/JCO.2011.35.6345
199. Shaw AT, Kim D-W, Nakagawa K, et al. Crizotinib versus Chemotherapy in Advanced ALK-Positive Lung Cancer. *N Engl J Med*. 2013;368(25):2385-2394. doi:10.1056/NEJMoa1214886
200. Solomon BJ, Mok T, Kim D-W, et al. First-Line Crizotinib versus Chemotherapy in ALK-Positive Lung Cancer. *N Engl J Med*. 2014;371(23):2167-2177. doi:10.1056/NEJMoa1408440
201. Shaw AT, Kim D-W, Mehra R, et al. Ceritinib in ALK-Rearranged Non-Small-Cell Lung Cancer. *N Engl J Med*. 2014;370(13):1189-1197. doi:10.1056/NEJMoa1311107
202. Kim D-W, Mehra R, Tan DSW, et al. Activity and safety of ceritinib in patients with ALK-rearranged non-small-cell lung cancer (ASCEND-1): updated results from the multicentre, open-label, phase 1 trial. *Lancet Oncol*. 2016;17(4):452-463. doi:10.1016/S1470-2045(15)00614-2
203. Mok T, Spigel D, Felip E, et al. ASCEND-2: A single-arm, open-label, multicenter phase II study of ceritinib in adult patients (pts) with ALK-rearranged (ALK+) non-small cell lung cancer (NSCLC) previously treated with chemotherapy and crizotinib (CRZ). *J Clin Oncol*. 2015;33(15_suppl):8059. doi:10.1200/jco.2015.33.15_suppl.8059
204. Felip E, Orlov S, Park K, et al. ASCEND-3: A single-arm, open-label, multicenter phase II study of ceritinib in ALKi-naïve adult patients (pts) with ALK-rearranged (ALK+) non-small cell lung cancer (NSCLC). *J Clin*

- Oncol.* 2015;33(15_suppl):8060. doi:10.1200/jco.2015.33.15_suppl.8060
205. Nokihara H, Hida T, Kondo M, et al. Alectinib (ALC) versus crizotinib (CRZ) in ALK-inhibitor naive ALK-positive non-small cell lung cancer (ALK+ NSCLC): Primary results from the J-ALEX study. *J Clin Oncol.* 2016;34(15_suppl):9008. doi:10.1200/JCO.2016.34.15_suppl.9008
 206. Camidge DR. Taking aim at ALK across the blood-brain barrier. *J Thorac Oncol.* 2013;8(4):389-390. doi:10.1097/JTO.0b013e3182864e7c
 207. Zhang S, Anjum R, Squillace R, et al. The Potent ALK Inhibitor Brigatinib (AP26113) Overcomes Mechanisms of Resistance to First- and Second-Generation ALK Inhibitors in Preclinical Models. *Clin Cancer Res.* 2016;22(22):5527-5538. doi:10.1158/1078-0432.CCR-16-0569
 208. Sullivan I, Planchard D. Editorial on the article entitled "brigatinib efficacy and safety in patients with anaplastic lymphoma kinase (ALK)-positive non-small cell lung cancer in a phase I/II trial". *J Thorac Dis.* 2016;8(10):E1287-E1292. doi:10.21037/jtd.2016.10.57
 209. Chen Y, Fu L. Mechanisms of acquired resistance to tyrosine kinase inhibitors. *Acta Pharm Sin B.* 2011;1(4):197-207. doi:10.1016/J.APSB.2011.10.007
 210. Katayama R, Shaw AT, Khan TM, et al. Mechanisms of Acquired Crizotinib Resistance in ALK-Rearranged Lung Cancers. *Sci Transl Med.* 2012;4(120):120ra17-120ra17. doi:10.1126/scitranslmed.3003316
 211. Camidge DR, Bang Y-J, Kwak EL, et al. Activity and safety of crizotinib in patients with ALK-positive non-small-cell lung cancer: updated results from a phase 1 study. *Lancet Oncol.* 2012;13(10):1011-1019. doi:10.1016/S1470-2045(12)70344-3
 212. Kim D-W, Ahn M-J, Shi Y, et al. Results of a global phase II study with crizotinib in advanced ALK-positive non-small cell lung cancer (NSCLC). *J Clin Oncol.* 2012;30(15_suppl):7533. doi:10.1200/jco.2012.30.15_suppl.7533
 213. Bivona TG, Doebele RC. A framework for understanding and targeting residual disease in oncogene-driven solid cancers. *Nat Med.* 2016;22(5):472-478. doi:10.1038/nm.4091
 214. Rotow J, Bivona TG. Understanding and targeting resistance mechanisms in NSCLC. *Nat Rev Cancer.* 2017;17(11):637-658. doi:10.1038/nrc.2017.84
 215. Choi YL, Soda M, Yamashita Y, et al. EML4-ALK Mutations in Lung Cancer That Confer Resistance to ALK Inhibitors. *N Engl J Med.* 2010;363(18):1734-1739. doi:10.1056/NEJMoa1007478
 216. Gainor JF, Dardaei L, Yoda S, et al. Molecular Mechanisms of Resistance to First- and Second-Generation ALK Inhibitors in ALK-Rearranged Lung Cancer. *Cancer Discov.* 2016;6(10):1118-1133. doi:10.1158/2159-8290.CD-16-0596
 217. Ceccon M, Mologni L, Bisson W, Scapozza L, Gambacorti-Passerini C. Crizotinib-Resistant NPM-ALK Mutants Confer Differential Sensitivity to Unrelated Alk Inhibitors. *Mol Cancer Res.* 2013;11(2):122-132. doi:10.1158/1541-7786.MCR-12-0569
 218. Ou S-HI, Klempner SJ, Greenbowe JR, et al. Identification of a Novel HIP1-ALK Fusion Variant in Non-Small-Cell Lung Cancer (NSCLC) and Discovery of ALK I1171 (I1171N/S) Mutations in Two ALK-Rearranged NSCLC Patients with Resistance to Alectinib. *J Thorac Oncol.* 2014;9(12):1821-1825. doi:10.1097/JTO.0000000000000368
 219. Sasaki T, Okuda K, Zheng W, et al. The Neuroblastoma-Associated F1174L ALK Mutation Causes Resistance to an ALK Kinase Inhibitor in ALK-Translocated Cancers. *Cancer Res.* 2010;70(24):10038-10043. doi:10.1158/0008-5472.CAN-10-2956
 220. Chen Y, Takita J, Choi YL, et al. Oncogenic mutations of ALK kinase in neuroblastoma. doi:10.1038/nature07399
 221. Bresler SC, Wood AC, Haglund EA, et al. Differential Inhibitor Sensitivity of Anaplastic Lymphoma Kinase Variants Found in Neuroblastoma. *Sci Transl Med.* 2011;3(108):108ra114-108ra114. doi:10.1126/scitranslmed.3002950
 222. Sasaki T, Koivunen J, Ogino A, et al. A Novel ALK Secondary Mutation and EGFR Signaling Cause Resistance to ALK Kinase Inhibitors. *Cancer Res.* 2011;71(18):6051-6060. doi:10.1158/0008-5472.CAN-11-1340
 223. Doebele RC, Pilling AB, Aisner DL, et al. Mechanisms of resistance to crizotinib in patients with ALK gene rearranged non-small cell lung cancer. *Clin Cancer Res.* 2012;18(5):1472-1482. doi:10.1158/1078-0432.CCR-11-2906
 224. Heuckmann JM, Hölzel M, Sos ML, et al. ALK Mutations Conferring Differential Resistance to Structurally Diverse ALK Inhibitors. *Clin Cancer Res.* 2011;17(23):7394 LP - 7401. doi:10.1158/1078-0432.CCR-11-1648
 225. Zamo A, Chiarle R, Piva R, et al. Anaplastic lymphoma kinase (ALK) activates Stat3 and protects hematopoietic cells from cell death. *Oncogene.* 2002;21(7):1038-1047. doi:10.1038/sj.onc.1205152
 226. Amin AD, Rajan SS, Liang WS, et al. Evidence Suggesting That Discontinuous Dosing of ALK Kinase Inhibitors May Prolong Control of ALK+ Tumors. *Cancer Res.* 2015;75(14):2916-2927. doi:10.1158/0008-5472.CAN-14-3437
 227. Katayama R, Khan TM, Benes C, et al. Therapeutic strategies to overcome crizotinib resistance in non-small cell lung cancers harboring the fusion oncogene EML4-ALK. *Proc Natl Acad Sci.* 2011;108(18):7535-7540. doi:10.1073/pnas.1019559108
 228. Siegel RL, Miller KD, Jemal A. Cancer statistics, 2019. *CA Cancer J Clin.* 2019;69(1):7-34. doi:10.3322/caac.21551
 229. Travis WD, Brambilla E, Nicholson AG, et al. The 2015 World Health Organization Classification of Lung Tumors. *J Thorac Oncol.* 2015;10(9):1243-1260. doi:10.1097/JTO.0000000000000630

230. Stewart EL, Tan SZ, Liu G, Tsao M-S. Known and putative mechanisms of resistance to EGFR targeted therapies in NSCLC patients with EGFR mutations-a review. *Transl lung cancer Res.* 2015;4(1):67-81. doi:10.3978/j.issn.2218-6751.2014.11.06
231. Gainor JF, Shaw AT. Emerging Paradigms in the Development of Resistance to Tyrosine Kinase Inhibitors in Lung Cancer. *J Clin Oncol.* 2013;31(31):3987-3996. doi:10.1200/JCO.2012.45.2029
232. Wilson FH, Johannessen CM, Piccioni F, et al. A Functional Landscape of Resistance to ALK Inhibition in Lung Cancer. *Cancer Cell.* 2015;27(3):397-408. doi:10.1016/j.ccell.2015.02.005
233. Lovly CM, McDonald NT, Chen H, et al. Rationale for co-targeting IGF-1R and ALK in ALK fusion-positive lung cancer. *Nat Med.* 2014;20(9):1027-1034. doi:10.1038/nm.3667
234. Hrustanovic G, Olivas V, Pazarentzos E, et al. RAS-MAPK dependence underlies a rational polytherapy strategy in EML4-ALK-positive lung cancer. *Nat Med.* 2015;21(9):1038-1047. doi:10.1038/nm.3930
235. Bai RY, Ouyang T, Miething C, Morris SW, Peschel C, Duyster J. Nucleophosmin-anaplastic lymphoma kinase associated with anaplastic large-cell lymphoma activates the phosphatidylinositol 3-kinase/Akt antiapoptotic signaling pathway. *Blood.* 2000;96(13):4319-4327. Accessed January 24, 2018. <http://www.ncbi.nlm.nih.gov/pubmed/11110708>
236. Bai RY, Dieter P, Peschel C, Morris SW, Duyster J. Nucleophosmin-anaplastic lymphoma kinase of large-cell anaplastic lymphoma is a constitutively active tyrosine kinase that utilizes phospholipase C-gamma to mediate its mitogenicity. *Mol Cell Biol.* 1998;18(12):6951-6961. doi:10.1128/mcb.18.12.6951
237. Schönherr C, Yang H-L, Vigny M, Palmer RH, Hallberg B. Anaplastic lymphoma kinase activates the small GTPase Rap1 via the Rap1-specific GEF C3G in both neuroblastoma and PC12 cells. *Oncogene.* 2010;29(19):2817-2830. doi:10.1038/onc.2010.27
238. Garraway LA, Jänne PA. Circumventing Cancer Drug Resistance in the Era of Personalized Medicine. *Cancer Discov.* 2012;2(3):214-226. doi:10.1158/2159-8290.CD-12-0012
239. Davies HT, Crombie IK. Bias in cohort studies. *Hosp Med.* 2000;61(2):133-135.
240. Horner MJ, Ries LAG, Krapcho M, Neyman N, Aminou R, Howlader N, Altekruse SF, Feuer EJ, Huang L, Mariotto A, Miller BA, Lewis DR, Eisner MP, Stinchcomb DG EB. *SEER Cancer Statistics Review, 1975-2006, National Cancer Institute.*; 2009.
241. Wood KC. Mapping the Pathways of Resistance to Targeted Therapies. *Cancer Res.* 2015;75(20):4247-4251. doi:10.1158/0008-5472.CAN-15-1248
242. Stewart EL, Mascaux C, Pham N-A, et al. Clinical Utility of Patient-Derived Xenografts to Determine Biomarkers of Prognosis and Map Resistance Pathways in EGFR-Mutant Lung Adenocarcinoma. *J Clin Oncol.* 2015;33(22):2472-2480. doi:10.1200/JCO.2014.60.1492
243. Crystal AS, Shaw AT, Sequist L V., et al. Patient-derived models of acquired resistance can identify effective drug combinations for cancer. *Science (80-).* 2014;346(6216):1480-1486. doi:10.1126/science.1254721
244. Frese KK, Tuveson DA. Maximizing mouse cancer models. *Nat Rev Cancer.* 2007;7(9):654-658. doi:10.1038/nrc2192
245. Wang J, Wang B, Chu H, Yao Y. Intrinsic resistance to EGFR tyrosine kinase inhibitors in advanced non-small-cell lung cancer with activating EGFR mutations. *Onco Targets Ther.* 2016;9:3711-3726. doi:10.2147/OTT.S106399
246. Tabe Y, Jin L, Yixin Z, et al. Role of Stromal Microenvironment In Non-Pharmacological Resistance of CML to Tyrosine Kinase Inhibitors through Lyn/CXCR4 Interactions In Lipid Rafts. *Blood.* 2015;116(21). doi:10.1038/leu.2011.291
247. Klemm F, Joyce JA. Microenvironmental regulation of therapeutic response in cancer. *Trends Cell Biol.* 2015;25(4):198-213. doi:10.1016/j.tcb.2014.11.006
248. Cheng X, Chen H. Tumor heterogeneity and resistance to EGFR-targeted therapy in advanced nonsmall cell lung cancer: challenges and perspectives. *Onco Targets Ther.* 2014;7:1689-1704. doi:10.2147/OTT.S66502
249. Rangarajan A, Weinberg RA. Comparative biology of mouse versus human cells: modelling human cancer in mice. *Nat Rev Cancer.* 2003;3(12):952-959. doi:10.1038/nrc1235
250. Gonzalez FJ, Kimura S. Study of P450 function using gene knockout and transgenic mice. *Arch Biochem Biophys.* 2003;409(1):153-158. doi:10.1016/s0003-9861(02)00364-8
251. Hanahan D, Weinberg RA. The Hallmarks of Cancer. *Cell.* 2000;100(1):57-70. doi:10.1016/S0092-8674(00)81683-9
252. Holliday DL, Speirs V. Choosing the right cell line for breast cancer research. *Breast Cancer Res.* 2011;13(4):215. doi:10.1186/bcr2889
253. Brodaczewska KK, Szczylik C, Fiedorowicz M, Porta C, Czarnecka AM. Choosing the right cell line for renal cell cancer research. *Mol Cancer.* 2016;15(1):83. doi:10.1186/s12943-016-0565-8
254. Auman JT, McLeod HL. Colorectal Cancer Cell Lines Lack the Molecular Heterogeneity of Clinical Colorectal Tumors. *Clin Colorectal Cancer.* 2010;9(1):40-47. doi:10.3816/CCC.2010.n.005
255. Hughes P, Marshall D, Reid Y, Parkes H, Gelber C. The costs of using unauthenticated, over-passaged cell lines: how much more data do we need? *Biotechniques.* 2007;43(5):575, 577-578, 581-2 passim. doi:10.2144/000112598
256. Pfeifer W, Levi E, Petrogiannis-Haliotis T, Lehmann L, Wang Z, Kadin ME. A Murine Xenograft Model for Human CD30+ Anaplastic Large Cell Lymphoma: Successful Growth Inhibition with an Anti-CD30 Antibody (HeFi-1). *Am J Pathol.* 1999;155(4):1353-1359. doi:10.1016/S0002-9440(10)65237-6
257. Drexler HG, MacLeod RAF. Malignant hematopoietic cell lines: in vitro models for the study of anaplastic large-cell lymphoma. *Leukemia.* 2004;18(10):1569-1571. doi:10.1038/sj.leu.2403465

258. Thiele CJ. Neuroblastoma Cell Lines. *J Hum Cell Cult.* 1998;1:21-53.
259. McCullum EO, Williams BAR, Zhang J, Chaput JC. Random Mutagenesis by Error-Prone PCR. In: *Methods in Molecular Biology (Clifton, N.J.)*. Vol 634. ; 2010:103-109. doi:10.1007/978-1-60761-652-8_7
260. Muteeb G, Sen R. Random Mutagenesis Using a Mutator Strain. In: *Methods in Molecular Biology (Clifton, N.J.)*. Vol 634. ; 2010:411-419. doi:10.1007/978-1-60761-652-8_29
261. Sharifnia T, Rusu V, Piccioni F, et al. Genetic modifiers of EGFR dependence in non-small cell lung cancer. *Proc Natl Acad Sci U S A.* 2014;111(52):18661-18666. doi:10.1073/pnas.1412228112
262. Diehl P, Tedesco D, Chenchik A. Use of RNAi screens to uncover resistance mechanisms in cancer cells and identify synthetic lethal interactions. *Drug Discov Today Technol.* 2014;11:11-18. doi:10.1016/j.ddtec.2013.12.002
263. Shalem O, Sanjana NE, Hartenian E, et al. Genome-scale CRISPR-Cas9 knockout screening in human cells. *Science.* 2014;343(6166):84-87. doi:10.1126/science.1247005
264. Doudna JA, Charpentier E. Genome editing. The new frontier of genome engineering with CRISPR-Cas9. *Science (80-).* 2014;346(6213):1258096. doi:10.1126/science.1258096
265. Jinek M, Chylinski K, Fonfara I, Hauer M, Doudna JA, Charpentier E. A programmable dual-RNA-guided DNA endonuclease in adaptive bacterial immunity. *Science.* 2012;337(6096):816-821. doi:10.1126/science.1225829
266. Hale CR, Zhao P, Olson S, et al. RNA-guided RNA cleavage by a CRISPR RNA-Cas protein complex. *Cell.* 2009;139(5):945-956. doi:10.1016/j.cell.2009.07.040
267. Deltcheva E, Chylinski K, Sharma CM, et al. CRISPR RNA maturation by trans-encoded small RNA and host factor RNase III. *Nature.* 2011;471(7340):602-607. doi:10.1038/nature09886
268. Gilbert LA, Larson MH, Morsut L, et al. CRISPR-Mediated Modular RNA-Guided Regulation of Transcription in Eukaryotes. *Cell.* 2013;154(2):442-451. doi:10.1016/j.cell.2013.06.044
269. Gilbert LA, Horlbeck MA, Adamson B, et al. Genome-Scale CRISPR-Mediated Control of Gene Repression and Activation. *Cell.* 2014;159(3):647-661. doi:10.1016/j.cell.2014.09.029
270. Ran FA, Hsu PD, Wright J, Agarwala V, Scott DA, Zhang F. Genome engineering using the CRISPR-Cas9 system. *Nat Protoc.* 2013;8(11):2281-2308. doi:10.1038/nprot.2013.143
271. Konermann S, Brigham MD, Trevino AE, et al. Genome-scale transcriptional activation by an engineered CRISPR-Cas9 complex. *Nature.* 2015;517(7536):583-588. doi:10.1038/nature14136
272. Wieschaus E, Nusslein-Volhard C, Kluding H. Krüppel, a gene whose activity is required early in the zygotic genome for normal embryonic segmentation. *Dev Biol.* 1984;104(1):172-186. Accessed January 25, 2018. <http://www.ncbi.nlm.nih.gov/pubmed/6428949>
273. Jinek M, East A, Cheng A, Lin S, Ma E, Doudna J. RNA-programmed genome editing in human cells. *Elife.* 2013;2013(2). doi:10.7554/eLife.00471
274. Mali P, Yang L, Esvelt KM, et al. RNA-guided human genome engineering via Cas9. *Science (80-).* 2013;339(6121):823-826. doi:10.1126/science.1232033
275. Lieber MR. The Mechanism of Double-Strand DNA Break Repair by the Nonhomologous DNA End-Joining Pathway. *Annu Rev Biochem.* 2010;79(1):181-211. doi:10.1146/annurev.biochem.052308.093131
276. Lykke-Andersen J, Bennett EJ. Protecting the proteome: Eukaryotic cotranslational quality control pathways. *J Cell Biol.* 2014;204(4):467-476. doi:10.1083/jcb.201311103
277. Bolotin A, Quinquis B, Sorokin A, Ehrlich SD. Clustered regularly interspaced short palindrome repeats (CRISPRs) have spacers of extrachromosomal origin. *Microbiology.* 2005;151(Pt 8):2551-2561. doi:10.1099/mic.0.28048-0
278. Makarova KS, Grishin N V, Shabalina SA, Wolf YI, Koonin E V. A putative RNA-interference-based immune system in prokaryotes: computational analysis of the predicted enzymatic machinery, functional analogies with eukaryotic RNAi, and hypothetical mechanisms of action. *Biol Direct.* 2006;1(1):7. doi:10.1186/1745-6150-1-7
279. Gilbert LA, Larson MH, Morsut L, et al. CRISPR-mediated modular RNA-guided regulation of transcription in eukaryotes. *Cell.* 2013;154(2):442-451. doi:10.1016/j.cell.2013.06.044
280. Qi LS, Larson MH, Gilbert LA, et al. Repurposing CRISPR as an RNA-guided platform for sequence-specific control of gene expression. *Cell.* 2013;152(5):1173-1183. doi:10.1016/j.cell.2013.02.022
281. Groner AC, Meylan S, Ciuffi A, et al. KRAB-Zinc Finger Proteins and KAP1 Can Mediate Long-Range Transcriptional Repression through Heterochromatin Spreading. *PLoS Genet.* 2010;6(3). doi:10.1371/journal.pgen.1000869
282. Chavez A, Scheiman J, Vora S, et al. Highly efficient Cas9-mediated transcriptional programming. *Nat Methods.* 2015;12(4):326-328. doi:10.1038/nmeth.3312
283. Tanenbaum ME, Gilbert LA, Qi LS, Weissman JS, Vale RD. A protein-tagging system for signal amplification in gene expression and fluorescence imaging. *Cell.* 2014;159(3):635-646. doi:10.1016/j.cell.2014.09.039
284. Kampmann M. CRISPRi and CRISPRa Screens in Mammalian Cells for Precision Biology and Medicine. *ACS Chem Biol.* 2018;13(2):406-416. doi:10.1021/acschembio.7b00657
285. Nishimasu H, Ran FA, Hsu PD, et al. Crystal structure of Cas9 in complex with guide RNA and target DNA. *Cell.* 2014;156(5):935-949. doi:10.1016/j.cell.2014.02.001
286. Joung J, Konermann S, Gootenberg JS, et al. Genome-scale CRISPR-Cas9 knockout and transcriptional activation screening. *Nat Protoc.* 2017;12(4):828-863. doi:10.1038/nprot.2017.016
287. Shalem O, Sanjana NE, Zhang F. High-throughput functional genomics using CRISPR-Cas9. *Nat Rev Genet.* 2015;16(5):299-311. doi:10.1038/nrg3899

288. Sanjana NE, Shalem O, Zhang F. Improved vectors and genome-wide libraries for CRISPR screening. *Nat Methods*. 2014;11(8):783-784. doi:10.1038/nmeth.3047
289. Wang T, Wei JJ, Sabatini DM, Lander ES. Genetic screens in human cells using the CRISPR-Cas9 system. *Science*. 2014;343(6166):80-84. doi:10.1126/science.1246981
290. Koike-Yusa H, Li Y, Tan E-P, Velasco-Herrera MDC, Yusa K. Genome-wide recessive genetic screening in mammalian cells with a lentiviral CRISPR-guide RNA library. *Nat Biotechnol*. 2014;32(3):267-273. doi:10.1038/nbt.2800
291. Zhou Y, Zhu S, Cai C, et al. High-throughput screening of a CRISPR/Cas9 library for functional genomics in human cells. *Nature*. 2014;509(7501):487-491. doi:10.1038/nature13166
292. Doench JG, Fusi N, Sullender M, et al. Optimized sgRNA design to maximize activity and minimize off-target effects of CRISPR-Cas9. *Nat Biotechnol*. 2016;34(2):184-191. doi:10.1038/nbt.3437
293. Sun W, He B, Yang B, et al. Genome-wide CRISPR screen reveals SGOL1 as a druggable target of sorafenib-treated hepatocellular carcinoma. *Lab Invest*. 2018;98(6):734-744. doi:10.1038/s41374-018-0027-6
294. Ouyang Q, Liu Y, Tan J, et al. Loss of ZNF587B and SULF1 contributed to cisplatin resistance in ovarian cancer cell lines based on Genome-scale CRISPR/Cas9 screening. *Am J Cancer Res*. 2019;9(5):988-998. Accessed December 15, 2019. <http://www.ncbi.nlm.nih.gov/pubmed/31218106>
295. Jost M, Chen Y, Gilbert LA, et al. Combined CRISPR/a-Based Chemical Genetic Screens Reveal that Rigosertib Is a Microtubule-Destabilizing Agent. *Mol Cell*. 2017;68(1):210-223.e6. doi:10.1016/j.molcel.2017.09.012
296. Kumar M, Keller B, Makalou N, Sutton RE. Systematic Determination of the Packaging Limit of Lentiviral Vectors. *Hum Gene Ther*. 2001;12(15):1893-1905. doi:10.1089/104303401753153947
297. Bester AC, Lee JD, Chavez A, et al. An Integrated Genome-wide CRISPRa Approach to Functionalize lncRNAs in Drug Resistance. *Cell*. 2018;173(3):649-664.e20. doi:10.1016/j.cell.2018.03.052
298. le Sage C, Lawo S, Panicker P, et al. Dual direction CRISPR transcriptional regulation screening uncovers gene networks driving drug resistance. *Sci Rep*. 2017;7(1):17693. doi:10.1038/s41598-017-18172-6
299. Joung J, Engreitz JM, Konermann S, et al. Genome-scale activation screen identifies a lncRNA locus regulating a gene neighbourhood. *Nature*. 2017;548(7667):343-346. doi:10.1038/nature23451
300. Trigg RM, Lee LC, Prokoph N, et al. The targetable kinase PIM1 drives ALK inhibitor resistance in high-risk neuroblastoma independent of MYCN status. *Nat Commun*. 2019;10(1):5428. doi:10.1038/s41467-019-13315-x
301. Prokoph N, Probst NA, Lee LC, et al. IL10RA modulates crizotinib sensitivity in NPM1-ALK+ anaplastic large cell lymphoma. *Blood*. 2020;136(14):1657-1669. doi:10.1182/blood.2019003793
302. Stewart SA, Dykxhoorn DM, Palliser D, et al. Lentivirus-delivered stable gene silencing by RNAi in primary cells. *RNA*. 2003;9(4):493-501. doi:10.1261/RNA.2192803
303. Sarbassov DD, Guertin DA, Ali SM, Sabatini DM. Phosphorylation and Regulation of Akt/PKB by the Rictor-mTOR Complex. *Science (80-)*. 2005;307(5712):1098-1101. doi:10.1126/science.1106148
304. Menotti M, Ambrogio C, Cheong T-C, et al. Wiskott–Aldrich syndrome protein (WASP) is a tumor suppressor in T cell lymphoma. *Nat Med*. Published online December 3, 2018. doi:10.1038/s41591-018-0262-9
305. Aubrey BJ, Kelly GL, Kueh AJ, et al. An Inducible Lentiviral Guide RNA Platform Enables the Identification of Tumor-Essential Genes and Tumor-Promoting Mutations InVivo. *Cell Rep*. 2015;10(8):1422-1432. doi:10.1016/j.celrep.2015.02.002
306. Chavez A, Tuttle M, Pruitt BW, et al. Comparison of Cas9 activators in multiple species. *Nat Methods*. 2016;13(7):563-567. doi:10.1038/nmeth.3871
307. Szulc J, Wiznerowicz M, Sauvain M-O, Trono D, Aebischer P. A versatile tool for conditional gene expression and knockdown. *Nat Methods*. 2006;3(2):109-116. doi:10.1038/nmeth846
308. Wiznerowicz M, Trono D. Conditional suppression of cellular genes: lentivirus vector-mediated drug-inducible RNA interference. *J Virol*. 2003;77(16):8957-8961. doi:10.1128/JVI.77.16.8957-8961.2003
309. Piva R, Chiarle R, Manazza AD, et al. Ablation of oncogenic ALK is a viable therapeutic approach for anaplastic large-cell lymphomas. *Blood*. 2006;107(2):689-697. doi:10.1182/blood-2005-05-2125
310. Yang X, Boehm JS, Yang X, et al. A public genome-scale lentiviral expression library of human ORFs. *Nat Methods*. 2011;8(8):659-661. doi:10.1038/nmeth.1638
311. Kang BH, Jensen KJ, Hatch JA, Janes KA. Simultaneous Profiling of 194 Distinct Receptor Transcripts in Human Cells. *Sci Signal*. 2013;6(287):rs13-rs13. doi:10.1126/scisignal.2003624
312. Ng SY, Yoshida N, Christie AL, et al. Targetable vulnerabilities in T- and NK-cell lymphomas identified through preclinical models. *Nat Commun*. 2018;9(1):2024. doi:10.1038/s41467-018-04356-9
313. Durant L, Watford WT, Ramos HL, et al. Diverse Targets of the Transcription Factor STAT3 Contribute to T Cell Pathogenicity and Homeostasis. *Immunity*. 2010;32(5):605-615. doi:10.1016/J.IMMUNI.2010.05.003
314. Pomari E, Basso G, Bresolin S, et al. NPM-ALK expression levels identify two distinct subtypes of paediatric anaplastic large cell lymphoma. *Leukemia*. 2017;31(2):498-501. doi:10.1038/leu.2016.292
315. Iqbal J, Wright G, Wang C, et al. Gene expression signatures delineate biological and prognostic subgroups in peripheral T-cell lymphoma. *Blood*. 2014;123(19):2915-2923. doi:10.1182/blood-2013-11-536359
316. Piccaluga PP, Agostinelli C, Califano A, et al. Gene expression analysis of peripheral T cell lymphoma, unspecified, reveals distinct profiles and new potential therapeutic targets. *J Clin Invest*. 2007;117(3):823-834. doi:10.1172/JCI26833
317. Eckerle S, Brune V, Döring C, et al. Gene expression profiling of isolated tumour cells from anaplastic large

- cell lymphomas: insights into its cellular origin, pathogenesis and relation to Hodgkin lymphoma. *Leukemia*. 2009;23(11):2129-2138. doi:10.1038/leu.2009.161
318. Iqbal J, Weisenburger DD, Greiner TC, et al. Molecular signatures to improve diagnosis in peripheral T-cell lymphoma and prognostication in angioimmunoblastic T-cell lymphoma. *Blood*. 2010;115(5):1026-1036. doi:10.1182/blood-2009-06-227579
 319. Scarfo I, Pellegrino E, Mereu E, et al. Identification of a new subclass of ALK-negative ALCL expressing aberrant levels of ERBB4 transcripts. *Blood*. 2016;127(2):221-232. doi:10.1182/blood-2014-12-614503
 320. Tarantelli C, Gaudio E, Arribas AJ, et al. PQR309 Is a Novel Dual PI3K/mTOR Inhibitor with Preclinical Antitumor Activity in Lymphomas as a Single Agent and in Combination Therapy. *Clin Cancer Res*. 2018;24(1):120-129. doi:10.1158/1078-0432.CCR-17-1041
 321. Schleussner N, Merkel O, Costanza M, et al. The AP-1-BATF and -BATF3 module is essential for growth, survival and TH17/ILC3 skewing of anaplastic large cell lymphoma. *Leukemia*. 2018;32(9):1994-2007. doi:10.1038/s41375-018-0045-9
 322. Piva R, Pellegrino E, Mattioli M, et al. Functional validation of the anaplastic lymphoma kinase signature identifies CEBPB and BCL2A1 as critical target genes. *J Clin Invest*. 2006;116(12):3171-3182. doi:10.1172/JCI29401
 323. Voena C, Conte C, Ambrogio C, et al. The Tyrosine Phosphatase Shp2 Interacts with NPM-ALK and Regulates Anaplastic Lymphoma Cell Growth and Migration. *Cancer Res*. 2007;67(9):4278-4286. doi:10.1158/0008-5472.CAN-06-4350
 324. Gruss H, Boiani N, Williams D, Armitage R, Smith C, Goodwin R. Pleiotropic effects of the CD30 ligand on CD30-expressing cells and lymphoma cell lines. *Blood*. 1994;83(8).
 325. Cerchetti L, Damm-Welk C, Vater I, et al. Inhibition of Anaplastic Lymphoma Kinase (ALK) Activity Provides a Therapeutic Approach for CLTC-ALK-Positive Human Diffuse Large B Cell Lymphomas. Wutz A, ed. *PLoS One*. 2011;6(4):e18436. doi:10.1371/journal.pone.0018436
 326. Redaelli S, Ceccon M, Antolini L, et al. Synergistic activity of ALK and mTOR inhibitors for the treatment of NPM-ALK positive lymphoma. *Oncotarget*. 2016;7(45):72886-72897. doi:10.18632/oncotarget.12128
 327. Ceccon M, Mologni L, Giudici G, et al. Treatment Efficacy and Resistance Mechanisms Using the Second-Generation ALK Inhibitor AP26113 in Human NPM-ALK-Positive Anaplastic Large Cell Lymphoma. *Mol Cancer Res*. 2015;13(4):775-783. doi:10.1158/1541-7786.MCR-14-0157
 328. Redaelli S, Ceccon M, Zappa M, et al. Lorlatinib treatment elicits multiple on- and off-target mechanisms of resistance in ALK-driven cancer. *Cancer Res*. Published online October 15, 2018;canres.1867.2018. doi:10.1158/0008-5472.CAN-18-1867
 329. Li W, Xu H, Xiao T, et al. MAGECK enables robust identification of essential genes from genome-scale CRISPR/Cas9 knockout screens. *Genome Biol*. 2014;15(12):554. doi:10.1186/s13059-014-0554-4
 330. Patro R, Duggal G, Love MI, Irizarry RA, Kingsford C. Salmon provides fast and bias-aware quantification of transcript expression. *Nat Methods*. 2017;14(4):417-419. doi:10.1038/nmeth.4197
 331. Soneson C, Love MI, Robinson MD. Differential analyses for RNA-seq: transcript-level estimates improve gene-level inferences. *F1000Research*. 2016;4:1521. doi:10.12688/f1000research.7563.2
 332. McCarthy DJ, Chen Y, Smyth GK. Differential expression analysis of multifactor RNA-Seq experiments with respect to biological variation. *Nucleic Acids Res*. 2012;40(10):4288-4297. doi:10.1093/nar/gks042
 333. Love, M., Anders, S., Huber W. Differential analysis of count data—the deseq2 package. *Genome Biol*. 2014;15:550.
 334. Durinck S, Spellman PT, Birney E, Huber W. Mapping identifiers for the integration of genomic datasets with the R/Bioconductor package biomaRt. *Nat Protoc*. 2009;4(8):1184-1191. doi:10.1038/nprot.2009.97
 335. Sergushichev A. An algorithm for fast preranked gene set enrichment analysis using cumulative statistic calculation. *bioRxiv*. Published online June 20, 2016:060012. doi:10.1101/060012
 336. Alexa A, Rahnenführer J. topGO: Enrichment Analysis for Gene Ontology. doi:10.18129/B9.bioc.topGO
 337. Kassambara A. Survminer: Drawing Survival Curves using “ggplot2.” Published 2018. <https://cran.r-project.org/web/packages/survminer/index.html>
 338. Therneau TM. Survival: Survival Analysis. Published 2018. <https://cran.r-project.org/web/packages/survival/index.html>
 339. Li H, Handsaker B, Wysoker A, et al. The Sequence Alignment/Map format and SAMtools. *Bioinformatics*. 2009;25(16):2078-2079. doi:10.1093/bioinformatics/btp352
 340. Langmead B, Salzberg SL. Fast gapped-read alignment with Bowtie 2. *Nat Methods*. 2012;9(4):357-359. doi:10.1038/nmeth.1923
 341. Quinlan AR, Hall IM. BEDTools: a flexible suite of utilities for comparing genomic features. *Bioinformatics*. 2010;26(6):841-842. doi:10.1093/bioinformatics/btq033
 342. Robinson JT, Thorvaldsdóttir H, Winckler W, et al. Integrative genomics viewer. *Nat Biotechnol*. 2011;29(1):24-26. doi:10.1038/nbt.1754
 343. Kuhn RM, Haussler D, Kent WJ. The UCSC genome browser and associated tools. *Brief Bioinform*. 2013;14(2):144-161. doi:10.1093/bib/bbs038
 344. Sean D, Meltzer PS. GEOquery: A bridge between the Gene Expression Omnibus (GEO) and BioConductor. *Bioinformatics*. 2007;23(14):1846-1847. doi:10.1093/bioinformatics/btm254
 345. Carvalho BS, Irizarry RA. A framework for oligonucleotide microarray preprocessing. *Bioinformatics*. 2010;26(19):2363-2367. doi:10.1093/bioinformatics/btq431
 346. Kauffmann A, Gentleman R, Huber W. arrayQualityMetrics - A bioconductor package for quality assessment of microarray data. *Bioinformatics*. 2009;25(3):415-416. doi:10.1093/bioinformatics/btn647

347. Pagès H, Carlson M, Falcon S LN. AnnotationDbi: Manipulation of SQLite-based annotations in Bioconductor. R package version 1.46.0. Published online 2019. <https://bioconductor.org/packages/release/bioc/html/AnnotationDbi.html>
348. Ritchie ME, Phipson B, Wu D, et al. Limma powers differential expression analyses for RNA-sequencing and microarray studies. *Nucleic Acids Res.* 2015;43(7):e47. doi:10.1093/nar/gkv007
349. Dunning MJ, Smith ML, Ritchie ME, Tavaré S. beadarray: R classes and methods for Illumina bead-based data. 2007;23(16):2183-2184. doi:10.1093/bioinformatics/btm311
350. Dunning M, Lynch A, Eldridge M. illuminaHumanv4.db: Illumina HumanHT12v4 annotation data (chip illuminaHumanv4). Published online 2015.
351. Frankish A, Diekhans M, Ferreira AM, et al. GENCODE reference annotation for the human and mouse genomes. *Nucleic Acids Res.* 2019;47(D1):D766-D773. doi:10.1093/nar/gky955
352. Kanehisa M, Goto S. KEGG: Kyoto Encyclopedia of Genes and Genomes. *Nucleic Acids Res.* 2000;28(1):27-30. doi:10.1093/nar/28.1.27
353. Wang X, Spandidos A, Wang H, Seed B. PrimerBank: a PCR primer database for quantitative gene expression analysis, 2012 update. *Nucleic Acids Res.* 2012;40(D1):D1144-D1149. doi:10.1093/nar/gkr1013
354. How J, Warner M, Shustik C, Laneville P. Cytarabine and Etoposide (CYVE) as First-Line Therapy for Primary Central Nervous System Lymphoma. *Blood.* 2010;116(21):4895. doi:10.1182/blood.V116.21.4895.4895
355. Barbey S, Gogusev J, Mouly H, et al. DEL cell line: a "malignant histiocytosis" CD30+ t(5;6)(q35;p21) cell line. *Int J cancer.* 1990;45(3):546-553. Accessed January 27, 2018. <http://www.ncbi.nlm.nih.gov/pubmed/2307542>
356. Epstein AL, Kaplan HS. Biology of the human malignant lymphomas. I. Establishment in continuous cell culture and heterotransplantation of diffuse histiocytic lymphomas. *Cancer.* 1974;34(6):1851-1872. Accessed January 27, 2018. <http://www.ncbi.nlm.nih.gov/pubmed/4140017>
357. Morgan R, Smith SD, Hecht BK, et al. Lack of involvement of the c-fms and N-myc genes by chromosomal translocation t(2;5)(p23;q35) common to malignancies with features of so-called malignant histiocytosis. *Blood.* 1989;73(8):2155-2164. Accessed January 27, 2018. <http://www.ncbi.nlm.nih.gov/pubmed/2525056>
358. Mologni L, Cecon M, Pirola A, et al. NPM/ALK mutants resistant to ASP3026 display variable sensitivity to alternative ALK inhibitors but succumb to the novel compound PF-06463922. *Oncotarget.* 2015;6(8):5720-5734. doi:10.18632/oncotarget.3122
359. PrimerBank. Accessed January 27, 2018. <https://pga.mgh.harvard.edu/primerbank/>
360. Cas9 Activator Tool. Accessed January 27, 2018. <http://sam.genome-engineering.org/database/>
361. pLKO.1-puro shRNA protocol. Accessed August 16, 2020. <https://www.addgene.org/tools/protocols/plko/#C>
362. Foucquier J, Guedj M. Analysis of drug combinations: current methodological landscape. *Pharmacol Res Perspect.* 2015;3(3):e00149. doi:10.1002/prp2.149
363. Kocak H, Ackermann S, Hero B, et al. Hox-C9 activates the intrinsic pathway of apoptosis and is associated with spontaneous regression in neuroblastoma. *Cell Death Dis.* 2013;4(4):e586. doi:10.1038/cddis.2013.84
364. Zhang W, Yu Y, Hertwig F, et al. Comparison of RNA-seq and microarray-based models for clinical endpoint prediction. *Genome Biol.* 2015;16:133. doi:10.1186/s13059-015-0694-1
365. Chiarle R, Simmons WJ, Cai H, et al. Stat3 is required for ALK-mediated lymphomagenesis and provides a possible therapeutic target. *Nat Med.* 2005;11(6):623-629. doi:10.1038/nm1249
366. Costa DB, Kobayashi S, Pandya SS, et al. CSF concentration of the anaplastic lymphoma kinase inhibitor crizotinib. *J Clin Oncol.* 2011;29(15):e443-5. doi:10.1200/JCO.2010.34.1313
367. Katayama R, Sakashita T, Yanagitani N, et al. P-glycoprotein Mediates Ceritinib Resistance in Anaplastic Lymphoma Kinase-rearranged Non-small Cell Lung Cancer. *EBioMedicine.* Published online 2016. doi:10.1016/j.ebiom.2015.12.009
368. Weilemann A, Grau M, Erdmann T, et al. Essential role of IRF4 and MYC signaling for survival of anaplastic large cell lymphoma. *Blood.* 2015;125(1):124-132. doi:10.1182/blood-2014-08-594507
369. Bandini C, Pupuleku A, Spaccarotella E, et al. IRF4 Mediates the Oncogenic Effects of STAT3 in Anaplastic Large Cell Lymphomas. *Cancers (Basel).* 2018;10(1):21. doi:10.3390/cancers10010021
370. Doebele RC, Pilling AB, Aisner DL, et al. Mechanisms of Resistance to Crizotinib in Patients with ALK Gene Rearranged Non-Small Cell Lung Cancer. *Clin Cancer Res.* 2012;18(5):1472-1482. doi:10.1158/1078-0432.CCR-11-2906
371. Cecon M, Merlo MEB, Mologni L, et al. Excess of NPM-ALK oncogenic signaling promotes cellular apoptosis and drug dependency. *Oncogene.* 2016;35(29):3854-3865. doi:10.1038/ncr.2015.456
372. Prutsch N, Gurnhofer E, Suske T, et al. Dependency on the TYK2/STAT1/MCL1 axis in anaplastic large cell lymphoma. *Leukemia.* Published online August 21, 2018. doi:10.1038/s41375-018-0239-1
373. Béguelin W, Sawh S, Chambwe N, et al. IL10 receptor is a novel therapeutic target in DLBCLs. *Leukemia.* 2015;29(8):1684-1694. doi:10.1038/leu.2015.57
374. Feigin ME, Xue B, Hammell MC, Muthuswamy SK. G-protein-coupled receptor GPR161 is overexpressed in breast cancer and is a promoter of cell proliferation and invasion. *Proc Natl Acad Sci U S A.* 2014;111(11):4191-4196. doi:10.1073/pnas.1320239111
375. Merighi S, Battistello E, Giacomelli L, et al. Targeting A3 and A2A adenosine receptors in the fight against cancer. *Expert Opin Ther Targets.* 2019;23(8):669-678. doi:10.1080/14728222.2019.1630380
376. Xie J, Merrett JE, Jensen KB, Proud CG. The MAP kinase-interacting kinases (MNKs) as targets in

- oncology. *Expert Opin Ther Targets*. 2019;23(3):187-199. doi:10.1080/14728222.2019.1571043
377. Hou J, Lam F, Proud C, Wang S. Targeting Mnk for cancer therapy. *Oncotarget*. 2012;3(2):118-131. doi:10.18632/oncotarget.453
378. Dreas A, Mikulski M, Milik M, Fabritius C-H, Brzózka K, Rzymiski T. Mitogen-activated Protein Kinase (MAPK) Interacting Kinases 1 and 2 (MNK1 and MNK2) as Targets for Cancer Therapy: Recent Progress in the Development of MNK Inhibitors. *Curr Med Chem*. 2017;24(28):3025-3053. doi:10.2174/0929867324666170203123427
379. Wu H, Hu C, Wang A, et al. Discovery of a BTK/MNK dual inhibitor for lymphoma and leukemia. *Leukemia*. 2016;30(1):173-181. doi:10.1038/leu.2015.180
380. Lyapichev KA, Tang G, Li S, et al. MYC expression is associated with older age, common morphology, increased MYC copy number, and poorer prognosis in patients with ALK+ anaplastic large cell lymphoma. *Hum Pathol*. Published online November 2020. doi:10.1016/j.humpath.2020.11.002
381. Turner SD, Yeung D, Hadfield K, Cook SJ, Alexander DR. The NPM-ALK tyrosine kinase mimics TCR signalling pathways, inducing NFAT and AP-1 by RAS-dependent mechanisms. *Cell Signal*. 2007;19(4):740-747. doi:10.1016/j.cellsig.2006.09.007
382. Ott GR, Cheng M, Learn KS, et al. Discovery of Clinical Candidate CEP-37440, a Selective Inhibitor of Focal Adhesion Kinase (FAK) and Anaplastic Lymphoma Kinase (ALK). *J Med Chem*. 2016;59(16):7478-7496. doi:10.1021/acs.jmedchem.6b00487
383. Schaller MD. Cellular functions of FAK kinases: insight into molecular mechanisms and novel functions. *J Cell Sci*. 2010;123(7):1007 LP - 1013. doi:10.1242/jcs.045112
384. Georger B, Schulte J, Zwaan CM, et al. Phase I study of ceritinib in pediatric patients (Pts) with malignancies harboring a genetic alteration in ALK (ALK+): Safety, pharmacokinetic (PK), and efficacy results. *J Clin Oncol*. 2015;33(15_suppl):10005. doi:10.1200/jco.2015.33.15_suppl.10005
385. Dagogo-Jack I, Shaw AT. Crizotinib resistance: implications for therapeutic strategies. *Ann Oncol*. 2016;27(suppl_3):iii42-iii50. doi:10.1093/annonc/mdw305
386. Ho AS, Liu Y, Khan TA, Hsu DH, Bazan JF, Moore KW. A receptor for interleukin 10 is related to interferon receptors. *Proc Natl Acad Sci U S A*. 1993;90(23):11267-11271. doi:10.1073/pnas.90.23.11267
387. Donnelly RP, Dickensheets H, Finbloom DS. The Interleukin-10 Signal Transduction Pathway and Regulation of Gene Expression in Mononuclear Phagocytes. *J Interf Cytokine Res*. 1999;19(6):563-573. doi:10.1089/107999099313695
388. Berti FCB, Pereira APL, Cebinelli GCM, Trugilo KP, Brajão de Oliveira K. The role of interleukin 10 in human papilloma virus infection and progression to cervical carcinoma. *Cytokine Growth Factor Rev*. 2017;34:1-13. doi:10.1016/J.CYTOGFR.2017.03.002
389. Finbloom DS, Winestock KD. *IL-10 Induces the Tyrosine Phosphorylation of Tyk2 and Jak1 and the Differential Assembly of STAT1 and STAT3 Complexes in Human T Cells and Monocytes.*; 1995.
390. Weber-Nordt RM, Riley JK, Greenlund AC, Moore KW, Darnell JE, Schreiber RD. Stat3 recruitment by two distinct ligand-induced, tyrosine-phosphorylated docking sites in the interleukin-10 receptor intracellular domain. *J Biol Chem*. 1996;271(44):27954-27961. doi:10.1074/JBC.271.44.27954
391. S-y AH, H-y Wei S, L-f Mui A, Miyajima A, Moore KW. Functional Regions of the Mouse Interleukin-10 Receptor Cytoplasmic Domain. *Mol Cell Biol*. 1995;15(9):5043-5053. doi:10.1128/mcb.15.9.5043
392. Wehinger J, Gouilleux F, Groner B, Finke J, Mertelsmann R, Weber-Nordt RM. IL-10 induces DNA binding activity of three STAT proteins (Stat1, Stat3, and Stat5) and their distinct combinatorial assembly in the promoters of selected genes. *FEBS Lett*. 1996;394(3):365-370. doi:10.1016/0014-5793(96)00990-8
393. Kasprzycka M, Marzec M, Liu X, Zhang Q, Wasik MA. Nucleophosmin/anaplastic lymphoma kinase (NPM/ALK) oncoprotein induces the T regulatory cell phenotype by activating STAT3. *Proc Natl Acad Sci*. 2006;103(26):9964-9969. doi:10.1073/pnas.0603507103
394. Knörr F, Damm-Welk C, Ruf S, et al. Blood cytokine concentrations in pediatric patients with anaplastic lymphoma kinase-positive anaplastic large cell lymphoma. *Haematologica*. 2018;103(3):477-485. doi:10.3324/haematol.2017.177972
395. Hoareau-Aveilla C, Valentin T, Daugrois C, et al. Reversal of microRNA-150 silencing disadvantages crizotinib-resistant NPM-ALK(+) cell growth. *J Clin Invest*. 2015;125(9):3505-3518. doi:10.1172/JCI78488
396. Song TL, Nairismägi M-L, Laurensia Y, et al. Oncogenic activation of the STAT3 pathway drives PD-L1 expression in natural killer/T-cell lymphoma. *Blood*. 2018;132(11):1146-1158. doi:10.1182/blood-2018-01-829424
397. Spaccarotella E, Pellegrino E, Ferracin M, et al. STAT3-mediated activation of microRNA cluster 17-92 promotes proliferation and survival of ALK-positive anaplastic large cell lymphoma. *Haematologica*. 2014;99(1):116-124. doi:10.3324/haematol.2013.088286
398. Hamedani FS, Cinar M, Mo Z, Cervania MA, Amin HM, Alkan S. Crizotinib (PF-2341066) induces apoptosis due to downregulation of pSTAT3 and BCL-2 family proteins in NPM-ALK+ anaplastic large cell lymphoma. *Leuk Res*. 2014;38(4):503-508. doi:10.1016/j.leukres.2013.12.027
399. Boulland M-L, Meignin V, Leroy-Viard K, et al. Human Interleukin-10 Expression in T/Natural Killer-Cell Lymphomas. *Am J Pathol*. 1998;153(4):1229-1237. doi:10.1016/S0002-9440(10)65667-2
400. Bard JD, Gelebart P, Anand M, Amin HM, Lai R. Aberrant expression of IL-22 receptor 1 and autocrine IL-22 stimulation contribute to tumorigenicity in ALK+ anaplastic large cell lymphoma. *Leukemia*. 2008;22(8):1595-1603. doi:10.1038/leu.2008.129
401. Yoon S, Jones BC, Logsdon NJ, et al. Structure and Mechanism of Receptor Sharing by the IL-10R2 Common Chain. *Structure*. 2010;18(5):638-648. doi:10.1016/j.str.2010.02.009

402. Moore KW, de Waal Malefyt R, Coffman RL, O'Garra A. INTERLEUKIN-10 AND THE INTERLEUKIN-10 RECEPTOR. *Annu Rev Immunol*. 2001;19(1):683-765. doi:10.1146/annurev.immunol.19.1.683
403. Werner MT, Zhang Q, Wasik MA. From Pathology to Precision Medicine in Anaplastic Large Cell Lymphoma Expressing Anaplastic Lymphoma Kinase (ALK+ ALCL). *Cancers (Basel)*. 2017;9(12):138. doi:10.3390/cancers9100138
404. Furtek SL, Backos DS, Matheson CJ, Reigan P. Strategies and Approaches of Targeting STAT3 for Cancer Treatment. *ACS Chem Biol*. 2016;11(2):308-318. doi:10.1021/acscchembio.5b00945
405. Reilley MJ, McCoon P, Cook C, et al. STAT3 antisense oligonucleotide AZD9150 in a subset of patients with heavily pretreated lymphoma: results of a phase 1b trial. *J Immunother Cancer*. 2018;6(1):119. doi:10.1186/s40425-018-0436-5
406. Minard-Colin V, Brugières L, Reiter A, et al. Non-Hodgkin Lymphoma in Children and Adolescents: Progress Through Effective Collaboration, Current Knowledge, and Challenges Ahead. *J Clin Oncol*. 2015;33(27):2963-2974. doi:10.1200/JCO.2014.59.5827
407. Gritti G, Boschini C, Rossi A, et al. Primary treatment response rather than front line stem cell transplantation is crucial for long term outcome of peripheral T-cell lymphomas. *PLoS One*. 2015;10(3):e0121822. doi:10.1371/journal.pone.0121822
408. Lobello C, Tichý B, Bystrý V, et al. Analysis of Mutational Landscape in Systemic Anaplastic Large Cell Lymphoma Identifies Novel Prognostic Markers. *Blood*. 2019;134(Supplement_1):1490. doi:10.1182/blood-2019-126501
409. Torossian A, Broin N, Frentzel J, et al. Blockade of crizotinib-induced BCL2 elevation in ALK-positive anaplastic large cell lymphoma triggers autophagy associated with cell death. *Haematologica*. 2019;104(7):1428-1439. doi:10.3324/haematol.2017.181966
410. Fontana D, Ceccon M, Gambacorti-Passerini C, Mogni L. Activity of second-generation ALK inhibitors against crizotinib-resistant mutants in an NPM-ALK model compared to EML4-ALK. *Cancer Med*. 2015;4(7):953-965. doi:10.1002/cam4.413
411. Li Y, Wang K, Song N, et al. Activation of IGF-1R pathway and NPM-ALK G1269A mutation confer resistance to crizotinib treatment in NPM-ALK positive lymphoma. *Invest New Drugs*. 2020;38(3):599-609. doi:10.1007/s10637-019-00802-7
412. Zdzalik D, Dymek B, Grygielewicz P, et al. Activating mutations in ALK kinase domain confer resistance to structurally unrelated ALK inhibitors in NPM-ALK-positive anaplastic large-cell lymphoma. *J Cancer Res Clin Oncol*. 2014;140(4):589-598. doi:10.1007/s00432-014-1589-3
413. Forde S, Matthews JD, Jahangiri L, et al. Paediatric Burkitt lymphoma patient-derived xenografts capture disease characteristics over time and are a model for therapy. *Br J Haematol*. n/a(n/a). doi:10.1111/bjh.17043
414. Gillet J-P, Varma S, Gottesman MM. The Clinical Relevance of Cancer Cell Lines. *JNCI J Natl Cancer Inst*. 2013;105(7):452-458. doi:10.1093/jnci/djt007
415. Sausville EA, Burger AM. Contributions of Human Tumor Xenografts to Anticancer Drug Development. *Cancer Res*. 2006;66(7):3351-3354. doi:10.1158/0008-5472.CAN-05-3627
416. Cassidy JW, Caldas C, Bruna A. Maintaining Tumor Heterogeneity in Patient-Derived Tumor Xenografts. *Cancer Res*. 2015;75(15):2963 LP - 2968. doi:10.1158/0008-5472.CAN-15-0727
417. Houghton PJ, Morton CL, Tucker C, et al. The pediatric preclinical testing program: Description of models and early testing results. *Pediatr Blood Cancer*. 2007;49(7):928-940. doi:10.1002/pbc.21078
418. Shultz LD, Lyons BL, Burzenski LM, et al. Human lymphoid and myeloid cell development in NOD/LtSz-scid IL2R gamma null mice engrafted with mobilized human hemopoietic stem cells. *J Immunol*. 2005;174(10):6477-6489. doi:10.4049/jimmunol.174.10.6477
419. Turner SD, Tooze R, MacLennan K, Alexander DR. Vav-promoter regulated oncogenic fusion protein NPM-ALK in transgenic mice causes B-cell lymphomas with hyperactive Jun kinase. *Oncogene*. 2003;22(49):7750-7761. doi:10.1038/sj.onc.1207048
420. Turner SD, Merz H, Yeung D, Alexander DR. CD2 promoter regulated nucleophosmin-anaplastic lymphoma kinase in transgenic mice causes B lymphoid malignancy. *Anticancer Res*. 2006;26(5A):3275-3279. <http://europepmc.org/abstract/MED/17094440>
421. Giuriato S, Foisseau M, Dejean E, et al. Conditional TPM3-ALK and NPM-ALK transgenic mice develop reversible ALK-positive early B-cell lymphoma/leukemia. *Blood*. 2010;115(20):4061-4070. doi:10.1182/blood-2008-06-163386
422. Chiarle R, Gong JZ, Guasparri I, et al. NPM-ALK transgenic mice spontaneously develop T-cell lymphomas and plasma cell tumors. *Blood*. 2003;101(5):1919-1927. doi:10.1182/blood-2002-05-1343
423. Illert AL, Kreutmair S, Klingenberg C, et al. IDENTIFICATION AND CHARACTERISATION OF THE LYMPHOMA-INITIATING CELL (LIC) POPULATION IN AN ALCL MOUSE MODEL. *Hematol Oncol*. 2017;35(S2):163. doi:10.1002/hon.2438_19
424. Shoumariyeh K, Schneider N, Poggio T, et al. A novel conditional NPM-ALK-driven model of CD30+ T-cell lymphoma mediated by a translational stop cassette. *Oncogene*. 2020;39(9):1904-1913. doi:10.1038/s41388-019-1058-1
425. Malcolm TIM, Villarese P, Fairbairn CJ, et al. Anaplastic large cell lymphoma arises in thymocytes and requires transient TCR expression for thymic egress. *Nat Commun*. 2016;7:10087. doi:10.1038/ncomms10087
426. *European Medicines Agency Assessment Report Alunbrig Procedure No. EMEA/H/C/004248/0000.*; 2018. <https://www.ema.europa.eu/en/documents/assessment-report/alunbrig-epar-public-assessment->

- report_en.pdf
427. Freireich EJ, Gehan EA, Rall DP, Schmidt LH, Skipper HE. Quantitative comparison of toxicity of anticancer agents in mouse, rat, hamster, dog, monkey, and man. *Cancer Chemother reports*. 1966;50(4):219-244.
 428. U.S. Department of Health and Human Services Food and Drug Administration Center for Drug Evaluation and Research (CDER). Guidance for Industry Estimating the Maximum Safe Starting Dose in Initial Clinical Trials for Therapeutics in Adult Healthy Volunteers. Published 2005. Accessed October 9, 2020. <https://www.fda.gov/media/72309/download>
 429. Byrne AT, Alférez DG, Amant F, et al. Interrogating open issues in cancer precision medicine with patient-derived xenografts. *Nat Rev Cancer*. 2017;17(4):254-268. doi:10.1038/nrc.2016.140
 430. Sun C, Wang L, Huang S, et al. Reversible and adaptive resistance to BRAF(V600E) inhibition in melanoma. *Nature*. 2014;508(7494):118-122. doi:10.1038/nature13121
 431. Das Thakur M, Salangsang F, Landman AS, et al. Modelling vemurafenib resistance in melanoma reveals a strategy to forestall drug resistance. *Nature*. 2013;494(7436):251-255. doi:10.1038/nature11814
 432. Zitvogel L, Kepp O, Kroemer G. Immune parameters affecting the efficacy of chemotherapeutic regimens. *Nat Rev Clin Oncol*. 2011;8(3):151-160. doi:10.1038/nrclinonc.2010.223
 433. Tanaka H, Matsushima H, Nishibu A, Clausen BE, Takashima A. Dual therapeutic efficacy of vinblastine as a unique chemotherapeutic agent capable of inducing dendritic cell maturation. *Cancer Res*. 2009;69(17):6987-6994. doi:10.1158/0008-5472.CAN-09-1106
 434. Tanaka H, Matsushima H, Mizumoto N, Takashima A. Classification of chemotherapeutic agents based on their differential in vitro effects on dendritic cells. *Cancer Res*. 2009;69(17):6978-6986. doi:10.1158/0008-5472.CAN-09-1101
 435. Stadler S, Singh VK, Knorr F, Damm-Welk C, Woessmann W. Immune Response against ALK in Children with ALK-Positive Anaplastic Large Cell Lymphoma. *Cancers (Basel)*. 2018;10(4). doi:10.3390/cancers10040114
 436. Liu P, Zhao L, Kepp O, Kroemer G. Crizotinib - a tyrosine kinase inhibitor that stimulates immunogenic cell death. *Oncoimmunology*. 2019;8(7):1596652. doi:10.1080/2162402X.2019.1596652
 437. Liu P, Zhao L, Pol J, et al. Crizotinib-induced immunogenic cell death in non-small cell lung cancer. *Nat Commun*. 2019;10(1):1486. doi:10.1038/s41467-019-09415-3
 438. Theocharides APA, Rongvaux A, Fritsch K, Flavell RA, Manz MG. Humanized hemato-lymphoid system mice. *Haematologica*. 2016;101(1):5-19. doi:10.3324/haematol.2014.115212
 439. Jones DTW, Banito A, Grünewald TGP, et al. Molecular characteristics and therapeutic vulnerabilities across paediatric solid tumours. *Nat Rev Cancer*. 2019;19(8):420-438. doi:10.1038/s41568-019-0169-x
 440. Spix C, Pastore G, Sankila R, Stiller CA, Steliarova-Foucher E. Neuroblastoma incidence and survival in European children (1978-1997): report from the Automated Childhood Cancer Information System project. *Eur J Cancer*. 2006;42(13):2081-2091. doi:10.1016/j.ejca.2006.05.008
 441. Smith MA, Seibel NL, Altekruse SF, et al. Outcomes for children and adolescents with cancer: challenges for the twenty-first century. *J Clin Oncol*. 2010;28(15):2625-2634. doi:10.1200/JCO.2009.27.0421
 442. Maris JM, Hogarty MD, Bagatell R, Cohn SL. Neuroblastoma. *Lancet*. 2007;369(9579):2106-2120. doi:10.1016/S0140-6736(07)60983-0
 443. Park JR, Bagatell R, London WB, et al. Children's Oncology Group's 2013 blueprint for research: neuroblastoma. *Pediatr Blood Cancer*. 2013;60(6):985-993. doi:10.1002/pbc.24433
 444. Bresler SC, Weiser DA, Huwe PJ, et al. ALK mutations confer differential oncogenic activation and sensitivity to ALK inhibition therapy in neuroblastoma. *Cancer Cell*. 2014;26(5):682-694. doi:10.1016/j.ccell.2014.09.019
 445. George RE, Sanda T, Hanna M, et al. Activating mutations in ALK provide a therapeutic target in neuroblastoma. *Nature*. 2008;455(7215):975-978. doi:10.1038/nature07397
 446. Wang HQ, Halilovic E, Li X, et al. Combined ALK and MDM2 inhibition increases antitumor activity and overcomes resistance in human ALK mutant neuroblastoma cell lines and xenograft models. *Elife*. 2017;6. doi:10.7554/eLife.17137
 447. Guan J, Tucker ER, Wan H, et al. The ALK inhibitor PF-06463922 is effective as a single agent in neuroblastoma driven by expression of ALK and MYCN. *Dis Model Mech*. 2016;9(9):941-952. doi:10.1242/dmm.024448
 448. Siaw JT, Wan H, Pfeifer K, et al. Brigatinib, an anaplastic lymphoma kinase inhibitor, abrogates activity and growth in ALK-positive neuroblastoma cells, Drosophila and mice. *Oncotarget*. 2016;7(20):29011-29022. doi:10.18632/oncotarget.8508
 449. Friboulet L, Li N, Katayama R, et al. The ALK inhibitor ceritinib overcomes crizotinib resistance in non-small cell lung cancer. *Cancer Discov*. 2014;4(6):662-673. doi:10.1158/2159-8290.CD-13-0846
 450. Xu F, Li H, Sun Y. Inhibition of Axl improves the targeted therapy against ALK-mutated neuroblastoma. *Biochem Biophys Res Commun*. 2014;454(4):566-571. doi:10.1016/j.bbrc.2014.10.126
 451. Wood AC, Krytska K, Ryles HT, et al. Dual ALK and CDK4/6 Inhibition Demonstrates Synergy against Neuroblastoma. *Clin Cancer Res*. 2017;23(11):2856-2868. doi:10.1158/1078-0432.CCR-16-1114
 452. Sharma GG, Mota I, Mologni L, Patrucco E, Gambacorti-Passerini C, Chiarle R. Tumor Resistance against ALK Targeted Therapy-Where It Comes From and Where It Goes. *Cancers (Basel)*. 2018;10(3). doi:10.3390/cancers10030062
 453. Saris CJ, Domen J, Berns A. The pim-1 oncogene encodes two related protein-serine/threonine kinases by alternative initiation at AUG and CUG. *EMBO J*. 1991;10(3):655-664.
 454. Wang Z, Bhattacharya N, Weaver M, et al. Pim-1: a serine/threonine kinase with a role in cell survival,

- proliferation, differentiation and tumorigenesis. *J Vet Sci.* 2001;2(3):167-179.
455. Zhu N, Ramirez LM, Lee RL, Magnuson NS, Bishop GA, Gold MR. CD40 signaling in B cells regulates the expression of the Pim-1 kinase via the NF-kappa B pathway. *J Immunol.* 2002;168(2):744-754. doi:10.4049/jimmunol.168.2.744
 456. Miura O, Miura Y, Nakamura N, et al. Induction of tyrosine phosphorylation of Vav and expression of Pim-1 correlates with Jak2-mediated growth signaling from the erythropoietin receptor. *Blood.* 1994;84(12):4135-4141.
 457. Merkel AL, Meggers E, Ocker M. PIM1 kinase as a target for cancer therapy. *Expert Opin Investig Drugs.* 2012;21(4):425-436. doi:10.1517/13543784.2012.668527
 458. Zha J, Harada H, Yang E, Jockel J, Korsmeyer SJ. Serine phosphorylation of death agonist BAD in response to survival factor results in binding to 14-3-3 not BCL-X(L). *Cell.* 1996;87(4):619-628.
 459. Gu JJ, Wang Z, Reeves R, Magnuson NS. PIM1 phosphorylates and negatively regulates ASK1-mediated apoptosis. *Oncogene.* 2009;28(48):4261-4271. doi:10.1038/onc.2009.276
 460. Madhunapantula S V., Sharma A, Robertson GP. PRAS40 Deregulates Apoptosis in Malignant Melanoma. *Cancer Res.* 2007;67(8):3626-3636. doi:10.1158/0008-5472.CAN-06-4234
 461. Zhang F, Beharry ZM, Harris TE, et al. PIM1 protein kinase regulates PRAS40 phosphorylation and mTOR activity in FDCP1 cells. *Cancer Biol Ther.* 2009;8(9):846-853. doi:10.4161/cbt.8.9.8210
 462. Xie Y, Xu K, Dai B, et al. The 44 kDa Pim-1 kinase directly interacts with tyrosine kinase Etk/BMX and protects human prostate cancer cells from apoptosis induced by chemotherapeutic drugs. *Oncogene.* 2006;25(1):70-78. doi:10.1038/sj.onc.1209058
 463. Natarajan K, Bhullar J, Shukla S, et al. The Pim kinase inhibitor SGI-1776 decreases cell surface expression of P-glycoprotein (ABCB1) and breast cancer resistance protein (ABCG2) and drug transport by Pim-1-dependent and -independent mechanisms. *Biochem Pharmacol.* 2013;85(4):514-524. doi:10.1016/j.bcp.2012.12.006
 464. Chen J, Kobayashi M, Darmanin S, et al. Pim-1 plays a pivotal role in hypoxia-induced chemoresistance. *Oncogene.* 2009;28(28):2581-2592. doi:10.1038/onc.2009.124
 465. Xu J, Xiong G, Cao Z, et al. PIM-1 contributes to the malignancy of pancreatic cancer and displays diagnostic and prognostic value. *J Exp Clin Cancer Res.* 2016;35(1):133. doi:10.1186/s13046-016-0406-z
 466. Kuo H-P, Ezell SA, Hsieh S, et al. The role of PIM1 in the ibrutinib-resistant ABC subtype of diffuse large B-cell lymphoma. *Am J Cancer Res.* 2016;6(11):2489-2501. Accessed March 28, 2019. <http://www.ncbi.nlm.nih.gov/pubmed/27904766>
 467. Cheng H, Huang C, Xu X, et al. PIM-1 mRNA expression is a potential prognostic biomarker in acute myeloid leukemia. *J Transl Med.* 2017;15(1):179. doi:10.1186/s12967-017-1287-4
 468. Liao Y, Feng Y, Shen J, et al. Clinical and biological significance of PIM1 kinase in osteosarcoma. *J Orthop Res.* 2016;34(7):1185-1194. doi:10.1002/jor.23134
 469. Mahadevan D, Spier C, Della Croce K, et al. Transcript profiling in peripheral T-cell lymphoma, not otherwise specified, and diffuse large B-cell lymphoma identifies distinct tumor profile signatures. *Mol Cancer Ther.* 2005;4(12):1867-1879. doi:10.1158/1535-7163.MCT-05-0146
 470. Brunen D, de Vries RC, Liefink C, Beijersbergen RL, Bernards R. PIM Kinases Are a Potential Prognostic Biomarker and Therapeutic Target in Neuroblastoma. *Mol Cancer Ther.* 2018;17(4):849-857. doi:10.1158/1535-7163.MCT-17-0868
 471. Cortes J, Tamura K, DeAngelo DJ, et al. Phase I studies of AZD1208, a proviral integration Moloney virus kinase inhibitor in solid and haematological cancers. *Br J Cancer.* 2018;118(11):1425-1433. doi:10.1038/s41416-018-0082-1
 472. Martin-Sanchez E, Odqvist L, Rodriguez-Pinilla SM, et al. PIM kinases as potential therapeutic targets in a subset of peripheral T cell lymphoma cases. *PLoS One.* 2014;9(11):e112148. doi:10.1371/journal.pone.0112148
 473. Debryne DN, Bhatnagar N, Sharma B, et al. ALK inhibitor resistance in ALK1174L-driven neuroblastoma is associated with AXL activation and induction of EMT. *Oncogene.* 2016;35(28):3681-3691. doi:10.1038/onc.2015.434
 474. Debryne DN, Dries R, Sengupta S, et al. BORIS promotes chromatin regulatory interactions in treatment-resistant cancer cells. *Nature.* 2019;572(7771):676-680. doi:10.1038/s41586-019-1472-0
 475. Kogita A, Togashi Y, Hayashi H, et al. Activated MET acts as a salvage signal after treatment with alectinib, a selective ALK inhibitor, in ALK-positive non-small cell lung cancer. *Int J Oncol.* 2015;46(3):1025-1030. doi:10.3892/ijo.2014.2797
 476. Nguyen LN, Ma D, Shui G, et al. Mfsd2a is a transporter for the essential omega-3 fatty acid docosahexaenoic acid. *Nature.* 2014;509(7501):503-506. doi:10.1038/nature13241
 477. Toyokawa G, Takenoyama M, Watanabe S, et al. Dramatic response to crizotinib in an ALK-positive adenocarcinoma patient with disseminated intravascular coagulation. *J Thorac Oncol.* 2013;8(11):e96-8. doi:10.1097/JTO.0b013e3182a008ed
 478. Isaac M, Siu A, Jongstra J. The oncogenic PIM kinase family regulates drug resistance through multiple mechanisms. *Drug Resist Updat.* 2011;14(4-5):203-211. doi:10.1016/j.drug.2011.04.002
 479. Hsi ED, Jung S-H, Lai R, et al. Ki67 and PIM1 expression predict outcome in mantle cell lymphoma treated with high dose therapy, stem cell transplantation and rituximab: a Cancer and Leukemia Group B 59909 correlative science study. *Leuk Lymphoma.* 2008;49(11):2081-2090. doi:10.1080/10428190802419640
 480. Warnecke-Eberz U, Bollschweiler E, Drebber U, et al. Prognostic impact of protein overexpression of the proto-oncogene PIM-1 in gastric cancer. *Anticancer Res.* 2009;29(11):4451-4455. Accessed March 28,

2019. <http://www.ncbi.nlm.nih.gov/pubmed/20032391>
481. Peltola K, Hollmen M, Maula S-M, et al. Pim-1 Kinase Expression Predicts Radiation Response in Squamocellular Carcinoma of Head and Neck and Is under the Control of Epidermal Growth Factor Receptor. *Neoplasia*. 2009;11(7):629-IN1. doi:10.1593/NEO.81038
 482. Jiang R, Wang X, Jin Z, Li K. Association of Nuclear PIM1 Expression with Lymph Node Metastasis and Poor Prognosis in Patients with Lung Adenocarcinoma and Squamous Cell Carcinoma. *J Cancer*. 2016;7(3):324-334. doi:10.7150/jca.13422
 483. Reiser-Erkan C, Erkan M, Pan Z, et al. Hypoxia-inducible proto-oncogene Pim-1 is a prognostic marker in pancreatic ductal adenocarcinoma. *Cancer Biol Ther*. 2008;7(9):1352-1359. doi:10.4161/cbt.7.9.6418
 484. Tursynbay Y, Zhang J, Li Z, et al. Pim-1 kinase as cancer drug target: An update. *Biomed reports*. 2016;4(2):140-146. doi:10.3892/br.2015.561
 485. Xiang X, Yuan D, Liu Y, et al. PIM1 overexpression in T-cell lymphomas protects tumor cells from apoptosis and confers doxorubicin resistance by upregulating c-myc expression. *Acta Biochim Biophys Sin (Shanghai)*. 2018;50(8):800-806. doi:10.1093/abbs/gmy076
 486. Kim JH, Kim WS, Yun Y, Park C. Epstein–Barr virus latent membrane protein 1 increases chemo-resistance of cancer cells via cytoplasmic sequestration of Pim-1. *Cell Signal*. 2010;22(12):1858-1863. doi:10.1016/j.cellsig.2010.07.013
 487. Yuan LL, Green AS, Bertoli S, et al. Pim kinases phosphorylate Chk1 and regulate its functions in acute myeloid leukemia. *Leukemia*. 2014;28(2):293-301. doi:10.1038/leu.2013.168
 488. Wein L, Loi S. Mechanisms of resistance of chemotherapy in early-stage triple negative breast cancer (TNBC). *The Breast*. 2017;34:S27-S30. doi:10.1016/j.breast.2017.06.023
 489. Le X, Antony R, Razavi P, et al. Systematic Functional Characterization of Resistance to PI3K Inhibition in Breast Cancer. *Cancer Discov*. 2016;6(10):1134-1147. doi:10.1158/2159-8290.CD-16-0305
 490. Zemskova M, Sahakian E, Bashkirova S, Lilly M. The PIM1 Kinase Is a Critical Component of a Survival Pathway Activated by Docetaxel and Promotes Survival of Docetaxel-treated Prostate Cancer Cells. *J Biol Chem*. 2008;283(30):20635-20644. doi:10.1074/jbc.M709479200
 491. Xie Y, Burcu M, Linn DE, Qiu Y, Baer MR. Pim-1 Kinase Protects P-Glycoprotein from Degradation and Enables Its Glycosylation and Cell Surface Expression. *Mol Pharmacol*. 2010;78(2):310-318. doi:10.1124/mol.109.061713
 492. Cao L, Wang F, Li S, Wang X, Huang D, Jiang R. PIM1 kinase promotes cell proliferation, metastasis and tumor growth of lung adenocarcinoma by potentiating the c-MET signaling pathway. *Cancer Lett*. 2019;444:116-126. doi:10.1016/j.canlet.2018.12.015
 493. Bellon M, Lu L, Nicot C. Constitutive activation of Pim1 kinase is a therapeutic target for adult T-cell leukemia. *Blood*. 2016;127(20):2439-2450. doi:10.1182/BLOOD-2015-11-685032
 494. Białopiotrowicz E, Górniak P, Noyszewska-Kania M, et al. Microenvironment-induced PIM kinases promote CXCR4-triggered mTOR pathway required for chronic lymphocytic leukaemia cell migration. *J Cell Mol Med*. 2018;22(7):3548-3559. doi:10.1111/jcmm.13632
 495. Mazzacurati L, Lambert QT, Pradhan A, Griner LN, Huszar D, Reuther GW. The PIM inhibitor AZD1208 synergizes with ruxolitinib to induce apoptosis of ruxolitinib sensitive and resistant JAK2-V617F-driven cells and inhibit colony formation of primary MPN cells. *Oncotarget*. 2015;6(37):40141-40157. doi:10.18632/oncotarget.5653
 496. Cen B, Xiong Y, Song JH, et al. The Pim-1 Protein Kinase Is an Important Regulator of MET Receptor Tyrosine Kinase Levels and Signaling. *Mol Cell Biol*. 2014;34(13):2517-2532. doi:10.1128/MCB.00147-14
 497. Wu Y, Deng Y, Zhu J, Duan Y, Weng W, Wu X. Pim1 promotes cell proliferation and regulates glycolysis via interaction with MYC in ovarian cancer. *Onco Targets Ther*. 2018;11:6647. doi:10.2147/OTT.S180520
 498. Iwahara T, Fujimoto J, Wen D, et al. Molecular characterization of ALK, a receptor tyrosine kinase expressed specifically in the nervous system. *Oncogene*. 1997;14(4):439-449. doi:10.1038/sj.onc.1200849
 499. Vernersson E, Khoo NKS, Henriksson ML, Roos G, Palmer RH, Hallberg B. Characterization of the expression of the ALK receptor tyrosine kinase in mice. *Gene Expr Patterns*. 2006;6(5):448-461. doi:https://doi.org/10.1016/j.modgep.2005.11.006
 500. Zaenker P, Gray ES, Ziman MR. Autoantibody Production in Cancer—The Humoral Immune Response toward Autologous Antigens in Cancer Patients. *Autoimmun Rev*. 2016;15(5):477-483. doi:https://doi.org/10.1016/j.autrev.2016.01.017
 501. Voena C, Menotti M, Mastini C, et al. Efficacy of a Cancer Vaccine against ALK-Rearranged Lung Tumors. *Cancer Immunol Res*. 2015;3(12):1333-1343. doi:10.1158/2326-6066.CIR-15-0089
 502. Damm-Welk C, Siddiqi F, Fischer M, et al. Anti-ALK Antibodies in Patients with ALK-Positive Malignancies Not Expressing NPM-ALK. *J Cancer*. 2016;7(11):1383-1387. doi:10.7150/jca.15238
 503. Awad MM, Mastini C, Blasco RB, et al. Epitope mapping of spontaneous autoantibodies to anaplastic lymphoma kinase (ALK) in non-small cell lung cancer. *Oncotarget*. 2017;8(54):92265-92274. doi:10.18632/oncotarget.21182
 504. Knörr F, Weber S, Singh VK, et al. Epitope mapping of anti-ALK antibodies in children with anaplastic large cell lymphoma. *Clin Immunol*. 2018;195:77-81. doi:10.1016/j.clim.2018.07.008
 505. Cheever MA, Allison JP, Ferris AS, et al. The Prioritization of Cancer Antigens: A National Cancer Institute Pilot Project for the Acceleration of Translational Research. *Clin Cancer Res*. 2009;15(17):5323 LP - 5337. doi:10.1158/1078-0432.CCR-09-0737
 506. Montgomery RB, Makary E, Schiffman K, Goodell V, Disis ML. Endogenous anti-HER2 antibodies block HER2 phosphorylation and signaling through extracellular signal-regulated kinase. *Cancer Res*.

- 2005;65(2):650-656.
507. Carpenter EL, Haglund EA, Mace EM, et al. Antibody targeting of anaplastic lymphoma kinase induces cytotoxicity of human neuroblastoma. *Oncogene*. 2012;31(46):4859-4867. doi:10.1038/onc.2011.647
 508. Sano R, Krytska K, Larmour CE, et al. An antibody-drug conjugate directed to the ALK receptor demonstrates efficacy in preclinical models of neuroblastoma. *Sci Transl Med*. 2019;11(483). doi:10.1126/scitranslmed.aau9732
 509. Stylianou DC, Auf der Maur A, Kodack DP, et al. Effect of single-chain antibody targeting of the ligand-binding domain in the anaplastic lymphoma kinase receptor. *Oncogene*. 2009;28(37):3296-3306. doi:10.1038/onc.2009.184
 510. Passoni L. ALK as a novel lymphoma-associated tumor antigen: identification of 2 HLA-A2.1-restricted CD8+ T-cell epitopes. *Blood*. 2002;99(6):2100-2106. doi:10.1182/blood.V99.6.2100
 511. Passoni L, Gallo B, Biganzoli E, et al. In vivo T-cell immune response against anaplastic lymphoma kinase in patients with anaplastic large cell lymphomas. *Haematologica*. 2006;91(1):48-55. Accessed June 30, 2019. <http://www.ncbi.nlm.nih.gov/pubmed/16434370>
 512. K Singh V, Werner S, Hackstein H, et al. Analysis of nucleophosmin-anaplastic lymphoma kinase (NPM-ALK)-reactive CD8(+) T cell responses in children with NPM-ALK(+) anaplastic large cell lymphoma. *Clin Exp Immunol*. 2016;186(1):96-105. doi:10.1111/cei.12842
 513. Duyster J, Bai R-Y, Morris SW. Translocations involving anaplastic lymphoma kinase (ALK). *Oncogene*. 2001;20(40):5623-5637. doi:10.1038/sj.onc.1204594
 514. Ducray SP, Natarajan K, Garland GD, Turner SD, Egger G. The Transcriptional Roles of ALK Fusion Proteins in Tumorigenesis. *Cancers (Basel)*. 2019;11(8). doi:10.3390/cancers11081074
 515. Pulford K, Lamant L, Morris SW, et al. Detection of anaplastic lymphoma kinase (ALK) and nucleolar protein nucleophosmin (NPM)-ALK proteins in normal and neoplastic cells with the monoclonal antibody ALK1. *Blood*. 1997;89(4):1394-1404.
 516. Delsol G, Lamant L, Mariamé B, et al. A New Subtype of Large B-Cell Lymphoma Expressing the ALK Kinase and Lacking the 2; 5 Translocation. *Blood*. 1997;89(5):1483-1490. doi:10.1182/blood.V89.5.1483
 517. Tort F, Pinyol M, Pulford K, et al. Molecular characterization of a new ALK translocation involving moesin (MSN-ALK) in anaplastic large cell lymphoma. *Lab Invest*. 2001;81(3):419—426. doi:10.1038/labinvest.3780249
 518. Honorat J-F, Ragab A, Lamant L, Delsol G, Ragab-Thomas J. SHP1 tyrosine phosphatase negatively regulates NPM-ALK tyrosine kinase signaling. *Blood*. 2006;107(10):4130-4138. doi:10.1182/blood-2005-06-2421
 519. Falini B, Pulford K, Pucciarini A, et al. Lymphomas expressing ALK fusion protein(s) other than NPM-ALK. *Blood*. 1999;94(10):3509-3515.
 520. Locatelli F, Mauz-Koerholz C, Neville K, et al. Brentuximab vedotin for paediatric relapsed or refractory Hodgkin's lymphoma and anaplastic large-cell lymphoma: a multicentre, open-label, phase 1/2 study. *Lancet Haematol*. 2018;5(10):e450-e461. doi:10.1016/S2352-3026(18)30153-4
 521. Atabay E, Wang Q, Chiara A, et al. Identifying Novel Mechanisms of Resistance to Tyrosine Kinase Inhibitors in Anaplastic Large Cell Lymphoma. *Blood*. 2019;134(Supplement_1):5060-5060. doi:10.1182/blood-2019-132188
 522. John TD, Naik S, Leung K, Sasa G, Martinez C, Krance RA. Allogeneic hematopoietic cell transplant following crizotinib monotherapy for relapsed/refractory anaplastic large cell lymphoma. *Pediatr Transplant*. 2018;22(5):e13210. doi:10.1111/petr.13210
 523. Ruf S, Hebart H, Hjalgrim LL, et al. CNS progression during vinblastine or targeted therapies for high-risk relapsed ALK-positive anaplastic large cell lymphoma: A case series. *Pediatr Blood Cancer*. 2018;65(6):e27003. doi:10.1002/psc.27003
 524. Nakai R, Fukuhara S, Maeshima AM, et al. Alectinib, an anaplastic lymphoma kinase (ALK) inhibitor, as a bridge to allogeneic stem cell transplantation in a patient with ALK-positive anaplastic large-cell lymphoma refractory to chemotherapy and brentuximab vedotin. *Clin case reports*. 2019;7(12):2500-2504. doi:10.1002/ccr3.2543
 525. Shaw AT, Felip E, Bauer TM, et al. Lorlatinib in non-small-cell lung cancer with ALK or ROS1 rearrangement: an international, multicentre, open-label, single-arm first-in-man phase 1 trial. *Lancet Oncol*. 2017;18(12):1590-1599. doi:10.1016/S1470-2045(17)30680-0
 526. Kim D-W, Tiseo M, Ahn M-J, et al. Brigatinib in Patients With Crizotinib-Refractory Anaplastic Lymphoma Kinase-Positive Non-Small-Cell Lung Cancer: A Randomized, Multicenter Phase II Trial. *J Clin Oncol*. 2017;35(22):2490-2498. doi:10.1200/JCO.2016.71.5904
 527. Peters S, Camidge DR, Shaw AT, et al. Alectinib versus Crizotinib in Untreated ALK-Positive Non-Small-Cell Lung Cancer. *N Engl J Med*. Published online 2017:NEJMoa1704795. doi:10.1056/NEJMoa1704795
 528. Hida T, Nokihara H, Kondo M, et al. Alectinib versus crizotinib in patients with ALK-positive non-small-cell lung cancer (J-ALEX): an open-label, randomised phase 3 trial. *Lancet*. 2018;390(10089):29-39. doi:10.1016/S0140-6736(17)30565-2
 529. Montero J. A new hope for neuroblastoma treatment? *Sci Transl Med*. 2019;11(523):eaaz9769. doi:10.1126/scitranslmed.aaz9769
 530. Claeys S, Denecker G, Durinck K, et al. ALK positively regulates MYCN activity through repression of HBP1 expression. *Oncogene*. 2019;38(15):2690-2705. doi:10.1038/s41388-018-0595-3
 531. Hu G, Feldman AL. Drivers of crizotinib resistance in ALK+ ALCL. *Blood*. 2020;136(14):1573-1575. doi:10.1182/blood.2020007226

532. Moti N, Malcolm T, Hamoudi R, et al. Anaplastic large cell lymphoma-propagating cells are detectable by side population analysis and possess an expression profile reflective of a primitive origin. *Oncogene*. 2015;34(14):1843-1852. doi:10.1038/onc.2014.112
533. Boesch M, Zeimet AG, Fiegl H, et al. High prevalence of side population in human cancer cell lines. *Oncoscience*. 2016;3(3-4):85-87. doi:10.18632/oncoscience.300
534. WANG Y, YIN C, FENG L, MA L, WEI Y, SHENG G. Sorting, identification and enrichment of side population cells in THP-1 acute monocytic leukemia cells. *Oncol Rep*. 2013;29(5):1923-1931. doi:10.3892/or.2013.2316
535. Huang B, Huang YJ, Yao ZJ, et al. Cancer Stem Cell-Like Side Population Cells in Clear Cell Renal Cell Carcinoma Cell Line 769P. Bhowmick NA, ed. *PLoS One*. 2013;8(7):e68293. doi:10.1371/journal.pone.0068293
536. Kim KH, Cheong H-J, Kim S-J, et al. Side Population of Multiple Myeloma and Multiple Myeloma Stem Cell. *Blood*. 2014;124(21). doi:10.1182/blood.V124.21.5786.5786
537. Pelekanou V, Notas G, Athanasouli P, et al. APRIL and BAFF increase breast cancer cell stemness. *bioRxiv*. Published online October 2017:151902. doi:10.1101/151902
538. Bertolini G, Roz L, Perego P, et al. Highly tumorigenic lung cancer CD133+ cells display stem-like features and are spared by cisplatin treatment. *Proc Natl Acad Sci U S A*. 2009;106(38):16281-16286. doi:10.1073/pnas.0905653106
539. Dallas NA, Xia L, Fan F, et al. Chemoresistant Colorectal Cancer Cells, the Cancer Stem Cell Phenotype, and Increased Sensitivity to Insulin-like Growth Factor-I Receptor Inhibition. *Cancer Res*. 2009;69(5):1951-1957. doi:10.1158/0008-5472.CAN-08-2023
540. Huang B, Fu SJ, Fan WZ, et al. PKC ϵ inhibits isolation and stemness of side population cells via the suppression of ABCB1 transporter and PI3K/Akt, MAPK/ERK signaling in renal cell carcinoma cell line 769P. *Cancer Lett*. 2016;376(1):148-154. doi:10.1016/j.canlet.2016.03.041
541. Fukunaga-Kalabis M, Herlyn M. Beyond ABC: Another Mechanism of Drug Resistance in Melanoma Side Population. *J Invest Dermatol*. 2012;132(10):2317-2319. doi:10.1038/JID.2012.220
542. Gross E, L'Faqih-Olive F-E, Ysebaert L, et al. B-chronic lymphocytic leukemia chemoresistance involves innate and acquired leukemic side population cells. *Leukemia*. 2010;24(11):1885-1892. doi:10.1038/leu.2010.176
543. Abel E V., Kim EJ, Wu J, et al. The Notch Pathway Is Important in Maintaining the Cancer Stem Cell Population in Pancreatic Cancer. Fernandez-Zapico M, ed. *PLoS One*. 2014;9(3):e91983. doi:10.1371/journal.pone.0091983
544. Zhang C, Li C, He F, Cai Y, Yang H. Identification of CD44+CD24+ gastric cancer stem cells. *J Cancer Res Clin Oncol*. 2011;137(11):1679-1686. doi:10.1007/s00432-011-1038-5
545. Zhou J, Wang H, Cannon V, Wolcott K, Song H, Yates C. Side population rather than CD133+ cells distinguishes enriched tumorigenicity in hTERT-immortalized primary prostate cancer cells. *Mol Cancer*. 2011;10(1):112. doi:10.1186/1476-4598-10-112
546. Yamazaki H, Wilson Xu C, Naito M, et al. Regulation of cancer stem cell properties by CD9 in human B-acute lymphoblastic leukemia. *Biochem Biophys Res Commun*. 2011;409(1):14-21. doi:10.1016/j.bbrc.2011.04.098
547. Lau WM, Teng E, Chong HS, et al. CD44v8-10 Is a Cancer-Specific Marker for Gastric Cancer Stem Cells. *Cancer Res*. 2014;74(9):2630-2641. doi:10.1158/0008-5472.CAN-13-2309
548. Huang F-F, Wu D-S, Zhang L, et al. Inactivation of PTEN increases ABCG2 expression and the side population through the PI3K/Akt pathway in adult acute leukemia. *Cancer Lett*. 2013;336(1):96-105. doi:10.1016/j.canlet.2013.04.006
549. Teshima K, Nara M, Watanabe A, et al. Dysregulation of BMI1 and microRNA-16 collaborate to enhance an anti-apoptotic potential in the side population of refractory mantle cell lymphoma. *Oncogene*. 2014;33(17):2191-2203. doi:10.1038/onc.2013.177
550. Chen W, Zhang X, Chu C, et al. Identification of CD44+ cancer stem cells in human gastric cancer. *Hepatogastroenterology*. 2013;60(124):949-954. doi:10.5754/hge12881
551. El-Khattouti A, Selimovic D, Haikel Y, Megahed M, Gomez CR, Hassan M. Identification and analysis of CD133+ melanoma stem-like cells conferring resistance to taxol: An insight into the mechanisms of their resistance and response. *Cancer Lett*. 2014;343(1):123-133. doi:10.1016/j.canlet.2013.09.024
552. Bleau A-M, Hambardzumyan D, Ozawa T, et al. PTEN/PI3K/Akt pathway regulates the side population phenotype and ABCG2 activity in glioma tumor stem-like cells. *Cell Stem Cell*. 2009;4(3):226-235. doi:10.1016/j.stem.2009.01.007
553. Lessard J, Sauvageau G. Bmi-1 determines the proliferative capacity of normal and leukaemic stem cells. *Nature*. 2003;423(6937):255-260. doi:10.1038/nature01572
554. Salcido CD, Larochelle A, Taylor BJ, Dunbar CE, Varticovski L. Molecular characterisation of side population cells with cancer stem cell-like characteristics in small-cell lung cancer. *Br J Cancer*. 2010;102(11):1636-1644. doi:10.1038/sj.bjc.6605668
555. Xia H, Cao J, Li Q, et al. Hepatocellular Carcinoma-propagating Cells are Detectable by Side Population Analysis and Possess an Expression Profile Reflective of a Primitive Origin. *Sci Rep*. 2016;6(1):34856. doi:10.1038/srep34856
556. Wu C-P, Zhou L, Xie M, et al. Identification of Cancer Stem-Like Side Population Cells in Purified Primary Cultured Human Laryngeal Squamous Cell Carcinoma Epithelia. Cao J, ed. *PLoS One*. 2013;8(6):e65750. doi:10.1371/journal.pone.0065750

557. Hoe SLL, Tan LP, Jamal J, et al. Evaluation of stem-like side population cells in a recurrent nasopharyngeal carcinoma cell line. *Cancer Cell Int.* 2014;14(1):101. doi:10.1186/s12935-014-0101-0
558. Yi X-J, Zhao Y-H, Qiao L-X, Jin C-L, Tian J, Li Q-S. Aberrant Wnt/ β -catenin signaling and elevated expression of stem cell proteins are associated with osteosarcoma side population cells of high tumorigenicity. *Mol Med Rep.* 2015;12(4):5042-5048. doi:10.3892/mmr.2015.4025
559. Marhold M, Tomasich E, El-Gazzar A, et al. HIF1 α Regulates mTOR Signaling and Viability of Prostate Cancer Stem Cells. *Mol Cancer Res.* 2015;13(3):556-564. doi:10.1158/1541-7786.MCR-14-0153-T
560. Murase M, Kano M, Tsukahara T, et al. Side population cells have the characteristics of cancer stem-like cells/cancer-initiating cells in bone sarcomas. *Br J Cancer.* 2009;101(8):1425-1432. doi:10.1038/sj.bjc.6605330
561. Kreso A, Dick JE. Evolution of the Cancer Stem Cell Model. *Cell Stem Cell.* 2014;14(3):275-291. doi:10.1016/j.stem.2014.02.006
562. Dieter SM, Ball CR, Hoffmann CM, et al. Distinct Types of Tumor-Initiating Cells Form Human Colon Cancer Tumors and Metastases. *Cell Stem Cell.* 2011;9(4):357-365. doi:10.1016/j.stem.2011.08.010
563. Quintana E, Shackleton M, Foster HR, et al. Phenotypic Heterogeneity among Tumorigenic Melanoma Cells from Patients that Is Reversible and Not Hierarchically Organized. *Cancer Cell.* 2010;18(5):510-523. doi:10.1016/j.ccr.2010.10.012
564. Newton TC, Wolcott K, Roberts SS. Comparison of the side populations in pretreatment and postrelapse neuroblastoma cell lines. *Transl Oncol.* 2010;3(4):246-251. doi:10.1593/tlo.09301
565. Clarke MF, Dick JE, Dirks PB, et al. Cancer Stem Cells—Perspectives on Current Status and Future Directions: AACR Workshop on Cancer Stem Cells. *Cancer Res.* 2006;66(19):9339-9344. doi:10.1158/0008-5472.CAN-06-3126
566. Nguyen L V., Vanner R, Dirks P, Eaves CJ. Cancer stem cells: an evolving concept. *Nat Rev Cancer.* 2012;12(2):133-143. doi:10.1038/nrc3184